Nutrient Limitation of Marine Phytoplankton

Thomas J. Browning

Thesis submitted to The University of Oxford for the degree of Doctor of Philosophy in Earth Sciences

Department of Earth Sciences and St Anne's College, University of Oxford

Hilary Term 2014

Supervised by Dr. Heather A. Bouman, Prof. Gideon M. Henderson,

& Dr. C. Mark Moore

Nutrient Limitation of Marine Phytoplankton

Thomas J. Browning, St Anne's College

Thesis submitted to The University of Oxford for the degree of Doctor of Philosophy in Earth Sciences

Hilary Term 2014

Abstract

PHYTOPLANKTON across the majority of the world's oceans are thought to be limited by the availability of either nitrate or iron (Fe). However, the spatial resolution of experiments confirming this is low. Two thesis chapters present the results of bottle enrichment experiments at high spatial resolution across (i) the South Subtropical Convergence (SSTC) in the South Atlantic, and (ii) the Scotia Sea-Drake Passage sector of the Southern Ocean. These studies have added detail to the boundaries of limiting nutrients in these regions. Patterns of Fast Repetition Rate fluorometry (FRRf) derived parameters, physiological regulation of these parameters including influences of community structure, and the environmental controls driving them are analysed. Given its role as an essential micronutrient, there has been much effort in constraining potential sources of bioavailable Fe to the ocean, with one such source receiving recent interest: erupted ash from volcanoes. Bottle-scale ash-incubation experiments alongside conventional iron additions and laboratory ash-leaching experiments were conducted, the results of which suggest phytoplankton would respond strongly to ash deposition in the High Nitrate, Low Chlorophyll (HNLC) areas of the Southern Ocean. Particularly notable was the evidence these experiments provided for potential (co-)limitation of phytoplankton in these waters by the micronutrient manganese. The first three chapters of this thesis highlight a number of biogeochemical implications of trace metal stress, particularly that of Fe stress. Therefore, the ability to map the oceanographic extent of Fe-stressed regions using remote sensing would represent a particularly useful advance in marine biogeochemistry. Theoretically it could be possible to map Fe stress from space using satellite images of chlorophyll fluorescence, yet there are important uncertainties that need to be addressed before this can be carried out. In particular, a better understanding of the midday non-photochemical quenching driven reductions in chlorophyll fluorescence occurring at the time satellite images are captured is required. Analysis of over 200 non-photochemical quenching experiments collected over three research cruises, has allowed us to explore non-photochemical quenching and its relevance for using sunlight induced chlorophyll fluorescence to assess broad patterns of Fe stress. Our results have confirmed that satellite fluorescence quantum yields have the potential to reveal broad regions of Fe stress, however a dynamic non-photochemical quenching correction derived from our experiments and analysis was necessary to achieve this.

Nutrient Limitation of Marine Phytoplankton

Thomas J. Browning, St Anne's College

Thesis submitted to The University of Oxford for the degree of Doctor of Philosophy in Earth Sciences

Hilary Term 2014

Extended Abstract

PHYTOPLANKTON across the majority of the world's oceans are thought to be limited by the availability of either the 'macronutrient' nitrate or the essential trace-metal 'micronutrient' iron (Fe). However, the spatial resolution of experiments confirming this is low. Two thesis chapters present the results of bottle enrichment experiments at high spatial resolution across (i) the South Subtropical Convergence (SSTC) in the South Atlantic, and (ii) the Scotia Sea-Drake Passage region of the Southern Ocean. These studies have added detail to the occasionally subtle boundaries of nutrient limitation in these regions. Patterns of Fast Repetition Rate fluorometry (FRRf) derived parameters, physiological regulation of these parameters including influences of community structure, and the environmental controls driving them are analysed. Particularly evident on the South Atlantic cruise was the ability for FRRf measurements to delineate between systems with subtle changes in available nutrients. Unique physiological signatures were observed in Drake Passage, suggested to be the result of severe micronutrient limitation. Both of these studies have broadened understanding of factors regulating phytoplankton ecophysiology in these regions, as well as contributing to understanding which can be transferred to other regions, laboratory work, and theoretical studies.

Given the fundamental role of Fe in regulating phytoplankton across large areas of the world's oceans, there has been much interest in investigating potential sources of bioavailable Fe to the ocean. One such source has received recent interest: erupted ash from volcanoes. A number of studies have investigated the release of nutrients from ash, attempted to identify phytoplankton blooms subsequent to ash fall using remote sensing, and assessed the response of phytoplankton cultures to ash supply in the laboratory. Our field campaign mapping Fe stress provided an ideal opportunity to answer important questions about ash driven fertilisation of marine phytoplankton. By conducting a number of ash-addition incubation experiments alongside conventional Fe-only additions in the field, and laboratory ash-leaching experiments, interesting results pertaining to ash supply to High Nitrate, Low Chlorophyll (HNLC) regions of the Southern Ocean were found. Of particular interest was the evidence these experiments provided for potential (co-)limitation of phytoplankton in these waters by another essential trace-metal micronutrient. Although the evidence for Fe or nitrate limitation patterns dominating the global ocean is strong, theoretical arguments, laboratory work, and some field studies

have suggested the potential for co-limitation or even proximal limitation of phytoplankton by another nutrient in some regions of the ocean. Our results provide tentative additional support to this hypothesis, meriting further field-based studies.

Given the array of biogeochemical implications of Fe stress, the ability to map such regions using remote sensing would represent a particularly useful advance in marine biogeochemistry. Theoretically it may be possible to map Fe stress from space using satellite images of chlorophyll fluorescence, yet there are important uncertainties that need to be addressed before this can be carried out. In particular, a better understanding of the midday Non-Photochemical Quenching (NPQ) driven reductions in chlorophyll fluorescence occurring at the time satellite images are captured is required. If, for example, different phytoplankton communities showed relatively different amounts of NPQ, this variability would need to be corrected for prior to the signal being used to infer anything about potential Fe stress. Analysis and discussion of how the extensive field dataset generated over three research cruises, including more than 200 NPQ experiments, has allowed us to explore NPQ and its relevance for using Sunlight Induced Chlorophyll Fluorescence (SICF) to assess broad patterns of Fe stress. Our experiments suggested the light regime a phytoplankton community inhabited controlled its NPQ characteristics, with dynamic light regimes accompanying a more vigorous mixing of phytoplankton throughout the water column appearing to increase NPQ. Empirically, a good correlation was found between sea surface temperature and the relative amount of NPQ being expressed, providing a method for dynamically correcting satellite fluorescence signals for NPQ. Our results confirmed that satellite fluorescence quantum yields have the potential to reveal broad regions of Fe stress however the dynamic NPQ correction developed was necessary to achieve this.

Acknowledgements

Firstly I would like to thank my supervisors Heather Bouman, Gideon Henderson and Mark Moore for giving me plenty of opportunity for taking my projects in the directions they ended up going in and for the continued advice, assistance, and resources throughout the past three and a half years. Thanks also to my thesis examiners, Ros Rickaby and Richard Geider, for interesting discussion during the viva and for helpful comments which improved this thesis.

Thanks also to: Alan Hsieh, Tristan Horner, Alex Thomas, Phil Holdship, Steve Wyatt, Thomas Jackson, Elaine Sherrott, and Yasuko Nakajima from the Earth Sciences department in Oxford for their help with either running samples, learning new methods, or sorting out admin for me. Christian Utschig for his help in running the phytoplankton absorption spectra during his summer in Oxford. OceanBUG and Climotope group members for the regular science meetings and pub trips. Tamsin Mather and David Pyle for their assistance and enthusiasm in the volcanic ash fertilisation project. From PML Glen Tarran for his thorough instruction on running flow cytometry samples, Malcolm Woodward for fast and reliable nutrient data and good times on cruises and science meetings, and Trevor Platt and Shubha Sathyendranath for inviting me to the INDO-MARECLIM conference in Kerala. From NOCS, Tommy Ryan-Keogh for sharing his bioassay experiment expertise, Christian Schlosser for trace-metal measurements and discussions, and Duncan Purdie and John Gittens for their assistance with the HPLC system. Fellow GEOTRACERS Bjorn, Alan, Alex, Rosin, Will, Robyn, Matt, Debbie and everyone else involved - especially Maeve Lohan and Angie Milne for their help and advice with everything to do with trace metals. From the DIMES cruise Andrew Watson and Alberto Naveira Garabato for welcoming us to participate, and Katie Sheen, Alex Brearley, Neill Mackay, and Ben Mills amongst others for making it a fun cruise to be on. Brian King and Ed Mawji for their assistance with supplying shipboard data. Finally thanks to the captains, crew and NMF technicians on the three cruises - particularly Paul, Richie and Steve for invaluable assistance with the trace-metal-clean towed-fish on the DIMES cruise.

NERC, the UK-GEOTRACES consortium and Burdett Coutts are acknowledged for funding this opportunity and St Anne’s College for the facilities they have provided.

Finally, for good times whilst at Oxford: JP, Dan, Dom, Shaun, Alex, Lucien, Harry, Ana, Michael, John H., Johnny, both Jonny’s, Connor, Chelsea, Colin, and my family - thanks!

Contents

List of Figures

List of Tables

1 Introduction

PHYTOPLANKTON are free floating single celled photosynthetic microbial organisms. Phytoplankton photosynthesis couples the cycling of carbon and other elements through the atmosphere, ocean and geosphere, and as such is a fundamental component of the Earth System (Kump et al., 1999; Sarmiento and Gruber, 2006). It has been clearly shown that marine primary productivity has significant climatological (e.g. Falkowski et al., 1998), and ecological (e.g. Duffy and Stachowicz, 2006) importance, and therefore advancing our understanding in this field has been identified as a key goal of global change research (Falkowski et al., 2000). Phytoplankton are estimated to contribute around 50 Pg of organic carbon to annual global net primary production (Field et al., 1998), which is the carbon fixed through photosynthesis and made available to higher trophic levels. This represents around half of the total value for the global biosphere (Field et al., 1998). Around a third of this carbon is transported to the deep ocean interior (Falkowski et al., 1998), thus making marine primary productivity an important contributor to the oceanographic regulation of atmospheric pCO_2 (Volk and Hoffert, 1985; Takahashi et al., 2002).

This chapter introduces the concept of nutrient limitation of marine phytoplankton and some basic aspects of photosynthesis and chlorophyll fluorescence theory to familiarise the reader with some understanding assumed in subsequent chapters. The study regions focussed on in this thesis are also briefly described. Full details are not given where they are either unnecessary for, or are sufficiently introduced in, subsequent chapters. The chapter concludes with a brief statement of research objectives outlining research presented in Chapters 2 to 5.

1.1 Nutrient limitation in the ocean

Factors that regulate the total biomass, community structure, and physiological status of phytoplankton are of great importance for understanding global biogeochemical cycles (e.g. Falkowski, 1994). Identifying and understanding these factors is essential for further advancing the field of global phytoplankton dynamics (Falkowski, 1994; Moore et al., 2013; Le Quéré et al., 2005). One critical controlling factor is the availability of nutrients in the surface ocean where phytoplankton live (Moore et al., 2013). Phytoplankton are made up of 30 or so naturally occurring elements which they must obtain in some chemical form from their external environment (Sterner and Elser, 2002). Therefore if at sufficiently low concentration in the upper ocean, one or more of these nutrients may limit the abundance and functionality of phytoplankton (i.e. phytoplankton are said to be 'nutrient limited', with the physiological expression of this nutrient limitation often being referred to as 'nutrient stress' – see Box 1). Furthermore, the condition of limited nutrient availability can lead to shifts in phytoplankton community structure towards the dominance of species that have a physiological advantage (Falkowski and Oliver, 2007). Alongside regulation of community structure, nutrient availability may also select for intra-specific physiological characteristics which allow for survival and growth in a particular nutrient regime (e.g. Cullen, 1992; Follows and Dutkiewicz, 2011).

Feedback mechanisms between phytoplankton evolution and their growth environment have been crucial in developing modern day ocean biogeochemistry (e.g. Morel et al., 2008; Williams and Rickaby, 2012). For example, a central theme of this thesis is the consideration of iron (Fe) limitation of phytoplankton, which is thought to exist across a significant areal extent of the modern ocean (De Baar et al., 2005; Boyd et al., 2007). Life evolved around 4 billion years ago in a heavily reducing (i.e. low oxygen) Achaean

ocean (Canfield, 1998). As Fe was readily available in its soluble Fe (II) form, organisms incorporated Fe into cellular components to mediate redox reactions. The evolution of a pair of photosystems 0.5 to 1.5 billion years later that used water as an electron donor, and generated O_2 in the process, led to relatively rapid oxygenation of the oceans (Barber, 2008). This radically reduced the availability of soluble, bioavailable Fe (II), as upon oxygenation Fe (III) rapidly precipitates out of solution.

Box 1: Nutrient limitation terms and concepts (adapted from Moore et al., 2013 and Cullen et al., 1991)

Limitation: a general term that encompasses restriction of the standing stock of phytoplankton or the growth rate of phytoplankton.

Nutrient stress: the physiological expression of nutrient limitation. Note that it is possible for phytoplankton to be limited by a nutrient but show limited detectible physiological responses to the limitation.

Blackman and Liebig limitation: two conceptual forms of nutrient limitation in plants. Liebig limitation refers to limitation of the amount of biomass that can be synthesised whilst Blackman limitation refers to the limitation of cellular growth rates.

Steady state versus starvation: steady state nutrient limitation refers to a condition of unchanging phytoplankton growth rates over time (achievable even when the overall standing stock of phytoplankton is restricted by nutrient availability), whilst starvation indicates a declining growth rate.

Proximal versus co-limitation: proximal limitation refers to a single factor which is limiting phytoplankton, without which an increase in growth rate or standing stock cannot be stimulated. Co-limitation refers to a condition where two or more abiotic factors are limiting phytoplankton. With regards to nutrient co-limitation this would be ascribed to a condition where two or more nutrients are simultaneously drawn down to levels where addition of both of these is required to stimulate growth. The term (co)limitation will hereafter be taken to refer to a condition where there is uncertainty if an abiotic factor is proximally or co-limiting.

The global distribution of nutrients in the modern ocean is regulated by a complex interplay between ocean physics, chemistry and biology. Ocean currents transport nutrients and are a fundamental control on resultant distributions of nutrients in the ocean. Water movement in the ocean is driven by atmospheric circulation (and therefore, amongst other drivers, solar heating, the Coriolis effect), changes in buoyancy (as a result

of changes in temperature or the freshwater balance), and physical barriers to motion (continental crust and seafloor bathymetry). Phytoplankton themselves exert a strong control on the nutrient distribution in the ocean. Phytoplankton photosynthesis requires light, therefore incorporation of nutrients into organic material during phytoplankton growth is restricted to a relatively thin (always less than a few hundred metres) illuminated layer at the surface of the ocean. The light field in this layer is controlled by the incident irradiance flux at the surface, transfer across the air-sea interface, and absorption or scattering in the water column by silt, phytoplankton, dissolved organic matter, and by water itself (Kirk, 1994). In a more complex interplay of processes, light absorbed by phytoplankton over some integrated time period is also controlled by the rate and depth of wind driven surface mixing of the water column which can transport phytoplankton through a steep light gradient on a timescale of hours to days (Kirk, 1994; Falkowski and Raven, 1997; Sathyendranath and Platt, 1988).

As available light is used by phytoplankton in photosynthesis, and nutrients are incorporated into organic matter, phytoplankton material can sink though the water column, either as whole, parts, or aggregations of cells or as faecal pellets from heterotrophic zooplankton. Respiring bacteria can consume this organic matter and release 'remineralised' nutrients that can be re-used by phytoplankton in an efficient cyclical process (Karl, 2002). If sinking phytoplankton material escapes remineralisation and sinks below depths where there is mixing to the surface, this material is said to be exported (Eppley and Peterson, 1979). Such export of organic material is termed the 'biological pump' and is important for regulating carbon and nutrient transfer from the surface ocean to deeper waters (Volk and Hoffert, 1985). An important regulatory factor with regards to rapid near-surface remineralisation versus successful sinking and export is phytoplankton or zooplankton faecal pellet size – larger particles, which sink faster and

are more resilient to grazing or remineralisation, are more efficiently exported. Consequently, in the high latitude regions export production is lower (up to ~50% of total carbon fixed) than in subtropical gyre regions of the central ocean basins (~5-10%), as a result of generally larger phytoplankton cell sizes and less efficient near-surface recycling of organic matter. Nutrients transported to greater depths via this export process enrich deep waters with nutrients and upwelling of these waters to the surface, which occurs in certain regions of the oceans, can supply nutrients to the photic zone and enhance primary productivity. If sinking organic material reaches the seafloor and accumulates, the nutrients in this material may be released into the bottom boundary layer and can potentially be mixed to the surface (Elrod et al., 2004), or could be buried to form sedimentary rock formations which may not have contact with the ocean for millions of years before re-exposure after tectonic uplift or sea level fall and subsequent weathering.

Added complexity to the system emerges when considering the different nutrients required by phytoplankton and how their biological requirements and chemical nature alter limitation patterns in the ocean. For example there is a biological requirement for magnesium (Mg), sulphur (S), potassium (K), and calcium (Ca), yet the elevated concentrations and long residence times (millions of years) of these elements in the oceans prevents them from ever reaching limiting levels (note that for a steady state system, the residence time of an element is dictated by the ratio of the flux in or out of the ocean to the total inventory of the element in the ocean). On the other hand cobalt (Co) also has a biological function (Saito et al., 2002; Price and Morel, 1990), and a very short residence time of around 300 years (Broecker and Peng, 1982), yet has never directly been shown to be limiting phytoplankton growth in the ocean. This is likely a result of the low absolute requirement of the element, coupled with the zinc (Zn) or

cadmium (Cd) substitution that can occur to carry out many of the same functions (Morel et al., 2003).

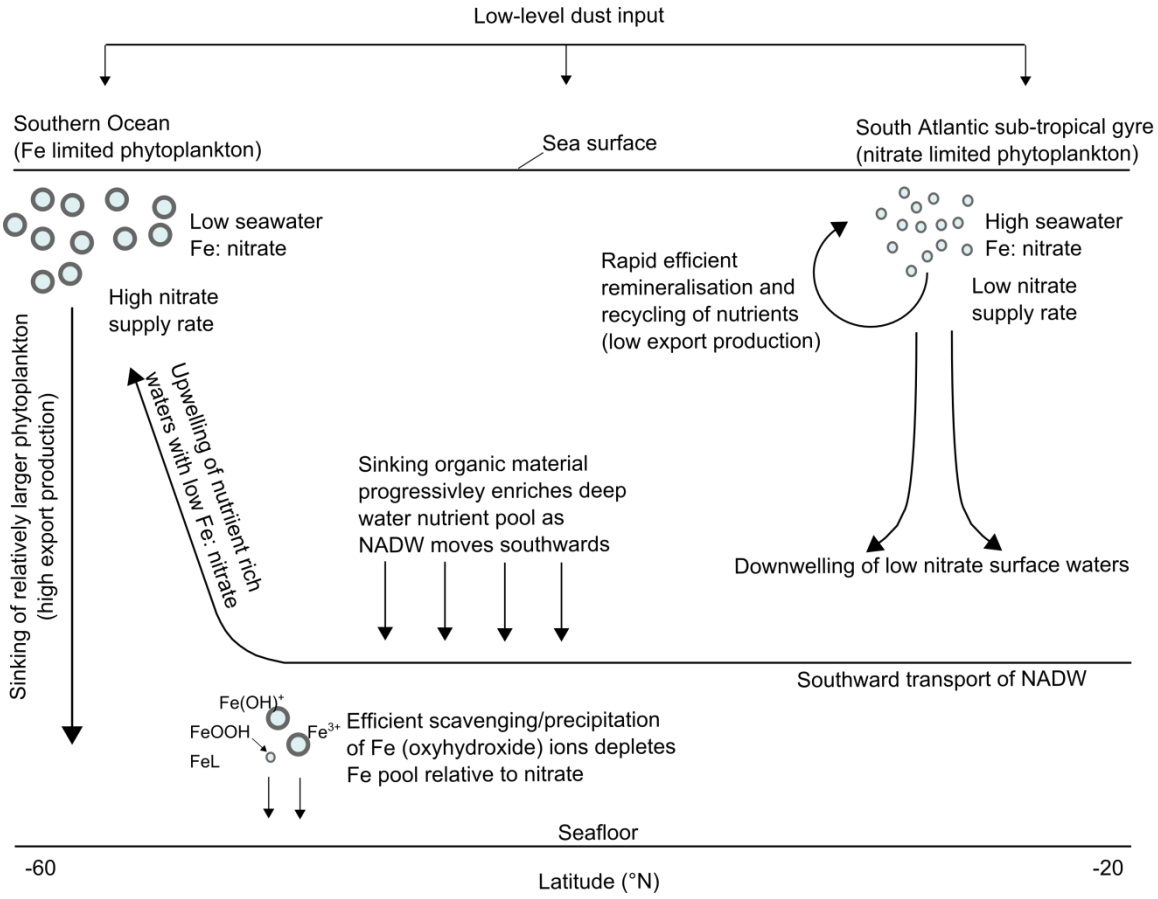

Figure 1.1: Conceptual development of broad scale nutrient limitation patterns in the South Atlantic and Southern Ocean. Filled circles represent relative phytoplankton particle size. Downward arrows represent particle sinking and export. Circular arrows represent organic matter remineralisation and nutrient recycling. Two example particle reactive Fe ions are given that are readily scavenged onto sinking particles. Fe can also precipitate out of solution (e.g. FeOOH), although this is regulated by binding to organic ligands, for which the structure can be highly variable (here simply denoted as FeL).

Identifying a particular limiting nutrient or group of co-limiting nutrients (two or more simultaneously limiting nutrients – see Box 1) in the ocean has proved difficult (Cullen et al., 1992; Saito et al., 2008), yet the ability to carry this out has improved markedly in the last few decades (Moore et al., 2013). Methods attempting to do this typically involve adding an element or group of elements to a phytoplankton sample and then observing the phytoplankton response over a particular time interval relative to a control (i.e. non-

amended) sample. Most often this is conducted in bottles and various 'bottle effects' (drivers imposed on phytoplankton that are not representative of their natural environment, for example contamination with toxic metals) can limit the ability of the results to unambiguously identify a limiting nutrient (Cullen et al., 1992). A classic example is that of early bottle experiments investigating Fe limitation in the ocean. Until recently, methods used to collect and incubate samples in bottle experiments were inadequate for maintaining unaltered trace metal conditions in control bottles (Huntsman and Sunda, 1980). For example, rubber seals on bottle caps would release Fe in the control (non-amended) bottles, provoking a similar response from phytoplankton in these bottles to those with purposeful Fe addition. It was not until the development of effective trace-metal-clean techniques that the results of such experiments demonstrated evidence for some degree of Fe limitation in regions of the oceans (Martin and Fitzwater, 1988). Similarly, identifying subtle variability in co-limitation patterns has proven difficult to assess as a result of the significant effort in conducting and interpreting a matrix of simultaneous incubations spiked with various concoctions of the elements thought to be potentially co-limiting (Saito et al. 2008, Moore et al., 2013).

Despite this array of complexity some clear broad-scale patterns of nutrient limitation have been observed in the ocean, which, at least conceptually, are relatively easily explained (Figure 1.1). Deep upwelling waters such as those found in the Southern Ocean, the Northern and Equatorial Pacific, and coastal regions associated with eastern boundary currents (e.g., Californian and Peruvian upwelling systems) bring with them Fe: nitrate ratios that are lower than phytoplankton requirements (Moore et al., 2006; Hutchins et al., 1998; Parekh et al., 2005; Ito et al., 2005). The reason for this is that nitrate is less particle reactive than Fe and is scavenged less efficiently by sinking particles (Johnson et al., 1997; Boyd and Ellwood, 2010). A result of this is that

phytoplankton growth depletes Fe, before nitrate, to levels that can set an upper limit on the phytoplankton standing stock. A number of mesoscale (i.e., km scale) experiments observing phytoplankton stimulation (i.e., an increase in phytoplankton biomass) following purposeful Fe addition to these waters have generated considerable evidence to support this (Boyd et al., 2007) (most notably, this experimental design eliminates any of the bottle effects discussed previously). Conversely, in the sub-tropical gyres of the world's oceans, deep water (i.e., high nitrate) upwelling is absent, thus nitrate resupply rate is low and nitrate concentrations are drawn down to levels that limit the standing crop of phytoplankton (Dugdale and Goering, 1967; Ryther and Dunstan, 1971; Eppley et al., 1979). Rapid efficient cycling of organic matter (i.e. phytoplankton growth, sinking, remineralisation, upward mixing) has been suggested to result in a low but continuous supply of nitrate to phytoplankton that maintains a limited standing crop (e.g., Karl et al., 2002; Moore et al., 2008). As a result of the low macronutrient concentrations setting a limit on the total phytoplankton crop that can be supported, relatively small supplies of Fe, for example from aeolian dust, together with ecosystem recycling can be sufficient to fulfil phytoplankton community requirements for this element in these regions.

1.2 Photosynthesis and chlorophyll fluorescence

1.2.1 Light reactions of photosynthesis

It is the aim of this thesis to add detail to some of the concepts of nutrient limitation introduced above. Critical to achieving this has been the use of a tool that has become fundamental to this area of research, chlorophyll fluorescence, which requires some basic level of understanding before the reader considers the work in the subsequent chapters. Nutrient limitation and chlorophyll fluorescence is closely coupled to photosynthesis and

so a brief outline of the key mechanisms and components involved in this process is given first. In the following section the focus is the 'light reactions' of photosynthesis (Equation 1.1), those reactions leading to the generation of protons and electrons from the 'splitting' of water:

$$2H_2O + light \xrightarrow{chlorophyll-a} 4H^+ + 4e^- + O_2 \quad \textbf{(1.1)}$$

where chlorophyll-a is the ubiquitous light harvesting pigment in plants, and light has been denoted as a substrate (i.e., some of the energy of the absorbed light is stored in the products). These protons and electrons are subsequently used in the synthesis of energy storage molecules - adenosine triphosphate (ATP), and reductant – most notably, nicotinamide adenine dinucleotide phosphate hydrogen (NADPH).

Downstream utilisation of these products in the carbon fixation reactions requires no light and hence these are termed the 'dark reactions'. The dark reactions are not described in detail here because they are not immediately involved in chlorophyll-a fluorescence emission, and because of the relatively low quotas of components involved in these reactions for the potentially limiting nutrients discussed in Chapters 2-5. In their simplest sense the light reactions of photosynthesis represent a flow of electrons driven by energy from incident photons. A critical by-product of this electron transport is the generation of a proton (pH) gradient across the thylakoid membrane that allows for ATP production via ATP synthase. Electrons and protons sourced from these reactions restore $NADP^+$ to NADPH, whereon it can be used once again as a supply of electrons and protons for the fixation of CO_2 in the dark reactions of photosynthesis. The process requires two types of functional centres located within the thylakoid membrane of chloroplasts: light harvesting complexes (LHC's), where photons are absorbed and their energy transferred by pigment-protein complexes, and reaction centres (RC's), where this

light energy is converted to photochemical energy. Electron passage through the components involved in the photosynthetic light reactions can be conceptually described by the Z-scheme. The components and processes of this scheme are illustrated and explained in Figure 1.2. Electron transport and ATP generation in the thylakoid membrane is, however, not limited to this suite of reactions: ATP can also be generated (in the absence of NADPH generation) via the light-dependant cycling of electrons around PSI (Arnon et al., 1965), the Mehler reactions (via reduction of O_2 generated by water splitting to form H_2O), or via midstream oxidases (MOXs). Collectively, these ATP and NADPH synthesis mechanisms act to balance cellular ATP/NADPH supply and demand (Falkowski and Raven, 1997; Behrenfeld et al., 2008).

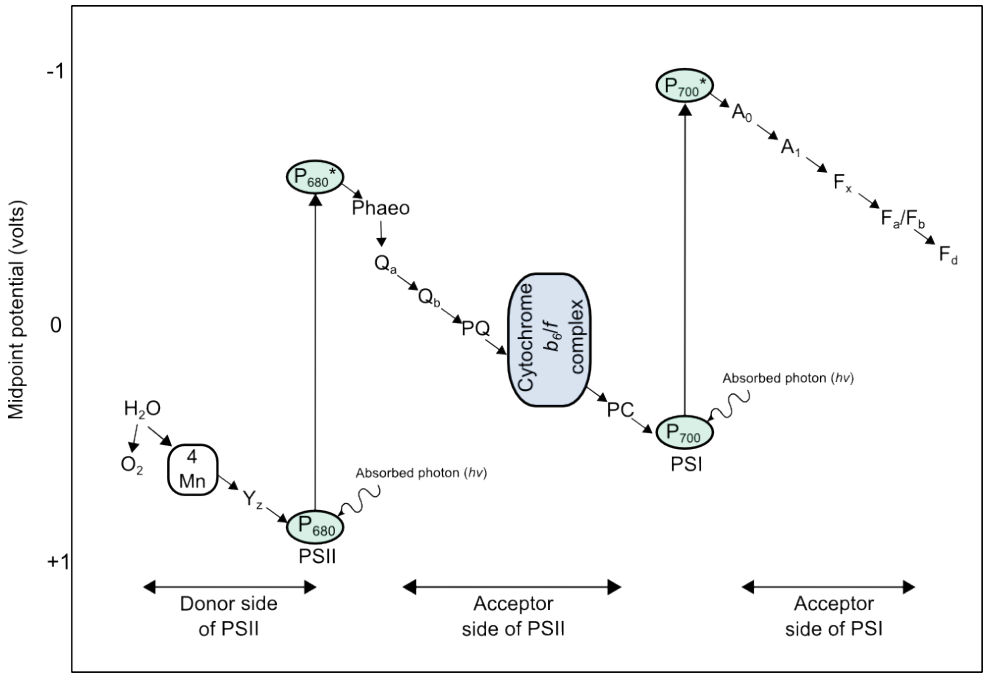

Figure 1.2: The Z-scheme of the light reactions of photosynthesis, which conceptualises electron flow through the light reactions of photosynthesis (adapted from Falkowski and Raven, 1997). The relative midpoint potential of photosynthetic electron carriers is indicated by their vertical positioning in the figure (a midpoint potential is measure of the tendency of a compound to take electrons from another compound, i.e., a large negative value indicates the compound is a strong reductant). A chlorophyll-a molecule in PSII (P_{680}) absorbs an incident photon, either directly or via a cascade of energy transfer though light harvesting/transfer pigments. The energy from this absorbed photon excites an electron in the P_{680} molecule into an excited state: P_{680}^*. To fill the electron hole in P_{680}^* an electron is 'drawn' from a cluster of 4 Mn atoms via the amino acid Tyrosine (Y_z) which originates from the oxidation of H_2O (often referred to as 'water

splitting'). In the process of this O_2 is evolved (requiring the liberation of 4 electrons from H_2O per generation of one O_2 molecule). The reactions leading to P_{680}^* re-reduction from H_2O are referred to as being on the 'donor side' of PSII. Meanwhile, the electron in an excited state in P_{680}^* can be transferred via the formation of a reduced phaeophytin (phaeo) anion intermediate to plastoquinone-a (Q_a) (a quinine bound to a protein) and then to plastoquinone-b (Q_b). Q_b dissociates from its binding site diffuses into the thylakoid membrane (becoming part of the PQ pool). Q_b diffuses across the thylakoid membrane until it reaches and reduces the cytochrome b_6/f complex. The absorption of a second photon by the PSI reaction centre chlorophyll molecule, P_{700}, excites an electron of this chlorophyll molecule into a higher energy level, and the electron residing in cytochrome b_6/f can be transferred via plastocyanin (PC) to this molecule to fill its electron hole. Reactions between phaeophytin and P_{700} are referred to as being on the 'acceptor side' of PSII. The previously excited electron from P_{700} is transferred down a cascade of electron carriers (A_o: a chlorophyll monomer; A_1: phylloquinone; F_x: an iron sulphur complex; F_A/F_B: iron-containing proteins; F_d: ferredoxin molecule), eventually going on to reduce $NADP^+$.

1.2.2 Chlorophyll fluorescence

Chlorophyll fluorescence is the emission of red light from chlorophyll-a molecules subsequent to absorption of actinic light (Falkowski and Kiefer, 1985) ('actinic' light refers to photosynthetically active light termed photosynthetically available radiation (PAR) which is the 400-700 nm electromagnetic radiation length range). Specifically, this fluorescence is a result the energy dissipation accompanying the electron transition from an excited to lower energy state. Under non-stressed conditions fluorescence emanates from P_{680} chlorophyll molecules in PSII and is regulated on the basis of the energy pathway of absorbed photons (Figure 1.3). This energy pathway is itself a function of reaction centre state: if Q_a is in reduced state and is incapable of accepting an electron from P_{680}^*, the energy of the previously absorbed photon is reemitted as fluorescence (Duysens and Sweers, 1963). Ultimately, utilisation rates of ATP and NADPH in the dark reactions and/or other cellular processes set an upper limit on the rate the light reactions of photosynthesis proceed, and when light absorption exceeds utilisation, excess photon energy must be dissipated if it is not to cause cell damage (termed 'photoinhibition' or 'photodamage'). Phytoplankton have evolved several mechanisms to do this, which principally result in dissipating excess absorbed light energy as heat. These mechanisms are collectively termed non-photochemical quenching

(NPQ) as a result of them reducing (quenching) fluorescence emission in a non-photochemical manner (i.e. as heat) (Krause and Weis, 1991; Müller et al., 2001).

1.2.3 Active fluorescence measurements

For a given incident excitation irradiance, the *in vivo* chlorophyll fluorescence flux emanating from a sample is closely related to the quantity of chlorophyll-a present; therefore absolute levels of actively stimulated florescence (i.e., using a light flash within the PAR wavelengths – most instrumentation uses blue light) are used routinely in oceanographic work for estimation of chlorophyll-a concentrations (Lorenzen, 1966). Because of NPQ mechanisms that fluctuate in magnitude throughout the day, alongside a host of other potential controls, such a relationship is an oversimplification and leads to errors in derived concentrations (but is often used nevertheless; note that this is not the case for *in vitro* fluorescence measured on chlorophyll extracted in a solvent). As understanding of fluorescence in photosystems improved (e.g., Malkin and Kok, 1966; Mauzerall, 1972; Falkowski et al., 1986), methodologies were developed in attempt to extract physiological information from detected fluorescence signals. For example a conceptually simple methodology, termed pump-and-probe fluorometry (Figure 1.4), involves illuminating a phytoplankton sample previously acclimated (i.e., given time to adjust physiologically to its environment) in the dark (to 'relax' reaction centres – see Figure 1.2) with a sub-saturating ('probe') light flash, giving a minimum fluorescence value, F_o, representing fluorescence with most reaction centres in an open state and a high proportion of photon energy utilisation for photochemistry (Mauzerall, 1972). After a short time period (10-100 μs) the sample is then exposed to a heavy light dose ('pump' flash), closing all reaction centres (i.e. all reaction centres are 'occupied' processing the energy of absorbed photons). This is then shortly followed by another probing light flash which gives a maximal fluorescence value, F_m. From these simple measurements, and

knowing that absorbed photon energy can only have one of three fates in the photosystem (Figure 1.3), a parameter theoretically representing a maximal photochemical efficiency of PSII (i.e., the probability of PSII reaction centres using available excitation energy for photochemistry) can be generated, termed F_v/F_m (Eq. 1.2):

$$\phi_p = \frac{k_p}{(k_f + k_p + k_d)} = \frac{(\phi F_m - \phi F_o)}{\phi F_m} = \frac{(F_m - F_o)}{F_m} = \frac{F_v}{F_m} \quad \textbf{(1.2)}$$

where

$$\phi F_o = \frac{k_f}{(k_f + k_p + k_d)}, \text{ and} \quad \textbf{(1.3)}$$

$$\phi F_m = \frac{k_f}{(k_f + k_d)} \quad \textbf{(1.4)}$$

(all notation is defined in the text or in Figure 1.3).

A significant advance in chlorophyll fluorescence methodology was the development of Fast Repetition Rate fluorometry (FRRf) (Kolber et al., 1998), which built upon advances of the pump-and-probe method (Falkowski et al., 1986). Instead of pump and probe flashes, this method employs a series of rapid blue light flashes ('flashlets') incident on a sample, which individually are sub-saturating: all reaction centres do not close with each light flash. However, the progression of the flash sequence leads to a gradual increase in fluorescence as reaction centres gradually close (i.e. there is insufficient time between flashes for reaction centres to relax back to F_o), and a plateau in fluorescence when all reaction centres are eventually closed (Figure 1.5). The fluorescence transient (f) at time t, can then be fitted to the following biophysical model (Kolber et al., 1998):

$$f(t) = F_o + (F_m - F_o)\left[C(t)\frac{1-p}{1-C(t)p}\right] \quad \textbf{(1.5)}$$

where p is a connectivity parameter (i.e. the degree of sharing of absorbed photon energy between reaction centres), and the fraction of closed reaction centres ($C(t)$) can be determined using:

$$\frac{dC(t)}{dt} = i(t)\sigma_{PSII}\frac{1-C(t)}{1-C(t)p} - \frac{C(t)}{\tau_{Qa}} \quad \textbf{(1.6)}$$

where i(t) is the flash intensity (Kolber et al., 1998), σ_{PSII} is the functional absorption cross section of PSII, and τ_{Qa} is the time for electron transport between Q_a and Q_b (see text below).

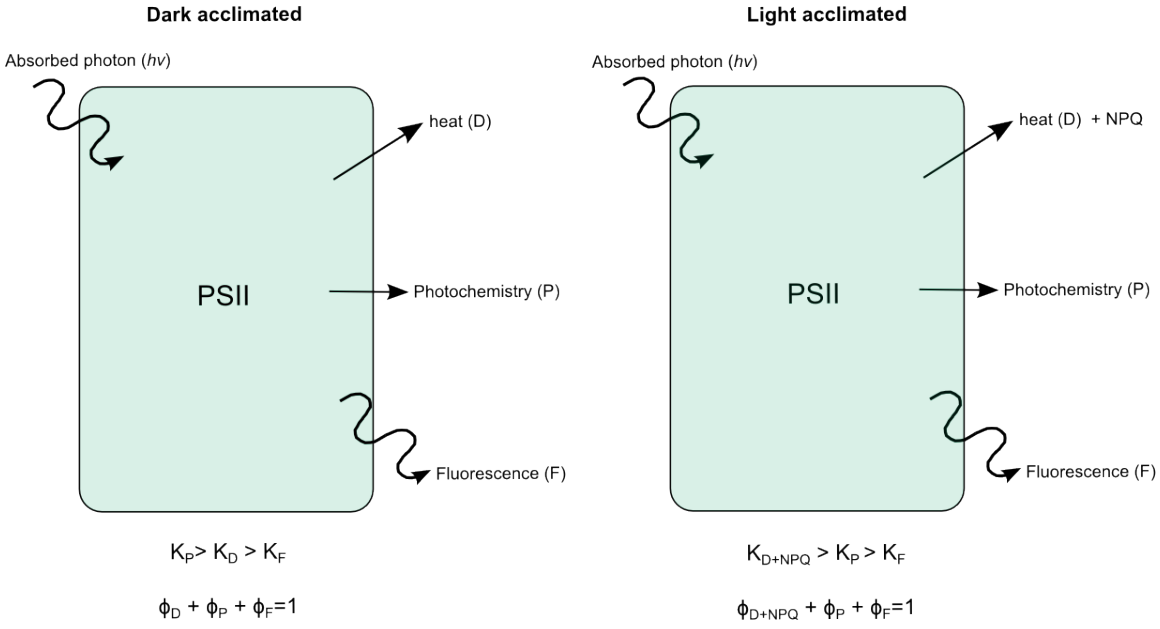

Figure 1.3: Energetic fate of a photon absorbed by photosystem II. The energy of an absorbed photon can either be directed towards photochemistry (P) (i.e., ATP and NADPH synthesis), lost as heat (D), or reemitted as fluorescence (F). Non-photochemical quenching (NPQ) represents a reduction in the proportion of energy directed towards fluorescence, which is not due to an increase in the proportion directed towards photochemistry. Theoretically NPQ only occurs under conditions of incident irradiance (i.e., in a non-dark acclimated sample). The respective rate constants (k) and yields (ϕ) of each process depends upon reaction centre state (see main text).

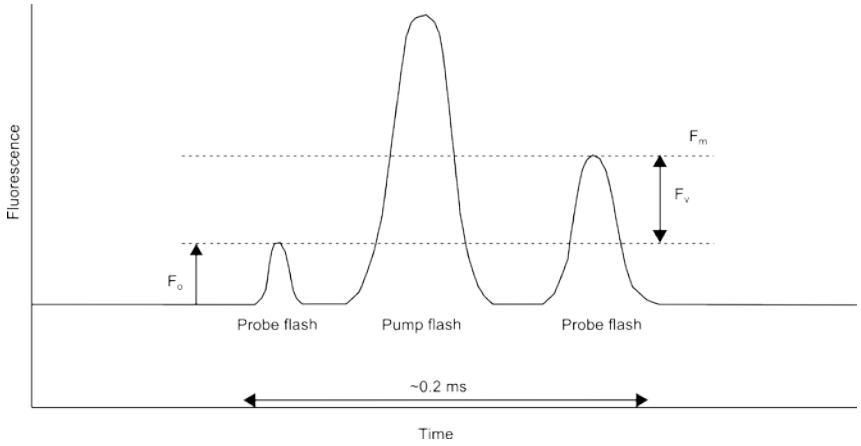

Figure 1.4: Schematic representation of the pump and probe methodology and determination of F_v/F_m.

Maximal fluorescence (F_m) is determined from the plateaux of the curve fit, and as for pump-and-probe fluorometry, a value of F_v/F_m obtained. Crucially, this protocol additionally provides a rapid measurement of effective PSII size, σ_{PSII} (Kolber et al., 1998). Values of σ_{PSII} characterise the gradient of the fluorescence rise from F_o to F_m: a rapid rise indicates larger and/or more efficient LHC's per associated RCII transporting absorbed photon energy to the RCII. Note that although σ_{PSII} is given units of area, it is not actually measured physically – it is the inferred probability of photon absorption and transfer to RCII based on the fluorescence response (Falkowski and Raven, 1997). Measurements of σ_{PSII} are interesting for understanding environmental or genetic regulation of PSII size (e.g. Behrenfeld et al., 2006; Suggett et al., 2009; Strzepek et al., 2012), but also have the advantage of allowing rapid quantification of RCII light absorption by phytoplankton, which coupled with photochemical efficiencies from F_v/F_m and incident light intensities, allow for direct estimation of the electron transport rate (ETR) through RCII (Suggett et al., 2011).

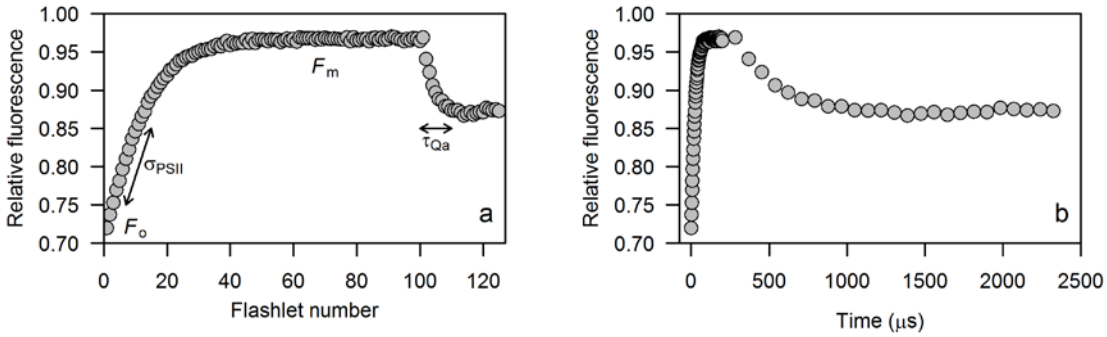

Figure 1.5: Fast Repetition Rate fluorometry (FRRf)-derived fluorescence transient, with respect to (a) flashlet, and (b) time, for an example Southern Ocean sample. F_o = minimum fluorescence estimated by extrapolating from the fluorescence retrieved in the first flashlet back to the y-axis. F_m = maximum fluorescence. σ_{PSII} = functional absorption cross section of PSII, effectively corresponding to the initial gradient of the fluorescence transient. The reduction in fluorescence at flashlets > 100 represents the relaxation of reaction centres as electrons are transferred downstream of Q_a towards Q_b and the PQ pool. This is achieved by increasing the time period between individual subsaturating flashes to 25 μs (b). The reciprocal of the estimated time for F_m to plateau at a fluorescence < F_m is thus referred to as the Q_a to Q_b electron transfer rate.

By conducting controlled manipulation of the light environment a phytoplankton sample is experiencing, alongside simultaneous FRRf measurements (a protocol collectively termed a 'rapid light curve' (RLC)), a relative ETR (rETR) versus irradiance curve can be generated (where the 'relative' term indicates ETR per RCII, rather than the total ETR through a cell or per unit biomass or seawater volume). Akin to conventional ^{14}C-derived carbon fixation versus irradiance curves (Steeman-Nielsen, 1952; Platt et al., 1980), these allow derivation of some parameters useful for understanding the physiological condition of phytoplankton (Figure 1.6). Maximal electron transport rates represent maximal rates of electron flow per RCII, where the number of incident absorbed photons is not a factor limiting rETR and thus rETR cannot be further enhanced by increasing incident PAR (Falkowski and Raven, 1997). The gradient in the region of the graph where incident light intensity is limiting (i.e., rETR is not maximal) is termed the light limed slope, α_{ETR}, which theoretically equates to σ_{PSII}, representing light absorption and delivery to RCs. The optimum light intensity, E_k, is equal to $rETR_{max}$ normalised to α_{ETR},

representing a theoretical 'optimal' irradiance for phytoplankton (Platt and Sathyendranath, 2007).

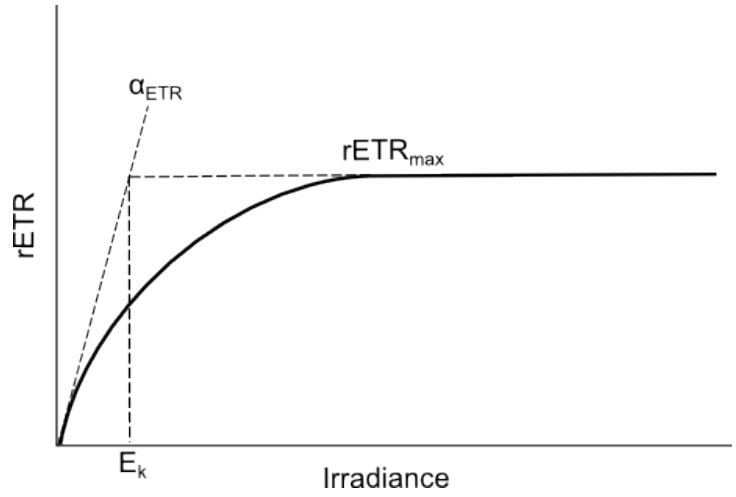

Figure 1.6: Relative electron transport rate (rETR) versus irradiance curve. $rETR_{max}$ represents the maximum electron transfer rate per RCII achievable at any irradiance. α_{ETR} represents the gradient of the initial slope, representing photon absorption and energy transfer capability of light harvesting pigments (effectively equating to σ_{PSII} in Figure 1.5). $E_k = rETR_{max}/\alpha_{ETR}$, and represents a theoretical 'optimum' irradiance.

Although not carried out within the current work, a subsequent step that could have been applied to rETR's presented in Chapters 2 and 3 of this thesis is multiplication of rETR by a term representing the number of RCII's per unit chlorophyll-a, to obtain a chlorophyll-specific ETR. Thus with this measurement, alongside simultaneous measurement of chlorophyll-a concentrations would have allowed for estimation of ETR (through RCII's) at the ecological level (Suggett et al., 2010). Further, this could then be multiplied by an estimate of the mass of carbon fixed per unit electron transport through RCII to yield a carbon fixation rate per unit irradiance. These subsequent terms are difficult to estimate, likely show significant variability between phytoplankton communities and growth regimes, and hence are currently rarely used for this purpose (e.g., Lawrenz et al., 2013).

In addition to estimation of rETR, RLC's can be used to evaluate how chlorophyll-a fluorescence reduces with an increase in incident irradiance – i.e., they can be used to estimate NPQ. Direct measurements of NPQ in the field are scarce (e.g., Morrison et al., 2003; Schallenberg et al., 2008), with new observations presented and discussed in detail in Chapter 5.

The final stage of the fluorescence transient in Figure 1.5 is a series of relaxation flashes. These flashes are identical to the excitation flashes yet are spaced further apart (25 µs compared to 1 µs in the saturation phase). The time take for F_m to relax back to a lower fluorescence plateau (τ_{Qa}) is theoretically inversely proportional to Q_a to Q_b electron transfer rates ($1/\tau_{Qa}$) and hence the re-reduction of P_{680}. Such rates can be controlled by re-oxidation rates of redox components further downstream (e.g. the PQ pool - Figure 1.2).

1.2.4 Sunlight induced chlorophyll fluorescence

Downwelling solar radiation stimulates chlorophyll-a fluorescence that is resolvable as a small but distinct peak in upwelling irradiance spectra (Kishino et al., 1984; Topliss, 1985), detectable from space by the moderate resolution imaging spectroradiometer (MODIS) and medium resolution imaging spectrometer (MERIS) sensors on earth orbiting satellites (Abbott and Letelier, 1999). This peak can be quantified by subtracting a baseline interpolated between irradiances retrieved within bands (i.e., channels where MODIS retrieves values of radiance) at two wavelengths on either side of the peak fluorescence band, generating a fluorescence line height (FLH) (Figure 1.7).

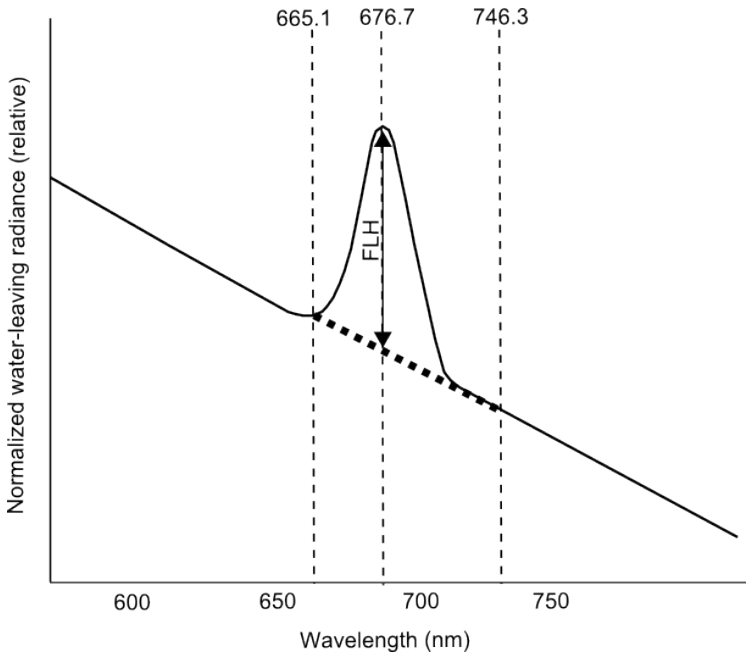

Figure 1.7: Geometric calculation of fluorescence line height (FLH) . A baseline (thick dashed line) is generated by interpolating between two bands (narrow vertical dashed lines) on either side of the chlorophyll-a fluorescence peak band (dashed line at 676.7 nm), and then subtracting this baseline from the fluorescence peak to yield a fluorescence line height (FLH) (note that a 676.7 nm channel was chosen for MODIS rather than the true chlorophyll-a fluorescence maximum at 685 nm due to interference with an oxygen absorption band around this wavelength).

FLH is primarily controlled by chlorophyll-a concentration (e.g. Huot et al., 2005; Behrenfeld et al., 2009), and therefore correlations between the two have been used in a number of studies to estimate chlorophyll-a concentration in 'case 2' waters where routine methods are hampered by heavy contamination with non-algal suspended particles and coloured dissolved substances (i.e. waters typically found in coastal regions) (e.g. Hu et al., 2005). Normalising FLH to satellite-detected chlorophyll (as estimated using a method other than fluorescence - e.g., O'Reilly, 2000), generates a parameter effectively corresponding to the fluorescence quantum yield - potentially revealing a signal related to phytoplankton physiological state (Abbott and Letelier, 1999; Letelier et al., 1997).

1.2.5 Chlorophyll fluorescence and nutrient limitation

An early use for measurements of maximum photochemical efficiency, F_v/F_m, was to identify regions of nutrient limited phytoplankton growth, with the premise that sub-optimal nutrient conditions would reduce values as reaction centre efficiency or functionality decreased (Geider et al., 1993a; Kolber et al., 1988, 1990). Early laboratory studies (Kolber et al., 1988; Geider et al., 1993b) and some field studies (Kolber et al., 1990, Geider et al., 1993a) supported this, however it has subsequently become evident that there is greater complexity in the parameter (Behrenfeld and Milligan 2013, Behrenfeld et al., 1996; Moore et al., 2008; Parkhill et al., 2001; Schrader et al, 2011; Suggett et al., 2009). High values of F_v/F_m, close to the theoretical maximum have been found in several field studies occupying oligotrophic waters, for which nutrient addition bioassay experiments have demonstrated the extant phytoplankton population to be limited by macronutrient availability (Behrenfeld et al., 2006; Moore et al., 2008). Similarly, high values of F_v/F_m have been found in laboratory studies where phytoplankton are grown under conditions where a nutrient is continuously supplied, but at rates low enough to regulate total phytoplankton biomass in the culture (termed 'steady state' nutrient limitation – see Box 1) (Parkhill et al., 2001; Schrader et al, 2011). An explanation for these findings is that macronutrient concentrations can be at levels limiting the total phytoplankton standing stock, but provided the phytoplankton are not starved of a nutrient, photosynthetic efficiency remains maximal (Cullen et al., 1991, Moore et al., 2008; Schrader et al., 2011; Behrenfeld and Milligan, 2013). Starvation of phytoplankton from any essential nutrient tends to result in decreased F_v/F_m as reaction centres are expected to become dysfunctional - as was observed in earlier laboratory studies (e.g. Kolber et al., 1988; Geider et al., 1993b).

Much greater uncertainty exists for the fluorescence response of phytoplankton living under variable severities of Fe deficiency (Behrenfeld and Milligan, 2013). Low F_v/F_m values are observed routinely in waters shown to be Fe limited, yet results differ for laboratory studies growing phytoplankton under steady state Fe limitation or Fe starvation (Peers and Price, 2004; Behrenfeld and Milligan, 2013). What is more conclusive is that several studies have found Fe stress responses in both steady state Fe-limited and Fe-starved phytoplankton cultures to include an increase in chlorophyll fluorescence by pigment complexes energetically 'uncoupled' to reaction centres (Behrenfeld et al., 2006; Schrader et al., 2011; Ryan-Keogh et al., 2012). Such 'disconnected' light harvesting complexes increase F_o and F_m and thus reduce F_v/F_m, and appear explain the widespread finding of depressed F_v/F_m values in Fe-limited waters.

Fe stress is not only reflected in FRRf measurements as depressed values of F_v/F_m. General trends of coincident elevated σ_{PSII} and a reduced Q_a to Q_b electron transfer rate ($1/\tau_{QA}$) have also been observed (Moore et al., 2007; Boyd and Abraham, 2001; Hutchins et al., 2002; Behrenfeld et al., 2006; Hopkinson et al., 2007). Elevated values of σ_{PSII} under Fe stress have been explained on the basis of more LHC's per reaction centre (e.g. Greene et al., 1992), as a result of the Fe requirement for LHCs being much lower than that of RC's (Raven, 1999; Behrenfeld and Milligan, 2013). Decreased $1/\tau_{Qa}$ is expected to be a result of the high Fe requirements for components downstream of PSII (cytochrome b_6/f; PSI) that result in a rapidly reduced PQ pool limiting upstream Q_a to Q_b electron flow rates (Greene et al., 1992; Moore et al., 2007). Similarly to F_v/F_m, measurements reflecting fluorescence quantum yields (i.e. the ratio of light fluoresced by chlorophyll to light absorbed, more often simply reported as measurements of F_o or F_m normalised to chlorophyll) have been observed to reflect Fe stress: elevated quantum

yields (i.e. more fluorescence per chlorophyll) are typically observed (Geider et al., 1993b; Sakshaug and Holm-Hansen, 1977; Schrader et al., 2011), although these can show greater variability than F_v/F_m, possibly dependant on relative levels of Fe stress (Greene et al., 1992). An improved understanding of fluorescence quantum yields have been identified as necessary for improving estimates of chlorophyll concentrations, or extracting physiological information, from solar-stimulated fluorescence detected by satellite sensors (Huot et al., 2005).

It is important to state clearly that, whilst used widely in studies assessing the nutrient stress status of phytoplankton, nutrients are only one of several controls on FRRf signatures. Recent studies have demonstrated an important control of the phytoplankton community structure signature on FRRf derived parameters (Moore et al., 2005, 2006; Suggett et al., 2004, 2009, Strzepek et al., 2012). Field and laboratory work have both revealed clear trends in physiological attributes of the phytoplankton community controlling values of F_v/F_m and σ_{PSII} when grown under nutrient replete conditions, and it has therefore been suggested that nutrient limitation signals could impose small scale variability on a signal largely regulated by phytoplankton community structure (Suggett et al., 2009). Similarly, the light environment phytoplankton are experiencing also reflects an important control on FRRf-derived parameter characteristics, with elevated incident irradiances inducing time-scale dependant NPQ photoprotective mechanisms alongside possible photodamage or PSII down regulation (Horton et al., 1996; Milligan et al., 2012; Behrenfeld et al., 1998). Such light induced changes in FRRf characteristics are strongly dependant on the conditions under which the measurement is made, and the particular FRRf parameter in question. It is with attention to these complex interactions that FRRf data in the following chapters is presented and interpreted.

1.3 Study regions and research cruises

The focus study regions of this thesis have been the South Atlantic and Scotia Sea-Drake Passage sector of the Southern Ocean (Figure 1.8). All three research cruises were conducted in the austral autumn-summer-spring period (it should be noted that as such there is an unavoidable seasonal bias in our field data). Each science chapter (Chapters 2-5) introduces the particular region in question in the context of the results being presented - this section provides only a brief introductory commentary of field work conducted. Two UK-GEOTRACES cruises (October-November 2010 and January 2012 respectably) occupied the bigeochemically dynamic Atlantic sector of the sub-Antarctic - subtropical gyre divide, termed the South Subtropical Convergence (SSTC). From a biogeochemical perspective, this region was chosen by the GEOTRACES planning workshop (http://www.bodc.ac.uk/geotraces/cruises/section_maps/atlantic_ocean/documents/geotraces_atlantic_report.pdf) as remote sensing images show this to be a zone of persistently elevated chlorophyll-a concentrations relative to waters to the north and south (Figure 1.8d), and constraining the sources and supply rates of micronutrients supporting this elevated phytoplankton standing stock was thus particularly pertinent to the objectives of the GEOTRACES programme (Henderson et al., 2007). This cruise transect enabled depth resolved sampling of two distinct biogeochemical provinces – cold, high macronutrient, sub-Antarctic waters, and warmer, macronutrient deplete, subtropical gyre type waters (Figure 1.8b-c) - for investigation of phytoplankton ecophysiology discussed in Chapters 2 and 5.

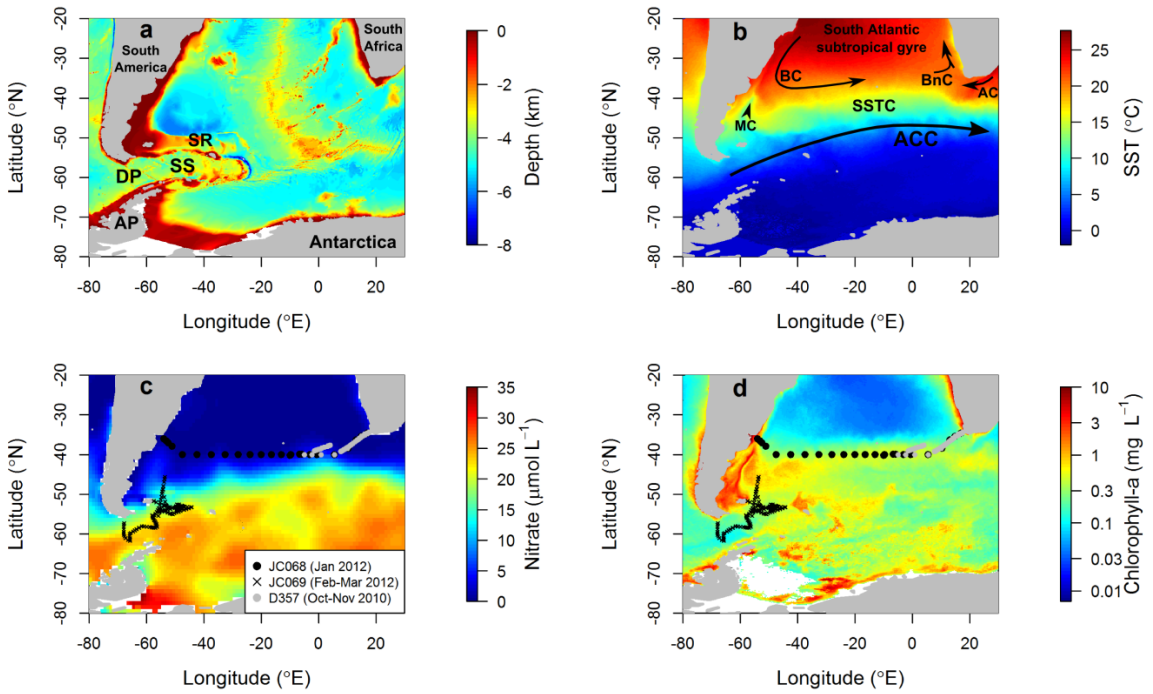

Figure 1.8: Oceanographic parameters for regions encountered on research cruises. (a) bathymetry; (b) MODIS 2012-2013 austral summer sea surface temperature (SST); (c) World Ocean Circulation Experiment (WOCE) austral summertime nitrate concentrations; (d) MODIS 2012-2013 austral summer surface chlorophyll-a concentrations. Some key geographic and oceanographic features are shown in (a) and (b) respectably; and sampling locations are shown in (c) and (d). DP = Drake Passage; SS = Scotia Sea; SR = Scotia Ridge; AP = Antarctic Peninsula; ACC = Antarctic Circumpolar Current; MC = Malvinas Current; BC = Brazil Current; BnC = Benguela Current; AC = Agulhas Current; SSTC = South Subtropical Convergence.

The Southern Ocean research cruise (February-March 2012) was a 'cruise of opportunity' where the cruise objective of the main scientific party was to characterise and quantify mixing in the Antarctic Circumpolar Current (ACC) through a region of dynamic bathymetry - part of the Diapycnal and Isopycnal Mixing Experiment (DIMES) programme (e.g., Watson et al., 2013; Sheen et al., 2013). A trace-metal-clean towed fish (a torpedo shaped instrument towed along the side of the ship, with water pumped on-ship via acid cleaned tubing and a diaphragm pump) was used on this cruise to collect surface seawater for the various phytoplankton measurements, nutrient concentrations and bioassay experiments discussed in Chapters 3-5. Similarly to the South Atlantic UK-GEOTRACES programmes, this oceanographic transect also occupied a

biogeochemcally dynamic transition zone, where phytoplankton depleted ACC waters in Drake Passage appear to interact with shallow bathymetry and coastlines surrounding the Scotia Sea to generate some of the largest phytoplankton blooms in the Southern Ocean - readily observable in remote sensing images (Figure 1.8a, d).

1.4 Thesis objectives

As mentioned previously, it is one of the aims of this thesis to add detail to a broad scale conceptual system of nitrate versus Fe limitation throughout the ocean. Firstly, the spatial resolution of experiments confirming the presence or absence of Fe or macronutrient limitation is low (Moore et al., 2013). Chapters 2 and 3 present bottle experiments at high spatial resolution that add detail to the subtle boundaries of nutrient limitation in our study regions and attempt to interpret observed patterns. Patterns of FRRf-derived parameters, physiological regulation of these parameters including community influences, and the environmental controls driving them are also analysed.

Given the fundamental role of Fe in regulating phytoplankton in large regions of the ocean, there has been much interest in constraining an Fe budget for the ocean together with investigating potential sources of Fe to the ocean (Fung et al., 2000; Henderson et al., 2007). One such source has had recent interest: erupted ash from volcanoes (Duggen et al., 2010). A number of studies have investigated the release of nutrients from ash (Jones and Gislason, 2008; Olgun et al., 2011, 2013; Censi et al., 2010), attempted to identify phytoplankton blooms subsequent to ash fall (Hamme et al., 2010), and investigated the response of phytoplankton to ash supply in the laboratory (Duggen et al., 2007; Hoffmann et al., 2012). Our field campaign mapping spatial patterns of nutrient limitation provided an ideal opportunity to answer important questions about ash driven fertilisation of marine phytoplankton. By conducting a number of ash-addition incubation

experiments alongside conventional Fe-only additions we found interesting results pertaining to ash delivery to HNLC regions. These results are presented and discussed in Chapter 4. Of particular interest was the evidence this provided for potential (co)limitation of phytoplankton in these waters by another essential trace metal nutrient. Although the evidence for widespread limitation of phytoplankton by either nitrate or Fe only is strong, theoretical arguments (e.g., Saito et al., 2008; Moore et al., 2013), laboratory studies (e.g., Morel et al., 1994; Peers and Price, 2004) and some field studies (e.g., Bertrand et al., 2007; Moore et al., 2006a; Crawford et al., 2003; Hutchins et al., 2001) have suggested the potential for co-limitation or even proximal limitation of phytoplankton by another nutrient in some regions of the ocean and our results provide an intriguing addition to this hypothesis.

Given the array of biogeochemical implications of Fe stress, the possibility of mapping such regions using remote sensing, which would dwarf even the largest of field campaigns, is an exciting possibility (Behrenfeld et al., 2009). The ability to do this confidently would allow monitoring of the location and extent of Fe-stressed regions on a global scale and thus would be an invaluable tool for biological oceanography, biogeochemical cycling, and monitoring environmental change (Behrenfeld et al., 2009; Cullen, 2009; Behrenfeld and Milligan 2013). Theoretically it may be possible to map Fe stress from space using satellite images of chlorophyll fluorescence (Behrenfeld et al., 2009), yet there are important uncertainties that need to be addressed before this can be carried out (Cullen, 2009). In particular, the NPQ-driven reductions in chlorophyll fluorescence at the time a satellite image is captured require a better understanding. If, for example, different phytoplankton populations showed relatively different amounts of NPQ, this variability would need to be corrected for before the signal could be used to infer anything about potential Fe stress. Chapter 5 presents analysis and discussion of

how the extensive field dataset generated on our cruises have allowed us to explore NPQ and its relevance for using SICF for assessing broad spatial patterns of Fe stress.

2 Nutrient Regimes Control Phytoplankton Ecophysiology in the South Atlantic

A reformatted version of this chapter was published as: *Browning, Bouman, Moore, Schlosser, Tarran, Woodward, & Henderson* (2014), Nutrient regimes control phytoplankton ecophysiology in the South Atlantic, *Biogeosciences*, 11, 463–479.

Abstract

Fast Repetition Rate fluorometry (FRRf) measurements of phytoplankton photophysiology from an across-basin South Atlantic cruise (as part of the GEOTRACES programme) characterised two dominant ecophysiological regimes that were interpreted on the basis of nutrient limitation. South of the South Subtropical Convergence (SSTC) in the northern sub-Antarctic sector of the Antarctic Circumpolar Current (ACC) in the Eastern Atlantic Basin, waters are characterised by elevated chlorophyll concentrations, a dominance by larger phytoplankton cells, and low apparent photochemical efficiency (F_v/F_m). Shipboard 24-hour iron (Fe) addition incubation experiments confirmed that Fe stress was primarily responsible for the low F_v/F_m, with Fe addition to these waters, either within the artificial bottle additions or naturally occurring downstream enrichment from Gough Island, significantly increasing F_v/F_m values. To the north of the SSTC at the southern boundary of the South Atlantic Gyre, phytoplankton are characterised by high values of F_v/F_m, which coupled with the low macronutrient concentrations and increased presence of picocyanobacteria, are interpreted as conditions of Fe replete, balanced macronutrient-limited growth. Spatial correlation was found between F_v/F_m

and Fe:nitrate ratios, supporting the suggestion that the relative supply ratios of these two nutrients can control patterns of limitation and consequently the ecophysiology of phytoplankton in subtropical gyre and ACC regimes.

2.1 Introduction

THE chlorophyll concentrations of the world's surface oceans are well constrained through satellite images of ocean colour. However, knowledge of the standing crop of phytoplankton is insufficient to understand the role of ocean primary production on global nutrient and carbon cycles, which will also be strongly influenced by the phytoplankton community structure and physiological status (Katz et al., 2004; Behrenfeld and Falkowski, 1997). In turn, the ecology and physiology of phytoplankton are regulated by multiple driving factors including light, temperature, nutrient availability, and grazing rates (Boyd et al., 2010). Globally, nutrient limitation of phytoplankton standing crops and growth rates has been shown to be dominated by the availability of fixed inorganic nitrogen, primarily in the form of nitrate, and iron (Fe) (Moore et al., 2013). However, the spatial resolution of data describing nutrient limitation is low, with large areas remaining poorly sampled (Moore et al., 2013). Such under-sampling is partly a result of the effort involved in conducting, and difficulties in unambiguously interpreting, shipboard bioassay incubation experiments where the phytoplankton population has been removed from their in situ environment (Cullen et al., 1992; Moore et al., 2013). The physiological assessment of phytoplankton communities using Fast Repetition Rate fluorometry (FRRf) represents a possible means of rapidly diagnosing nutrient limitation of phytoplankton (Greene et al., 1994). However, a variety of factors can influence FRRf derived photophysiological parameters (e.g. the apparent photochemical efficiency, F_v/F_m) under multi-faceted ecophysiological regimes (Behrenfeld et al., 2006; Moore et al., 2006a, 2008; Suggett et al., 2009; Schrader et al., 2011; Behrenfeld and Milligan, 2013). Thus, while many studies have suggested that FRRf signatures are influenced by nutrients, the prevailing light climate, and/or the phytoplankton community structure, the factors that dominate the signal under different

circumstances remain a subject of debate (Suggett et al., 2009; Behrenfeld and Milligan, 2013).

Although the exact causative mechanisms remain to be fully established (Behrenfeld and Milligan, 2013), Fe additions to Fe-limited waters have been repeatedly shown to increase F_v/F_m (Greene et al., 1994; Kolber et al., 1994; Behrenfeld et al., 1996; Olson, 2000; Boyd and Abraham, 2001; Sosik & Olson, 2002; Moore et al., 2006a, 2007). In contrast, in macronutrient-limited subtropical gyre waters F_v/F_m values have typically been found to be higher than for Fe-limited waters and insensitive to nitrate and/or phosphate additions (Behrenfeld et al., 2006; Moore et al., 2008; see also Parkhill et al. (2001) for analogous laboratory experiments). The reasons for this differential response remain uncertain, although one possibility is that the phytoplankton in these waters are living under conditions of balanced nutrient-limited growth, rather than starvation, as a result of sustained nutrient (re-)supply due to rapid efficient recycling (Moore et al., 2008).

The South Subtropical Convergence (SSTC) is the intersection point of low macronutrient subtropical gyre waters and high macronutrient ACC waters and therefore represents one of the most dynamic nutrient environments in the oceans (Ito et al., 2005). Satellite images show chlorophyll concentrations in the SSTC are typically elevated with respect to subtropical gyre waters further north and Antarctic Circumpolar Current (ACC) waters to the south throughout the year, although peak concentrations are found during austral spring and summer (Longhurst, 1998). Suggested mechanisms explaining the enhanced phytoplankton standing crop of the SSTC principally revolve around the idea that convergence of subtropical gyre waters, generally considered to be limited by the availability of nitrate (e.g. Dugdale and Goering, 1967; Ryther and Dunstan, 1971; Eppley, et al., 1979), and ACC waters, generally considered to be limited by Fe

availability (e.g. Boyd et al., 2000), provide both nitrate and Fe to the region, thus producing a nutrient regime that is capable of supporting elevated phytoplankton standing crops (Longhurst, 1998; Ito et al., 2005). The stability of the upper water column, critical for controlling water-column irradiance, has also been suggested as an important control of phytoplankton standing crop in the region. For example, the mixing of warm subtropical waters southwards across the SSTC has been suggested to provide thermal stability to the water column and therefore, through shallower mixing, increased light availability (Longhurst, 1998; Llido et al., 2005).

This chapter reports data on phytoplankton photophysiology and community structure from a South Atlantic cruise encountering strong gradients in nutrient environments during two crossings of the SSTC. These data, together with the results from a suite of 24-hour Fe addition incubation experiments, offer an improved knowledge of the phytoplankton standing crop, community structure, and photophysiology in the region, in addition to providing strong field evidence for the dominant controls on FRRf signals in these regimes. The detailed sections of photophysiological parameters along the transect, together with supporting ancillary data, clearly demonstrate how the system is controlled by the contrasting conditions of low macronutrient, subtropical gyre-type waters and low Fe, high macronutrient sub-Antarctic ACC waters.

2.2 Methods

2.2.1 General

2.2.1.1 Cruises

Data was collected on the RRS James Cook (JC068), as Section GA10 of the GEOTRACES programme. The cruise took place in mid-austral summer (28 December 2011 – 25 January 2012) and followed a track, mostly at 40°S, occupying 21 stations

between Cape Town, South Africa and Montevideo, South America (Figure 2.1). One station (Station 9) was occupied immediately to the east (i.e. downstream) of Gough Island – a volcanic island situated at 40.32° S, 9.92° W.

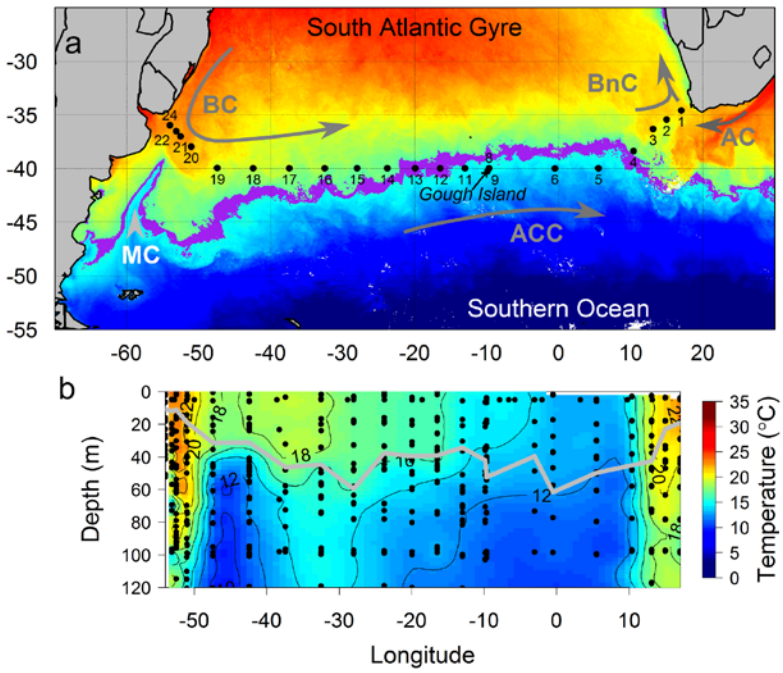

Figure 2.1: Water temperature around the Atlantic SSTC. (a) MODIS monthly composite image of sea-surface temperature (SST) for January 2012. Dominant surface water masses and sampling stations are labelled (AC: Agulhas Current; ACC: Antarctic Circumpolar Current; BC: Brazil Current; BnC: Benguela Current; MC: Malvinas (Falklands) Current). Purple colouring represents SST = 16 °C (+/- 0.5 °C) and is shown as a practical definition of the SSTC location. Gough Island is located next to Station 9. (b) Cross-basin section of CTD water temperature. Grey line indicates the mixed layer depth (MLD).

2.2.1.2 CTD data

Vertical profiles of temperature, salinity, fluorescence and (occasionally) photosynthetically available radiation (PAR) were collected using a Seabird 911 CTD. Mixed-layer depths (MLD) were calculated using the threshold method of de Boyer Montégut et al. (2004). In this method, the MLD is identified as the depth where density changes by a threshold value (0.125 kg m^{-3}) relative to one at a near-surface reference depth (10 m). A linear interpolation between observed levels is then used to estimate the

exact depth where the difference criterion is met (de Boyer Montégut et al., 2004; Suga et al., 2004). Using this finite difference criterion has been shown to better represent the MLD compared to integral and regression methods (Thomson and Fine, 2003; de Boyer Montégut et al., 2004). The euphotic depth (z_{eu}) was calculated from PAR profiles and is here defined as the depth where PAR reduced to 1% of values at the surface. At stations where no PAR profiles were obtained, a correlation between chlorophyll and the diffuse attenuation coefficient for PAR $K_{d(PAR)}$ (calculated from profiles where PAR was collected) was used to estimate $K_{d(PAR)}$ and therefore z_{eu} using $z_{eu} = 4.6/K_{d(PAR)}$. Continuous (every 10 minutes) measurements of surface PAR were also made throughout the cruise by two CM 6B pyranometers (Kipp & Zonen) mounted on ship.

2.2.1.3 Remote sensing

To examine the spatial and temporal variability in both chlorophyll-a and sea surface temperature (SST), and to monitor how the boundaries of the ACC and subtropical gyre provinces varied over the sampling period, satellite images from the Moderate Resolution Imaging Spectroradiometer (MODIS) were downloaded in daily, three day, eight day and monthly composite formats from the ocean colour website (http://oceancolor.gsfc.nasa.gov/).

2.2.2 Nutrient concentrations

2.2.2.1 Macronutrients

The dissolved macronutrients silicate, phosphate and nitrate + nitrite (hereafter simply referred to as nitrate) were analysed on-board ship by Malcolm Woodward using a micromolar Bran and Luebbe AAIII segmented flow, colourimetric autoanalyser with 4 analytical channels (nitrate+nitrite, nitrite, phosphate, silicate), using methods described in Woodward and Rees (2001). The results were checked against a certified nutrient

reference material, made by KANSO Technos, Japan. Clean analytical, handling and sampling techniques were employed according to the GO-SHIP repeat hydrography manual (Hydes et al, 2010).

2.2.2.2 Trace metal concentrations

Surface seawater samples for trace metal analysis and incubation experiments were pumped from a towed fish at a depth of 2 to 3 m. The seawater was pumped to a trace metal clean sampling container via a completely enclosed system with the suction provided by a Teflon diaphragm pump. Samples were filtered in-line through a 0.2 μm cartridge filter (AcroPak1000™) directly into acid cleaned low density polyethylene (LDPE) sample bottles. Discrete water samples from depth were obtained via 20 litre Niskin sampling bottles deployed on a titanium frame CTD rosette using a Kevlar cable. Dissolved samples for trace metal analysis were collected after filtration through 0.2 μm cartridge filters (AcroPak500™), with slight overpressure provided by a clean air compressor.

Seawater samples for trace metal analysis were acidified with concentrated ultra-pure hydrochloric acid (Romil, UpA) to pH 1.6 (0.023 M H^+), and shipped to the National Oceanography Centre (Southampton, UK). Trace metal samples were analysed under clean air conditions by Christian Schlosser, using a modified method previously outlined by Milne et al. (2010), using isotope dilution inductively coupled plasma mass spectrometry (ID-ICP/MS (Thermo Element XR)). To validate analysed sample concentrations, seawater standards (SAFe and GEOTRACES) were analysed with each batch of samples. Values agreed within the consensus values for SAFe and GEOTRACES (SAFe S: 0.09 ± 0.03 nmol Fe kg^{-1} (consensus 0.09 ± 0.01 nmol Fe kg^{-1}), GEOTRACES GS: 0.56 ± 0.05 nmol Fe kg^{-1} (consensus 0.52 ± 0.07 nmol Fe kg^{-1})). The precision for replicate analyses was between 1-3%. The manifold blank was 0.056 ±

0.016 nmol Fe kg^{-1}, and the limit of detection (3 x standard deviation of the blank) was determined to 0.032 ± 0.020 nmol Fe kg^{-1}.

2.2.3 Phytoplankton community structure

2.2.3.1 Accessory pigment composition

Samples for High Performance Liquid Chromatography (HPLC) (0.5–2 L) were filtered onto 0.7 µm Whatman GF/F filters, which were immediately flash-frozen in liquid nitrogen and then stored in a −80 °C freezer. Pigments were extracted into 90% acetone by sonication and then analysed using a Thermo HPLC system following the method described in Gibb et al. (2000). Pigments were identified using diagnostic retention times and comparison of individual pigment absorption spectra from a known spectral library. Chlorophyll-a and pigment mixture standards were included in each run to calibrate retention times for the accessory pigments.

Total accessory pigments (∑AP) were defined in this study as the sum of: chlorophyll-c3, chlorophyll-c2, peridinin, 19´-butanoyloxyfucoxanthin, fucoxanthin, 19´-hexanoyloxyfucoxanthin, prasinoxanthin, violoxanthin, diadinoxanthin, alloxanthin, zeaxanthin, lutein, gyroxanthin, chlorophyll-b, divinyl chlorophyll-a, and β-carotene. We found resultant concentrations to closely resemble chlorophyll-a biomass (∑AP = *chl-a* +0.038, R^2=0.8) (Trees et al., 2000). Fractional contributions of individual diagnostic pigments to total accessory pigments were subsequently calculated.

2.2.3.2 Phytoplankton absorption spectra

Phytoplankton absorption samples were collected by filtering 0.5 – 1 L seawater onto GF/F filters and flash-freezing the filter papers in liquid nitrogen before transfer to a -80°C freezer for storage. Measurements were made using the hot methanol extraction method of Kishino (1985) using a Shimadzu UV-2550 spectrophotometer equipped with

an integrating sphere over the visible range (350-750 nm). Optical densities for total (i.e. prior to methanol extraction) and detrital (after extraction) particles were corrected for optical pathlength amplification arising from scattering caused by the filter, according to the method of Cleveland and Weidemann (1993). Phytoplankton absorption coefficients (a_{ph}) were calculated by subtracting the detrital absorption spectra from the total absorption spectra. Pigment-specific absorption coefficients (a^*_{ph}) were calculated by dividing a_{ph} by the HPLC-determined chlorophyll-a concentration.

2.2.3.3 Flow Cytometric Analysis

Concentrations of nanophytoplankton, photosynthetic picoeukaryotes (PPEs), *Synechococcus*, *Prochlorococcus*, and total heterotrophic bacteria were analysed by analytical flow cytometry (AFC). Samples (2 mL) were fixed with neutralised paraformaldehyde (1% final concentration) and left for 10 minutes in the dark at room temperature before being flash-frozen in liquid nitrogen. Samples were then transported and stored in a -80°C freezer prior to AFC analysis.

Samples were thawed at room temperature and analysed using a FACSort flow cytometer (Becton Dickenson, Oxford, United Kingdom) according to the methods described in Davey et al. (2008) and Zubkov et al. (2003). An aliquot of sample (500 µL) was stained with 50 µL of 1% SYBR Green 1 DNA dye (SYBR Green diluted 100x in potassium citrate) for identification of total bacteria. Half of the remaining 1.5 mL was used for the purpose of identifying *Synechoccocus*, PPEs, and nanophytoplankton, and the other half for identifying *Prochlorococcus.* The FACsort instrument counted particles and measured chlorophyll fluorescence (>650 nm), orange fluorescence (585 +/- 21 nm), SYBR Green fluorescence, and side scatter (light scattered at 90 degrees to the plane of vertically polarised argon ion laser exciting at 488 nm). Samples were analysed in duplicate for 3 minutes at a flow rate of ~170 µL min^{-1} for counts of nanophytoplankton,

PPEs, *Synechococcus*, and *Prochlorococcus*. SYBR Green stained samples were analysed for 1 minute at a flow rate of ~60 µL min^{-1} for counts of total bacteria.

Data analysis and cell counts were carried out in WinMDI Version 2.8 (Joseph Trotter) flow cytometry analysis software. Scatter plots of orange fluorescence versus red fluorescence were used to discriminate and enumerate *Synechococcus* from other pico- and nanophytoplankton, and plots of side scatter versus red fluorescence (with *Synechococcus* gated out) were used to enumerate PPEs and nanophytoplankton. Plots of side scatter versus orange fluorescence were then used to gate out *Synechococcus* from plots of side scatter versus red fluorescence that were then used to enumerate *Prochlorococcus.* Total bacteria were enumerated from plots of side scatter versus SYBR Green fluorescence.

2.2.4 Fast Repetition Rate Fluorometry

A Fast Repetition Rate fluorometer (FRRf) ($FAST^{tracka\ II}$ with integrated $FAST^{act}$ base unit, Chelsea Technologies Group Ltd.) was used to make measurements of phytoplankton photophysiology on samples from multiple depths in the euphotic zone. In a single acquisition protocol, the FRRf was set to deliver 64 sequences of one hundred 1 µs saturation flashes at 1 µs intervals followed by twenty five 1 µs relaxation flashes at 84 µs intervals. Rapid Light Curves (RLC) were also run for all surface and subsurface chlorophyll maximum (SCM) samples. The RLC protocol was a series of identical FRRf single acquisitions (same settings as for single acquisitions, except sequences per acquisition were reduced to 32), performed under a series of 15 progressively higher PAR intensities ranging from 6 to 1434 µmol photons $m^{-2}s^{-1}$ delivered from the integrated $FAST^{act}$ system. Each illumination step in the RLC lasted for 180 seconds, with 10 second dark steps in between.

Samples were dark-acclimated in opaque plastic bottles for at least 30 minutes prior to analysis and maintained at sea surface temperature by incubating in a water bath of flowing seawater from the ship's underway system. Blanks were run for the majority of samples using the following procedure (after Cullen and Davis, 2003): an aliquot of roughly 3 mL of sample was gently filtered using a 0.2 μm pore size Nalgene syringe filter unit and a single acquisition FRRf measurement made using the same FRRf settings as the unfiltered sample. The average of fluorescence of a blank was taken (i.e. the mean fluorescence of 125 repetitions of the flash sequence). Minimal variable fluorescence was found in all sample blanks. All sample fluorescence values were subsequently blank-corrected by subtracting the blank from unfiltered samples before any further analysis.

Fluorescence transients were fit using the model of Kolber et al. (1998) in FASTpro (V1.5) software supplied with the instrument (Chelsea Technologies Group Ltd.). Parameter recovery using this software was checked against previous analysis methods performed in a MATLAB^{TM} environment using custom codes (Laney, 2003; Moore et al., 2006b; Moore, unpub.). F_v/F_m was calculated as $(F_m\text{-}F_o)/F_m$ (where F_o is the fluorescence at the zeroth flashlet and F_m is the maximum fluorescence), with functional absorption cross sections (σ_{PSII}) recovered from the fit to the model of Kolber et al. (1998), effectively corresponding to the initial gradient of the fluorescence transients. The decline in fluorescence during relaxation flashes in the FRRf single acquisition protocol represents plastoquinone Q_A re-oxidation in PSII, where the dominant decay component, τ_{QA}, represents the timescale of electron flow between plastoquinones A and B. Relative electron transport rates per RCII (ETR) were calculated from the RLC data using Eq. 2.1 (Gorbunov et al., 2001):

$$ETR = E\ \sigma_{PSII} \left(\frac{F_q{'}/F_m{'}}{F_v/F_m}\right) \quad \textbf{(2.1)}$$

where E is the ambient PAR intensity supplied by the FAST^{act} system, $F_q' = F_m' - F_o'$, and prime symbols indicate the measurements were made under actinic light. Calculated ETR's were then fitted to the following function (adapted from Platt et al., 1980):

$$\frac{\mathrm{ETR}}{\mathrm{E}} = \left(\frac{\mathrm{ETR_{max}}}{\mathrm{E}}\right)\left(1 - \mathrm{e}^{\left(\frac{-\alpha_{\mathrm{ETR}}\mathrm{E}}{\mathrm{ETR_{max}}}\right)}\right) \quad \textbf{(2.2)}$$

where $\mathrm{ETR_{max}}$ represents the maximum light saturated ETR plateau and α_{ETR} represents the gradient of the light-limited slope and will effectively be proportional to σ_{PSII}. Normalisation of ETR to irradiance provides a more statistically robust fitting method (Silsbe and Kromkamp, 2012), particularly improving fit quality at high irradiance. The optimum light intensity E_k was calculated as $\mathrm{ETR_{max}}/\alpha_{ETR}$. Example curve fits of ETR/E versus E are provided in Appendix 1 (Fig. A1.1).

2.2.5 Incubation experiments

Nine trace metal-clean, 1 L polycarbonate bottles were filled with trace metal clean water either from the towed fish described previously or, for samples from the SCM, from the titanium frame CTD rosette (see Figure 2.6a for depths). When sampling from the towed fish, bottles were filled close to midnight to avoid any effects of light stress on phytoplankton photophysiology. Three bottles were sub-sampled immediately for initial measurements of photophysiology and chlorophyll-a concentrations. For all experiments, samples for chlorophyll-a analysis (100 mL) were filtered onto 0.7 µm Whatman GF/F filter papers then extracted overnight in the dark in 10 mL 90% acetone in a -20 °C freezer, before measurement on a calibrated Trilogy fluorometer (Turner designs) following the method of Holm-Hansen et al. (1965). Of the remaining six bottles, 3 were spiked with 200 µL $FeCl_3$ in a 10% HCl solution resulting in a final Fe concentration of 2 nmol L^{-1} and 3 bottles were sealed immediately with no amendment. The 3 amended and

3 control (non amended) bottles were sealed around the lids with Parafilm^{TM}, double bagged, and placed in an on-deck incubator filled with continuously replenished sea-surface water from the ship's underway water system to limit temperature change of the samples. The incubator was shaded with blue screening to provide 35% of above surface irradiance.

After 24 hours the bottles were sub-sampled for photophysiology and fluorometric chlorophyll-a concentration. Iron-stressed waters were defined as those that produced a statistically significant ($p<0.01$ level using a one-tailed Student's t-test) F_v/F_m increase in the Fe-amended bottles over that of the control (non-amended) bottles. Values of $\Delta F_v/F_m$ were calculated, where $\Delta F_v/F_m$ = average F_v/F_m Fe amended bottles – average F_v/F_m control bottles (Ryan-Keogh et al., 2013). Chlorophyll-a concentrations were not expected to increase in response to the amendments, as 24 hours is too short a period for phytoplankton to display a significant biomass increase in response to relief of nutrient limitation (e.g. Greene et al., 1992; Ryan-Keogh et al., 2013). The short duration of our bottle experiments will minimise significant changes in the taxonomic composition of the phytoplankton community during the incubation, resulting in F_v/F_m differences likely being indicative of direct physiological changes only (Moore et al., 2008; Suggett et al., 2009; Ryan-Keogh et al., 2013).

Samples for macronutrients (nitrate, phosphate and silicate) and trace metals were taken prior to the bottle filling procedure described above, and for some experiments macronutrient samples were also sub-sampled for each of the three initial bottles. No samples for macronutrients were taken after the 24-hour incubation period as previous studies have shown insignificant changes, even where F_v/F_m responses are seen, due to the short nature of the incubation time (Ryan-Keogh et al. 2013). All sampling, sub-sampling, and Fe spiking was carried out using trace metal-clean techniques, either in a

trace metal clean container on the ship or in a trace metal clean laminar flow hood in the ship laboratory (Fe spiking only).

2.3 Results

2.3.1 General hydrography

The SSTC can be traced almost continuously around the globe between 35-45°S and divides the anticyclonic circulation of the southern hemisphere gyres from the cyclonic circulation of the ACC. The convergence results in a region of strong downwelling and sharp surface temperature and salinity gradients (Figure 2.1; Lutjeharms, 1985). The SSTC has been defined operationally as a band of elevated chlorophyll concentrations (0.2 – 0.3 mg chlorophyll-a m^{-3}, Longhurst, 1998), although this becomes poorly constrained in the Western Atlantic. A more practical definition for the Atlantic sector of the SSTC is to use sea-surface temperature, with a contour of 16 °C corresponding well to the nutrient gradients associated with the two water masses involved (Figure 2.1 and Figure 2.2). The latitude of the SSTC is seasonally dependant, with flow rates of the Agulhas Current (AC) and the Brazil Current (BC) increasing in austral summer (Walker, 1986; Matano et al., 1993), resulting in a southward expansion of South Atlantic Gyre waters and a resultant southward shift in the SSTC. In the western basin, the southward shift in the intersection point of the BC and Malvinas Current (MC) (the BC-MC confluence) in austral summer has been shown to be caused by an acceleration of water flow in the subtropical gyre and a weakened MC (Matano et al., 1993).

Mixed-layer depths showed consistent values of between ~40-60 m throughout the central basin (40°W to 15°E), reducing to <25 m nearer South African and South American coasts (Figure 2.1b). The light climate experienced by phytoplankton in the upper mixed layer is a function of the attenuation coefficient ($K_{d(PAR)}$) (which in open

ocean waters is mainly a function of phytoplankton biomass), the MLD, and above surface incident irradiance levels. Consequently, the lower $K_{d(PAR)}$ values, the similar-to-shallower MLDs, and similar incident above surface irradiances would have resulted in higher light levels in sub-tropical gyre mixed layers than sub-Antarctic ones. For example, using two representative stations where rosette deployments included a PAR sensor in addition to the CTD package (Stations 5, representing sub-Antarctic waters, and 18, representing sub-tropical gyre waters) we calculated mean MLD irradiances using the method described in Venables and Moore (2010). For a fixed integrated daytime irradiance for both, calculated values showed the gyre-type mixed layer irradiance to be around double that for the station in sub-Antarctic waters.

2.3.2 Nutrients

2.3.2.1 Macronutrients

Concentrations of nitrate and phosphate were depleted (< 0.3 µmol L^{-1} nitrate) in surface waters (0-50 m), and higher (5-12 µmol L^{-1} nitrate) at greater depths, apart from in the sub-Antarctic ACC waters south of the SSTC in the eastern basin where elevated concentrations (~5 µmol L^{-1} nitrate) were seen to extend into the surface waters (Figure 2.2a-b). Concentrations of silicate were uniformly low (<1 µmol L^{-1}) in surface waters (0-50 m depth) apart from near the South American coast where concentrations increased markedly (Figure 2.2c). For example, silicate concentrations reached 10 µmol L^{-1} at 5 m depth at Station 22, and 22 µmol L^{-1} at Station 24 (2 m depth) in close proximity to the Plata River outflow. Silicate concentrations remained low in surface waters (0-50 m depth) near the South African coast, yet increased significantly at depths of greater than ~50 m (reaching 7 µmol L^{-1} at 60 m depth). A notable feature in the sections of nitrate and phosphate, and to a lesser extent silicate, were elevated concentrations at depths greater than ~50 m for Stations 18 - 19 around 45°W. This feature also coincided with

relatively colder waters (see Figure 2.1b), and lower dissolved oxygen. This region of the transect was identified as being in a zone of depressed sea surface height (http://eddy.colorado.edu/ccar/data_viewer/index) for the time period of station sampling, suggestive of a cyclonic mesoscale eddy driving upwelling of deeper, colder, elevated nutrient waters.

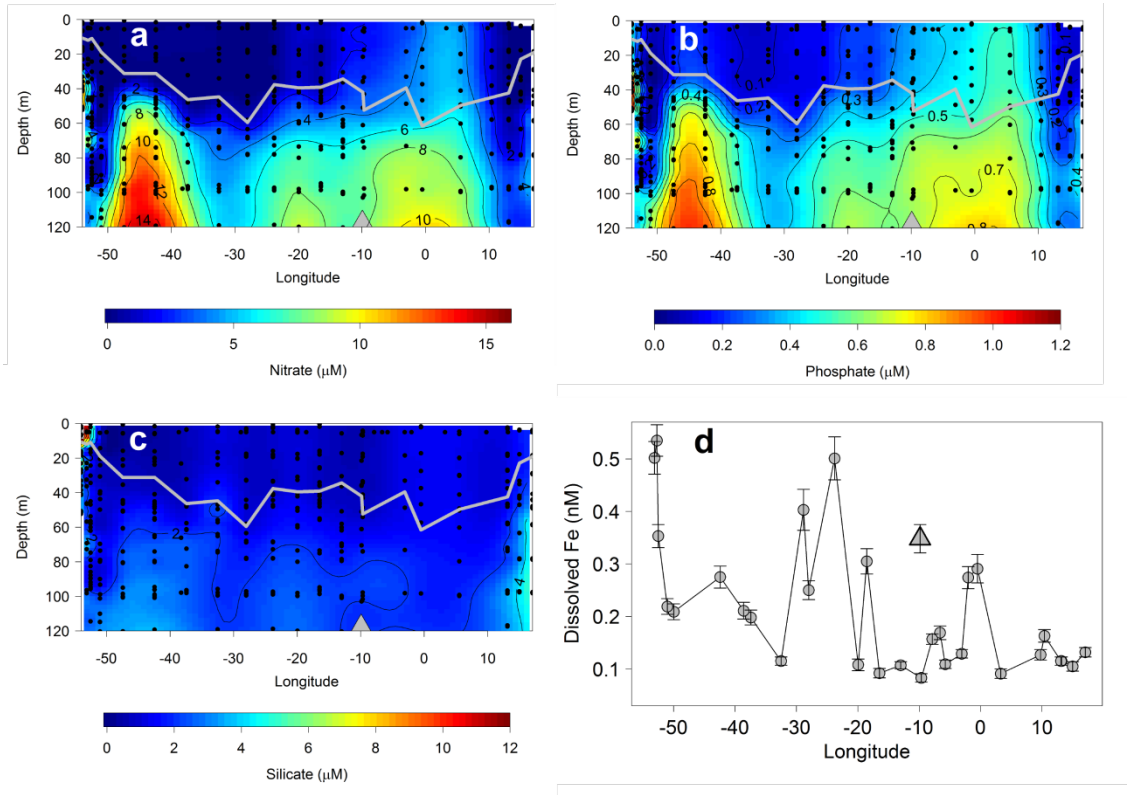

Figure 2.2: Cross-basin section of nutrient concentrations: (a) nitrate; (b) phosphate; (c) silicate. Grey lines indicate the MLD and grey triangles indicate the location of Gough Island. (d) Surface (~2-5 m) dissolved Fe concentrations. Error bars represent the standard deviation calculated as the accuracy of the spike ratio (~4%) and the counting accuracy of the ICP-MS. The point labelled with a triangle represents the DFe concentration for Station 9 (next to Gough Island).

2.3.2.2 Micronutrients

Surface dissolved Fe concentrations (DFe) showed low but variable surface concentrations throughout the cruise track (0.083 to 0.535 nmol L^{-1}, Figure 2.1d). Consistently low concentrations (<0.16 nmol L^{-1}) were seen east of 10.5°E in the surface AC waters of the Eastern Atlantic. Sub-Antarctic ACC surface waters showed more

variable concentrations, reaching a maximum of 0.348 nmol L^{-1} in Station 9 (proximal to Gough Island). On crossing the SSTC between Stations 13 and 14 (See Figure 2.1a), a significant increase in DFe concentrations occured, reaching a value of 0.501 nmol L^{-1}, which is comparable to those in surface waters in close proximity to the South American coast. To the west of 33°W concentrations showed an increase towards the South American coast, with values reaching a maximum of 0.535 nmol L^{-1} in next to the Plata River.

2.3.3 Chlorophyll-a concentrations

Satellite images show surface chlorophyll concentrations in the SSTC that are typically elevated with respect to waters further north (southern hemisphere subtropical gyres) and south (the ACC) throughout the year, although peak concentrations are found during austral spring and summer (September to February) (Figure 2.3a-f). The band of elevated chlorophyll coinciding with the SSTC shows a southward shift in austral summer associated with increased AC and BC flow and a resultant southward expansion of the subtropical gyre (Figure 2.3). In association with the trajectory of the SSTC (which occupies lower latitudes in the eastern basin than the western basin, Figure 2.1a), the band of elevated chlorophyll concentrations is typically found further north in the eastern portion of the basin. For example, peak chlorophyll concentrations at 40°S for the austral spring-summer of 2011-2012 are seen in November 2011 for the western basin (40°W to 20°W) and February 2012 for the eastern basin (10°W to 10°E).

Profiles of chlorophyll-a concentrations revealed elevated and depth-uniform values (0.2 – 0.7 mg m^{-3}) within the mixed layer for sub-Antarctic ACC waters in the central eastern basin, whilst low surface concentrations (<0.2 mg m^{-3}) and elevated deep concentrations (typically >0.4 mg m^{-3} and reaching a maximum of 1.46 mg m^{-3}) were observed in the

higher temperature regions of the western basin and nearer to the South African coast (Figure 2.3a and b). Elevated mixed-layer chlorophyll-a concentrations were seen at the station in close proximity to the Plata River (~0.7 to 0.9 mg m^{-3}).

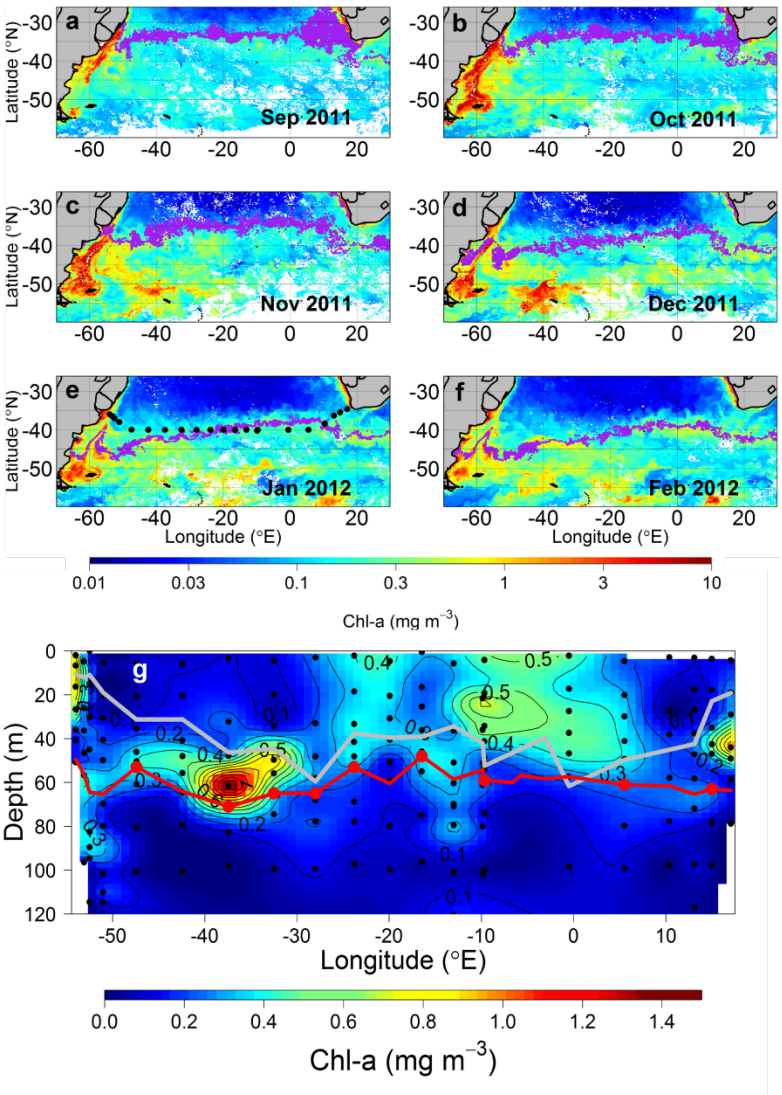

Figure 2.3: Chlorophyll-a concentrations. MODIS monthly composite images (a-f) of chlorophyll-a concentrations for September 2011 – February 2012 around the Atlantic SSTC. Sampling locations are labelled for the January 2012 image, which was the month of in situ sampling. Purple colouring represents SST = 16 °C (+/- 0.5 °C) and is shown as a practical definition of the SSTC location. (g) Cross-basin section of HPLC-derived chlorophyll-a concentrations. Note the different scales for (a-f) and (g). Grey line is the MLD. The red line is the euphotic depth (z_{eu}) here defined as the 1% light depth, with red dots indicating where direct PAR measurements were used to calculate the depth and remaining variability reflecting z_{eu} estimated using a derived chlorophyll- $K_{d(PAR)}$ relationship ($K_{d(PAR)}$ = 0.016 Chlorophyll-a + 0.068).

2.3.4 Phytoplankton community structure

Specific absorption coefficients were low in the eastern basin in comparison with the rest of the transect (Figure 2.4a), suggesting the presence of larger phytoplankton cells relative to the subtropical gyre-type regimes (Ciotti et al., 2002; Yentsch and Phinney, 1989). Correspondingly, AFC results showed higher concentrations of nanophytoplankton in the eastern basin (Figure 2.4b). Elevated concentrations of smaller cells (picophytoplankton) are seen in these waters and at SCM depths in subtropical gyre-type waters, which also included elevated concentrations of *Synechococcus* and *Prochlorococcus* (Figure 2.4d-e).

HPLC samples showed elevated 19´-hexanoyloxyfucoxanthin (19´-Hex) contributions (Figure 2.5g) in the eastern basin between 13°E to 10°W (generally >40% contribution to total accessory pigment biomass) suggestive of haptophytes dominating phytoplankton communities in this region. However, 19´-Hex also contributed significantly to accessory pigments in the western basin and closer to the South African coast (e.g. >30% contribution in SCM waters in AC waters of Stations 1 and 2, and generally greater than 20% in waters shallower than 80 m depth west of 10°W), although the photoprotective pigment zeaxanthin (Figure 2.5d), a diagnostic pigment of cyanobacteria, was also found to contribute significantly to the total pigment complement (up to 36% in surface waters of Station 1). Elevated contributions of divinyl chlorophyll-a (Figure 2.5h) in some of these samples were indicative of *Prochlorococcus*, matching with elevated *Prochlorococcus* abundances measured by AFC (Figure 2.4e and Figure 2.5h). Elevated contributions of peridinin (Figure 2.5a), the unambiguous marker pigment for dinoflagellates, were found in the eastern basin, yet its contribution to total accessory pigments generally remained only around 10% in this region.

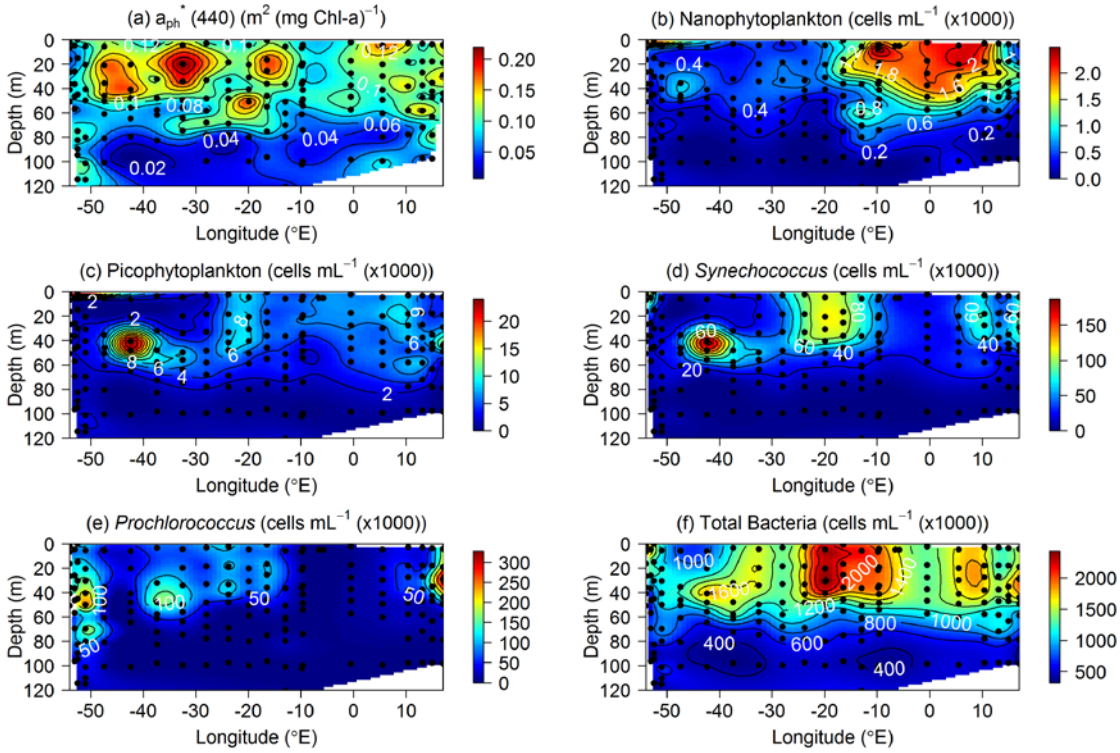

Figure 2.4: Analytical fluow cytometry (AFC) and specific absorption of phytoplankton at 440 nm. Cross-basin (depth-longitude) sections of (a) specific phytoplankton absorption at 440 nm, and analytical flow cytometry counts of: (b) nanophytoplankton; (c) photosynthetic picoeukaryotes; (d) *Synechococcus*; (e) *Prochlorococcus*; (f) total bacteria.

High contributions of the photoprotective pigment diadinoxanthin (reaching 17% contribution, Figure 2.5b) were found in surface waters (<50 m depth) across the whole transect, as has been observed in previous studies of haptophyte-dominated waters (e.g. Gibb et al., 2000; Gibb et al., 2001). The highest fucoxanthin contributions (Figure 2.5e) were observed in the stations furthest west along the cruise track within close proximity to the Plata River (up to 77% contribution at 40 m depth in Station 24), suggestive of diatoms dominating these waters. Elevated fucoxanthin contributions are also observed in the high macronutrient feature identified in Section 3.2.1 (reaching 50% at 100 m depth at Station 18), which is suggestive of an increased contribution of diatoms to total chlorophyll biomass. However, as total chlorophyll-a biomass is very low in this region (<0.1 mg m^{-3}, Figure 2.3b), the actual biomass of diatoms would also be low. Similarly, elevated contributions of 19´-butanoyloxyfucoxanthin (19´-But) at depths below ~60 m

were observed across large parts of the transect, however the low chlorophyll concentrations at these depths indicated the total biomass of phytoplankton types containing this pigment (e.g. Chrysophyceae, Pelagophyceae) were relatively low.

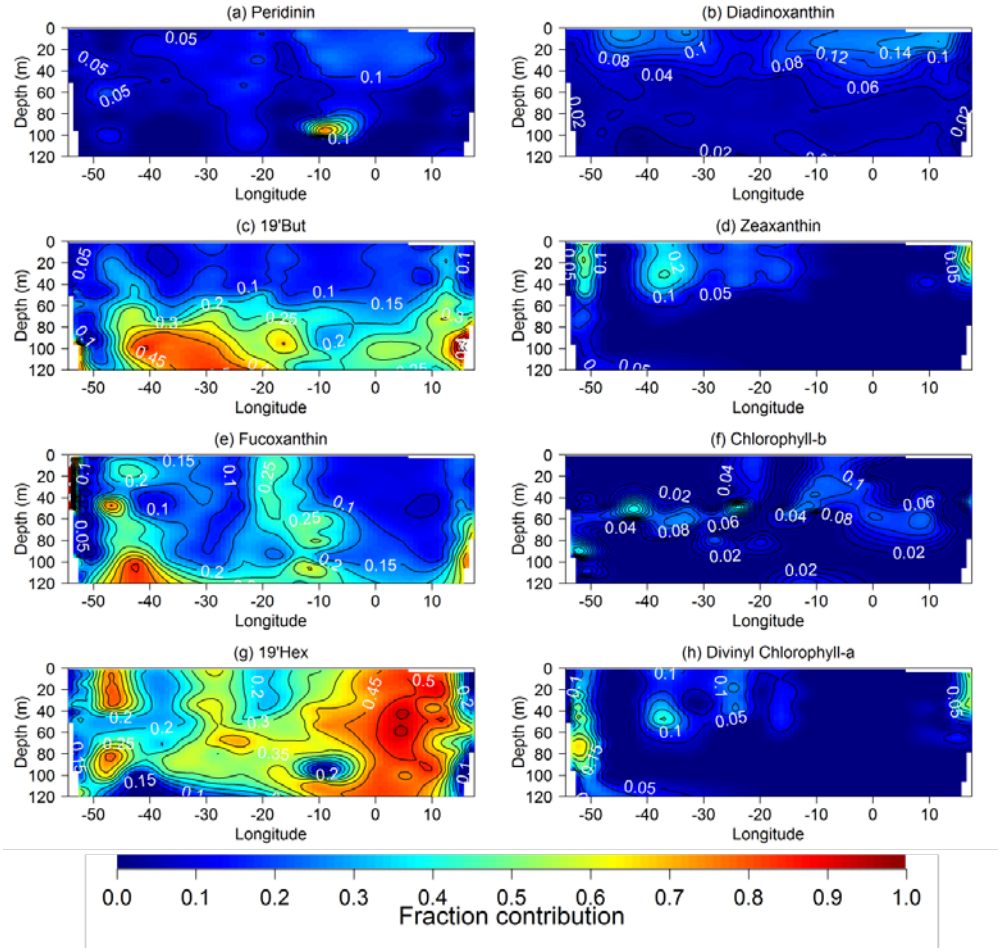

Figure 2.5: Cross-basin (depth-longitude) sections of the contribution of major accessory pigments to total accessory pigments. (19'-Hex =19' hexanoyloxyfucoxanthin, 19'-But = 19' butanoyloxyfucoxanthin).

2.3.5 Phytoplankton photophysiology

The section of F_v/F_m in Figure 2.6a shows strong variations of photophysiology along the transect, which again match up with the distinct regimes identified from previously described temperature, macronutrient, chlorophyll-a and phytoplankton community data. Low values of F_v/F_m (F_v/F_m <0.3) are seen throughout the mixed layer in the sub-Antarctic ACC waters of the eastern basin with increases at greater depths. An exception

to this is the station occupied next to Gough Island (Station 9), where elevated F_v/F_m (F_v/F_m >0.3) can be discerned throughout the mixed layer. Higher F_v/F_m is seen at all depths in subtropical gyre-type waters in the western basin (west of 35°W) and in AC waters (>13°E). Off the South African coast, small but clear F_v/F_m reductions occur at the SCM. Slightly more longitudinal variability was found in surface water (<10 m) F_v/F_m values than for deeper samples. Values of σ_{PSII} showed a less clear trend than F_v/F_m (Figure 2.6b), although a general trend of inverse co-variability with F_v/F_m can be discerned (e.g. for 0 to 50 m, R^2=0.3, p<0.001), with higher values generally seen in sub-Antarctic waters. Lowest σ_{PSII} values were observed next to the South American coast. Trends in $1/\tau_{QA}$ were not clear, with significant depth and longitudinal variability. Despite this there was some indication of reduced values in ACC waters south of the SSTC.

RLC parameters again showed a less clear spatial trend than F_v/F_m, yet some broad characteristics of the different regions can be discerned (Figure 2.6c-d, see also Fig. A1.1 in Appendix A1). Surface samples from thermally-stratified subtropical gyre-type waters (west of 25°W and east of 10°E) show higher ETR_{max} and E_k values than SCM samples. Particularly large differences, with highest recorded ETR_{max} and E_k surface values, were observed for Stations 1 (nearest the South African coast), 19 and 20 (near the South American coast). Sub-Antarctic ACC waters south of the SSTC in the eastern basin show less variability between surface and SCM depths, and have ETR_{max} and E_k values in between that of the surface and SCM samples from subtropical waters. As expected, values of α_{ETR} followed trends in σ_{PSII} (R^2=0.53).

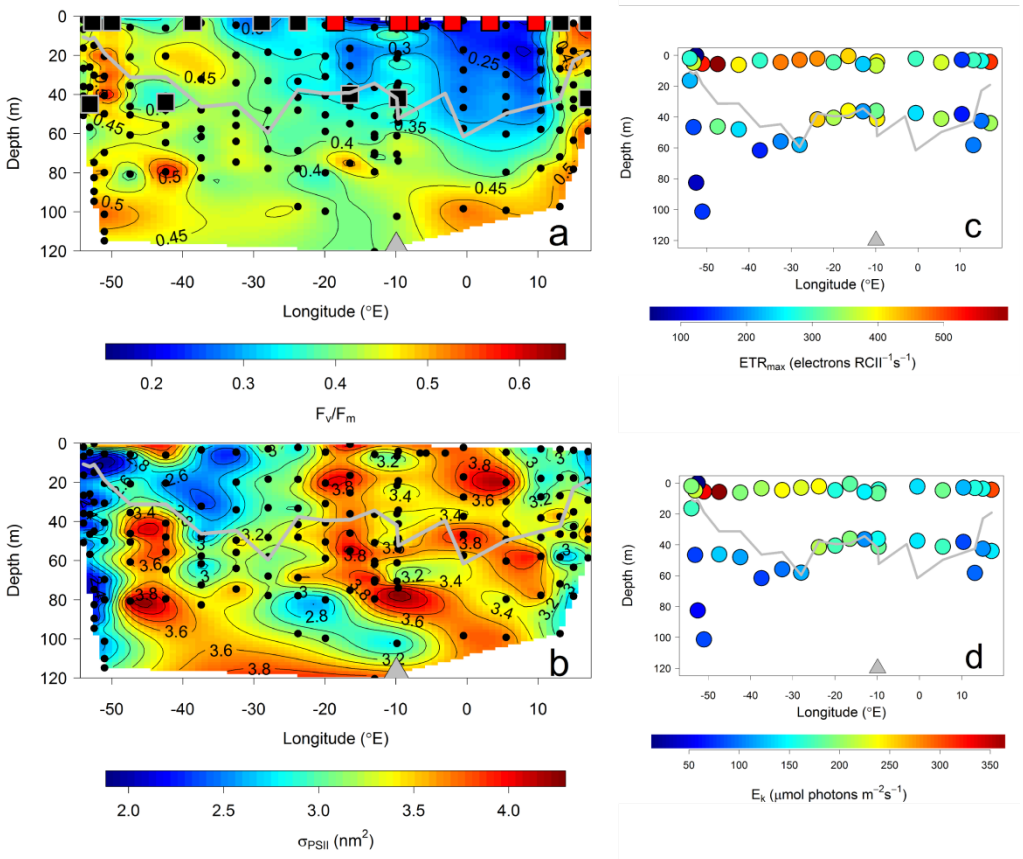

Figure 2.6: Cross-basin sections of FRRf-derived photophysiological parameters: (a) F_v/F_m; (b) σ_{PSII}; (c) relative ETR$_{max}$; (d) E_k. Black and red squares in (a) indicate the location of Fe addition incubation experiments (black = no significant response from Fe amendment; red = statistically significant response). Grey lines indicate the MLD, grey triangles indicate the location of Gough Island.

2.3.6 Fe addition experiments

The Fe addition experiments showed clear (t-test $p < 0.01$) F_v/F_m responses from Fe-amended bottles over that of the control bottles for surface waters in the eastern basin between 10°E and 20°W (IF3 to IF8 in Figure 2.7 7a-b, see also Appendix A2 for full list of F_v/F_m values for each experiment bottle). Within these experiments, a notable east-to-west reduction in response was observed in surface water amendments between IF3 and IF8 (e.g. $\Delta F_v/F_m$ values of 0.16 for IF3, decreasing to 0.063 for IF8). No significant F_v/F_m response to Fe amendment was seen either side of this zone. Furthermore no statistically significant F_v/F_m responses to Fe amendment were seen for the five SCM

experiments conducted (Figure 2.7b), although it should be noted that no SCM Fe-amendment experiments were conducted where the largest surface water responses were seen (IF3 to IF6). Significant changes in chlorophyll-a concentrations were also not observed in the majority of experiments.

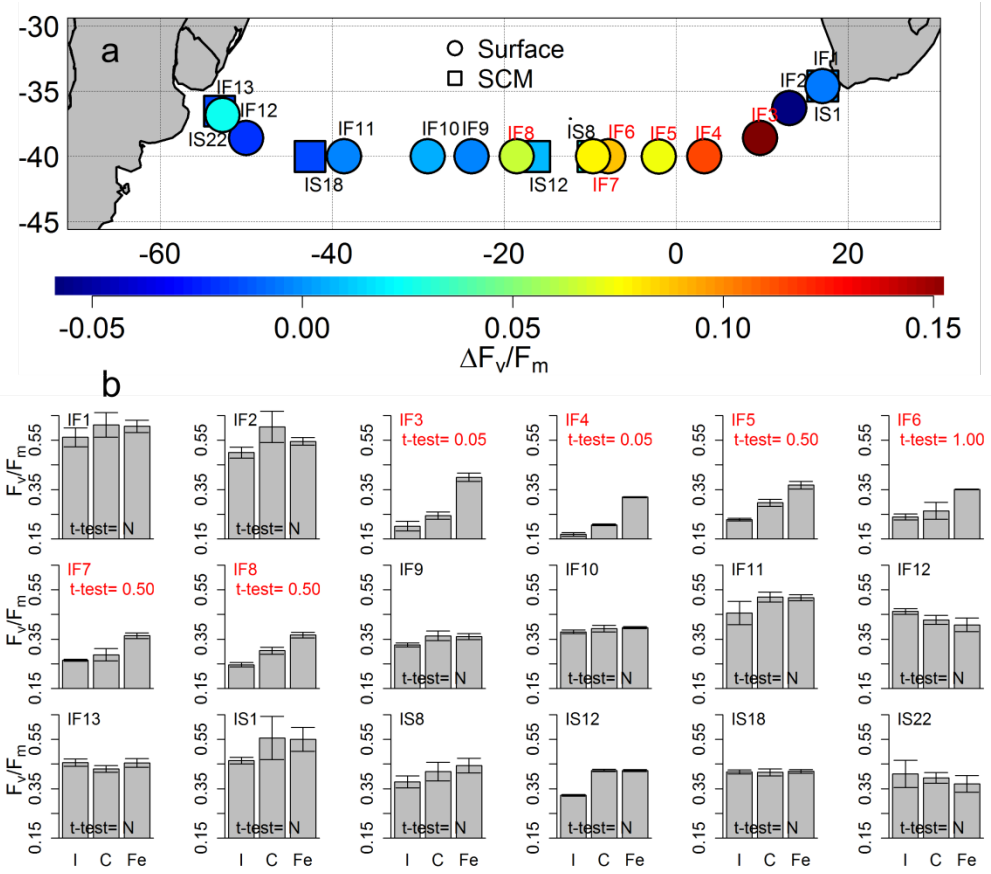

Figure 2.7: Fe incubation locations and results. (a) Locations of experiments coloured according to $\Delta F_v/F_m$ values ($\Delta F_v/F_m$ = F_v/F_m Fe amended bottle – F_v/F_m control bottle). IF = Incubation Fish (indicating trace-metal-clean tow-fish water used for the experiment, highlighted on the map as a filled circle), IS = Incubation Station (indicating SCM trace-metal-clean water from the titanium CTD rosette was used, highlighted on the map as a filled square). Experiments with statistically significant responses (t-test $p<0.01$) are highlighted with red labels. (b) F_v/F_m for incubation experiments. I = Initial, C = Control (incubated for 24 hours with no amendment), Fe = Fe spiked (incubated for 24 hours after 2 nmol L^{-1} $FeCl_3$ addition). Bars = mean of three bottle replicates; error bars = standard deviation. Student's one tailed t-test significance levels (%) are shown, with significant results labelled in red (N= no significant difference between control and Fe amended bottles).

2.4 Discussion

2.4.1 Patterns of phytoplankton photophysiology in and around the SSTC

The section of F_v/F_m (Figure 2.6a), together with ancillary chemical and phytoplankton data (Figure 2.2 to Figure 2.5) and the Fe incubation experiments (Figure 2.7) demonstrates a clear division of this ocean section into two regimes: 1) low macronutrient, sufficient Fe, and higher F_v/F_m to the north of the SSTC; and 2) elevated macronutrient, insufficient Fe, and lower F_v/F_m to the south. Several factors are thought to control values of F_v/F_m, including light climate, the particular phytoplankton taxa present and the nutrient regime (Suggett et al., 2009). Using accessory pigment, AFC, irradiance and experimental data however, we can eliminate the first two controls and demonstrate that macronutrient and Fe availability govern the majority of variability in this parameter for our study region.

Light stress has been shown to result in photodamage to reaction centre proteins (e.g. Horton et al., 1996; Raven, 2011), or the down-regulation of PSII (e.g. Milligan et al., 2012). However, any resultant reductions in F_v/F_m might be expected to reduce F_v/F_m principally in the high irradiance surface of the stratified low macronutrient regions, rather than the ACC waters. Irrespectively light induced changes in F_v/F_m would also not explain the observed differences in F_v/F_m between experimental treatments (Figure 2.7). The taxonomic composition of the phytoplankton community can potentially influence F_v/F_m signatures, with a general trend of decreasing F_v/F_m observed with decreasing cell size when grown under the same environmental conditions (Suggett et al., 2009). However, we performed correlation analysis between F_v/F_m and indices of community structure for the upper 50 m water column depth, which showed trends opposite to that expected from this control (Table 1). Significant negative correlations were found

between F_v/F_m and the contribution of 19´-Hex to total accessory pigments, whilst a positive correlation was found between F_v/F_m and the contribution of zeaxanthin to total accessory pigments. This is indicative of lower F_v/F_m being found in phytoplankton communities with higher haptophyte to cyanobacteria ratios, which is inconsistent with that expected under nutrient replete conditions (Suggett et al., 2009). Furthermore, in terms of the significant F_v/F_m responses from the Fe-addition experiments in the ACC waters south of the SSTC (Figure 2.7), net differential growth sufficient to generate taxonomic shifts in the bottles is unlikely over the short 24-hour timescale (Moore et al., 2008; Ryan-Keogh et al., 2013), as evidenced by the generally insignificant changes in total chlorophyll-a.

Laboratory studies have demonstrated that macronutrient starvation can lead to reductions in F_v/F_m due to reduced reaction centre functionality (e.g. Kolber et al., 1988; Geider et al., 1993b). However, this type of nutrient stress actually appears rare in the open ocean (although see Kolber et al., 1990; Geider et al., 1993a), where more steady-state macronutrient stress appears to result in maintained F_v/F_m values (MacIntyre et al., 1997; Parkhill et al., 2001; Behrenfeld et al., 2006; Kruskopf and Flynn, 2006; Moore et al., 2008; Schrader et al., 2011). The high F_v/F_m values observed in waters with nitrate concentrations of less than 0.02 µmol L^{-1} are consistent with such an interpretation (Figure 2.2a and Figure 2.6a). In contrast, Fe limitation both in terms of starvation and possibly steady-state limitation, has been observed to result in depressed values of F_v/F_m that is relieved upon the addition of Fe, both in culture (Geider et al, 1993b; Greene, 1991; Greene, 1992; Vassiliev et al., 1995; Sharader et al. 2011) and in situ (Greene, 1994; Kolber, 1994; Vassiliev et al., 1995; Behrenfeld, 1996; Olson, 2000; Boyd and Abraham, 2001; Sosik & Olson, 2002; Moore, 2007) although note that high F_v/F_m was observed under steady-state Fe-limited diatom cultures by Peers and Price (2004). In a

similar manner, our observations of F_v/F_m recovery south of the SSTC after Fe enrichment (Figure 2.7), together with a step-wise elimination of the other potential controls discussed above, allows us to confidently ascribe the observed low F_v/F_m values to Fe stress.

Table 2.1: Simple linear regression statistics for potential controls on F_v/F_m (0-50 m) and $\Delta F_v/F_m$

Potential controlling variable for F_v/F_m	Correlation direction	R^2	p
DFe	Ns	0.037	ns
Nitrate	Negative	0.12 (0.38)	<0.0005 (<0.0001)
DFe: nitrate	Positive	0.18 (0.51)	<0.01 (<0.0001)
Phosphate	Negative	0.17 (0.33)	<0.0001 (<0.0001)
Silicate	Ns	0.015	ns
Chlorophyll	Ns	0.022	ns
19´-Hex: ∑AP	Negative	0.23	<0.0001
Zeaxanthin: ∑AP	Positive	0.22	<0.0001
19´-But: ∑AP	Ns	0.00016	ns
Fucoxanthin: ∑AP	ns	0.015	Ns
a^*_{ph} (440)	ns	0.041	Ns
MLD	negative	0.22	<0.0001
Temperature	positive	0.46	<0.0001
Depth	positive	0.040	<0.05
Potential controlling variable for $\Delta F_v/F_m$			
F_v/F_m	negative	0.75	0.0001
DFe	ns	0.083	Ns
Nitrate	positive	0.59 (0.79)	<0.005 (0.0001)
DFe: nitrate	negative	0.36 (0.73)	0.05 (<0.0005)

Note "ns" = "not significant" (p>0.05). Values in parenthesis are included for log transformation of the potential forcing variable where this significantly improved the correlation. AC = accessory pigments.

Two mechanisms have been put forward to explain depressed F_v/F_m values in Fe-limited waters. Firstly, as Fe is an essential component of the photosynthetic apparatus, its absence could potentially limit the functionality of PSII reaction centres (e.g. Greene et al., 1994; Kolber et al., 1994). However, more recent work has suggested that low F_v/F_m

values may originate from the production of excess disconnected light harvesting complexes (DLHC) under conditions of Fe-limited growth (Behrenfeld et al. 2006; Schrader et al., 2011; Ryan-Keogh et al., 2012; Fraser et al., 2013). Excess pigments energetically uncoupled from a functional reaction centre will not contribute to photochemistry but could contribute to total fluorescence (i.e. increase F_o and F_m), and hence reduce F_v/F_m independently of F_v (Schrader et al., 2011; Ryan-Keogh et al., 2012). As such, depressed values of F_v/F_m would characterise a Fe-stress physiological response, but without any coincident dysfunctionality of reaction centres or impairment of carbon fixation efficiencies (Behrenfeld and Milligan, 2013). Consequently, depressed F_v/F_m in the sub-Antarctic waters south of the SSTC may still correspond to conditions of balanced Fe limitation of the phytoplankton standing crop, in a similar manner to the expected macronutrient limitation of waters to the north of the front.

The data collected in this study provides clear field evidence that high F_v/F_m signatures can be produced in low Fe waters provided that coincident low macronutrient concentrations are found (compare Figure 2.2a, b, d with Figure 2.6a and also see Figure 2.8). For example, AC waters in the east of the cruise track show F_v/F_m >0.5 yet DFe concentrations are less than 0.16 nmol L^{-1}. There is some evidence from laboratory experiments that Fe-macronutrient co-limited phytoplankton show elevated F_v/F_m (Schrader et al., 2011). This observation together with subsequent F_v/F_m reductions following macronutrient re-supply have been suggested to be due to the macronutrient requirement for DLHC synthesis (Schrader et al., 2011). With our current suite of experiments it is not possible to conclude whether or not the waters of the AC were Fe-macronutrient co-limited, although the addition of fixed nitrogen would likely have been required to stimulate any significant increase in the standing crop of phytoplankton.

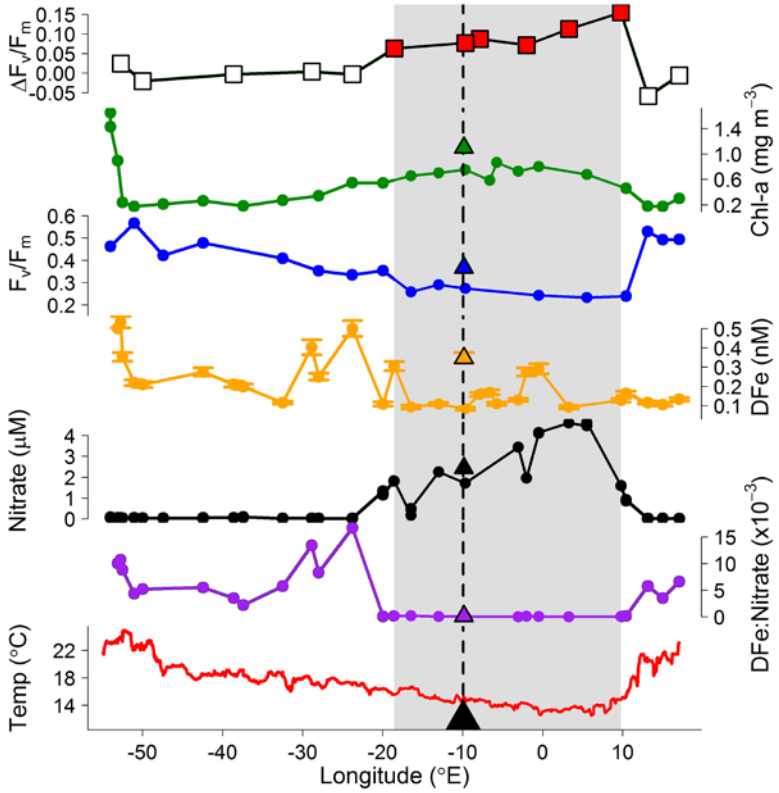

Figure 2.8: Across-basin summary of environmental and ecophysiological parameters: $\Delta F_v/F_m$ from Fe addition incubation experiments; chlorophyll-a; F_v/F_m; nitrate; DFe; DFe:nitrate; ship's underway temperature. All measurements are from the surface (<10 m depth) apart from F_v/F_m, shown for 20 m to reduce the influence of long-lived photodamage/PSII down-regulation on measurements. For $\Delta F_v/F_m$, red squares = statistically-significant response from Fe amended bottles. The grey shaded region highlights the Fe-limited zone as indicated by significant Fe amendment responses. Triangular symbols represent measurements from the station next to Gough Island, the location of which is highlighted by the large black triangle and dashed line.

More generally, these results also suggest that Fe-stressed conditions may not easily be identified solely on the basis of DFe concentrations (compare Figure 2.2d with Figure 2.6a, and also see Figure 2.8). Measurements of DFe include soluble, colloidal, inorganic and ligand-bound fractions and considerable uncertainty persists as to the relative bioavailability of these fractions to phytoplankton (Shaked and Lis, 2012 and references therein). For the same measured DFe concentration, the ability for the available Fe to support the growth of the extant phytoplankton population might be expected to be higher in the subtropical gyre-type waters encountered compared with the ACC waters both as a result of the lower phytoplankton standing stock reducing competition for the

metal and the generally smaller cell sizes increasing surface-area-to-volume ratios and hence the kinetics of metal uptake (Hudson and Morel, 1990; Shaked et al., 2005).

Whilst at the level of an individual phytoplankton cell the factors controlling Fe limitation are complex, our data support suggestions that regions of Fe limitation are characterisable on the basis of the relative supply of DFe and nitrate (Parekh et al., 2005). Loss of Fe to scavenging in the deep ocean results in waters upwelling from depth (such as occurs strongly within the ACC) having lower DFe:nitrate ratios than that of phytoplankton requirements (Johnson et al., 1997; Ito et al., 2005; Parekh et al., 2005; Sunda, 2012). Formation and subsequent export of organic material would therefore be expected to deplete Fe to levels that are limiting to phytoplankton growth in such regions. In contrast depletion of macronutrients under weaker replenishment from depth in subtropical gyre waters, alongside some level of external Fe supply (for example from dust), results in the gradual development of macronutrient limitation (Moore et al., 2013). Accordingly, across-transect values of the surface DFe:nitrate ratio suggested a good spatial correlation with both F_v/F_m, and the proximal response of the phytoplankton community to Fe replenishment as indicated by $\Delta F_v/F_m$, in our study region (Figure 2.8). Moreover the degree of Fe stress showed a stronger spatial relationship with both DFe:nitrate and even nitrate than with DFe, with these relationships appearing non-linear (shown visually in Figure 2.8, and by simple linear regression in Table 1). Similarly Fe:macronutrient supply ratios effectively dictate the broad patterns of nutrient limitation that develop in regional (Ito et al., 2005) and global (Aumont et al., 2003; Moore et al., 2004) biogeochemical models. For example, the derived parameter Fe*, the difference between DFe and phosphate concentrations weighted by an assumed biological uptake ratio of the two nutrients ($R_{F:P}$), has been used to delineate Fe or macronutrient limited regions (Ito et al., 2005; Parekh et al., 2005).

Values of σ_{PSII} broadly show an inverse relationship to F_v/F_m (Fig. 6b), potentially indicating either larger connected LHC's and/or less operational reaction centres per LHC under Fe stressed conditions (Vassiliev et al., 1995; Behrenfeld and Milligan, 2013). The less clear spatial pattern of σ_{PSII} than for F_v/F_m may result from an enhanced taxonomic signature for this physiological trait (Suggett et al., 2004; Moore et al., 2005, 2006b; Suggett et al., 2009). RLC parameters showed a less clear across-transect trend than F_v/F_m, instead being dominated by vertical gradients within the gyre-type waters (see differences in parameters between surface water samples and below mixed layer depth samples in Figure 2.6c and d). This difference is likely related to photoacclimation, as the light environment phytoplankton are experiencing above and below the mixed layer is expected to be quite different. Specifically, elevated ETR_{max} and E_k of surface samples compared to SCM samples (below the mixed layer) likely reflect acclimation to the increased irradiance encountered here (Moore et al., 2006b). In contrast, RLC parameters displayed less vertical variability between surface waters and those at the base of the mixed layer in ACC waters of the eastern basin: deep (~40 m) and shallow (~5 m) values of ETR_{max} and E_k were in between that of surface and SCM samples from the subtropical gyre-type regions to the east and west. Such a pattern likely resulted from these phytoplankton communities acclimating to mean mixed layer depth irradiances.

2.4.2 Controls on the development of the SSTC bloom

Satellite images suggest a band of elevated chlorophyll concentrations around the SSTC in austral summer (Figure 2.3a-f). Note that the SSTC chlorophyll band can be distinguished from the Fe-fertilised band downstream of South Georgia and the Scotia Ridge further to the south (e.g. Sokolov and Rintoul, 2007; Moore and Abbott, 2002). Increasing chlorophyll concentrations are observed at the SSTC between September 2011 and February 2012, which could be a result of increased light availability through a

combination of increased surface irradiance and reduced mixed-layer depths (de Boyer Montégut et al., 2004). However, as we have demonstrated, phytoplankton in these waters are limited by Fe availability in January 2012. Consequently the sustained and even increased chlorophyll into February 2012 may be indicative of a maintained Fe supply to this region.

The expected response of phytoplankton to natural Fe supply in these waters is particularly well demonstrated by Fe enrichment from Gough Island, which sits centrally in the Atlantic Basin at 40°S within the region of Fe-stress (Figure 2.8). The eastward-flowing surface currents pass over the shallow-subsurface topography surrounding the island, and weathered material is presumably transported off the island by streams and as windblown dust. Evidence for Fe delivery to waters surrounding Gough Island comes from increased DFe, similar to other islands that have been hypothesised or shown directly to supply Fe to HNLC waters, for example the Crozet Islands (Planquette et al., 2007) and Kerguelen (Blain et al., 2001; Bucciarelli et al., 2001; Blain et al., 2002, Blain et al., 2007). Indeed, both elevated chlorophyll-a concentrations and a recovery of F_v/F_m to higher values were observed for the single station occupied in the vicinity of Gough Island (Station 9), as might be expected upon relief of Fe limitation.

DFe was around 3-fold higher proximal to Gough Island than with the waters just to the north. Increases in F_v/F_m and chlorophyll were more modest (34% and 46% respectively), potentially reflecting the time required for phytoplankton entrained in the eastward flowing current to respond to Fe supply from Gough Island. For instance, the increase in F_v/F_m between the two stations (8 and 9) was comparable to the increase observed for the 24 hour duration Fe-amendment experiment using water collected at Station 8 (26% increase for IF7, Figure 2.7b). Moreover, there is no reason to suspect a linear correlation between Fe concentration and F_v/F_m or chlorophyll (e.g. Cullen et al.,

1992, also see Table 1 and Figure 2.8). Similarly, there was relatively little indication of any significant species shifts accompanying the natural Fe-fertilisation, with contributions of major diagnostic pigments remaining relatively constant (e.g. mixed layer fucoxanthin remained at ~10% contribution for both stations). Although our data from Station 8 suggest Fe-fertilisation from Gough Island is spatially limited to the north, the downstream (longitudinal) Fe-fertilisation distance from Gough Island remains to be tested.

2.5 Conclusions

FRRf measurements of phytoplankton photophysiology alongside chlorophyll-a concentrations, community structure, macronutrients and DFe, together with results from a suite of 24-hour Fe-addition incubation experiments from a cruise in the South Atlantic, have characterised two regimes on the basis of nutrient limitation. The primary limiting nutrient of the elevated chlorophyll, relatively larger cell-dominated sub-Antarctic ACC waters south of the SSTC in the Eastern Atlantic Basin in mid-austral summer has been shown to be Fe. Increasing Fe availability in this region results in increased F_v/F_m values (bottle enrichment experiments and natural enrichment from Gough Island) and chlorophyll-a concentrations (natural enrichment from Gough Island). To the north of the SSTC, as seen close to the South African coast and in the western section of the cruise transect, the phytoplankton standing crop showed elevated F_v/F_m and an enhanced contribution of smaller cells, which are hypothesised to be limited by macronutrient availability.

Our results indicated poorer spatial correlation of DFe with values of F_v/F_m than with DFe:nitrate ratios. Interestingly, the boundary between Fe-stressed and non-stressed regions was associated with a DFe:nitrate ratio of between $4x10^{-4}$ and $5x10^{-3}$ mol:mol,

which is comparable with the extended average Redfield phytoplankton requirements of ~$1x10^{-3}$ mol:mol (Quigg et al., 2011). Phytoplankton cells should not be directly sensitive to the local ratio of potentially limiting nutrients, responding rather to absolute availability (Moore et al., 2013). Consequently, as in other systems (Hutchins et al., 1998; Moore et al., 2006a; Ryan-Keogh et al., 2013) and theoretical studies (Parekh et al., 2005; Ito et al., 2005), the observed relationship of Fe stress with DFe:nitrate likely reflects large-scale controls on upper ocean nutrient limitation generated by gradients in relative nutrient supply ratios (Ito et al., 2005). Moreover, future work on physiological responses to changing nitrate availability under conditions close to those where Fe is potentially co-limiting (Ryan-Keogh et al., 2013) might allow further assessment of whether F_v/F_m reductions following nitrate additions reflect co-limitation of phytoplankton by Fe and nitrate (Schrader et al., 2011) or simply a transition across a tipping point from nitrate to Fe limitation. Our results also suggested that other factors, including bioavailability, community structure, macronutrient availability and subsequent overall biological demand likely need to be considered alongside absolute DFe concentrations when assessing the potential for the development of regional Fe limitation. Such considerations may be particularly pertinent as the global coverage of DFe data increases rapidly though the GEOTRACES programme.

3 Strong ecophysiological response of phytoplankton to an environmental gradient in the Southern Ocean

Abstract

Photophysiological responses of phytoplankton communities to a suite of environmental changes were assessed on an austral summer-autumn cruise in the Southern Ocean. Clear gradients in the apparent photosynthetic efficiency parameter (F_v/F_m), functional absorption cross sections (σ_{PSII}), reaction centre-II (RCII) specific maximum electron transport rates ($rETR_{max}$) and light limited slopes (α_{ETR}) were observed between productive waters around the North Scotia Ridge (NSR) and the oligotrophic Drake Passage (DP). These photophysiological shifts were likely influenced, yet could not be fully explained, by changes in phytoplankton community structure. Responses of phytoplankton communities to addition of iron (Fe) in a suite of bottle scale manipulation experiments lacked clarity in spatial patterns as a result of the dynamic nature of well mixed NSR waters alongside expected (co-)limitation of some phytoplankton communities by a micronutrient other than Fe, as evidenced by enhanced responses to supply of multiple trace metals through concurrent volcanic ash addition experiments. Contrasting with published field data for the Southern Ocean, phytoplankton communities in DP, expected to be under the most severe micronutrient stress in the cruise region, showed depressed σ_{PSII}. Calculating daily-integrated relative electron transport using modelled mixed layer irradiance and parameters derived from rETR versus irradiance curves for NSR and DP regimes suggested significantly lower RCII-specific electron transport in DP. This is inconsistent with expected patterns of cellular

reaction centre density, and a hypothesis is suggested for this to be a result of the limited ATP and NADPH requirements of slow growing DP phytoplankton communities.

3.1 Introduction

SURFACE waters of the Southern Ocean have year-round elevated concentrations of the macronutrients nitrate and phosphate yet phytoplankton concentrations can be persistently very low (Cullen, 1991). Numerous studies have been designed to investigate this condition and have collectively developed the current paradigm that the availability of light, and concentrations of the essential trace-metal micronutrient Fe, tend to set an upper limit on phytoplankton growth and thereby prevent macronutrient depletion (Mitchell et al., 1991; Nelson and Smith, 1991; de Baar et al., 2005; Boyd et al. 2007). Furthermore, studies have shown that Fe-light co-limitation of phytoplankton plays a fundamental role in regulating not only algal concentrations, but also community structure and physiological attributes (Strzepek et al., 2012; Boyd, 2002; Moore et al., 2007). Both of these factors – which are yet to be reliably observable using remote sensing - are crucial for understanding this biogeochemical system and how it will be affected by future environmental changes (Boyd, 2002; Boyd and Doney, 2002; Le Quéré et al., 2005; Nair et al., 2008; Bouman et al., 2003; Cullen and Lewis, 1995; Behrenfeld et al., 2009).

Fe or light stress, either sub- or supra-optimal with regards to light, induces strong photophysiological responses in phytoplankton (Behrenfeld and Milligan, 2013; Falkowski and Raven, 1997). These photophysiological responses are frequently characterised using specific fluorescence attributes of phytoplankton, yet some of these fluorescence signatures still remain to be unambiguously reconciled with their physiological cause (Behrenfeld and Milligan, 2013). In particular, physiological explanations are yet to be fully resolved where complex iron–light acclimatory

mechanisms are occurring (Sunda and Huntsman, 1997; Strzepek and Harrison, 2004). This is particularly the case for Southern Ocean phytoplankton ecotypes experiencing high variability in these environmental variables (Strzepek et al., 2012).

The Drake Passage (DP)-Scotia Sea region of the Southern Ocean exhibits one of the strongest along-current chlorophyll gradients of the Antarctic Circumpolar Current (ACC). Waters entering the DP from the Pacific sector of the Southern Ocean are extremely phytoplankton poor (oligotrophic) after an extended period of isolation from micronutrient supply (Fan et al., 2006; Boyd et al., 2012). Prior to entering DP, ACC flow at this latitude has almost been uninterrupted zonally and transport of this current over the shallow and rough bathymetry of the Scotia Sea induces some of the strongest turbulent diapycnal mixing in the Southern Ocean (Naveira Garabato et al., 2004; Watson et al., 2013). This mixing combined with the interaction of waters with coastlines have collectively been hypothesised to supply Fe to surface waters, relieve phytoplankton of this growth limiting nutrient, and result in the subsequent chlorophyll blooms in the Scotia Sea observed routinely in satellite images (Moore and Abbott, 2002; Korb and Whitehouse, 2004; Comiso et al., 1993; Sullivan et al., 1993; Holeton et al., 2005; Hopkinson et al., 2007; Holm-Hansen et al., 2004; Nielsdóttir et al., 2012, Ardelan et al., 2010; Venables and Moore, 2010).

Because of these unique attributes, the DP-Scotia Sea region represents an ideal natural laboratory for diagnosing the response of Southern Ocean phytoplankton community structure and photophysiology to a gradient in trace-metal supply. In this study a cruise track from the productive northern Scotia Ridge (NSR) to the low-chlorophyll DP was used to monitor changes in phytoplankton ecophysiology and controlling environmental parameters. Whilst important questions remain to be answered, these measurements, together with the photophysiological responses of phytoplankton in bottle-scale trace

metal addition experiments, have been used to delineate three major photophysiological regimes representative of Southern Ocean waters. Additionally, we have suggested that parameters derived from electron transport rate (ETR) based light curves could potentially allow us to put these results into context with regards to primary productivity and phytoplankton standing stocks.

3.2 Methods

3.2.1 General

Sampling was undertaken in February-March 2012 on the RRS James Cook (JC069) occupying a transect between waters north of the Falkland Islands, along the NSR, and into DP (see Figure 1.8). Samples were either collected using near-surface water from CTD-rosette deployments (5-20 m depth) or a trace metal clean towed fish at around 3 m depth. The towed-fish used a teflon diaphragm pump connected to a clean air compressor to provide suction, and tow-fish to laboratory tubing was cleaned with 10% HCl and Milli-Q washes at the beginning of the cruise and anytime contamination of tubing was thought possible. The pump was turned off when on station, and when turned back on, 30 minutes of flushing time was given prior to any sampling.

Mixed layer depths (MLD) were calculated for sites where CTD profiling was carried out. MLDs were calculated using the threshold method of de Boyer Montegut et al. (2004), where the MLD was identified as the depth where density changes by a threshold value (0.125 kg m^{-3}) relative to that at 10 m depth. Continuous (1 minute resolution) measurements of surface photosynthetically available radiation (PAR) were also made throughout the cruise by two CM 6B pyranometers (Kipp & Zonen) mounted on ship, alongside underway measurements of temperature and salinity. Satellite images of sea surface temperature (SST), chlorophyll-a concentration, and PAR were downloaded in a

range of time-averaged composite formats from the NASA ocean colour website (http://oceancolor.gsfc.nasa.gov/).

3.2.2 Macronutrient and trace metal concentrations

Samples for dissolved macronutrients silicate, phosphate and nitrate + nitrite (hereafter referred to as nitrate) were frozen at -20 °C before being analysed by Malcolm Woodward in the UK (Plymouth Marine Lab) using a micromolar Bran and Luebbe AAIII segmented flow, colourimetric autoanalyser following methods described in Woodward and Rees (2001).

Samples for trace metal analysis were collected from the trace-metal-clean tow-fish system described previously. Samples were filtered in-line through 0.2 µm cartridge filter (AcroPak1000™) into acid washed low density polyethylene (LDPE) sample bottles and acidified with concentrated ultra-pure quartz-distilled hydrochloric acid to pH 1.6 (0.023 M H^+). Trace metal samples were analysed using a modified method from Milne et al. (2010) by isotope dilution inductively coupled plasma mass spectrometry (ID-ICP/MS (Thermo Element XR)) by Christian Schlosser (National Oceanography Centre, Southampton).

3.2.3 Phytoplankton community structure

High performance liquid chromatography (HPLC) samples (0.5–2 L) were filtered onto 0.7 µm Whatman GF/F filters, immediately frozen in liquid nitrogen before storage in a −80 °C freezer. Pigments were extracted into 90% acetone by sonication and analysed using a Thermo HPLC system following the method described in Gibb et al. (2000). The matrix factorisation program CHEMTAX was used to aid with interpretation of the pigments in terms of contributing taxonomic groups to total chlorophyll-a biomass (Mackey et al., 1996) using starting pigment ratios for the different taxonomic groups

from Wright et al. (1996). Using microscopy data, Wright et al. (1996) defined two haptophyte categories, haptophyte-N (represented by *Emiliana huxleyi*) and haptophyte-S (represented by *Phaeocyctis antarctica*). As we did not verify contributions with microscopy, we combined CHEMTAX-derived contributions for each of these categories. In addition to HPLC samples, triplicate samples for fluorometric chlorophyll-a analysis were measured on-ship by filtering samples (100 mL) through 0.7 µm Whatman GF/F filter papers, extracting in the dark in 10 mL 90% acetone for 12-24 hours in a -20 °C freezer, before measuring on a calibrated Turner Designs Trilogy fluorometer (Holm-Hansen et al., 1965).

Cell concentrations of nanophytoplankton, photosynthetic picoeukaryotes (PPEs), *Synechococcus* and *Prochlorococcus* were analysed by analytical flow cytometry (AFC). Samples (2 mL) were fixed with neutralised paraformaldehyde (1% final concentration) and left for 10 minutes in the dark at room temperature before being frozen in liquid nitrogen and transferred to a -80 °C freezer. Samples were thawed at room temperature and analysed using a FACSort flow cytometer according to the methods described in Davey et al. (2008). Data analysis and cell counts were carried out in WinMDI Version 2.8 (Joseph Trotter) flow cytometry analysis software (see Tarran et al. (2001) for example cluster analysis of PPEs, nanophytoplankton, and coccolithophores; and Tarran et al. (1999) for *Synechococcus* and *Prochlorococcus*). Because of preservation (freezing), coccolithophores were likely damaged when analysed, and counts were therefore interpreted qualitatively.

3.2.4 Light absorption spectra of phytoplankton

Samples for phytoplankton absorption were collected and stored as for HPLC samples. Measurements were made using the hot methanol extraction method of Kishino et al.

(1985) using a Shimadzu UV-2550 spectrophotometer equipped with an integrating sphere over the visible range. Optical densities for total (i.e. prior to methanol extraction) and detrital (after extraction) particles were corrected for optical path-length amplification arising from scattering by the filter using the method of Cleveland and Weidemann (1993). Phytoplankton absorption coefficients (a_{ph}) were calculated by subtracting the detrital absorption spectra from the total absorption spectra. Pigment-specific absorption coefficients (a^*_{ph}) were calculated by dividing a_{ph} by HPLC-determined chlorophyll-a concentration. Values of a^*_{ph} at 440 nm (a^*_{ph} (440)) were used as a qualitative indicator for phytoplankton size (Ciotti et al., 2002; Yentsch and Phinney, 1989).

3.2.5 Fast Repetition Rate fluorometry (FRRf)

In a single acquisition protocol, the FRRf ((FAST$^{tracka\ II}$ with integrated FAST^{act} base unit, Chelsea Technologies Group Ltd.)) was set to deliver 64 sequences of one hundred 1 µs sub-saturating flashes at 1 µs intervals followed by twenty five 1 µs relaxation flashes at 84 µs intervals. The RLC protocol was a series of identical FRRf single acquisitions (same settings as for single acquisitions, except sequences per acquisition were reduced to 32), performed under a series of 14 progressively higher PAR intensities ranging from 6 to 1434 µmol photons $m^{-2}s^{-1}$ delivered from the integrated FAST^{act} system. Each illumination step in the RLC lasted for 180 seconds, with 10 second dark steps in between.

Samples were dark-acclimated in opaque plastic bottles for at least 30 minutes prior to analysis and maintained at sea surface temperature by incubating in a water bath of flowing seawater from the ship's underway system. Blanks were run for the majority of samples using the following procedure (after Cullen and Davis, 2003): an aliquot of

roughly 3 mL of sample was gently filtered using a 0.2 μm pore size Nalgene syringe filter unit and a single acquisition FRRf measurement made using the same FRRf settings as the unfiltered sample. The average of fluorescence of a blank was taken (i.e. the mean fluorescence of 125 repetitions of the flash sequence). Minimal variable fluorescence was found in all sample blanks. All sample fluorescence values were subsequently blank-corrected by subtracting the blank from unfiltered samples before any further analysis. As found by Moore et al. (2008) for their study in the North Atlantic sub-tropical gyre, blank fluorescence was found to contribute to ~50% of the signal in the most oligotrophic regions of our study area in DP. Consequently, this correction had a significant effect on derived F_v/F_m values (Cullen and Davis, 2003), and further underscores the importance of implementing a blank correction in these systems.

Fluorescence transients were fit using the model of Kolber et al. (1998) in FASTpro (V1.5) software supplied with the instrument (Chelsea Technologies Group Ltd.). F_v/F_m was calculated as $(F_m\text{-}F_o)/F_m$ (where F_o is the fluorescence at the zeroth flashlet and F_m is the maximum fluorescence), with functional absorption cross sections (σ_{PSII}) recovered from the fit to the model of Kolber et al. (1998). These values of σ_{PSII} are weighted to the spectral region of excitation (light flashes are blue with a peak at ~478 nm, Figure 3.1a), and therefore may be biased by the spectral absorption characteristics of the phytoplankton community present (Figure 3.1b). Following Moore et al. (2006b) this bias was reduced by weighting σ_{PSII} (478) to the spectral distribution of above surface irradiance (an irradiance spectrum from the mid-latitude North Atlantic was used):

$$\sigma_{PSII,\ in\ situ} = \sigma_{PSII}(478)\ \frac{\sum_{400}^{700} a_{ph}^{*}(\lambda)\, E_{in\ situ}(\lambda)\ \sum_{400}^{700} E_{FRR}(\lambda)}{\sum_{400}^{700} a_{ph}^{*}(\lambda)\, E_{FRR}(\lambda)\ \sum_{400}^{700} E_{in\ situ}(\lambda)} \qquad \textbf{(3.1)}$$

Where $E_{in\ situ}(\lambda)$ and $E_{FRR}(\lambda)$ are the *in situ* (i.e. above surface irradiance) and FRR excitation spectra respectably. All quoted values of σ_{PSII} from herein refer to the spectrally corrected values.

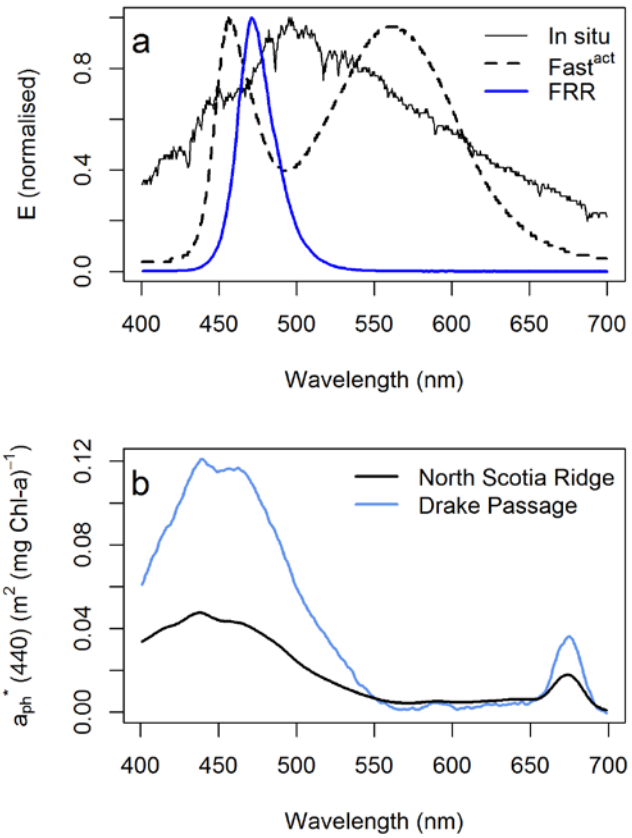

Figure 3.1: Irradiance and phytoplankton absorption spectra. (a) Excitation spectra of the FRR, FAST^{act} and typical in situ irradiance (spectrum above the sea surface in the mid-latitude North Atlantic). (b) Mean phytoplankton specific absorption spectra for the North Scotia Ridge (defined as region I) and Drake Passage (defined as region III). Absorption spectra have been smoothed with a 3-point running mean. See Figure 3.7 and text for definition of regimes I and III.

Relative electron transport rates (rETR) were calculated from the RLC data using Eq. 3.2 (Gorbunov et al., 2001):

$$rETR = E\ \sigma_{PSII} \left(\frac{F_q'/F_m'}{F_v/F_m}\right) \qquad \textbf{(3.2)}$$

where E is the ambient PAR intensity supplied by the FAST^{act} system, $F_q' = F_m' - F_o'$, prime symbols indicate the measurements were made under actinic light, and values of

σ_{PSII} are the spectrally corrected values referred to above (as in Suggett et al., 2006). Calculated rETR's were then fitted to the following function (adapted from Platt et al., 1980):

$$\frac{rETR}{E} = \left(\frac{rETR_{max}}{E}\right)\left(1 - e^{\left(\frac{-\alpha_{ETR}E}{rETR_{max}}\right)}\right) \quad \textbf{(3.3)}$$

where $rETR_{max}$ represents the maximum light saturated ETR plateau and α_{ETR} represents the gradient of the light-limited slope. Normalisation of ETR to irradiance provides a more statistically robust fitting method (Silsbe and Kromkamp, 2012), and improved fit quality at high irradiance where values of rETR were often noisy. The optimum light intensity E_k was calculated as ETR_{max}/ α_{ETR}. Example curve fits of ETR/E versus E are provided in Appendix 1 (Fig. A1.2).

3.2.6 Fe and volcanic ash amendment experiments

Design of amendment experiments followed that of Ryan-Keogh et al. (2013) and Browning et al. (2014) (see Chapters 2 and 4 for further details). Briefly, between 12 and 15 1L polycarbonate bottles were filled with trace-metal-clean water from the towed fish described previously. Bottles were filled at night to reduce effects of light stress on phytoplankton photophysiology. Three bottles were sub-sampled immediately for initial measurements of photophysiology and fluorometric chlorophyll concentrations. Of the remaining bottles, 3 were spiked with 200 µL $FeCl_3$ in a 10% HCl solution resulting in a final Fe concentration of 2 nM, 3 were spiked with varying masses of rhyolite volcanic ash, 3 were spiked with varying masses of basalt volcanic ash, and 3 bottles were sealed immediately with no amendment. The 9 amended bottles and 3 control (non-amended) bottles were sealed around the lids with parafilm, double bagged, and incubated in an on-deck incubator filled with continuously replenished sea surface water from the ships

underway plumbing to limit temperature change of samples. The incubator was shaded with blue screening to reduce irradiance to 35% of above surface values.

After 24 hours the bottles were sub-sampled for photophysiology and chlorophyll concentrations. The index of phytoplankton response from the ash or Fe amendments was a statistically significant increased F_v/F_m over that of the control (non-amended) bottles. Values of $\Delta F_v/F_m$ were calculated ($\Delta F_v/F_m$ = F_v/F_m of amended waters (Fe or ash) – F_v/F_m control bottles) where larger positive values indicated a greater phytoplankton response to amendment (Ryan-Keogh et al., 2013; Browning et al., 2014). One experiment was conducted to assess the longer-term response of the phytoplankton to Fe and ash amendments (IF33). In this particular experiment bottles were sub-sampled for F_v/F_m measurements after 24 hours, but were then replaced in the incubator for a further 24 hours before taking measurements of both F_v/F_m and chlorophyll concentrations. The advantage of our bottle experiments being limited to a relatively short incubation period (i.e., less than 48 hours) is that this limits changes in the taxonomic composition of the phytoplankton community during the incubation, which in our experiments are intended to be indicative of physiology only (Moore et al., 2008; Suggett et al., 2009).

Samples for macronutrients (nitrate, phosphate and silicate) and trace metals were taken prior to the bottle filling procedure described above. All sampling, sub-sampling, ash and Fe spiking was carried out using trace-metal clean techniques in a trace-metal clean container on ship.

3.2.7 Quantifying differences in RCII electron transport between SR and DP

Our approach was as that of Hiscock et al. (2008), except ETR light response curve parameters were used in the place of ^{14}C incubation parameters. The advantage of this approach is the number of curves that were possible to attain throughout the cruise (i.e.

81 experiments relative to 36 in Hiscock et al., 2008). Incident PAR data from the entire cruise period was binned at 1 minute intervals and averaged to give a representative single day 1 minute resolution surface PAR dataset (note that when averaged over the same timescale, incident satellite-retrieved PAR showed minimal spatial variability across the latitudinal range encountered – see Results Section 3.3.1). For each minute these PAR values were then propagated through a 60 m mixed layer (representative of both NSR and DP waters) at 1 m depth intervals to give ~50, 000 discrete PAR occurrences using the following equation:

$$PAR(z) = PAR(0)e^{-K_{d(PAR)}z} \quad \textbf{(3.4)}$$

where PAR(z) is the modelled PAR at depth z, PAR(0) is PAR at the surface, and $K_{d(PAR)}$ is the diffuse attenuation coefficient for PAR. Average values of $K_{d(PAR)}$ were calculated for DP and NSR using the average chlorophyll-a concentrations for the two regimes and the equation of Venables and Moore (2010):

$$K_{d(PAR)} = 0.05 + 0.057Chl^{0.58}. \quad \textbf{(3.5)}$$

The calculation assumes a homogeneous chlorophyll-a concentration throughout the mixed layer, which although not always the case, was confirmed to generally be acceptable upon inspection of fluorescence depth-profiles. Average rETR for each light level from the suite RLCs were calculated for each region, and fit to Equation 3.3 to yield average light curve parameters for the two regions. The resultant equation was then used to calculate rETR's for each discrete PAR occurrence described previously. To account for spectral differences in phytoplankton light absorption between the $FAST^{act}$ light source and *in situ* irradiances (Figure 3.1a), rETR were weighted by a conversion factor calculated from *in situ* (North Atlantic spectrum described previously), $FAST^{act}$, and a_{ph} spectra. Spectral changes in light with depth were not considered, although it should be

noted that this could potentially have some imact on derived rETRs (e.g. Kirk, 1994; Sathyendranath and Platt, 1988). Calculated rETR values were then summed at each light level to produce a relative cumulative electron transport per RCII for each light level.

3.3 Results

3.3.1 Physical oceanography, irradiance, and nutrient regimes

Mixed-layer depths (MLD) varied between around 40 to 120 m with an average of 67 m and no clear spatial pattern (Figure 3.2a). The average irradiance experienced by open-ocean phytoplankton is mainly a function of incident irradiance, $K_{d(PAR)}$, and the MLD. As indicated by Figure 3.2a, measured MLDs were highly variable, mainly dependant on how recently a storm had passed through the region. Furthermore, shipboard PAR retrieved by the pyramometer reflects a snapshot of the irradiance at the time of sampling particular waters. To get a more representative longer term average PAR for the NSR and DP, a February-March 2012 average daily integrated mixed layer PAR was calculated using satellite chlorophyll-a and PAR data for the boxed regions in Figure 3.2a for a MLD range of 30 to 100 m. The average MLD irradiance ($\overline{PAR}_{MLD}$) was calculated using the method of Venables and Moore (2010):

$$\overline{PAR}_{MLD} = \frac{PAR_{sat}}{K_{d(PAR)}MLD}\left(1 - e^{K_{d(PAR)}MLD}\right) \quad \textbf{(3.6)}$$

where PAR_{sat} is the satellite-retrieved average integrated daytime PAR, and $K_{d(PAR)}$ was calculated with Equation 3.5 using the mean satellite-retrieved chlorophyll-a concentration for each box. For a given MLD, differences between the two regions were modest (driven by differences in $K_{d(PAR)}$), yet varied significantly with a change in MLD (i.e., for a 30 m MLD: DP $\overline{PAR}_{MLD}$= 11.0 mol photons m^{-2} day^{-1}; SR $\overline{PAR}_{MLD}$= 8.37 mol

photons m^{-2} day^{-1}, whilst for a 100 m MLD: DP $\overline{PAR}_{MLD}$= 3.8 mol photons m^{-2} day^{-1}; SR $\overline{PAR}_{MLD}$= 2.9 mol photons m^{-2} day^{-1}).

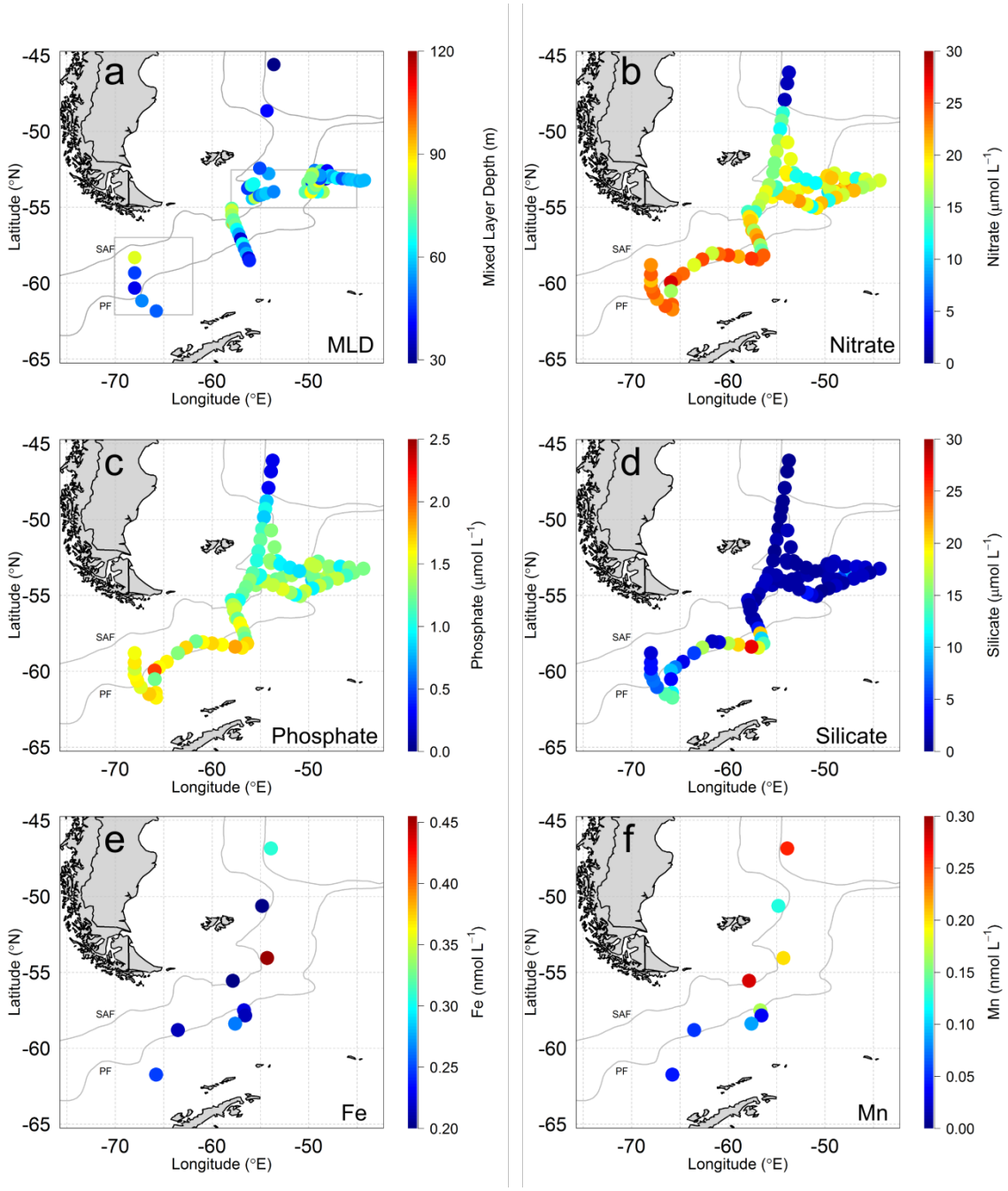

Figure 3.2: Maps of mixed layer depth (MLD) and nutrient concentrations: (a) MLD, (b-d) macronutrient (nitrate, phosphate and silicate) concentrations, and (e-f) micronutrient (Fe, Mn) concentrations. SAF = Sub-Antarctic front, PF = polar front (both from Orsi et al., 1995). Boxes in (a) are the regions over which average satellite-retrieved PAR and chlorophyll-a were been calculated (discussed in text).

Nitrate and phosphate concentrations both showed clear southward increases whilst silicate concentrations increased (reaching 27 nM) upon crossing south of the polar front (Figure 3.2b-d). As reported in detail in Chapter 4, Fe concentrations were generally low (~0.25 nM, although reaching 0.45 nM) and showed no clear spatial pattern (Figure 3.2e). Manganese (Mn) concentrations showed a clearer southward reduction and reached concentrations as low as 0.034 nM, which is amongst the lowest ever measured in seawater (Figure 3.2f).

3.3.2 Chlorophyll-a and phytoplankton community structure

During the cruise period satellite images of chlorophyll-a suggested a consistent phytoplankton bloom across the Scotia Ridge, east of South America and the Antarctic Peninsula, and persistently low chlorophyll-a concentrations in the central DP (Figure 3.3). Daily images revealed the blooming regions around the NSR were often composed of high and low chlorophyll filaments (Figure 3.3 inset). Matching the satellite data, HPLC-determined chlorophyll-a concentrations also showed generally elevated (mean chlorophyll-a of 0.57 mg m^{-3}), although variable (range = 0.05-2.04 mg m^{-3}), concentrations around the NSR, decreasing to lower values in DP (mean concentration of 0.057 mg m^{-3}) (Figure 3.4a).

Specific absorption at 440 nm (a_{ph}^{*} (440)) showed lower values around the NSR than the central Scotia Sea and DP regions, suggestive of larger cells in these higher chlorophyll waters (Figure 3.4b). The use of a_{ph}^{*} (440) values as an indicator of the relative amount of pigment packaging, and therefore cell size, was confirmed by the absence of spatial patterns in the 440 nm specific absorption values reconstructed using HPLC-derived pigment concentrations and the pigment specific absorption spectra of Bidigare et al. (1990). AFC results showed marked reductions in photosynthetic picoeukaryote (PPE)

concentrations between the NSR and DP (Figure 3.4c). Nanoeukaryotic phytoplankton concentrations displayed this trend less clearly, with concentrations at a number of sites in DP showing the same concentrations as the NSR (Figure 3.4d). Also of note was that the significant increase in chlorophyll-a concentrations at 57°S 57°W was not mirrored by an increase in nanoeukaryotic phytoplankton concentrations or an increase in cell size as indicated by a_{ph}^{*} (440) (Figure 3.4a, b, and d). Although likely widespread at low concentrations (Holligan et al., 2010), the presence of coccolithophores identified by AFC analysis suggested significant abundance only in close proximity to the Falkland Islands and in the zone highlighted on Figure 3.4d.

HPLC samples showed a dominant contribution of 19'-Hex and fucoxanthin to total accessory pigments around the NSR and 19'-Hex and 19'-But in the central Scotia Sea and DP region – identified by CHEMTAX as representing diatom-haptophyte and haptophyte dominated communities respectively (Figure 3.3). Prasinophytes, cryptophytes, chlorophytes and dinoflagellates made up small contributions to total chlorophyll-a (always totaling less than 25%). Cyanobacteria, as indicated by the photoprotective pigment zeaxanthin and AFC cell counts of *Synechococcus* and *Prochlorococcus*, were absent from all but the most northerly samples (<47°S for zeaxanthin and *Synechococcus*; *Prochlorococcus* was absent for all samples) (as also found by: Letelier and Karl, 1989; Detmer and Bathmann, 1997), whereas the haptophyte-diatom-dinoflagellate photoprotective pigment diadinoxanthin was ubiquitous (typically 10-20% contribution to total accessory pigments) throughout all samples (Figure 3.3).

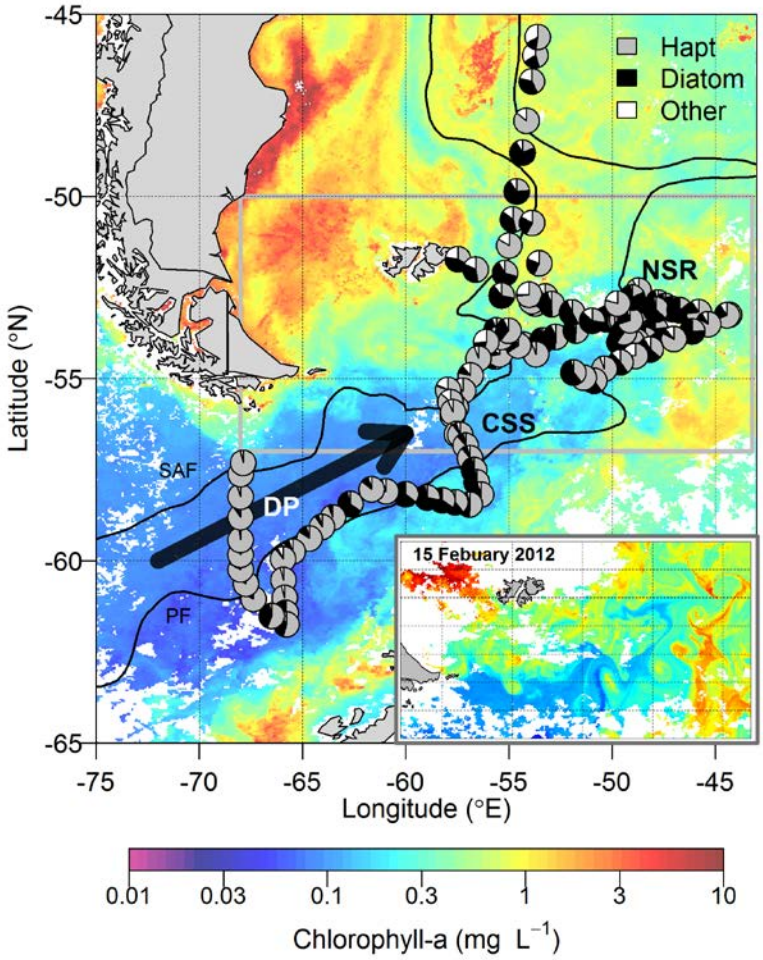

Figure 3.3: Satellite chlorophyll-a and community structure. February-March 2012 satellite chlorophyll-a composite with pie charts showing the relative contributions of dominant phytoplankton types to total chlorophyll-a (as estimated by CHEMTAX). "Hapt" = Haptophyte; "Other" fraction includes prasinophytes, dinoflagellates, cryptophytes, chlorophytes and cyanobacteria. Main sampling regions referred to in the text are labelled: NSR= North Scotia Ridge; CSS= Central Scotia Sea; DP= Drake Passage. Black arrow shows the general direction of the Antarctic Circumpolar Current (ACC). Inset shows 15th February 2012 chlorophyll-a concentration for the region shown by the grey box in the main figure, and highlights the high spatial variability in chlorophyll-a around the NSR.

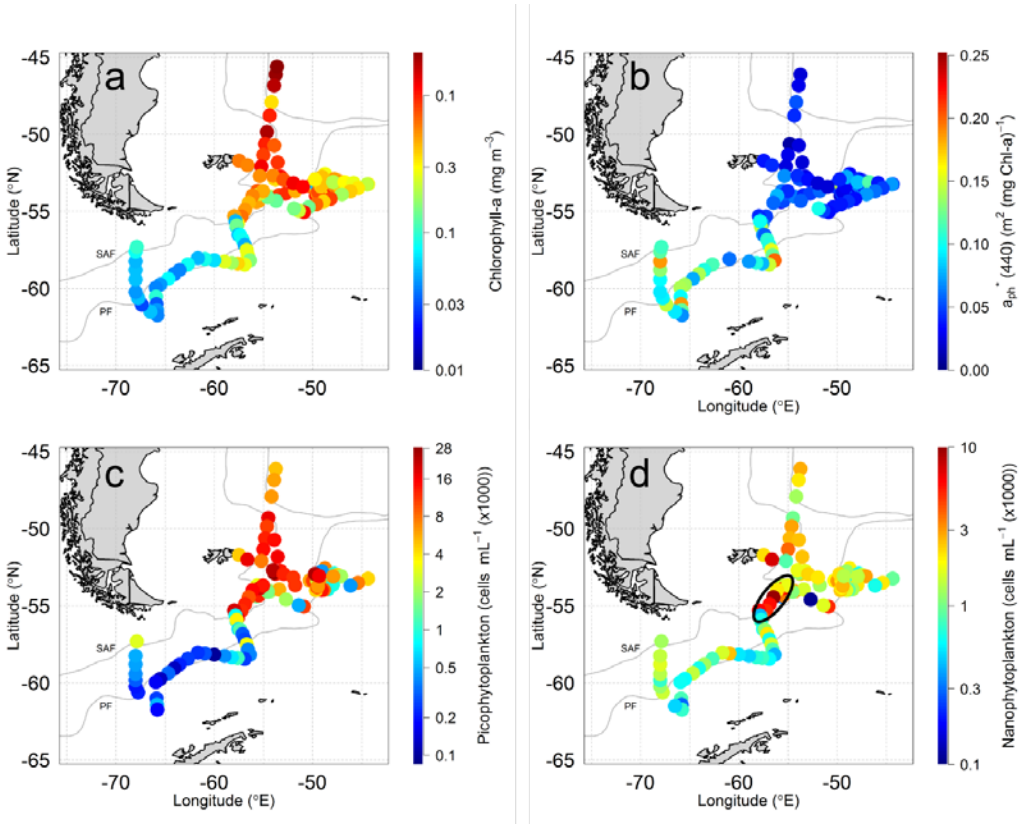

Figure 3.4: Chlorophyll-a concentrations and analytical flow cytometry (AFC) results. Maps of (a) chlorophyll-a concentration, (b) specific absorption at 440 nm, and (c-d) AFC cell counts. Ellipse in (d) highlights the region where coccolithophores were identified in AFC analysis.

3.3.3 Phytoplankton community photophysiology

Night time F_v/F_m and σ_{PSII} generally showed higher values in the NSR, F_v/F_m (but not σ_{PSII}) reduced into the central Scotia Sea, and both parameters showed further reductions into DP (Figure 3.5a-b). Strong daytime reductions in F_v/F_m were observed for NSR samples whist diel variability in σ_{PSII} was absent. The theoretical rate of electron transfer between quinones Q_a and Q_b, $1/\tau_{QA}$, also followed this trend, albeit less clearly, with lower values in DP than the NSR (Figure 3.6a). RLC parameters ETR_{max}, E_k and α_{ETR} all generally showed reductions on moving towards DP from the NSR (Figure 3.6b-d). A stronger correlation between night time ETR_{max} and α_{ETR} (R^2=0.89, p<0.001) was observed than between night time ETR_{max} and E_k (R^2=0.53, p<0.001) (the night time

criterion imposed to remove any possible influence of photoinhibitory or PSII down regulation effects on either parameter). A strong correlation was observed between night time σ_{PSII} and α_{ETR} (R^2=0.90, p<0.001).

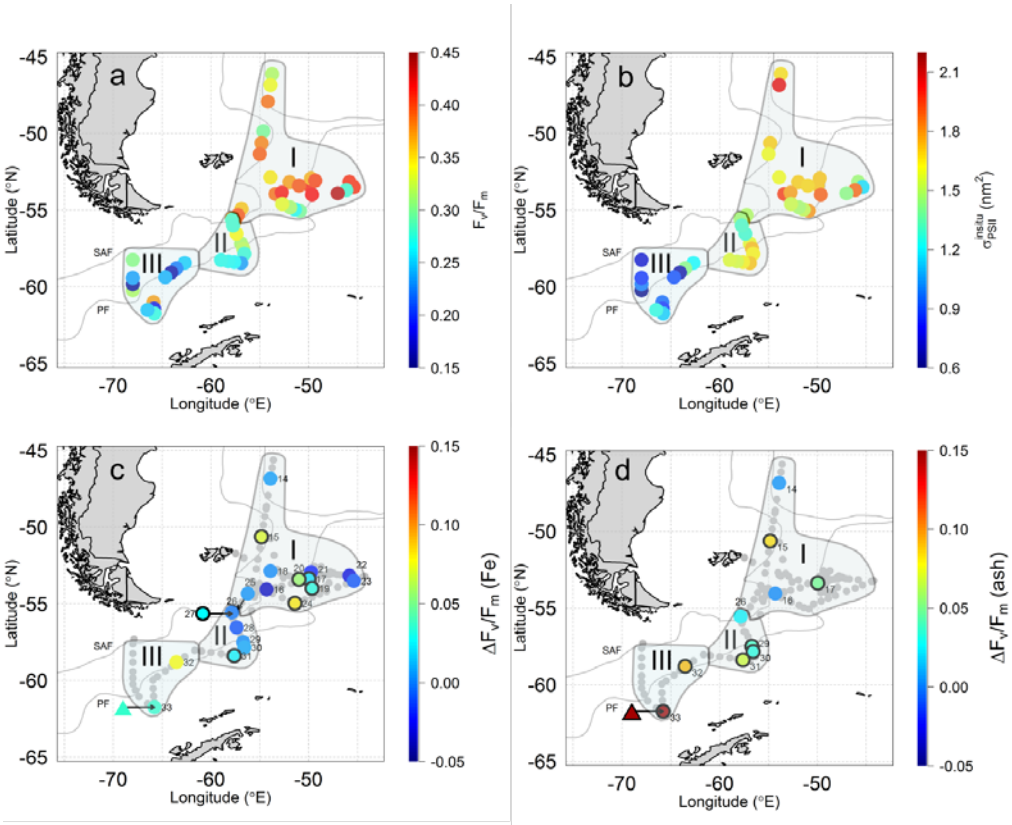

Figure 3.5: Photophysiological variability in phytoplankton communities. Night time values of (a) F_v/F_m and (b) σ_{PSII} (spectrally weighted – see methods). Three photophysiological regimes have been delineated based on the magnitude of the first principle component of the PCA displayed in Figure 3.7. Lower panels show phytoplankton community response to (c) Fe, and (d) ash addition as indicated by $\Delta F_v/F_m$. Ash addition results have been averaged for six replicate bottles amended with either basaltic or rhyolitic volcanic ash. Outlined symbols in (c-d) indicate statistically significant responses (t-test p<0.05). Experiment numbers are also labelled, and regular sampling sites are indicated by grey dots. The locations of experiments 25 and 27 are indicated by arrows. Triangle symbols indicate the response after 48 hours for experiment 33.

3.3.4 Community responses to Fe and volcanic ash amendment experiments

Fe incubation experiments showed no clear spatial trend in terms of F_v/F_m increases subsequent to Fe amendment relative to controls (Figure 3.5c, see also Appendix A2 for full list of F_v/F_m values for each experiment bottle). Statistically significant responses (t-test p<0.05) were seen north east of the Falkland Islands (experiment 15), around the

NSR (experiments 17, 19 and 20), in the more central Scotia Sea (experiments 24 and 27), and for one experiment in the DP (experiment 31). Significant reductions (t-test $p<0.025$) in σ_{PSII} were also observed alongside increases in F_v/F_m for experiments 17, 19 and 20 (i.e. NSR incubations), whilst a reduction was observed in experiment 28. No significant changes in chlorophyll concentrations or $1/\tau_{QA}$ were observed for any of the 24-hour duration experiments. As reported in Chapter 4, responses of phytoplankton to the mixture of trace metals added upon amendment with small quantities of volcanic ash were significantly more pronounced (Figure 3.5d). Where there was any response to either, F_v/F_m increases were always greater than for Fe amended bottles and for a number of experiments there were significant responses where none were detected for Fe addition. Furthermore, for the single experiment continued for 48 hours in DP, significant chlorophyll increases were observed in ash amended bottles whilst no response was observed in Fe-amended ones.

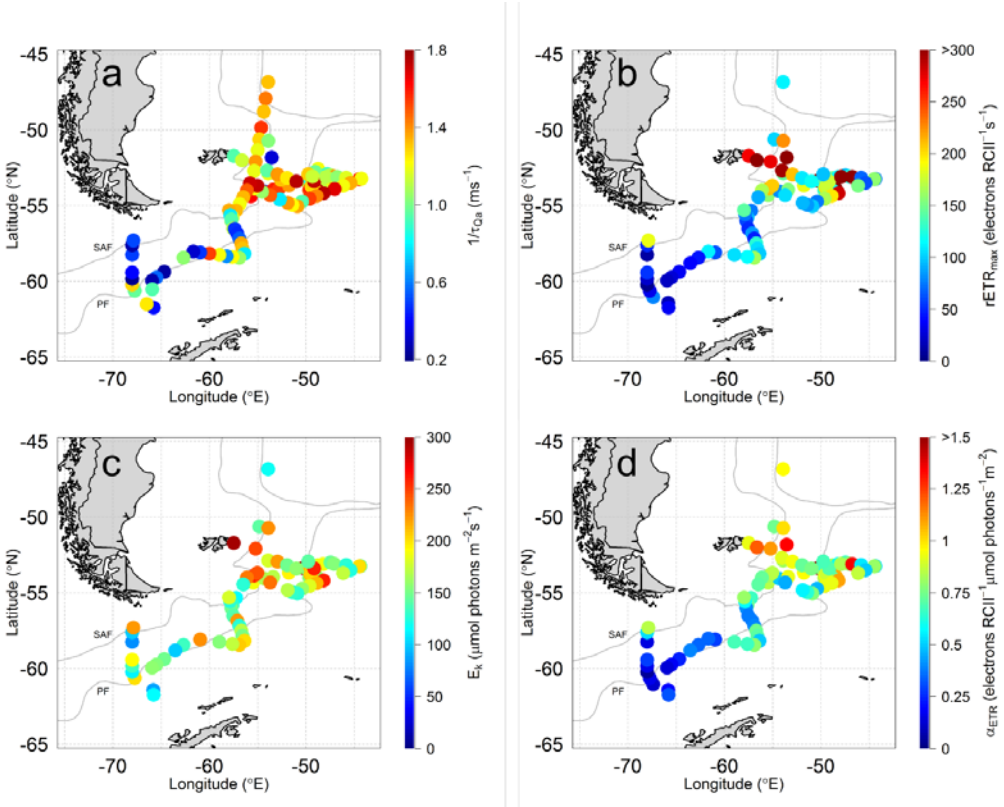

Figure 3.6: FRRf-derived $1/\tau_{Qa}$ and RLC parameters throughout the study region.

3.3.5 Assessment of correlation between ecophysiological and environmental variables

To assess for possible community structure or environmental dependencies of the photophysiological parameters F_v/F_m and σ_{PSII}, a principle component analysis (PCA) was performed for those variables displayed in Figure 3.7b. Despite being an *a priori* candidate for driving photophysiological variability, trace-metal availability, as indicated by seawater trace-metal concentrations or responses to Fe or ash addition, was not included in the analysis because of low sampling frequency. Rather, in this instance the PCA analysis was used to identify co-variability and eliminate other potential environmental controls. The eigenvalues of the data matrix showed that the first two principle components accounted for more than 70% of variability in the dataset, and furthermore that the first principle component (PC1) accounted for nearly 50% of the variability (Figure 3.7a). Thus, displaying the PCA in the PC1 versus PC2 plane revealed two dominant trends of co-variability, with most of the variability explained by PC1 (Figure 3.7b). All variables contributed significantly to the formation of PC1 apart from the contribution of haptophytes and diatoms to total chlorophyll-a, which formed PC2 alongside some contribution from variability in silicate concentration. Therefore, although displaying a continuous trend, values of PC1 could be used to subdivide the dataset into three environmental – photophysiological regimes (Figure 3.7b). When plotted spatially (Figure 3.7c), these regimes broadly occupied the three geographic regions encountered: the NSR, the central Scotia Sea, and DP. Furthermore, these regimes were found to delineate three distinct photophysiological regimes based on night time F_v/F_m and σ_{PSII} (Figure 3.5a-b).

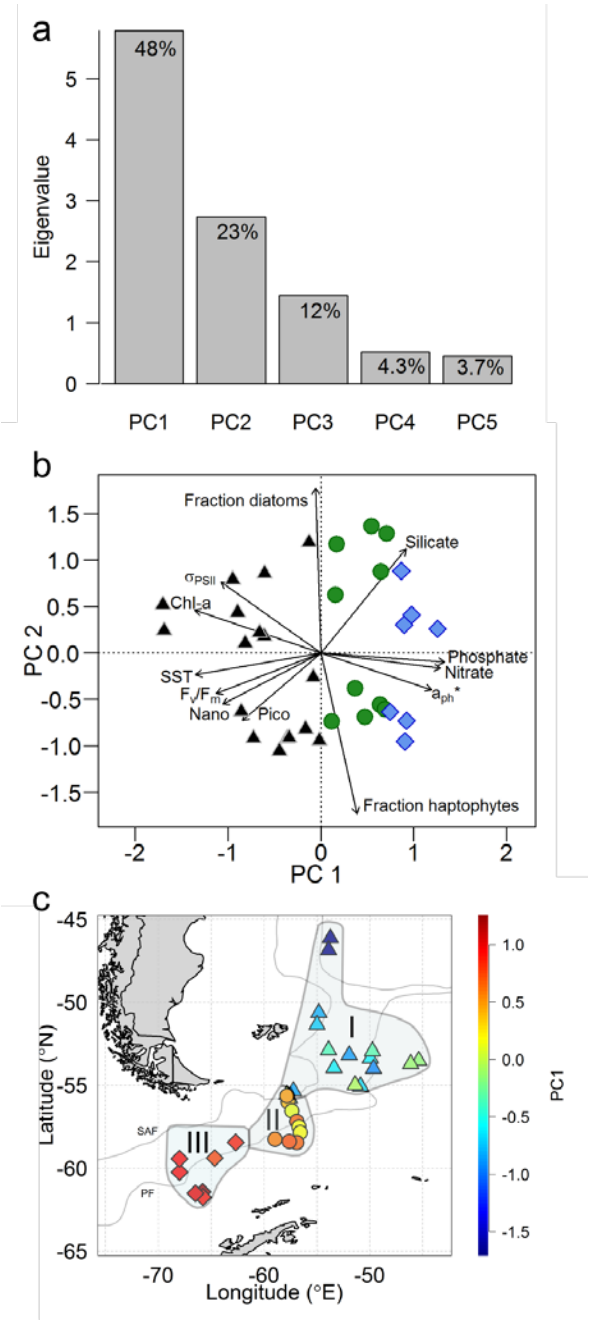

Figure 3.7: Principle component analysis (PCA) of photophysiological data and potentially controlling environmental variables. (a) Screeplot of eigenvalues associated with the first five principle axes of the data matrix used for the analysis. Percent variance explained by each principle component is labelled in each bar. (b) Projection of samples on the plane formed by the first two principle components, with symbols delineating three ranges in PC1, which are displayed geographically in (c). (c) Spatial variability in PC1, values of which divide the study region into three environmental-photophysiological regimes. Only samples collected at night time were included in the analysis to remove any variability in F_v/F_m induced by photoinhibition or PSII down regulation.

3.4 Discussion

As illustrated by the PCA analysis (Figure 3.7), the clear gradient observed in chlorophyll-a concentrations between the NSR and DP (Figure 3.3 and Figure 3.4a) was accompanied by equally pronounced changes in phytoplankton photophysiology (Figure 3.5 and Figure 3.6) and variations in community structure (Figure 3.3 and Figure 3.4b-d). In a spatially dynamic region such as the Scotia Sea, each sampling location has a unique set of interacting environmental and ecological factors that lead to the generation of a particular phytoplankton community expressing a physiological response to its growth environment. Despite this inevitable complexity, FRRf parameters displayed some clear spatial patterns throughout the cruise region (Figure 3.5) that matched the regimes previously delineated using the PCA analysis (Figure 3.7).

Chlorophyll-a concentrations, cell counts of nanophytoplankton and PPEs, and apparent PSII photochemical efficiency (F_v/F_m) correlated inversely with concentrations of nitrate and phosphate (Figure 3.7b), expected to be a result of sufficiency of these particular resources throughout all but the most northerly of samples (Figure 3.2b-c). The relative contribution of diatoms and haptophytes appeared to have other drivers, with silicate concentration being one such control, consistent with the enhanced requirement of this nutrient for diatoms (Figure 3.7b). A similar correlation strength was found between σ_{PSII} and the PC1 drivers macronutrient concentration and SST (e.g., negative correlation with phosphate, R^2=0.28, p<0.001; positive correlation with SST, R^2=0.31, p<0.001), and PC2 drivers' contribution of haptophytes (negative correlation, R^2= 0.28, p<0.001) or diatoms (positive correlation, R^2= 0.21, p<0.001), suggesting factors beyond community structure were influencing this photophysiological parameter (Suggett et al., 2009). Hence, using trends identified in the PCA analysis, alongside the responses of phytoplankton

communities to Fe and volcanic ash addition (Section 3.3.4 and Chapter 4), we suggest a dominant resource-control on community photophysiology that is now considered in a step-wise discussion of the three photophysiological-environmental regimes identified (Figure 3.5 and Figure 3.7).

Around the NSR, waters were characterised by relatively elevated nocturnal F_v/F_m and σ_{PSII} (regime I in Figure 3.5a-b), and rates of Q_a re-oxidation (Figure 3.6a). Elevated F_v/F_m and $1/\tau_{QA}$ is suggestive of sufficient micronutrient availability for reaction centre (RC) synthesis, however some F_v/F_m values were still somewhat lower than that expected for the present communities under optimal growth conditions (~0.4-0.65, Suggett et al., 2009) suggesting some phytoplankton communities were possibly close to the onset of resource (e.g., Fe) limitation. Indeed, amendment of phytoplankton with Fe produced some significant positive F_v/F_m responses suggesting spatial patchiness in Fe stress patterns and showing evidence of some communities having crossed into Fe limited growth conditions (Figure 3.5c). Similar patchiness was observed in patterns of chlorophyll-a concentrations (Figure 3.3 and Figure 3.4a), which again could be a result of mixing between waters of variable Fe availability. Within the NSR waters, no correlation between F_v/F_m and chlorophyll-a concentration was found ($R^2<0.001$, $p>0.9$). This is not particularly surprising as the onset of Fe stress is a physiological response that is itself a function of Fe bioavailability per cell relative to other resources; whereas the phytoplankton standing stock is a function of, amongst other controls (e.g. dilution, dispersion, grazing, light), bulk Fe supply to waters (e.g. Moore et al., 2013). Recovery of $1/\tau_{Qa}$ was not observed during 24 hour Fe addition incubation experiments where significant F_v/F_m responses were seen (for any experiments). However, elsewhere in the Southern Ocean, relief of Fe limitation produced reductions in $1/\tau_{Qa}$ rates only after incubations times of 72 hours - concluded to be due to the additional time required to

synthesise Fe-rich cytochrome b_6/f and/or PSI complexes (Moore et al., 2007; Hopkinson et al., 2007, although note this at odds with the interpretation of Greene et al., 1992). The strong daytime reductions in F_v/F_m observed in this regime were suggestive of significant photodamage or PSII down-regulation that did not relax during the 30 minute dark acclimation period, however this could also reflect some longer lived NPQ, such has been observed in diatom cultures (Milligan et al., 2012).

Concurrent elevated σ_{PSII} in this regime is also suggestive of communities being close to Fe stress, with resource-replete phytoplankton typically displaying lower values (e.g. Boyd and Abraham, 2001; Moore et al., 2007; Hopkinson et al., 2007). Supporting this were reductions in σ_{PSII} subsequent to Fe amendment for several (but not all) experiments in the region that showed simultaneous increases in F_v/F_m. A good correlation was observed between night time σ_{PSII} and chlorophyll-a concentration for NSR waters (R^2=0.52, p<0.0005), which could be interpreted as a factor regulating light availability, with lower light expected to favour larger σ_{PSII} to maintain light harvesting. However, for this region no significant correlation was found between σ_{PSII} and the MLD (p>0.5, n=14), which was the parameter shown to be the dominant control of average mixed layer irradiance for the two regions (i.e., over and above $K_{d(PAR)}$). Alternatively, the elevated σ_{PSII} could simply be an adaptive signature of the community being sampled - selected for under these conditions that are not reflected in culture isolates from other regions (Strzepek, et al. 2012).

At the southern limit of the NSR and in the central Scotia Sea, the continued reduction of PC1 (Figure 3.7c) was accompanied by a clear photophysiological shift to lower night time F_v/F_m, whilst σ_{PSII} was generally maintained at similar values (regime II in Figure 3.5a-b). Typically these observations would have been interpreted as a shift to Fe limited growth conditions (e.g. Behrenfeld and Milligan, 2013), yet our manipulation

experiments showed none-to-minimal response to Fe addition and strong responses to the concoction of trace metals supplied from low mass volcanic ash additions (Figure 3.5c-d). A conclusive explanation for this finding remains to be found and is discussed in detail in Chapter 4. Briefly, the low night time F_v/F_m in this regime is suggested to reflect the onset of a combination of Fe- and Mn (co)limitation (supplied by the ash but not the Fe spike), which is supported by the extremely low Mn seawater concentrations found, alongside the relatively enhanced availability of other biologically important metals. Again, although our interpretation is inconclusive, we suggest that without our coincident ash addition experiments it would have been difficult to assign the low F_v/F_m to Fe limited or trace metal co-limited conditions as there appears to be no diagnostic trait in variable chlorophyll fluorescence measurements to distinguish between the two. More easily explained are the maintained elevated values of σ_{PSII} that are commonly found under conditions of Fe limitation where RC construction is retarded whilst, with their lower micronutrient-resource requirement LHCs are still being synthesised (Greene et al., 1991, 1992; Geider et al., 1993b; Vassiliev et al., 1995; Davey and Geider, 2001; Boyd and Abraham, 2001; Moore et al., 2006a, 2007; Hopkinson et al., 2007).

An abrupt shift in this pattern was found however on moving west, further into the oligotrophic conditions of DP which had the highest values of PC1 (Figure 3.7b-c) (regime III in Figure 3.5a-b). Although inevitably susceptible to lower signal: noise ratios in variable fluorescence measurements, there was clear evidence of reductions in σ_{PSII} accompanying low F_v/F_m. This behaviour has rarely been seen in the ocean yet has been observed in the laboratory subsequent to Fe-starvation of phytoplankton cultures (Vassiliev et al., 1995). This reduction was interpreted by Vassiliev et al. (1995) to reflect an Fe stress induced disconnection of LHC from RCII, which is supported by more recent studies consistently finding disconnected LHCs under Fe stress (Bibby et al.,

2001; Desquilbet et al., 2003; Moseley et al., 2002). For example, Moseley et al. (2002) proposed the disconnection was a result of the reduced activity of Fe-containing aerobic oxidative cyclase, which catalyses the oxidative closure of the fifth ring characteristic of all chlorophylls (Allen et al., 2008). However, these studies have been focussed on PSI – light harvesting centre connectivity and relatively little exists in the literature regarding connectivity of antennae to PSII (although see Morales et al. (2001), for discussion relating to PSII in sugar beet leaves). Regardless, this interpretation would suggest one could identify between severities of Fe stress on a scale of low F_v/F_m – low σ_{PSII} (severe Fe stress), depressed F_v/F_m – elevated σ_{PSII} (moderate Fe stress), high F_v/F_m (Fe replete). The first characterises DP, yet because of the results of our amendment experiments, the interpretation cannot be attributed simply to Fe stress but more generally to trace metal stress (with an expectation of Mn (co)limitation, Chapter 4). As an alternative or additional explanation, phytoplankton could be reducing σ_{PSII} as a photoprotection mechanism to prevent reaction centre damage that would reduce photochemical efficiencies further still (e.g. Demmig-Adams et al., 1990).

Unfortunately, the response of low σ_{PSII} samples to Fe or ash addition during amendment experiments was not tested. DP waters were used for manipulation experiments, but in the particular waters experiment samples were collected from, none had a particularly low initial σ_{PSII}. However, as Vassiliev et al. (1995) reported rises and subsequent reductions in σ_{PSII} on timescales of 10-30 hours (see Figure 5b of Vassiliev et al., 1995), it could be hypothesised that significant changes in this parameter may not have been observed in our 24 hour duration experiments.

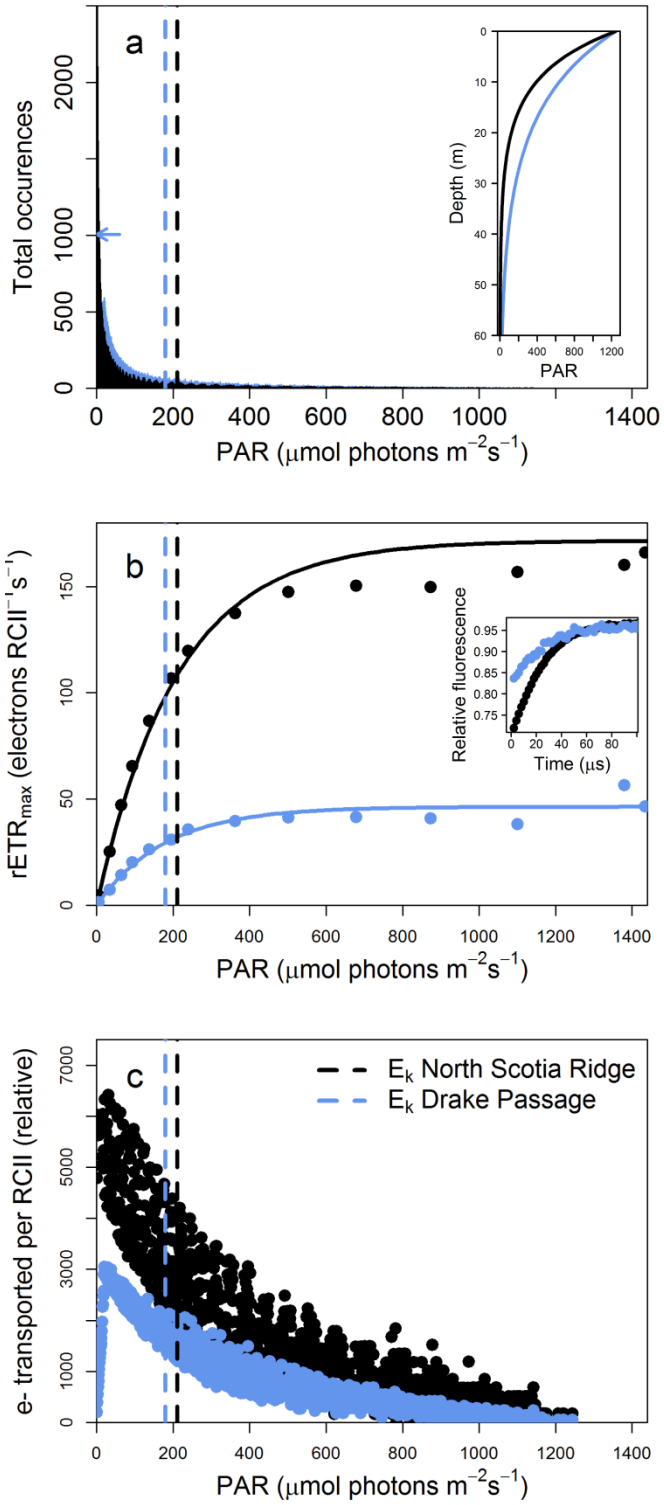

Figure 3.8: Reduced RCII electron flow as a potential result of resource limitation (approach as for Hiscock et al. (2008)). (a) Histogram of representative daily PAR occurrence at 1 m intervals throughout the mixed layer, (b) average light curves, and (c) relative daily cumulative electron flow per RCII for each PAR value (rounded integers) in (a), for NSR (black) and DP (blue) regions (regimes I and III respectably, defined in Figure 3.6 - Figure 3.7). Region-specific E_k values derived from the average RLCs are indicated by dashed lines. Insets show: (a) the decrease in PAR with depth for the midday maximum PAR value in the simulations; and (b)

regime-averaged relative fluorescence for the initial portion of the fluorescence transient, highlighting the reduced gradient (effectively σ_{PSII}) of DP phytoplankton communities that results in reduced α_{ETR}. The reduction in rETR for DP (blue) at low irradiances in (c) is a result of the relatively lower occurrence of these PAR values within the mixed layer (the maximum occurrence is highlighted with a blue arrow in (a) – the maximum for NSR extends beyond the y-axis limit) resulting from the shape of depth profiles of PAR generated for these low-$K_{d(PAR)}$ waters (inset in (a)).

Reductions in F_v/F_m, σ_{PSII}, and $1/\tau_{QA}$ between NSR and DP were accompanied by decreases in light curve parameters $rETR_{max}$ (ETR_{max} per RCII), α_{ETR}, and to a lesser extent, E_k (Figure 3.6b-d). Previous studies, away from the Southern Ocean, have found low values of $rETR_{max}$ to be a result of photoacclimation to low light intensities as a result of increases in cellular RC density, without coincident reductions in σ_{PSII} (Moore et al., 2006b; Chapter 1). However, reduced σ_{PSII} is controlling factor for the low $rETR_{max}$ found in DP (see Equation 3.2). Additionally, a reduction in temperature (from ~10 to ~2°C) could also be mediating the reduction between NSR and DP regimes by regulating enzyme-mediated rates of carbon fixation downstream of photosynthetic light reactions.

As for $rETR_{max}$, significantly lower light limited slopes (α_{ETR}) were found in DP than in the NSR (Figure 3.6d). This similar pattern to σ_{PSII} (R^2=0.9, $p<0.0001$) is expected to be the result of a common physiological control between the two (Falkowski and Raven, 1997), limiting transfer of light energy between LHCs and RCII. This reduction in α_{ETR} is of significance as it considerably reduces the total RCII-specific electron flow a given day, because phytoplankton are predominantly experiencing light levels less than E_k. For example, propagating cruise-averaged minute-resolution daily irradiance through a 60 m mixed layer resulted in 73% (DP) and 86% (NSR) of resultant irradiance values being less than a region-specific E_k (Section 3.2.7, Figure 3.8a). Moreover, calculating a daytime cumulative mixed layer rETR for the two regions using these irradiance values produced significantly lower values for DP, where 47% of the difference between the regions was at light levels less than E_k (Figure 3.8c). This potentially reinforces the

findings of Hiscock et al. (2008) who, using a similar type of analysis with ^{14}C-based photosynthesis-irradiance curves, suggested that Fe limitation was hindering primary production in the Southern Ocean specifically by reducing light use efficiencies. However, in the present study we can attribute this difference to both reductions in quantum yields (F_v/F_m) and light harvesting and transfer (σ_{PSII}), and possibly associate this with trace metal co-limitation rather than simply a lack of Fe. A caveat to this interpretation is the limitation inherent in calculating and using rETRs (i.e. electron transfer per RCII): reaction centre number per cell could ultimately be controlling rETRs as the two scale inversely (e.g. Moore et al., 2006b). However, performing the same analysis with chlorophyll or carbon specific ETRs would be expected to further exacerbate differences between DP and the NSR, due to the particularly heavy trace-metal requirement of reaction centres and therefore an expectation of fewer reaction centres per cell in DP.

The underlying physiology behind a micronutrient-stress-induced σ_{PSII} reduction is difficult to assess with the suite of parameters we measured, and therefore we can only speculate as to its meaning. As mentioned previously, an inverse relationship between F_v/F_m and σ_{PSII} has typically been observed between Fe-stressed and Fe-replete waters (e.g. Boyd and Abraham, 2001; Moore et al., 2007; Hopkinson et al., 2007). This has been interpreted as increased LHC: RCII with increasing severity of Fe stress that limits synthesis of RCII's but not LHC's. This photophysiological shift would favour increased electron transport per RCII to maintain ATP and NADPH production for cell metabolism and growth under Fe-stressed conditions (Behrenfeld et al., 1998; Behrenfeld et al., 2008). However, under the cold, particularly micronutrient–scarce conditions of Drake Passage, where growth rates are presumably low (e.g. Eppley, 1972; Raven and Geider, 1988; Sedwick et al., 1999; Reay et al., 2001; Hopkinson et al., 2007; Rose et al., 2009),

maintained ATP and NADPH production might be unnecessary, with only a limited demand for these to satisfy a slow metabolism. Importantly, this photophysiological response would limit the energetic cost of RCII repair likely accompanying a larger σ_{PSII}.

3.5 Conclusions

The availability of Fe and light limit the standing stock of phytoplankton in large areas of the Southern Ocean (Boyd, 2002). Furthermore, evidence for possible co-limitation by other essential micronutrients such as Mn and Co-containing vitamin B12 is growing (Bertrand et al., 2007; Middag et al., 2013; Chapter 4). Nutrient and light stress induce strong photophysiological signatures in phytoplankton yet there are uncertainties to be addressed when interpreting these signatures and their influence on phytoplankton standing stocks and growth rates – particularly for Southern Ocean phytoplankton communities (Strzepek et al., 2012). Here some key photophysiological traits have identified that vary largely independently of phytoplankton community structure along an environmental gradient in the Southern Ocean. Furthermore we have demonstrated a link between growth environment and variability in RCII-specific electron transport rates, which is difficult to explain on the basis of photoacclimation. Based on previous studies in the Southern Ocean, reduced σ_{PSII} and the resultant influence on α_{ETR} in DP were not anticipated. The oceanographic extent of this condition may be limited to those regions and seasons being most trace metal depleted (e.g. DP in austral summer). Indeed, the scarcity of field data showing reduced σ_{PSII} under micronutrient-stressed conditions may be representative of the rarity of this condition. Interestingly, although also observed by Vassiliev et al. (1995) this response in σ_{PSII} is not consistently found in laboratory studies starving phytoplankton of Fe either (Greene et al., 1991, 1992; Geider et al., 1993; Davey and Geider, 2001), although differences in culturing protocols in experiments (e.g.,

growth irradiance, temperature, acclimatory time period) could perhaps offer an explanation for this.

Although deemed to be strongly influenced by micronutrient stress, the underling physiology behind our observations remains inconclusive and we have only made suggestions as to their cause. New understandings of physiological responses of phytoplankton cultures to micronutrient stress are emerging (e.g. Allen et al., 2008; Thamatrakoln et al., 2013; Strzepek et al., 2012). Reconciling fluorescence-derived apparent photochemical efficiency and functional absorption cross sections with their physiological cause is a requirement for a more conclusive interpretation of ETR in natural, micronutrient stressed regions (e.g. Ryan-Keogh et al., 2013; Schrader et al., 2011; Strzepek et al., 2012). This is particularly important as diagnosis of phytoplankton ETR response to changes in micronutrient and light supply could be a valuable tool for both monitoring, and testing, phytoplankton responses to the multiple environmental changes projected to occur in the future (Boyd and Hutchins, 2012). Indeed, surface ocean warming in the Drake Passage region is projected to be amongst the fastest occurring globally (e.g., Boyd and Doney, 2002; Boyd et al., 2002), and thus may be a site where such monitoring could be most pertinent. Despite the clear ecological relevance of rETRs, quantifying electron transport may ultimately provide a method for estimating carbon-based primary productivity, although this does present substantial additional challenges (Lawrenz et al., 2013).

4 Strong responses of Southern Ocean phytoplankton communities to volcanic ash

A modified version of this chapter has been published as: *Browning, Bouman, Henderson, Mather, Pyle, Schlosser, Woodward, & Moore* (2014), Strong responses of Southern Ocean phytoplankton communities to volcanic ash, *Geophysical Research Letters.*

Abstract

Volcanic eruptions have been hypothesised as an iron supply mechanism for phytoplankton blooms, however little direct evidence of stimulatory responses has been obtained in the field. Here we present the results of 21 1-2 day bottle enrichment experiments from cruises in the South Atlantic and Southern Ocean that conclusively demonstrated a photophysiological and biomass stimulation of phytoplankton communities following supply of basaltic or rhyolitic volcanic ash. Furthermore, experiments in the Southern Ocean demonstrated significant phytoplankton community responses to volcanic ash supply in the absence of responses to addition of dissolved iron alone. At these sites, dissolved manganese concentrations were amongst the lowest ever measured in seawater and we therefore suggest that the enhanced response to ash may have been a result of the relief of manganese (co-)limitation. Our results imply that volcanic ash deposition events could trigger extensive phytoplankton blooms, potentially capable of significant impacts on regional carbon cycling.

4.1 Introduction

PHYTOPLANKTON growth in the high-nitrate low-chlorophyll (HNLC) regions of the world's oceans is limited by the availability of iron (Fe) (Boyd et al., 2007). Experiments that have artificially supplied Fe to HNLC waters triggered significant phytoplankton responses, typically including: an increase in overall biomass, an increased apparent efficiency of photochemical energy conversion (F_v/F_m), and a shift in the species composition of phytoplankton towards a diatom-dominated community (Boyd et al., 2007). This biogeochemical response to Fe fertilisation has the potential to sequester CO_2 from the atmosphere into the deep ocean. Although the efficiency of such sequestration remains uncertain, recent studies have suggested that significant carbon export is probable under the right conditions (Blain et al., 2007; Smetacek et al., 2012).

The delivery of volcanic ash to Fe-limited waters has been hypothesised as a natural fertilisation mechanism, whereby the dissolution of Fe-rich soluble salts on the surface of ash particles (or possibly the ash itself) supplies Fe and potentially relieves limitation (Duggen et al., 2010). Volcanic-ash fertilisation of remote Fe-limited waters was proposed to cause the detected atmospheric CO_2 drawdown after the Pinatubo 1991 eruption as a result of post-fertilisation increases in marine primary productivity (Watson et al., 1997). Furthermore, this fertilisation mechanism has been hypothesised to drive large-scale perturbations to biogeochemical cycles and climate observed in geological or ice-core records (Bay et al., 2004; Cather et al., 2009).

To date, evidence for the volcanic ash fertilisation hypothesis has generally relied on either measuring trace metals released from ash (e.g. Olgun et al., 2011, 2013; Duggen et al., 2007; Achterberg et al., 2013), detecting the response of phytoplankton cultured in the laboratory to ash addition (Duggen et al., 2007; Hoffman et al., 2012), or observing

post-eruptive phytoplankton blooms using remote sensing (Hamme et al., 2010; Langmann et al., 2010; Achterberg et al., 2013). Recent results from a bottle-enrichment experiment in the North Atlantic have demonstrated the fertilisation potential of Icelandic volcanic ash in a region not normally considered to be a classic HNLC system (Achterberg et al., 2013), while a positive phytoplankton community response to ash addition after a four-day time lag has recently been reported for the HNLC North Pacific (Mélançon et al., 2014). Until now, however, the response of phytoplankton to ash fertilisation in the Southern Ocean, the most biogeochemically significant HNLC system (Sigman et al., 2010), has remained untested. Here we present the results from a suite of Fe and volcanic-ash addition experiments conducted across a range of oceanic regimes (subtropical gyre, productive shelf, and HNLC waters – see Figure 1). These provide clear evidence for the potential for volcanic ash deposition to stimulate phytoplankton growth in the Southern Ocean.

4.2 Methods

Incubation experiments were carried out on consecutive cruises in the South Atlantic and Southern Ocean from January to March 2012 (Figure 4.1, Table 4.1, and Table 4.2). The experimental setup followed that described in Chapters 2 and 3, and involved pumping surface seawater (from 2-3 m depth with a trace-metal clean tow-fish system) into twelve 1 L bottles, analyzing initial phytoplankton condition from 3 of these bottles, spiking three sets of 3 replicates with either 2 nmol L^{-1} $FeCl_3$ (200 µL $FeCl_3$ in 10% HCl (Ryan-Keogh et al., 2013)), basaltic ash, or rhyolitic ash, and sealing the final 3 immediately with no amendment (using trace metal clean techniques at all stages, including seawater pumping). Bottles were placed in an on-deck incubator filled with continuously replenished sea-surface water from the ship's underway water system and shaded with

blue screening to provide 35% of above surface irradiance. After 24 hours incubation with ash or Fe (and 48 hours for experiment 12), the bottles were sub-sampled for phytoplankton photophysiology (using Fast Repetition Rate fluorometry (FRRf) (Kolber et al., 1998)), and chlorophyll concentrations (fluorometric technique (Holm-Hansen et al., 1965)). Active chlorophyll fluorescence measurements using FRRf, were used to calculate the apparent photochemical efficiency of photosystem II (F_v/F_m), providing a sensitive and rapidly responding indication of relief from Fe limitation (Behrenfeld and Milligan, 2013). Specifically, the index of a phytoplankton response from the ash or Fe amendments was a significant increase in F_v/F_m, over that of three control (non-amended) bottles ($\Delta F_v/F_m$ = F_v/F_m Fe or ash amended bottles – F_v/F_m control bottles (Ryan-Keogh et al., 2013)).

Two ash types were used for the 21 sets of fertilisation experiments conducted (3 replicates per experiment, therefore totalling 63 ash-enriched bottles): 34 were pristine basalt samples, collected downwind from Etna (Sicily) in Giardini Naxos following an overnight ash fall in November 2002; 29 were rhyolite samples, collected in 2008 from Chaitén (Chile) a few weeks after emplacement from a location 151 km downwind from the vent. Chaitén ash was sample 05-20A of Watt et al. (2009): longitude= -43.594; latitude= -71.112; ash layer thickness= 6 mm; modal grain size= 67 µm.

The various masses of ash used in experiments ranged between 0.1 and 250 mg ash L^{-1} of seawater, representing realistic ash fluxes to surface waters and dilution within the surface ocean mixed layer (i.e. dilution of hypothetical 0.004 mm or 11 mm thick ash layers (a relatively conservative range – see Figure 4.1) respectively over a 50 m mixed layer depth). The following works through this calculation.

<u>Bulk ash densities (as determined in the field)</u>

Etna = ~1.3×10^6 g m^{-3} (Scollo et al., 2007)

Chaitén = ~1×10^6 g m^{-3} (Watt et al., 2009)

Average = 1.15×10^6 g m^{-3}

Minimum loading (0.004 mm ash layer)

$$\text{Mass of 0.004 mm ash layer per m}^2 = \frac{0.004\ \text{mm}}{1000} \times 1.15 \times 10^6\ \text{g m}^{-3} = 4.6\ \text{g m}^{-2}$$

$$\text{Ash concentration when mixed over 50 m} = \frac{4.6\ \text{g}}{50\ \text{m}} = 0.1\ \text{gm}^{-3} = 0.1\ \text{mg L}^{-1}$$

Maximum loading (11 mm ash layer)

$$\text{Mass of 11 mm ash layer per m}^2 = \frac{11\ \text{mm}}{1000} \times 1.15 \times 10^6\ \text{g m}^{-3} = 12650\ \text{g m}^{-2}$$

$$\text{Ash concentration when mixed over 50 m} = \frac{12650\ \text{g}}{50\ \text{m}} = 254\ \text{g m}^{-3} = 254\ \text{mg L}^{-1}$$

At each site additional water samples were collected alongside experimental water to constrain the initial nutrient regime and phytoplankton community present. The phytoplankton community structure was determined by analyzing the accessory pigment composition using high-performance liquid chromatography (HPLC) (Gibb et al., 2000), and using the CHEMTAX program for assessing the contribution of phytoplankton types to total chlorophyll biomass (Mackey et al., 1996). Temperature, salinity and photosynthetically available radiation (PAR) data were collected continuously on both cruises by shipboard instruments. Level 3 satellite images of chlorophyll concentration were downloaded for the cruise periods from the NASA Ocean Colour website (http://oceancolor.gsfc.nasa.gov/). Total Ozone Mapping Spectrometer (TOMS) UV Aerosol Index products for the Hudson 1991 eruption period were downloaded from NASA (http://ozoneaq.gsfc.nasa.gov/index.md).

Dissolved seawater trace-metal concentrations were determined by Christian Schlosser (National Oceanography Centre, Southampton) using isotope dilution inductively

coupled plasma – mass spectrometry (ID-ICP-MS (Thermo Element XR)) for iron (Fe), zinc (Zn), copper (Cu), nickel (Ni) and cadmium (Cd), and standard addition ICP-MS for manganese (Mn) and cobalt (Co) (Milne et al., 2010). Macronutrient concentrations (nitrate+nitrite, nitrite, phosphate, and silicate) were determined by Malcolm Woodward at Plymouth Marine Labs using a segmented flow colourimetric autoanalyser (Woodward and Rees, 2001). Estimates of metal requirements for natural phytoplankton communities were taken from Bruland et al. (1991) based on data published by Martin et al. (1976) and Martin and Knauer (1973). Metal: P ratios for the natural phytoplankton communities in these studies were compared with seawater ratios determined in this study.

Short duration leaching experiments were conducted to characterise the release of trace metals from the two types of ash used. Masses of ash ranging between 4.5 and 25 mg were added to 10 mL of Milli-Q water in acid-washed Teflon vials, gently agitated for around one second and left for 2 hours. Ash loadings in the leaching experiments represented a balance of being reflective of the low loading of the incubation bottles in the field experiments, yet sufficient to produce a detectible change in metal concentrations in the solvent. An aliquot of the mixture was then filtered (0.2 µm Whatman Puradisc 30 disposable syringe filter) for analysis. A procedure was developed to quantify trace metals absorbed onto the sides of the vial during the two hour period. This involved discarding the remaining ash-solvent mixture, rinsing the vials 3 times with Milli-Q water, adding 2 mL of 5% HCl, leaving for one hour, and finally measuring the trace-metal concentrations redissolved from the vial wall into the acid. Low-blank, trace-metal clean, cleaning and handling techniques were used throughout and all leaching procedures were carried out in a trace-metal-clean laboratory. Three blanks were run with every six ash samples to quantify contamination from the beakers, syringes,

filters, and acid. Subsequent to blank correction, the trace metals in the Milli-Q water and those adsorbed to the sides of the vial were summed to give a total metal release from the ash (Table 4.2). Relative to seawater experiments this would represent an upper level of trace metal release due to the more acidic nature of Milli-Q over seawater and because the experiments were conducted at room temperature (ca. 20°C) rather than the colder conditions of the Southern Ocean.

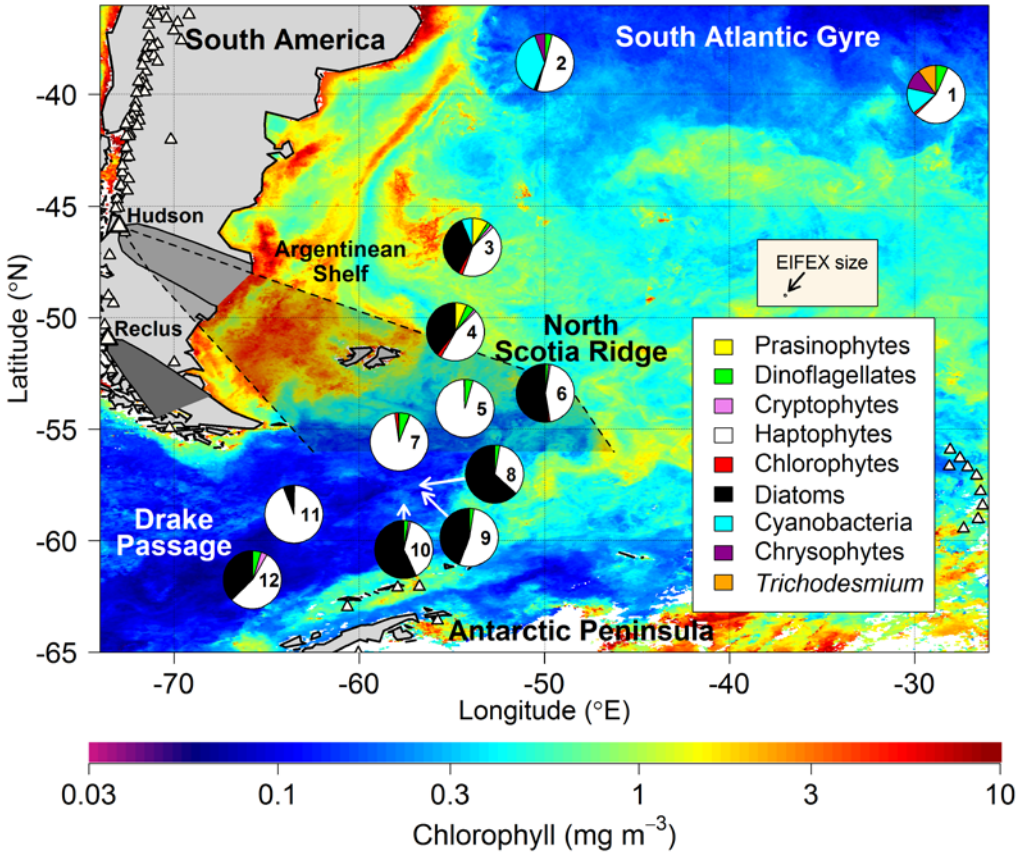

Figure 4.1: Phytoplankton types and chlorophyll concentrations at experimental sites. Background image shows a January-to-March 2012 satellite composite of chlorophyll concentrations from MODIS (http://oceancolor.gsfc.nasa.gov/). Overlain pie charts represent the dominant phytoplankton types present in waters at each experimental site. Experiment numbers are labelled. Triangles show the locations of volcanoes thought to have been active in the last 10, 000 years (Global Volcanism Program, http://www.volcano.si.edu/index.cfm). To illustrate the potential scale of natural ash additions in this region, volcanic ash deposition from two Quaternary volcanic eruptions are shown (grey shaded regions enclosed in solid lines): >10 mm isopach (ash thickness) for the Hudson 1991 eruption (Scasso et al., 1994) (light grey); and >30 mm isopach for the ca. 14.8 cal ka BP Reclus R1 eruption (Stern, 2008; Fontijn et al., 2014) (dark grey). Note that, although likely extending into open ocean waters, no Reclus isopachs (dark grey) have been mapped further south than the region highlighted. The shaded region bounded by the dashed line represents the 15th August 1991 Hudson ash cloud extent from the TOMS aerosol

index (UV Aerosol Index 4.5 a.u. contour, http://ozoneaq.gsfc.nasa.gov/index.md). For scale, the size of the 167 km^2 Fe-fertilised patch for the European Iron Fertilisation Experiment (EIFEX) is shown by a circle in the inset box.

4.3 Results and Discussion

Initial phytoplankton biomass, community structure, and macronutrient concentrations showed expected patterns for the oceanic provinces encountered. Chlorophyll concentrations increased from the South Atlantic Gyre to the Argentinean Shelf and North Scotia Ridge before declining significantly in the Drake Passage (Figure 4.1 and Table 4.1). Phytoplankton community structure showed a general north-to-south shift from haptophyte-cyanobacteria dominated communities in gyre waters to haptophyte-diatom dominated communities in the Southern Ocean (Figure 4.1). Nitrate and phosphate increased from low, depleted values in gyre waters to much increased values in the Drake Passage (Figure 4.2a), whilst silicate increased south of the polar front (Table 4.1). Concentrations of the trace-metal micronutrients Fe and manganese (Mn) generally demonstrated a north-to-south reduction (Figure 4.2b-c and Table 4.1). Concentrations of Mn in the surface waters of Drake Passage reached as low as 0.034 nmol L^{-1}, representing some of the lowest values ever measured in seawater, comparable with previous minimal Southern Ocean values (~0.04 nmol L^{-1}) (Middag et al., 2011; 2012; 2013). Bruland et al. (1991) reported metal: P values of (averages of the two studies, nmol L^{-1}:µmol L^{-1}): Fe = 5.1 (in situ dissolved seawater ratio measured in this study was 0.51); Zn = 1.32 (0.78); Mn = 0.39 (0.20); Cu = 0.28 (2.31); Ni = 0.28 (13.18); Cd = 0.26 (0.53). Although considerable plasticity in requirements needs to be taken into account (e.g., Twining and Baines, 2013), based on this comparison seawater ratios suggest an excess of phytoplankton community requirements for Zn, Cu, Ni, Cd, and deficiency of Fe and Mn.

Table 4.1: Initial (untreated) seawater nutrient, trace-metal and chlorophyll concentrations for experiments.

Cruise	Exp	Initial macronutrients (µmol L^{-1})			Initial trace metals (nmol L^{-1})													Initial chlorophyll (µg L^{-1})
		Nitrate	Phosphate	Silicate	Fe		Mn		Zn		Cu		Ni		Cd		Co	
JC068	1	0.03	0.13	0.9	0.40	±0.039	0.40	±0.039										0.18
JC068	2	0.04	0.04	0.73	0.21	±0.015	0.21	±0.015										0.26
JC069	3	1.75	0.27	0.35	0.31	±0.022	0.26	±0.009	0.24	±0.033	1.43	±0.098	4.10	±0.323	0.02	±0.002	0.01	±0.000	1.89
JC069	4	15.55	1.1	0.6	0.20	±0.021	0.12	±0.005	0.31	±0.036	0.67	±0.057	4.89	±0.358	0.11	±0.008	0.03	±0.002	1.27
JC069	5	20.58	1.38	0.98	0.45	±0.042	0.20	±0.010	3.10	±0.256	0.92	±0.066	5.24	±0.369	0.24	±0.019	0.03	±0.001	0.36
JC069	6	18.03	1.25	1.03															1.23
JC069	7	20.35	1.45	1.54	0.20	±0.015	0.28	±0.012	0.84	±0.102	0.77	±0.045	8.76	±0.469	0.31	±0.023	0.02	±0.000	0.14
JC069	8	16.21	1.31	20.56	0.23	±0.019	0.16	±0.007	1.77	±0.154	1.23	±0.079	5.97	±0.423	0.39	±0.020	0.03	±0.001	1.01
JC069	9	13.96	1.2	10.19	0.21	±0.018	0.03	±0.002	0.93	±0.085	1.06	±0.104	6.04	±0.342	0.26	±0.016	0.02	±0.000	0.67
JC069	10	25.15	1.8	27.04	0.26	±0.024	0.09	±0.004	2.26	±0.182	1.11	±0.088	6.35	±0.442	0.33	±0.022	0.02	±0.002	0.83
JC069	11	17.98	1.27	5.74	0.22	±0.018	0.05	±0.002	0.67	±0.069	0.97	±0.070	5.74	±0.347	0.17	±0.011	0.02	±0.001	0.09
JC069	12	22.68	1.61	14.18	0.25	±0.025	0.05	±0.002	0.77	±0.065	1.16	±0.083	5.98	±0.427	0.20	±0.011	0.02	±0.001	0.13

For trace metals, the dissolved seawater concentration ± the standard deviation is shown

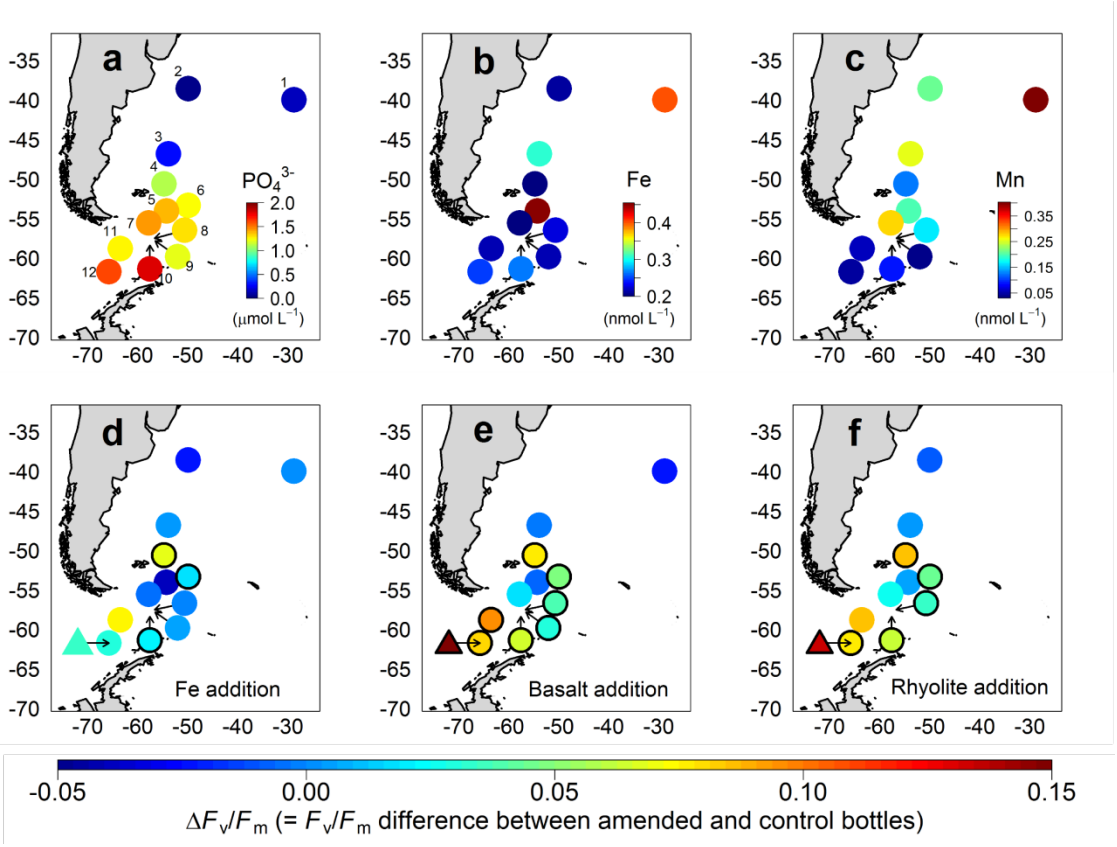

Figure 4.2: Seawater nutrient concentrations and the response of phytoplankton to iron and ash additions. Dots represent the locations of experiments, with colours representing the nutrient concentration (a-c) or the level of phytoplankton response (d-e). Experiment numbers are labelled in (a). Nitrate concentrations showed a strong correlation with phosphate (a) ($R^2 = 0.97$; $p<0.001$). For (d)-(e): $\Delta F_v/F_m = F_v/F_m$ of waters amended with iron spike (d) or ash (e and f) – F_v/F_m control bottles (Ryan-Keogh et al., 2013); circular symbols represent the response after 24 hours incubation, triangles after 48 hours incubation; black outlines around symbols indicate a statistically significant response from amended bottles over control bottles (t-test $p<0.05$). Arrows point to the sites of experiments 8, 9, 10 and 12 (labelled in (a)).

Of the 23 sets of triplicate bottles amended with ash, 18 sets produced statistically significant (t-test $p<0.05$) increases in F_v/F_m relative to control (non-amended) bottles. For the remaining 5 experiments, located in macronutrient-depleted South Atlantic waters (experiments 1 and 2) and three sites around the Falkland Islands (experiments 3, 5 and 7), there was no response to either Fe or ash addition. In marked contrast to previous experiments performed in the North Atlantic (Achterberg et al., 2013), phytoplankton responses to ash addition were always greater than those in Fe-spiked bottles (Figure 4.2d-f, Table 4.2, see also Appendix A2 for full list of F_v/F_m values for

each experiment bottle). Particularly enhanced responses from phytoplankton amended with ash, relative to those amended only with Fe, were found in the vicinity of Drake Passage (Figure 4.2d-f and also see Figure 4.3) – a region widely assumed to be severely Fe limited (Martin et al., 1990; Hopkinson et al., 2007), and containing some of the lowest chlorophyll concentrations in the Southern Ocean (<0.1 mg m^{-3}).

Table 4.2: Ash addition experiments conducted.

Cruise	Experiment	Mass basalt added (mg)				Mass rhyolite added (mg)			$\Delta F_v/F_m$ Fe	$\Delta F_v/F_m$ Basalt	$\Delta F_v/F_m$ Rhyolite
		Bas 1	Bas 2	Bas 3	Bas 4	Rhy 1	Rhy 2	Rhy 3			
JC068	1	18.8	27	20.8					0.004	0.004	
JC068	2					39.2	38.1	44.7	-0.020		-0.020
JC069	3	17.4	20.1	18.4		19.3	37.9	48.3	0.006	0.000	0.006
JC069	4	3.1	16.1	192.3		15.2	234.6	215.9	0.070*	0.078*	0.087*
JC069	5	1.7	196.6	61.3		1.7	14.6	253.8	-0.036	-0.004	0.007
JC069	6	2.1	16.4	169.2		2.1	13.4	139.7	0.019*	0.051*†	0.046*†
JC069	7	1.3	16.4	13.2		0.6	9	1	-0.002	0.020†	0.029†
JC069	8	3.8	6.3	60.7		10.9	0.1	11.4	0.002	0.040*	0.036*
JC069	9	4.1	19.1	0.1					0.007	0.032*	
JC069	10	5.5	0.7	22.8		17.3	14.1	26	0.024*	0.066*	0.065*
JC069	11	4.4	8.8	21.2		0.1	18.2	4.9	0.077	0.096*	0.087
JC069	12 (24hr)	2.3	4.8	8.5	18.7		35.8	6	0.033	0.083*	0.079*
JC069	12 (48hr)								0.035	0.149*†	0.135*†

* Significant (t-test $p<0.05$) F_v/F_m responses

† Significant (t-test $p<0.05$) chlorophyll responses

Note that all experiments were run for 24 hours. Only experiment 12 was continued for an additional 24 hours to assess the longer timescale response of phytoplankton to Fe or ash amendment. $\Delta F_v/F_m$ indicates the F_v/F_m difference between triplicate amended (Fe or ash) and control bottles.

In order to limit the potential for confounding taxonomic changes to influence the interpretation of physiological (F_v/F_m) responses (Suggett et al., 2009), experimental durations were typically kept short enough (24 hours) to prevent significant increases in biomass (Table 4.2). However, within the single experiment run over a longer timescale

in Drake Passage, both F_v/F_m and chlorophyll concentrations in the ash amended bottles increased significantly above that of the control and Fe amended bottles (Figure 4.3). Significantly enhanced physiological and growth responses were thus observed for ash-amended phytoplankton.

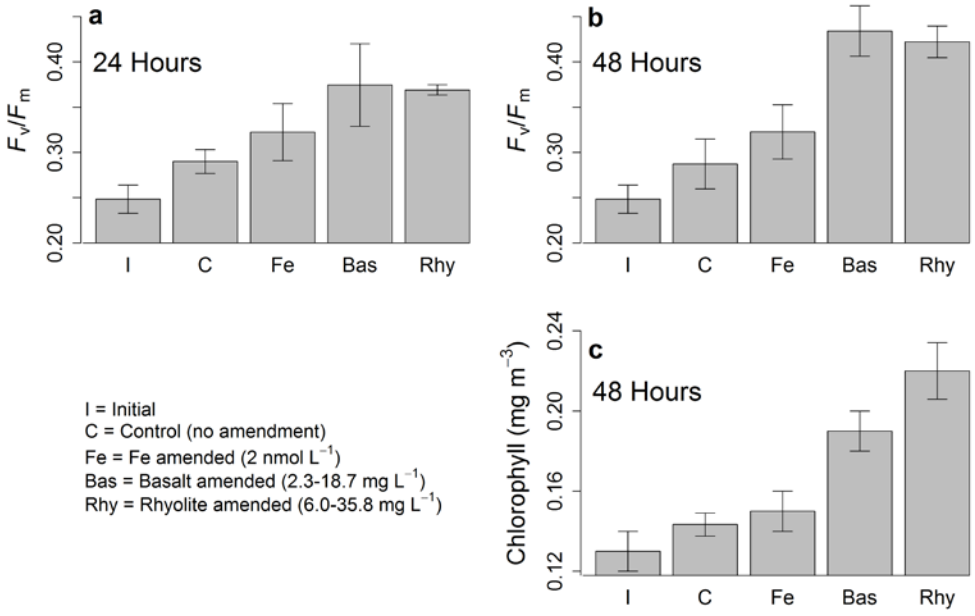

Figure 4.3: Phytoplankton response to ash addition in Drake Passage (Experiment 12): (a) and (b) show the initial photophysiological status and response after 24 and 48 hours respectively; (c) shows the initial chlorophyll concentration and response after 48 hours.

There are a number of possible explanations for why the volcanic ash additions stimulated phytoplankton more than Fe-only additions. A difference in total Fe supply between treatments appears to be unlikely for several reasons: (i) While some of the ash loadings were potentially capable of releasing more Fe than the 2 nmol L^{-1} Fe-spike (Figure 4.4), this level would typically already be expected to be capable of relieving phytoplankton Fe stress. Overall biological demand for Fe might be expected to be relatively lower in the Drake Passage, where the lowest phytoplankton concentrations were observed. Drake Passage sites nonetheless responded to ash addition but not to the Fe-only spike, while other sites responded significantly to the same Fe-only amendment.

(ii) Comparing the results of the laboratory ash leaching experiments for the two ash types suggested that the rhyolitic ash likely released significantly less Fe than the artificial Fe spike (see Table 4.3 and Figure 4.4). (iii) Despite differential Fe release per unit mass of ash (around 100% for a given ash type in leaching experiments, likely due to a heterogeneous distribution of soluble trace metals in/on the ash - see Table 4.3), alongside significant variability in total loadings (Figure 4.4), similar phytoplankton responses were observed across bottles. For example, within experiment 12 the mass of ash added to individual bottles varied by an order of magnitude yet the relative standard deviation of responses between bottles was less than 20%. Overall, the total Fe added during amendment (ash or spike) thus appeared to be an unlikely determining factor in phytoplankton responses.

Table 4.3: Summary of results from the volcanic ash leaching experiments.

Ash type	Metal (nmol / g ash)											
	Fe		Mn		Zn		Cu		Cd		Pb	
Basalt	589.10	±631.47	5.80	±4.32	5.072	±10.66	6.147	±5.83	0.001	±0.01	0.10	±0.17
Rhyolite	18.79	±13.29	12.50	±8.812	8.78	±9.28	5.503	±5.30	0.006	±0.01	0.01	±0.10

Values show metal release into Milli-Q water per gram of ash ± standard deviation for 6 replicates.

Addition of acidified $FeCl_3$ will increase oxidised Fe(III) to concentrations that would promote rapid Fe precipitation unless immediately complexed by biologically produced organic ligands (Schlosser et al., 2011). In contrast, ash may release significant reduced Fe (II) (e.g. from $FeCl_2$ or FeF_2 salts (Duggen et al., 2010)), which could persist in cold Southern Ocean waters for several hours prior to oxidation (Croot and Laan, 2002). Furthermore the dissolution or release kinetics of Fe from ash particles could result in a more continuous supply of Fe (II) for a limited period (~up to 1 hour (Olgun et al.,

2011)). As the Drake Passage waters were the coldest encountered (~2 °C for surface waters) and might be expected to be characterised by low organic ligand concentrations due to low overall biomass (Boye et al., 2001), semi-continuous Fe (II) delivery from ash resulting in a greater effective bioavailability to the resident phytoplankton population, could be considered possible. However, the ubiquity of the enhanced ash response across >3 orders of magnitude in ash loading (Figure 4.4), argues against such an explanation. We therefore consider (co-)limitation of phytoplankton by another essential trace metal nutrient to be the most likely explanation for the marked enhancement in phytoplankton response to ash addition.

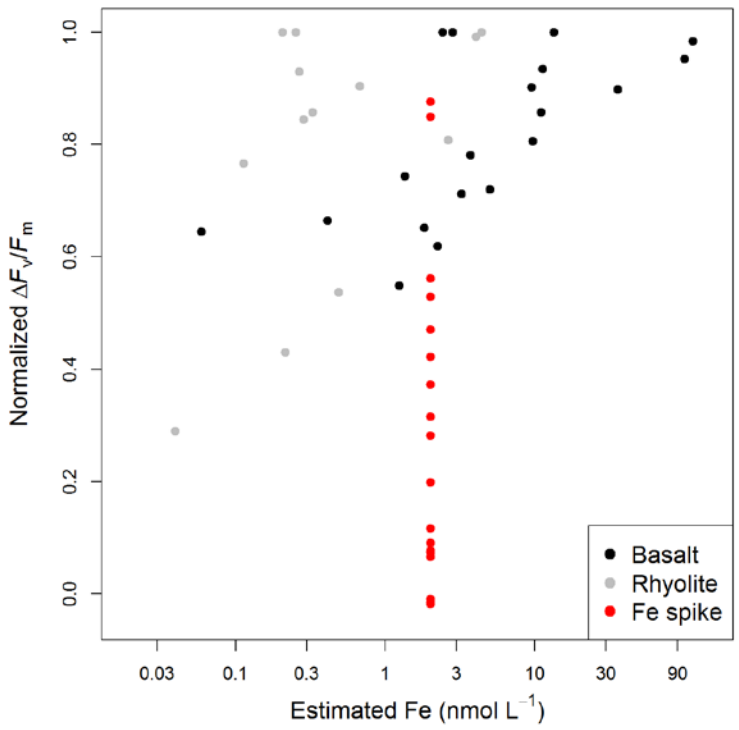

Figure 4.4: Phytoplankton response as a function of estimated Fe supply in bottle experiments. Each point represents a single ash or Fe amended bottle, and only experiments that showed a statistically significant response to either Fe or ash amendments are shown. Fe supply from volcanic ash was calculated using results from leaching experiments (i.e. Fe release per mass of ash multiplied by mass of ash added to each bottle). To make experiments more readily comparable, phytoplankton response to ash or Fe amendment ($\Delta F_v/F_m$, see Figure 4.2 caption) has been normalised to the maximum response observed in each experiment.

Co-limitation of phytoplankton by Mn in Drake Passage was suggested as early as 1990 by Martin and co-workers (Martin et al., 1990), although no subsequent direct evidence has been found. Our Mn data demonstrated surface concentrations in this region to be amongst the lowest ever measured in seawater (Figure 4.2c) (Middag et al., 2011, 2012, 2013), with dissolved Mn:Fe ratios as low as 0.16 being typically below phytoplankton cellular Mn:Fe ratios (Moore et al., 2013). Mn is required for a variety of biological processes, including as an essential and non-substitutable cofactor in the oxygen-evolving complex of photosystem II within the light reactions of photosynthesis (Morel et al., 2003). Moreover, Mn requirements and Mn:Fe ratios may be particularly enhanced under Fe limitation (Middag et al., 2013; Peers and Price, 2004), with relief of Fe-Mn co-limitation resulting in enhanced growth and F_v/F_m in laboratory phytoplankton cultures (Peers and Price, 2004). The basaltic ash released far more Fe than the rhyolitic ash, while, in contrast, both ashes released similar amounts of Mn (Table 4.3). Consequently, we suggest that the observed similarity in enhanced phytoplankton responses to both ash types indicates the potential significance of relief of Mn (co-)limitation.

The clear phytoplankton responses we observed to ash addition have important implications for Southern Ocean biogeochemistry. Enhanced phytoplankton growth following ash addition would be expected to increase the flux of CO_2 between the atmosphere and the surface ocean organic carbon pool, and potentially drive a shift to larger, more-rapidly sinking taxa (Boyd et al., 2007; Smetacek et al., 2012; Moore et al., 2007) enhancing carbon export to the deep ocean where it can remain sequestered for centuries or longer (Sigman et al., 2010; Williams and Follows, 2011). In comparison to the recent European Iron Fertilisation Experiment (EIFEX), where a few thousand tonnes of carbon was estimated to be sequestered from a fertilisation area of only 167 km^2 (Smetacek et al., 2012), the much larger aereal extent (Figure 4.1) and enhanced

stimulatory response (Figure 4.2d-f and Figure 4.3) that would likely accompany a major ash deposition event could potentially result in regionally or even globally significant carbon sequestration (Watson et al., 1997).

4.4 Conclusions and wider implications

Although requiring further verification, both of our suggested explanations for the significantly enhanced stimulatory response to ash over that of Fe alone (namely greater bioavailability of ash-released Fe (II) and/or the release of (co-)limiting Mn) would have important biogeochemical implications. Specifically, we suggest that significant changes in the biogeochemistry of Drake Passage, which currently represents some of the lowest-chlorophyll high-nitrate waters found anywhere in the surface ocean, may not simply depend on overall increases in Fe supply. Rather, the form of external Fe delivery may be significant and/or an accompanying Mn input might be required to drive significantly enhanced productivity and carbon export. Thus, for example, as sedimentary Fe sources might be expected to be accompanied by Mn (e.g. Measures et al., 2013; Hatta et al., 2013), the combined input of both Fe and Mn may be partially responsible for near coastal phytoplankton responses observed in Drake Passage (e.g. Hopkinson et al., 2007).

Irrespective of the exact cause for our observations, erupted volcanic material appears to be an effective fertiliser for this region. The Drake Passage and the western margin of the South Atlantic are areas of the Southern Ocean that are highly prone to tephra deposition from explosive volcanic eruptions (Olgun et al., 2011; Fontijn et al., 2014). Large late-Quaternary eruptions from volcanoes of both the Andean Austral and Southern Volcanic Zones have deposited considerable volumes of andesitic to rhyolitic tephra across the Drake Passage, and into Antarctica (Stern, 2008; Narcisi et al., 2012); while several eruptions per century from Patagonian volcanoes have delivered tephra to the western

reaches of the South Atlantic (Scasso et al., 1994). Rates and sizes of eruptions may well have varied significantly between peak-glacial and post-glacial times, depending on the extent of ice cover across Patagonia (Watt et al., 2013). Consequently, there is the potential for long timescale variability in the extent of ash-driven fertilisation and carbon export from these waters.

5 Satellite-detected fluorescence: decoupling non-photochemical quenching from iron stress signals in the South Atlantic and Southern Ocean

A modified version of this chapter has been published as: *Browning, Bouman, & Moore* (2014), Satellite detected fluorescence: decoupling non-photochemical quenching from iron stress signals in the Southern Ocean, *Global Biogeochemical Cycles.*

Abstract

Satellite detected sunlight induced chlorophyll fluorescence could offer valuable information about the physiological status of phytoplankton on a global scale. Realisation of this potential is confounded by the considerable uncertainty that exists in deconvolving the multiple ecophysiological processes that can influence the satellite signal. A dominant source of current uncertainty arises from the extent of reductions in chlorophyll fluorescence caused by the high light intensities phytoplankton are typically exposed to when satellite images are captured. In this study, results from over two hundred non-photochemical quenching (NPQ) experiments conducted on cruises spanning from subtropical gyre to Southern Ocean waters have confirmed that satellite fluorescence quantum yields have the potential to reveal broad regions of iron (Fe) stress. However, our results suggest significant variability in phytoplankton NPQ behaviour between oceanic regimes. Dynamic NPQ must therefore be considered to achieve a reliable interpretation of satellite fluorescence in terms of Fe stress. Specifically, significantly lower NPQ was found in stratified subtropical gyre-type waters than in

well-mixed Southern Ocean waters. Such variability is suggested to result from differences in incident irradiance fluctuation experienced by phytoplankton, with highly variable irradiance conditions likely driving phytoplankton to acclimate or adapt towards a higher dynamic NPQ capacity. Sea surface temperature empirically demonstrated the strongest correlation with NPQ parameters and is presented as a means of correcting the chlorophyll fluorescence signature for the region studied. With these corrections, a decadal composite of satellite austral summer observations is presented for the Southern Ocean, potentially reflecting spatial variability in the distribution and extent of Fe stress.

5.1 Introduction

CHLOROPHYLL fluorescence is the emission of red light, which at least under non-nutrient-stressed conditions, arises almost exclusively from chlorophyll-a pigments in photosystem II (PSII), subsequent to excitation by absorbed photons (Falkowski and Kiefer, 1985). Sunlight-induced chlorophyll fluorescence (SICF) has been studied and interpreted as an indicator of chlorophyll concentrations (e.g. Hu et al., 2005), photosynthetic rates (Kiefer et al., 1989; Topliss and Platt, 1986), and the photophysiological status of phytoplankton (Letelier et al., 1997; Morrison, 2003; Schallenberg et al., 2008; Behrenfeld et al., 2009; Morrison and Goodwin, 2010; Huot et al., 2005, 2013; Westberry et al., 2013). All three of these applications of SICF require estimation or calculation of the quantum yield of fluorescence (ϕ_F, see Table 5.1), the ratio of light fluoresced by chlorophyll-a pigments to total light absorbed by phytoplankton. Recently, studies have suggested that higher values of satellite-derived ϕ_F (ϕ_{sat}) could provide an indication of phytoplankton nutrient stress (Letelier et al., 1997; Huot et al., 2005), particularly under Fe-limiting growth conditions (Behrenfeld et al., 2009).

Fe stress has been shown to increase chlorophyll-a normalised fluorescence of phytoplankton in laboratory and field studies (Geider et al., 1993b; Sakshaug and Holm-Hansen, 1977; Schrader et al., 2011). The exact physiological mechanisms underlying this response are still debated, but are thought to be a combination of Fe stress induced shifts to a higher ratio of photosystem II (PSII) to largely non-fluorescent, but highly Fe rich photosystem I (PSI) (Strzepek and Harrison, 2004), together with an over-expression of energetically isolated pigment protein complexes (Schrader et al., 2011; Ryan-Keogh et al., 2012; Behrenfeld and Milligan, 2013). In contrast, increases in ϕ_F as a result of

macronutrient stress have only been observed where phytoplankton are starved of a macronutrient, thereby inhibiting the production of functional reaction centres (Kolber et al., 1988; Geider et al., 1993b; Parkhill et al., 2001). Consequently, across extensive regions of the world's oceans where phytoplankton are potentially under conditions of steady state macronutrient limitation rather than starvation (i.e. nutrient availability sets a limit on the standing stock, but nutrient (re-)supply may be rapid due to intense recycling (Moore et al., 2013)), it appears that the majority of PSII is fully functional and has relatively low ϕ_F (e.g. Moore et al., 2008). Regardless of the underlying physiological cause, the empirical relationship between Fe stress and ϕ_F presents an enticing possibility for the remote observation of Fe-stressed growth conditions using satellite detected ϕ_F (Behrenfeld et al., 2009). Unfortunately, such a simple relationship is confounded by the fact that Fe stress is not the only control of ϕ_F in the satellite data (Huot et al., 2005, 2013; Schallenberg et al., 2008; Behrenfeld et al., 2009).

Variability in two processes, photochemical quenching (qP) and non-photochemical quenching (NPQ) are particularly important in determining the chlorophyll fluorescence yield under ambient light conditions (Falkowski and Kiefer, 1985). Absorbed photon energy used in the photosynthetic light reactions competes with fluorescence and is termed qP (Kiefer and Reynolds, 1992), while NPQ refers to a suite of non-photochemistry related mechanisms that can reduce chlorophyll fluorescence (Müller et al., 2001). These NPQ mechanisms are a direct result of the need to dissipate excess absorbed photon energy as heat to limit photodamage (Raven, 2011). Antennae quenching (qE), which operates on timescales of seconds-minutes, describes thermal dissipation of absorbed photon energy, mainly due to cycling of the xanthophyll pigments (Demmig-Adams, 1990), while longer lived reaction centre quenching (qI) can

be related to photo-damage (Horton et al., 1996; Behrenfeld et al., 2009; Milligan et al., 2012).

Table 5.1: List of symbols and abbreviations used.

Symbol	Meaning
$< a_{ph} >_{blue}$	Average phytoplankton absorption coefficient spectrally weighted to the blue excitation flashes of the FRRf (m^{-1})
$< a_{ph} >_{in\ situ}$	Average phytoplankton absorption coefficient spectrally weighted to a clear sky irradiance spectrum (m^{-1})
$< a^*_{ph} >_{in\ situ}$	Average chlorophyll specific phytoplankton absorption coefficient spectrally weighted to a clear sky irradiance spectrum (m^2 (mg Chl)$^{-1}$)
B	Parameter representing NPQ in Eq. 4.
Chl	Analytically determined chlorophyll-a concentration (mg m^{-3})
Chl_{sat}	Satellite-derived chlorophyll-a concentration
F_{o} , F'	Minimum FRR fluorescence in the dark and light respectively
$F_{\mathrm{v}}/F_{\mathrm{m}}$	Apparent PSII photochemical efficiency
$iPAR_{\mathrm{FRR}}$	Spectrally neutral incident irradiance provided by the FAST^{act} system (µmol photons $m^{-2}s^{-1}$)
$iPAR_{\mathrm{sat}}$	Incident solar irradiance integrated over the 400 to 700 nm waveband (µmol photons $m^{-2}s^{-1}$)
$nFLH$	Normalised fluorescence line height, the NASA satellite-derived chlorophyll fluorescence product (mW cm^{-2} μm^{-1} sr^{-1})
ϕ_{F}	Quantum yield of fluorescence (%)
ϕ_{rel}, ϕ_{rel}'	Quantum yield of fluorescence as determined using FRR parameters and measured chlorophyll-a concentrations, measured in the dark and light respectively (arbitrary units)
ϕ_{sat}	Satellite-derived quantum yield of fluorescence without any NPQ correction (%)
$\phi_{\mathrm{sat}}(SST)$	Satellite-derived quantum yield of fluorescence with *SST* NPQ correction (%)
σ_{PSII}	Functional absorption cross-section of PSII

Satellite images of ocean colour are taken near midday under clear-sky conditions, when ϕ_{sat} values are impacted significantly by NPQ mechanisms. A suitable correction for NPQ is therefore essential if ϕ_{sat} is to be used as an indicator for another physiological signal (e.g. Fe stress) (Dandonneau and Neveux, 1997; Maritorena et al., 2000; Morrison 2003; Schallenberg et al., 2008; Behrenfeld et al., 2009). If all phytoplankton populations showed identical trends of fluorescence quenching with increasing irradiance, it would be easy to remove the effect of NPQ from ϕ_{sat} using the particular value of irradiance at the time of satellite image capture. Unfortunately, this appears not to be the case. NPQ has

been shown to depend strongly on the light acclimation state of the phytoplankton population (e.g. Milligan et al., 2012), while other potential controls including the phytoplankton species dominating the fluorescence signal and their photoacclimation state remain to be investigated. If NPQ effects cannot be removed confidently, it is clearly impossible to unambiguously ascribe variability in ϕ_{sat} to other physiological signals such as Fe stress.

Previous studies have highlighted the difficulty in correcting ϕ_{sat} signals for NPQ (Maritorena et al. 2000; Huot et al., 2005; Schallenberg et al., 2008; Behrenfeld et al., 2009). However, thus far NPQ studies in the field have generally been limited to a relatively small number of observations from discrete geographic regions (Morrison, 2003; Schallenberg et al., 2008), that were therefore incapable of revealing any ocean-basin scale variability in NPQ characteristics. Taking this into account, alongside evidence suggesting Fe stress increases ϕ_F of phytoplankton (Geider et al., 1993b; Sakshaug and Holm-Hansen, 1977; Schrader et al., 2011), the enticing possibility of being able to map regions of Fe stress on a global scale using ϕ_{sat} warrants efforts aimed at improving our understanding of NPQ. To this end, the NPQ of natural phytoplankton assemblages were investigated by detecting changes in ϕ_F under a range of incident light intensities for 229 samples across the South Atlantic and Southern Ocean. These experiments represent the NPQ response of phytoplankton communities from several distinct oceanic regimes: macronutrient-limited subtropical gyre waters; Fe-limited mesotrophic waters; Fe-limited high nutrient low chlorophyll (HNLC) waters; and Fe- and macronutrient-replete productive waters. Alongside every measurement the necessary ancillary data for interpretation of responses were collected, including a suite of high spatial resolution Fe-addition incubation experiments providing an assessment of Fe stress status in the regions encountered and the direct influence of Fe resupply on

fluorescence characteristics. Our results show that ϕ_{sat} holds significant promise for identifying regions of Fe stress provided the NPQ behaviour of the particular region can be characterised and hence corrected for. Highlighting potential limitations, we employ an NPQ correction parameter derived from our field observations and present a decadal composite of ϕ_{sat} for the Southern Ocean.

5.2 Methods

5.2.1 Cruises

Data were collected on three cruises: two in the South Atlantic (JC068 and D357) and one in the Scotia Sea – Drake Passage region of the Southern Ocean (JC069) (Figure 5.1). JC068 was carried out during January 2012 and spanned the South Atlantic Basin between 35 and 40˚S. D357 occupied the eastern portion of this same transect during October-November 2010. JC069 was undertaken during February-March 2012 and followed a cruise track through the Scotia Sea and Drake Passage.

5.2.2 CTD data

Vertical profiles of temperature, salinity, fluorescence and (on occasion for JC068 and D357 cruises) photosynthetically available radiation (PAR), were collected using a Seabird 911 CTD and a LI-COR Biospherical PAR sensor. Mixed-layer depths (MLD) were calculated using the threshold method of de Boyer Montégut et al. (2004), while euphotic depth (z_{eu} assumed to correspond to 1% of surface irradiance) was calculated from PAR profiles for JC068 and D357. For stations without PAR profiles during JC068, a relationship between chlorophyll and the diffuse attenuation coefficient for PAR ($K_{d(\mathrm{PAR})}$) was used to estimate $K_{d(\mathrm{PAR})}$ and therefore z_{eu} using $z_{eu} = 4.6/K_{d(\mathrm{PAR})}$. No underwater PAR data were available for JC069, so K_d was calculated as:

$$K_{d(\mathrm{PAR})} = 0.05 + 0.057Chl^{0.58} \quad \textbf{(5.1)}$$

after Venables and Moore (2010) using the Southern Ocean field data of Korb et al. (2008) and Moore et al. (2007). A stratification index for the euphotic zone was calculated as the difference in density between a reference surface depth (20 m) and z_{eu}.

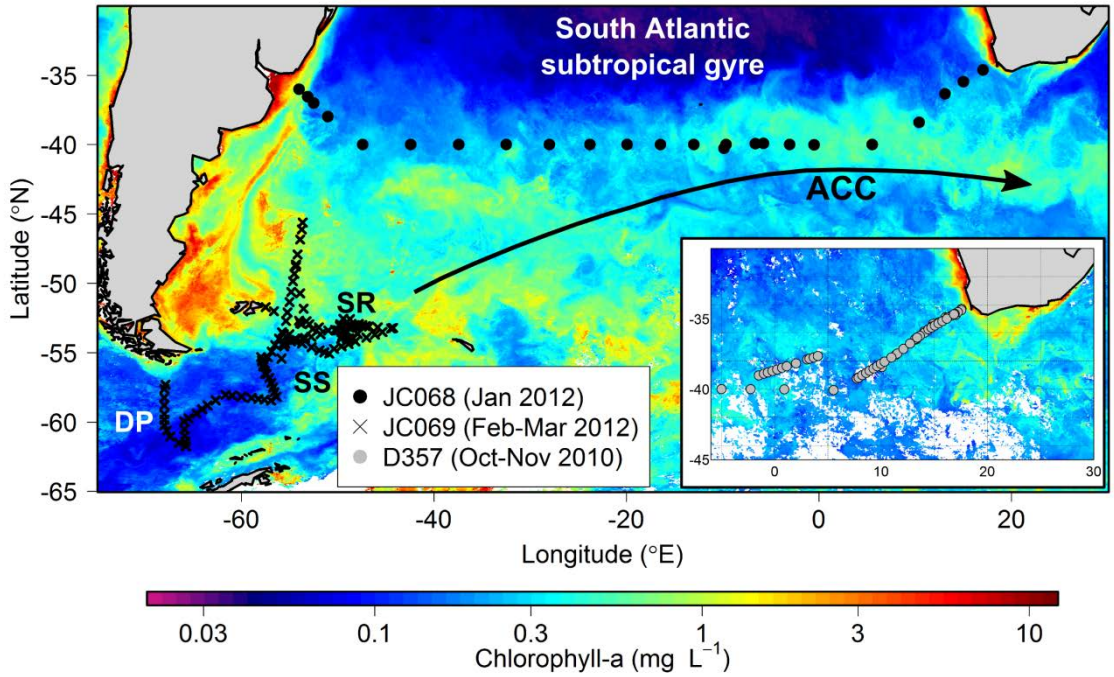

Figure 5.1: Map of non-photochemical quenching (NPQ) experiment locations for the different cruises (each symbol represents one experiment). Background is MODIS chlorophyll-a concentration composites for the time periods of the cruises (January-March 2012 for JC068 and JC069; mid-October to mid November for D357). The general trajectory of the Antarctic Circumpolar Current (ACC) is shown, alongside the locations of Drake Passage (DP), the Scotia Sea (SS), and the Scotia Ridge (SR).

5.2.3 Macronutrient and trace metal concentrations

Dissolved macronutrients silicate, phosphate and nitrate + nitrite (hereafter referred to as nitrate) were analysed by Malcolm Woodward at Plymouth Marine Labs using a micromolar Bran and Luebbe AAIII segmented flow, colourimetric autoanalyser using methods described in Woodward and Rees (2001). Samples were analysed on ship during JC068 and D357 cruises and frozen at -20 °C before being analysed in the UK for JC069.

Surface seawater samples for trace metal analysis and incubation experiments (Section 2.8) were collected with a towed fish at 2 to 3 m depth. The seawater was pumped into a trace metal clean sampling container using a Teflon diaphragm pump. Samples were filtered in-line through 0.2 µm cartridge filter (AcroPak1000™) into acid washed low density polyethylene (LDPE) sample bottles and acidified with concentrated ultra-pure hydrochloric acid (Romil, UpA) to pH 1.6 (0.023 M H^+). Trace metal samples were analysed by Christian Schlosser (National Oceanography Centre, Southampton) using a modified method from Milne et al. (2010) by isotope dilution inductively coupled plasma mass spectrometry (ID-ICP/MS (Thermo Element XR)).

5.2.4 Phytoplankton community structure

High Performance Liquid Chromatography (HPLC) samples (0.5–2 L) were filtered onto 0.7 µm Whatman GF/F filters, immediately frozen in liquid nitrogen and then stored in a −80 °C freezer. Pigments were extracted into 90% acetone by sonication and analysed using a Thermo HPLC system following the method described in Gibb et al. (2000). The matrix factorisation program CHEMTAX was used to aid with interpretation of the pigments in terms of contributing taxonomic groups to total chlorophyll-a biomass (Mackey et al., 1996). Starting pigment ratios for the different taxonomic groups were obtained from Wright et al. (1996) for Southern Ocean waters, and Veldhuis and Kraay (2004) for subtropical gyre type waters. In addition to HPLC analysis, triplicate samples for fluorometric chlorophyll-a analysis (100 mL) were measured on-ship by filtering samples through 0.7 µm Whatman GF/F filter papers, extracting in the dark in 10 mL 90% acetone for 12-24 hours in a -20 °C freezer, before measuring on a calibrated Turner Designs Trilogy fluorometer (Holm-Hansen et al., 1965).

In addition to pigment analysis, concentrations of nanophytoplankton, photosynthetic picoeukaryotes (PPEs), *Synechococcus* and *Prochlorococcus* were analysed by analytical flow cytometry (AFC). Samples (2 mL) were fixed with neutralised paraformaldehyde (1% final concentration) and left for 10 minutes in the dark at room temperature before being frozen in liquid nitrogen and transferred to a -80 °C freezer. Samples were thawed at room temperature and analysed using a FACSort flow cytometer according to the methods described in Davey et al. (2008). Data analysis and cell counts were carried out in WinMDI Version 2.8 (Joseph Trotter) flow cytometry analysis software.

5.2.5 Phytoplankton absorption spectra

Phytoplankton absorption samples were collected by filtering 0.5 – 1 L seawater onto 0.7 µm pore GF/F filters and freezing the filter papers in liquid nitrogen before transfer to a -80 °C freezer for storage. Measurements were made using the hot methanol extraction method of Kishino et al. (1985) using a Shimadzu UV-2550 spectrophotometer equipped with an integrating sphere over the visible range (350-750 nm). Optical densities for total (i.e. prior to methanol extraction) and detrital (after extraction) particles were corrected for optical path-length amplification arising from scattering by the filter using the method of Cleveland and Weidemann (1993). Phytoplankton absorption coefficients (a_{ph}) were calculated by subtracting the detrital absorption spectra from the total absorption spectra. Pigment-specific absorption coefficients (a^*_{ph}) were calculated by dividing a_{ph} by HPLC-determined chlorophyll-a concentration. Values of averaged spectrally-weighted absorption were calculated by weighting a_{ph} values to, (i) a clear sky irradiance spectrum at the sea surface from measurements in the mid-latitude North Atlantic ($<a_{ph}>_{in\ situ}$), and (ii) the spectrum of the blue excitation flashes from the Fast Repetition Rate fluorometer (FRRf) ($<a_{ph,}>_{blue}$).

5.2.6 Fast Repetition Rate fluorometer (FRRf) and Rapid Light Curves (RLC)

A FRRf (FAST$^{tracka\ II}$ with integrated FAST^{act} base unit, CTG Ltd.) was used for phytoplankton fluorescence measurements and characterising NPQ responses. In a single acquisition protocol, the FRRf was set to deliver 64 sequences of one hundred 1 µs subsaturating flashes at 1 µs intervals. Fluorescence transients were fitted to the model of Kolber et al. (1998) in FASTpro (V1.5) software (CTG Ltd.). Samples were collected throughout the day-night cycle and were always dark acclimated for at least 30 minutes prior to analysis (whilst being maintained at sea surface temperatures). FRRf measurements were corrected for blank fluorescence using 0.2 µm filtrates (Cullen and Davis 2003).

F_v/F_m was calculated as $(F_m\text{-}F_o)/F_m$ (where F_o is the fluorescence at t=0 and F_m is the maximum fluorescence) and functional absorption cross sections (σ_{PSII}) were recovered from the Kolber et al. (1998) model fit. A rapid light curve (RLC) protocol was configured to evaluate NPQ for surface samples (JC068, D357, JC069) and subsurface chlorophyll maximum (SCM) samples (JC068 and D357). The RLC protocol involved a series of identical FRRf single acquisitions (same settings as for single acquisitions, except sequences per acquisition were reduced to 32), performed under a sequence of 14 to 15 progressively increasing PAR ($iPAR_{FRR}$) intensities provided by the FAST^{act} unit, starting from 6 µmol photons $m^{-2}s^{-1}$ and increasing to 1434 µmol photons $m^{-2}s^{-1}$. Each illumination step in the RLCs lasted for 3 minutes, with 10 second dark steps in between. In order to assess the potential magnitude of spectral differences between the FAST^{act} and solar irradiance, light absorbed by phytoplankton was calculated by weighting $a_{ph}^{*}(\lambda)$ to the FAST^{act} irradiance spectrum and a clear sky irradiance spectrum. Differences were relatively minor, with absorption of $iPAR_{FRR}$ being slightly lower (15-25% lower for >90% of samples) and hence to first order could be neglected.

The relative chlorophyll fluorescence quantum yield of dark acclimated samples at F_o and in the light at F' (both of which will be proportional to the actual quantum yields), were calculated as:

$$\boldsymbol{\phi}_{rel} = \frac{F_o}{<a_{ph}>_{blue}} \quad \textbf{(5.2)}$$

and:

$$\boldsymbol{\phi}_{rel}{}' = \frac{F'}{<a_{ph}>_{blue}} \quad \textbf{(5.3)}$$

respectively. Calculation of relative quantum yield from FRRf data does not require division by $iPAR_{FRR}$, as the contribution of the background irradiance to the fluorescence stimulated during the flash sequence is negligible in comparison with the LED flashlets themselves.

Observed relationships between ϕ_{rel}' and irradiance were fitted to the following empirical equation:

$$\boldsymbol{\phi}_{rel}{}' = A\ iPAR_{FRR}{}^{B} \quad \textbf{(5.4)}$$

for $iPAR_{FRR}$ values greater than 300 µmol photons m^{-2} s^{-1}. For values of $iPAR_{FRR}$ lower than 300 µmol photons m^{-2} s^{-1} the response of ϕ_{rel}' was more complex due to decreasing qP (see for example Falkowski et al., 1986; Morrison, 2003). However, such irradiance levels are not generally representative of those encountered in situ at the time of MODIS satellite overpasses. Thus the relationship between ϕ_{rel}' and irradiance was initially chosen to be described using the simple empirical relationship of Equation 5.4, rather than a more mechanistic model (Morrison, 2003; Shallenberg et al., 2008; Morrison and Goodwin, 2010) both to facilitate more direct comparison with previous basin-scale work (Behrenfeld et al., 2009) and because the presence and quenching characteristics of any

potential pool of energetically isolated pigment protein complexes (Behrenfeld and Milligan, 2013) would likely complicate the application of currently available mechanistic models (Morrison and Goodwin, 2010).

5.2.7 MODIS satellite data products

Daily, monthly, and seasonal level 3 MODIS chlorophyll, phytoplankton absorption at 443 nm (Lee et al., 2002), normalised fluorescence line height (*nFLH*), instantaneous photosynthetically available radiation (*iPAR*), and sea surface temperature (*SST*) data products were downloaded for the time periods of the three cruises, in addition to seasonal climatology's for 2002-2012 (http://oceancolor.gsfc.nasa.gov/). All images were from NASA's latest reprocessing (2009 reprocessing for all data pre- 2011; 2013 reprocessing for 2011-2013) which includes removal of a temporal trend in *nFLH* data that existed prior to the 2009 reprocessing (http://oceancolor.gsfc.nasa.gov/REPROCESSING/R2009/modisa_calibration/).

Normalised FLH (*nFLH*, referred to as F_{sat} in Behrenfeld et al. (2009)) is a Level 3 NASA MODIS data product describing fluorescence emanating from the oceans normalised to incident satellite *iPAR* ($iPAR_{\text{sat}}$) (Abbott and Letelier, 1999; Behrenfeld et al., 2009). In order to obtain a quantum yield of fluorescence, values of *nFLH* need to be corrected for the fraction of $iPAR_{\text{sat}}$ actually absorbed by phytoplankton. Following the method of Behrenfeld et al. (2009), fields of spectrally averaged phytoplankton absorption were initially estimated from satellite derived chlorophyll-a concentrations (Chl_{sat}) using the equation of Bricaud et al. (1998):

$$< a_{ph} >_{in\ situ} = Chl_{sat} < a^{*}_{ph} >_{in\ situ} = A_p Chl_{sat}^{E_p} \quad \textbf{(5.5)}$$

where $< a_{ph} >_{in\ situ}$ is the average spectrally weighted phytoplankton absorption coefficient, $< a^*_{ph} >_{in\ situ}$ is the average chlorophyll specific absorption coefficient, and A_p and E_p are parameters from an empirical data fit (see Figure 5.2). A_p and E_p were initially set to 0.0147 and 0.684 respectively, as calculated by Behrenfeld et al. (2009) who used the data of Bricaud et al. (1998). Subsequently values were determined from our own dataset (see Section 2.5) to investigate the importance of regional variation in these parameters for resultant ϕ_{sat} fields. Satellite fields of a_{ph} at 443 nm (Lee et al., 2002) were also investigated as a means of normalising the fluorescence signal directly to phytoplankton absorption.

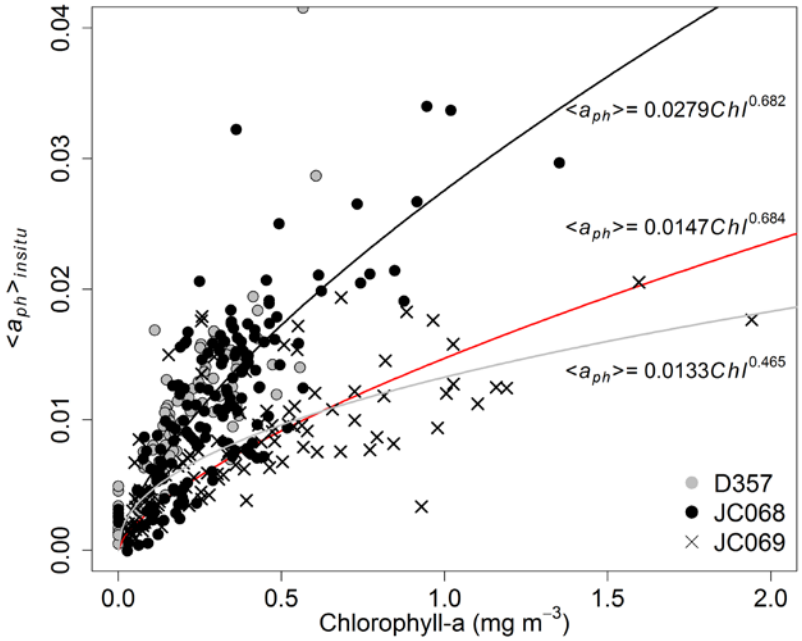

Figure 5.2: Relationship between values of average spectrally weighted phytoplankton absorption and chlorophyll-a concentrations for the three cruises. Lines and equations represent best model fits to JC068 and D357 (black line), JC069 (grey line), and the relationship used by Behrenfeld et al. (2009) who used the dataset of Bricaud et al. (1998) (red).

The final ϕ_{sat} algorithm of Behrenfeld et al. (2009), including corrections for phytoplankton absorption and other satellite corrections (see Behrenfeld et al., 2009), is:

$$\boldsymbol{\phi}_{sat} = 0.01 \frac{nFLH}{<a_{ph}>}. \quad \textbf{(5.6)}$$

As an initial approximation of NPQ, Behrenfeld et al. (2009) then applied a 1/*iPAR* correction in the form:

$$NPQ - corrected\ \boldsymbol{\phi}_{sat} = \boldsymbol{\phi}_{sat}\ \frac{iPAR}{1590} \quad \textbf{(5.7)}$$

where 1590 is equal to MODIS global average *iPAR* for the time period of their study (units of µmol photons m^{-2} s^{-1}).

The geometric calculation of *nFLH* (see Abbott and Letelier, 1999) should in theory remove any artefact introduced due to fluorescence from coloured dissolved organic matter (as is directly characterised in the field with the blank FRR measurements described in Section 2.6), which is supported by observations of spectrally resolved CDOM fluorescence by Chekaliuk and Hafez (2008). Therefore, despite CDOM fluorescence being found to contribute significantly to total fluorescence in the most oligotrophic waters encountered, as elsewhere (Moore et al., 2008), the baseline method used for the calculation of *nFLH* should in theory remain robust in these systems. However, we follow the recommendation of Huot et al. (2013), who suggest that uncertainty in satellite detected chlorophyll and fluorescence increases significantly below chlorophyll concentrations of 0.1 mg m^{-3}, in subsequent analysis by highlighting pixels with chlorophyll-a < 0.1 mg m^{-3} and suggesting these be interpreted with caution.

5.2.8 Fe-addition incubation experiments

Fe-addition incubation experiments were performed using trace metal clean seawater from the towed fish and followed the method described in Chapter 2 (Ryan-Keogh et al., 2013; Browning et al., 2014). Fe-limited waters were defined as those producing a statistically significant ($p<0.01$ level using a one-tailed Student's t-test) F_v/F_m increase

in Fe amended bottles over that of control (non-amended) bottles. Values of $\Delta F_v/F_m$ were calculated, where $\Delta F_v/F_m$ = average F_v/F_m Fe amended bottles – average F_v/F_m control bottles (Ryan-Keogh et al., 2013).

5.3 Results and discussion

5.3.1 Biogeochemical regimes encountered on cruises

Collectively, the three cruises encountered several oceanic provinces (Longhurst, 1998). JC068 passed through two clear regimes either side of the south subtropical convergence (SSTC), which was described in detail in Chapter 2. Warmer subtropical gyre-type waters next to the South African coast and in the Western Atlantic Basin were characterised by low macronutrient concentrations, low surface chlorophyll-a concentrations, distinct subsurface chlorophyll maxima (SCM), and elevated concentrations of smaller cells including *Synechococcus* and *Prochlorococcus*. Conversely, colder sub-Antarctic - Antarctic Circumpolar Current (ACC) waters to the south of the SSTC had elevated macronutrient concentrations, uniform chlorophyll-a concentrations through the mixed layer, and low concentrations of picocyanobacterial cells. ACC waters were shown to be Fe-limited on the basis of significant (t-test $p<0.01$) increases in F_v/F_m following Fe-amendment, while within subtropical gyre-type waters the standing crop of phytoplankton was likely limited by macronutrient availability (Chapter 2). D357 was carried out in the eastern portion of the JC068 transect during austral spring when the SSTC was occupying a more northerly location. Consequently the regime encountered was predominantly that of the ACC waters in the JC068 cruise.

JC069 passed through productive waters close to the South American continental shelf (chlorophyll-a concentrations >2 mg m^{-3}), both high and low chlorophyll-a filaments around the Scotia Ridge, and low chlorophyll-a waters in Drake Passage (lowest surface

concentration of <0.03 mg m^{-3}). Macronutrient concentrations increased from relatively low values next to the South American shelf (minimum of 1.8 µmol L^{-1} nitrate) to high values in the Scotia Sea and Drake Passage (up to 27.8 µmol L^{-1} nitrate). Phytoplankton community structure transitioned from a mixed population co-dominated by haptophytes and diatoms around the Scotia Ridge to haptophyte-dominated waters in Drake Passage. Physiological responses of phytoplankton to Fe replenishment were observed throughout this cruise, but showed no clear spatial trend.

5.3.2 Correlation of ϕ_{sat} with in situ matchups

F_v/F_m has been used routinely as an index of Fe limitation (Behrenfeld and Milligan, 2013), with fluorescence quantum yields (or more typically, chlorophyll normalised values of F_o or F_m), being reported less frequently. Overall, ϕ_{rel} and F_v/F_m were observed to be negatively correlated within the current study, although there was some evidence of cruise and/or spatial variability in the observed relationships (see Figure 5.3a). Furthermore inverse co-variability was observed between the response of ϕ_{rel} and F_v/F_m to Fe replenishment (Figure 5.3b), confirming that higher values of ϕ_{rel} were likely associated with regions of Fe stress across our wider study area..

Calculation of ϕ_{sat} values with the potential to reliably indicate relative levels of Fe stress requires appropriate NPQ correction and realistic parameterisation of light absorption by phytoplankton. Although light absorption by phytoplankton can be estimated on the basis of an empirical relationship with satellite-derived chlorophyll-a concentrations (e.g. Eq. 5.5, Figure 5.2), such relationships tend to be characterised by large scatter and hence it may be desirable to use satellite products representing phytoplankton absorption directly (Lee et al., 2002; Westberry et al., 2013). However, whilst same day match ups between remote sensing observations and in situ data revealed a good correlation for chlorophyll-a

(R^2=0.92, see Figure 5.5b), for phytoplankton absorption at 443 nm the correlation was markedly worse (R^2=0.18, Figure 5.5d) and hence we currently still rely on indirect phytoplankton absorption inferred from chlorophyll-a.

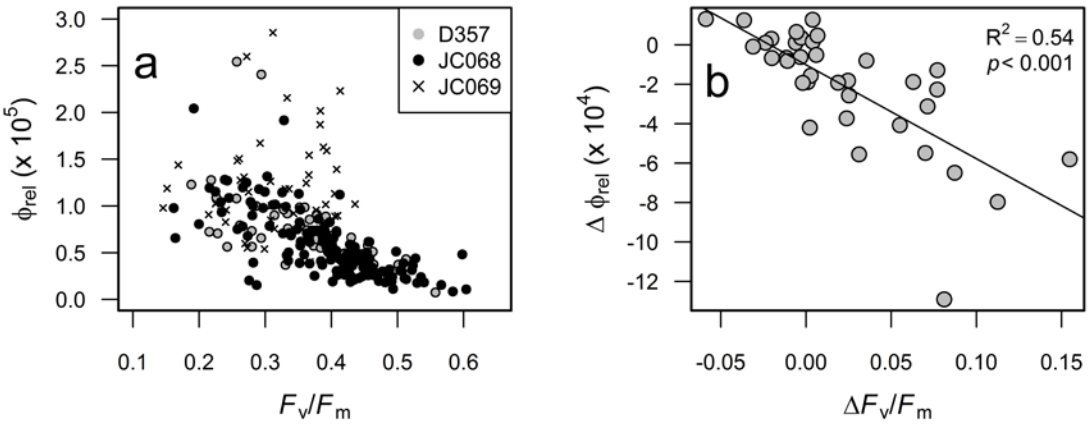

Figure 5.3: Correlations between the relative fluorescence quantum yield (ϕ_{rel}) and F_v/F_m. a) Night time ϕ_{rel} versus F_v/F_m for the three cruises. b) Inverse co-variability of Fe-addition phytoplankton response in terms of F_v/F_m and ϕ_{rel} parameters. Delta notation indicates difference between Fe-amended bottles and control bottles in terms of F_v/F_m and ϕ_{rel} parameters. For (b), $< a_{ph} >_{blue}$ (i.e., as required in Equation 5.2) was derived from its relationship with fluorometrically-determined chlorophyll-a concentration for each of the two cruises where incubation experiments were performed.

Attempts were made to calculate satellite fields of phytoplankton absorption using a regional relationship between phytoplankton absorption and surface chlorophyll concentration based on in situ observations (Figure 5.2), however, a lack of data points at high chlorophyll values resulted in poorly constrained non-linear model fits that propagated to lower chlorophyll values. This problem has been commented on previously when similar regional data sets have been used (Stuart et al., 2000; Sathyendranath et al., 2001). To overcome this we followed the method of Behrenfeld et al. (2009) who used the extensive, global absorption – chlorophyll dataset of Bricaud et al. (1998). This dataset is much better constrained at higher chlorophyll concentrations (up to 25 mg

chlorophyll-a m^{-3}). Potential bias may be introduced in using this model generated using data largely collected outside the Southern Ocean. In particular the low chlorophyll

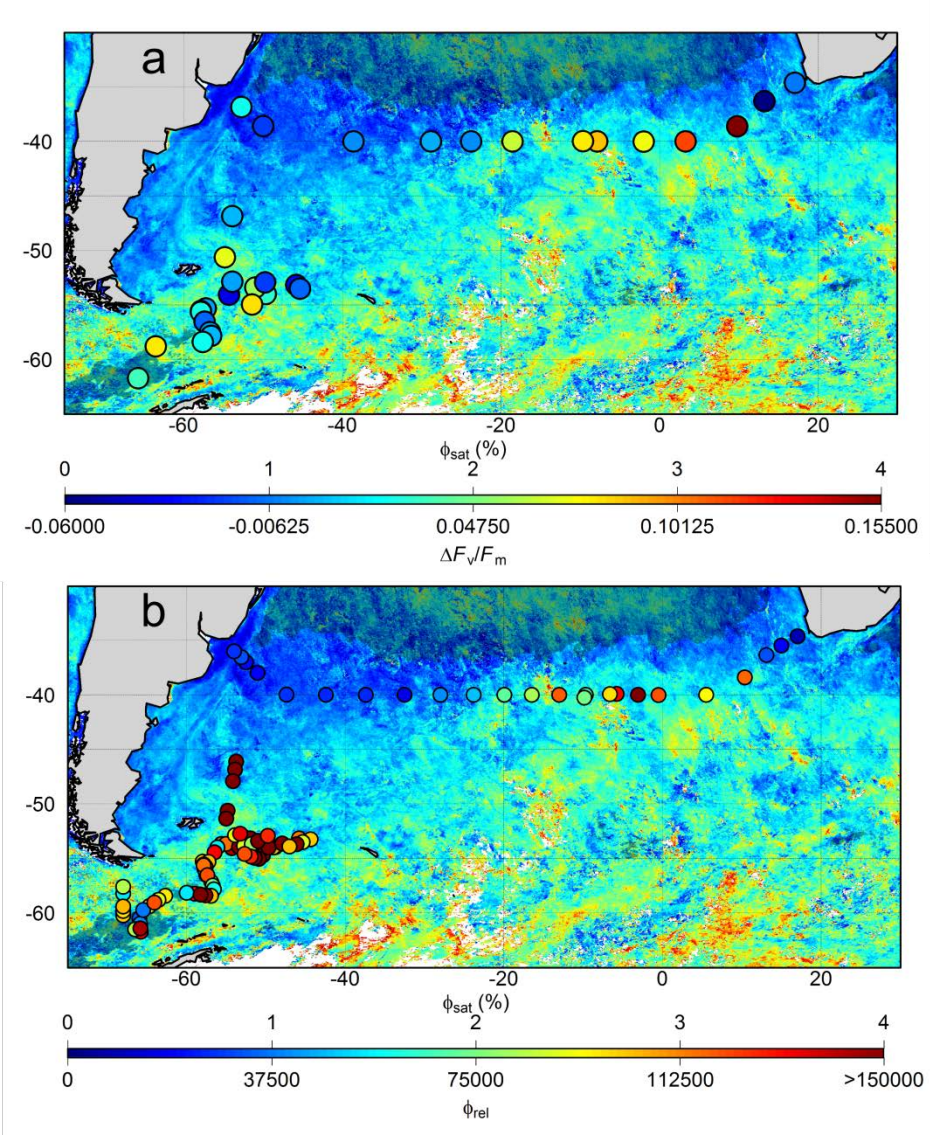

Figure 5.4: Satellite fluorescence quantum yield (ϕ_{sat}) and field matchups (ϕ_{rel}) for the three cruises. a) January-March 2012 (JC068 and JC069 cruise period) averaged ϕ_{sat} (not NPQ-corrected) with $\Delta F_v/F_m$ measurements over plotted. b) As for (a) but with ϕ_{rel} over plotted. Pixels with chlorophyll-a less than 0.1 mg m^{-3} in (a) and (b) are shaded.

values in the dataset of Bricaud et al. (1998) are biased to low-latitude, gyre-type waters dominated by picocyanobacteria rather than pico- and nanoeukaryotes that dominate the low chlorophyll waters of the Southern Ocean (Bouman et al., 2012). Indeed our data (Figure 5.2), along with other datasets from the Southern Ocean (Mitchell and Holm-

Hansen, 1991; Reynolds et al., 2001) show absorption values that fall below the best fit line of Bricaud et al. (1998) (i.e. lower absorption per chlorophyll-a concentration), likely as a result of a reduced contribution of photoprotective pigments to absorption, alongside increased pigment packaging effects due to generally larger cell sizes in these waters (e.g. Morel and Bricaud, 1981; Reynolds et al., 2001).

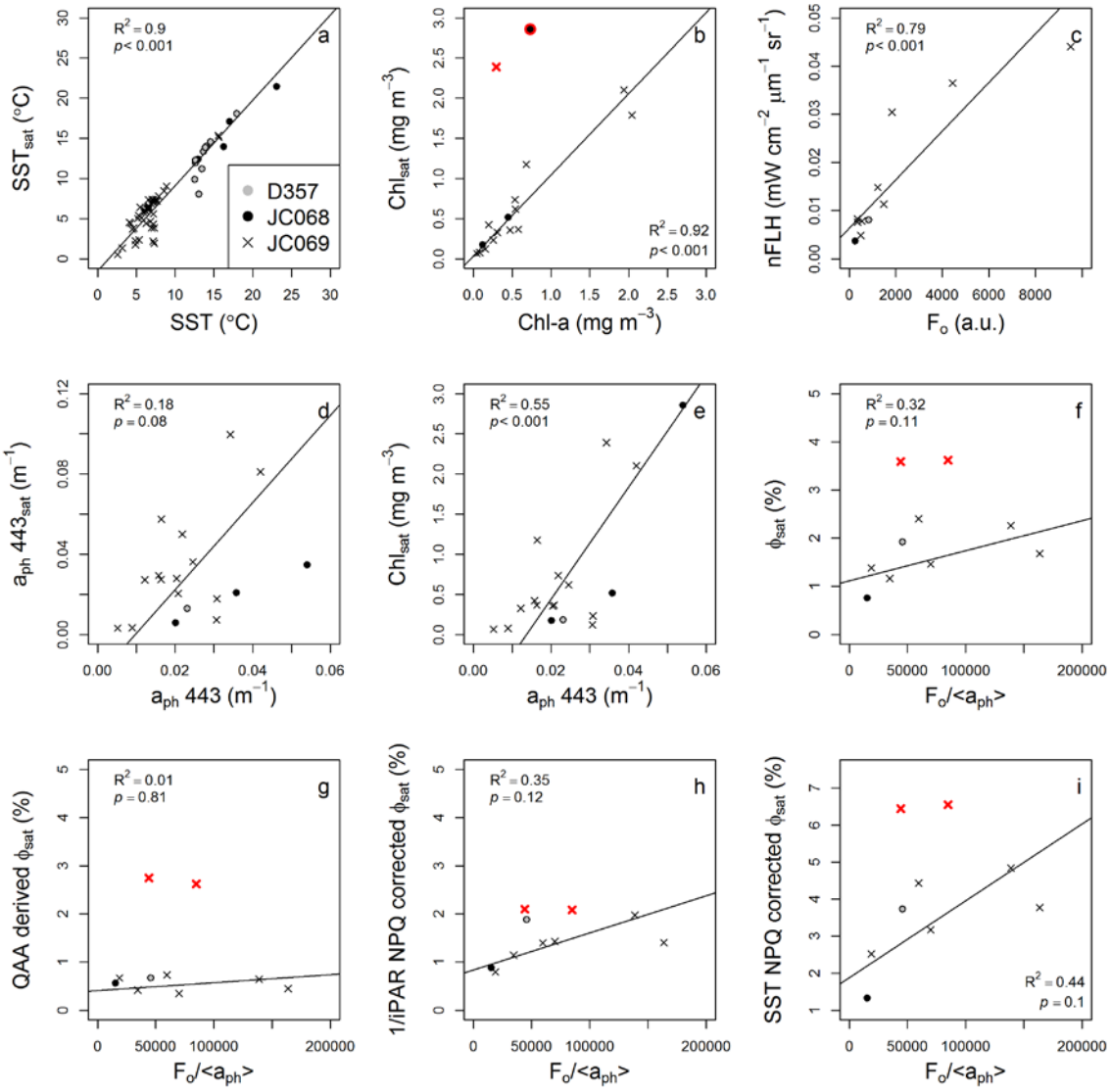

Figure 5.5: Correlation between same day satellite-field matchups. Lines and statistics are from type-2 linear regression models. Red symbols in (b) highlight outliers excluded from the regression, and in (f-i) highlight points with satellite chlorophyll<0.1 mg m^{-3} (i.e., quite likely unreliable – see main paper) that have been excluded from regressions.

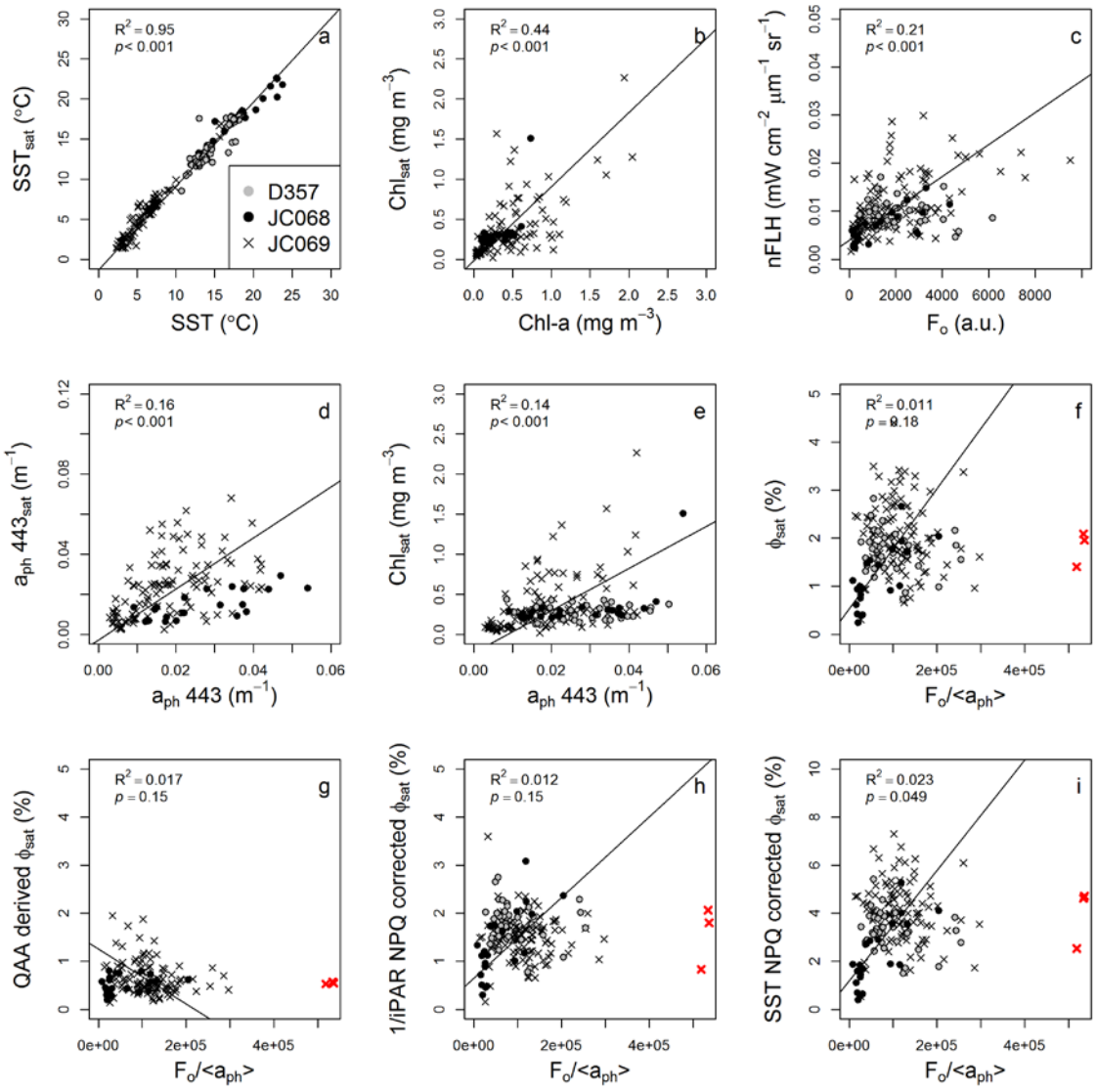

Figure 5.6: Correlation between monthly averaged satellite composite pixels and field matchups. Lines and statistics are from type-2 linear regression models. Red symbols in (f-i) highlight outliers excluded from regressions.

Correcting ϕ_{sat} for absorption but not NPQ (Figure 5.4, also see Figure 5.5 and Figure 5.6) revealed broadly similar, oceanographically coherent spatial patterns spatial patterns in ϕ_{sat} and the proximal response of the phytoplankton community to Fe replenishment as indicated by $\Delta F_v/F_m$, as well as ϕ_{sat} and dark acclimated values of ϕ_{rel} (Figure 5.4a and b respectively). Greater variability observed for both $\Delta F_v/F_m$ and ϕ_{rel} in the Scotia Sea region may result from high spatial dynamics in phytoplankton ecophysiology (Holm-Hansen et al., 2004) driven by the dynamic mixing environment that exists in this

region (e.g. Naveira Garabato et al., 2004), which consequently may cause longer time period composites to mask shorter timescale variability as observed in field measurements. Consistent with this, the limited number of same-day satellite matchups tended to show significantly better correlations for a range of retrieved products (see Figure 5.6). Although this initial relationship between non-NPQ corrected values of ϕ_{sat} with regions of Fe stress appears promising, we now consider whether significant differences in NPQ between regions could be resulting in biased satellite observations of ϕ_{sat}.

5.3.3 Controls on non-photochemical quenching

Field measurements of ϕ_{rel}' at progressively increasing *iPAR* showed significant variability in observed NPQ responses, with the relationship between ϕ_{rel}' and $iPAR_{FRR}$ varying for both surface (Figure 5.7) and SCM samples for all cruises. In particular the curves for JC068 could clearly be divided into two distinct zones of high and low NPQ which also corresponded to the two dominant ecophysiological regimes encountered on the cruise. Specifically, flatter relationships indicating minimal dynamic NPQ were observed in the warmer, low nitrate, Fe-replete subtropical gyre-type waters (dashed lines in Figure 5.7a-b), whilst enhanced dynamic NPQ was observed in the colder, high nitrate, Fe-limited (ACC type) waters (solid lines in Figure 5.7a-b). Normalising to low light values further emphasised that NPQ driven reductions in ϕ_{rel}' from ACC waters sampled on JC068 were typically around double that of the modest response observed in subtropical gyre waters (Figure 5.7b). Less coherent geographical variability was observed during the D357 and JC069 cruises, however a considerable spread of NPQ responses remained (Figure 5.7c-d).

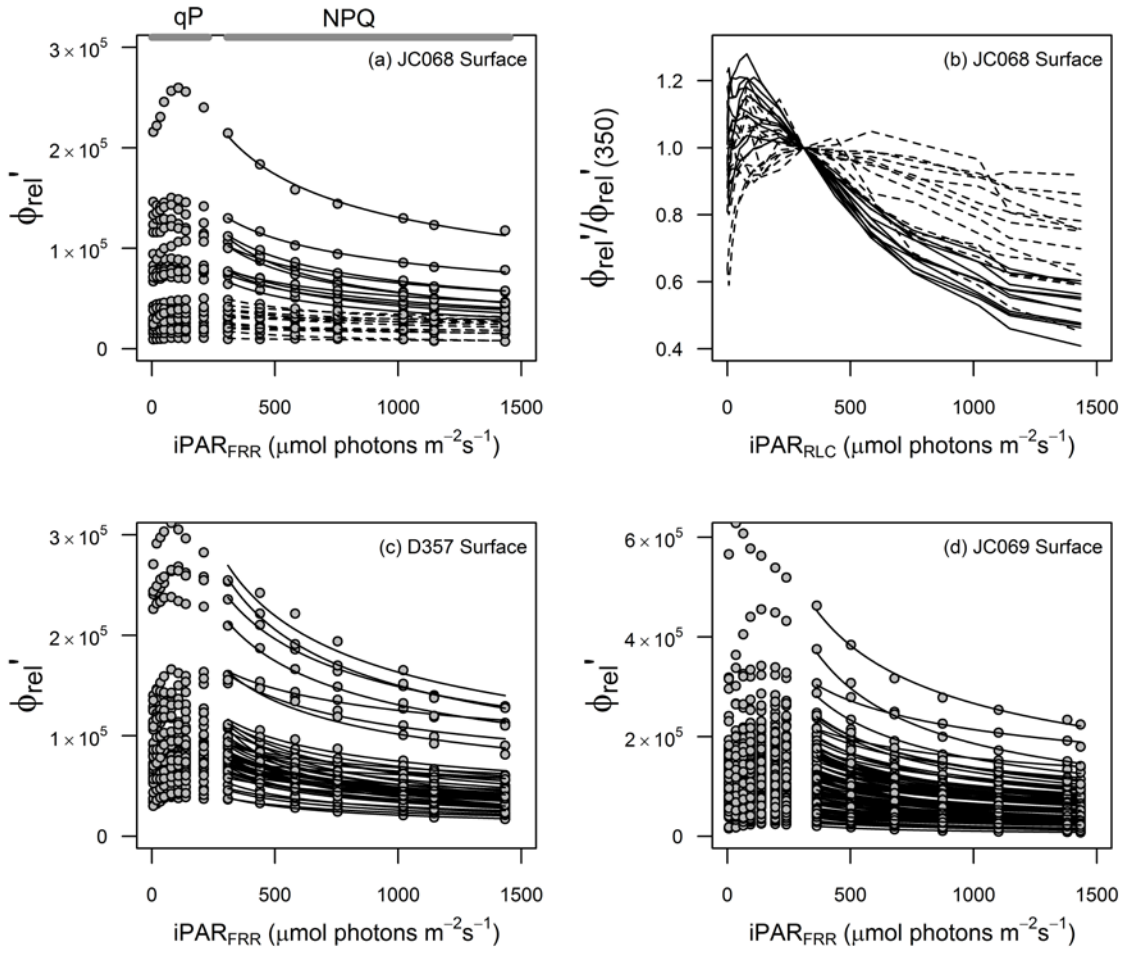

Figure 5.7: NPQ of surface samples for the three cruises. Dots represent data points, curves in (a), (c), and (d) represent best fit models to data points at *iPAR*>300 µmol photons $m^{-2}s^{-1}$. Dominant regions of qP and NPQ are highlighted in (a). (b) NPQ for surface waters in the two ecophysiological regimes encountered on JC068: ϕ_{rel}' at each light step have been normalised to ϕ_{rel}' at 350 µmol photons $m^{-2}s^{-1}$ to remove the influence of Fe limitation on yields. Resultant curves with steeper gradients have greater NPQ. Dashed lines in (a) and (b) distinguish the two distinct ecophysiological regimes identified on JC068.

In order to provide an index of the NPQ response, we fitted values of ϕ_{rel} at the upper range (>300 µmol photons m^{-2} s^{-1}) of $iPAR_{FRR}$ to Equation 5.4, to obtain the empirical parameter *B* (e.g. Milligan et al., 2012). A wide range of *B* values were found (between -0.84 and -0.057 for all experiments) with strong spatial variability suggesting that any robust NPQ correction method would have to account for such differences. Consequently, for the regions encountered on our cruises, a single $iPAR^{-1}$ correction, i.e. an assumed value of -1 for *B*, as used as an initial approximation in previous studies

(Behrenfeld et al., 2009), would not be capable of accurately accounting for NPQ, with highest discrepancies likely for subtropical gyre-type waters that displayed much lower dynamic NPQ at high *iPAR*.

In order to investigate potential ecophysiological drivers of the variable NPQ responses, correlation analyses were carried out between *B* and potential controlling factors (Figure 5.8). Despite almost certainly exerting some degree of control over fluorescence characteristics (e.g. Suggett et al., 2009) and therefore NPQ variability, neither trophic status (i.e. chlorophyll-a concentration) nor community structure (apart from cyanobacteria presence) showed a clear relationship with *B* (Figure 5.8f-h). Similarly, varying levels of Fe stress have been suggested to potentially enhance NPQ (*Cullen*, 2009), however the correlation of *B* with F_v/F_m was weak (R^2= 0.096, $p<0.001$), suggesting that this is unlikely the dominant driver (Figure 5.8d). In contrast, derived values of *B* were more strongly correlated with parameters relating to the light environment phytoplankton were experiencing. Observed relationships between *B* and mixed-layer depths (MLDs) (R^2= 0.32, $p<0.001$) and stratification indices (R^2= 0.33, $p<0.001$) both suggested that the highest dynamic NPQ responses occurred under conditions of deeper mixing and/or reduced near surface stratification (Figure 5.8a-b), as might be expected for phytoplankton populations having to cope with the more variable light regimes encountered in these environments, as compared to highly stratified systems. Such a pattern is consistent with laboratory studies of marine diatoms (Milligan et al., 2012; Lavaud et al., 2007). Data from the fluorometer linked to the ships underway flow-through system further supported these observations, with the typically observed diel fluorescence cycles characterised by daytime reductions (e.g. Dandonneau and Neveux, 1997) suggestive of much greater NPQ within the regions of deeper mixed layers on JC068.

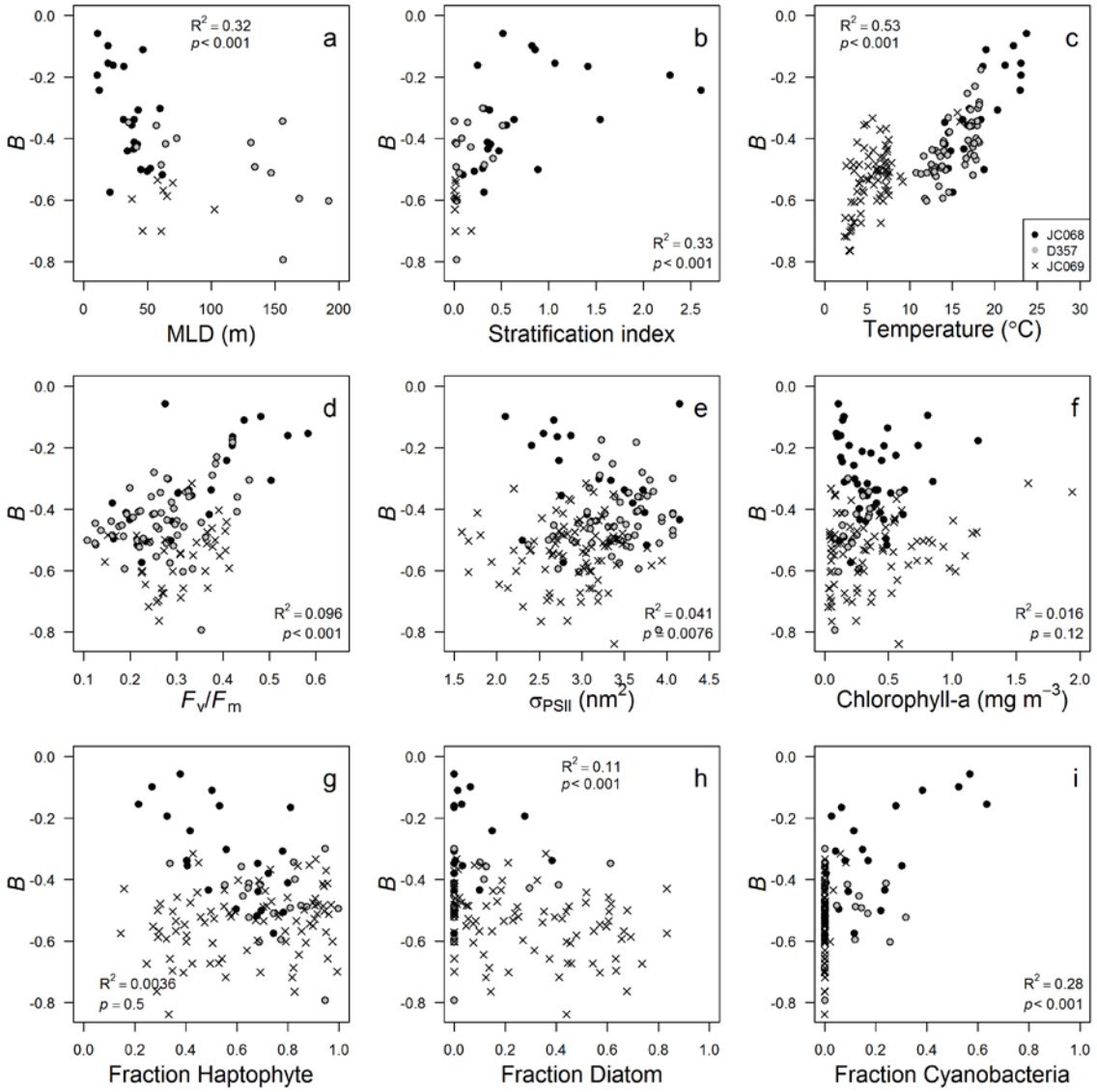

Figure 5.8: Potential controllers of NPQ. Relationships between *B*, the exponent representing ϕ_{rel}' decay in Equation 5.4, and possible controls (surface samples only).

Whilst being an unlikely candidate for driving NPQ variability at the physiological level, a clear correlation of *B* with sea surface temperature (*SST*) was found (R^2= 0.53, p<0.001) (Figure 5.8c). Such a relationship further highlights the strong geographical variability in the extent of NPQ. Moreover, *SST* is suggested to be a good predictor of *B* due to the relationship between upper ocean temperature with the extent of near surface stratification and MLD (Bouman et al., 2003). Consequently, relationships between the extent of NPQ (*B*) and community structure (i.e., with cyanobacteria: R^2= 0.28, p<0.001,

Figure 5.8i) may also be non-causal, with both responding instead to the same driver (Margalef, 1978; Cushing, 1989). Irrespective of the underlying controls, correlation between the extent of NPQ and *SST* is clearly of potential utility in NPQ-correcting fields of ϕ_{sat}.

5.3.4 Correcting for NPQ using *SST*

The observed linear model regression between *B* and *SST* allowed us to empirically predict values of *B* using satellite-retrieved values of *SST* (Figure 5.8c):

$$B = 0.019SST - 0.65. \quad \textbf{(5.8)}$$

Subsequent fields of *B* were hence used to NPQ-correct ϕ_{sat} to values expected at low light intensities according to:

$$\boldsymbol{\phi}_{sat}\,(SST) = \boldsymbol{\phi}_{sat}\left(\frac{350}{iPAR_{sat}}\right)^{B} \quad \textbf{(5.9)}$$

where ϕ_{sat} (*SST*) represents ϕ_{sat} with the *SST*-derived NPQ correction applied, 350 represents the low-light *iPAR* value chosen as the normalisation point (units of µmol photons $m^{-2}s^{-1}$), and $iPAR_{sat}$ represents irradiance at the time of image capture (units of µmol photons $m^{-2}s^{-1}$).

Using this correction, ϕ_{sat} (*SST*) fields were derived for the geographic region and time period of our cruises (Figure 5.9a). As for field measurements of ϕ_{rel}, *SST*-NPQ corrected ϕ_{sat} fields indicated strong geographic variability, with ACC waters having elevated ϕ_{sat} relative both to low chlorophyll (elevated *SST*) subtropical gyre-type waters and high chlorophyll (low *SST*) waters west of Patagonia. For comparison, applying a 1/*iPAR* correction (Eq. 5.7, Behrenfeld et al., 2009) to the same data (Figure 5.9b) resulted in clear differences, with higher ϕ_{sat} predicted in stratified subtropical gyres and

lower ϕ_{sat} at high latitudes as a result of over and under prediction of the actual extent of NPQ in these regions respectively.

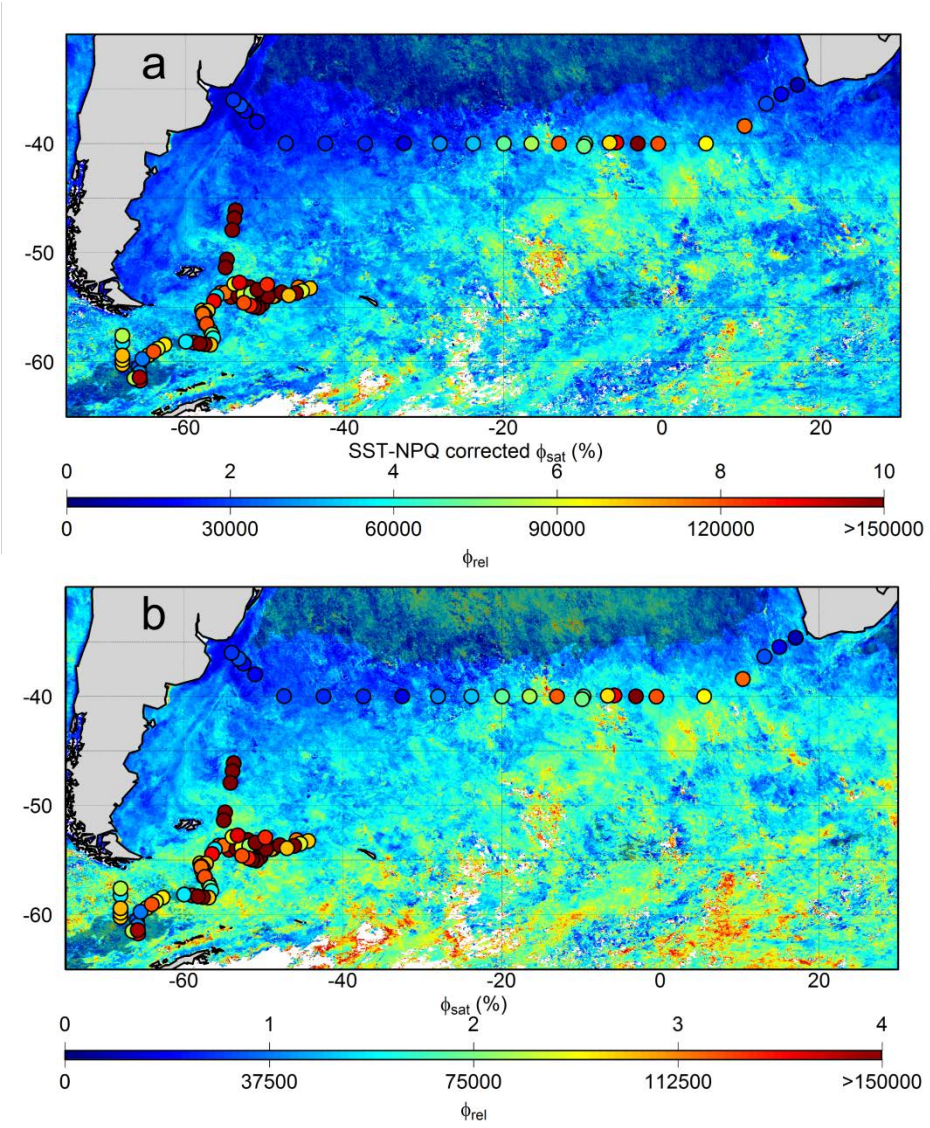

Figure 5.9: NPQ-corrected ϕ_{sat} for January-March 2012 with field measurements of ϕ_{rel} over plotted. Two NPQ corrections have been applied: a) *SST*-NPQ correction; b) 1/*iPAR* NPQ correction. Note that for (a) the correction function was only applied over the *SST* range for NPQ experiments (2 to 24 °C). Pixels with chlorophyll-a less than 0.1 mg m^{-3} are shaded.

5.3.5 Decadal composite of NPQ-corrected ϕ_{sat}

Extending the NPQ (*SST*) correction to all circumpolar waters for a 2002-2012 austral summer composite revealed clear spatial patterns in ϕ_{sat} (Figure 5.10a). Given the uncertainties involved in calculating ϕ_{sat}, caution clearly still needs to be applied in

attributing such spatial variability to Fe stress, although our field observations lend support to such an interpretation. Indeed, elevated values of the climatology of NPQ-corrected ϕ_{sat} (using *SST*) spatially correlated with summertime elevated nitrate (Figure 5.10c) and hence the broad so-called high-nitrate low-chlorophyll regime expected to be characterised by Fe stress (Moore et al., 2013). In contrast, using a 1/*iPAR* NPQ correction (Behrenfeld et al., 2009), which cannot account for spatial variability in the NPQ relationships we observed, produced fields of ϕ_{sat} that do not correlate with elevated summertime nitrate, in particular decreasing significantly south of 60°S and increasing in the sub-tropics (Figure 5.10b). Finer scale spatial variability in *SST*-NPQ corrected ϕ_{sat} might subsequently be related to regional scale Fe sources, for example over the Patagonian shelf and other potential sedimentary sources, dust deposition (Cassar et al., 2007), deep water upwelling (de Baar et al., 1995; Lefèvre et al., 1999), or iceberg discharge (Raiswell et al., 2008).

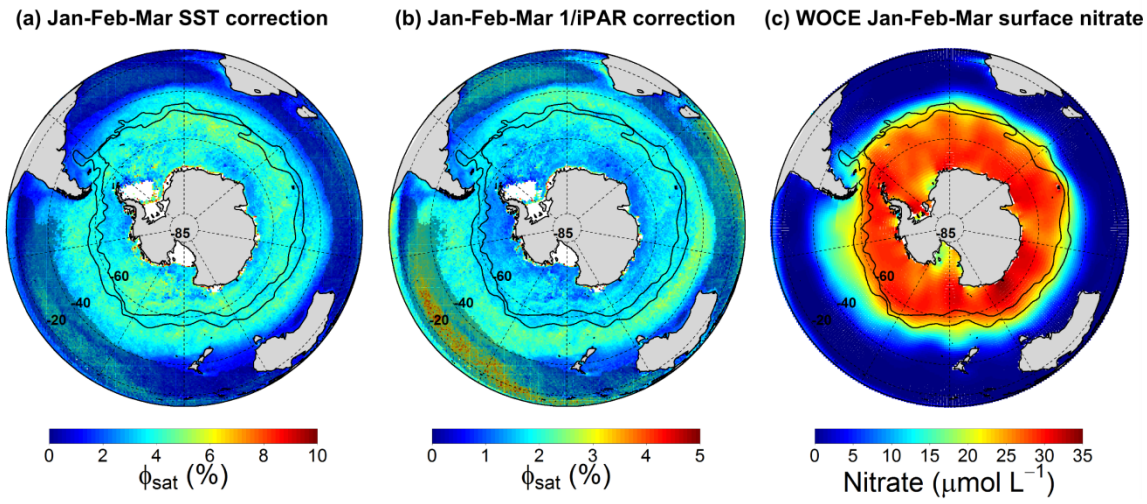

Figure 5.10: Southern Ocean 2002-2012 austral summertime composites of NPQ corrected ϕ_{sat}: a) NPQ (*SST*) corrected ϕ_{sat} (note that we have included data beyond the latitudinal bounds of our experiments and these regions should thus be interpreted with caution); b) 1/*iPAR* corrected ϕ_{sat}; c) WOCE austral summertime nitrate concentrations (http://woce.nodc.noaa.gov/wdiu/). Pixels with chlorophyll-a less than 0.1 mg m^{-3} in (a) and (b) are shaded. Black lines show locations of polar (inner) and sub-Antarctic (outer) fronts from Orsi et al. (1995).

5.4 Conclusions

Decades of field work on ships has been required to map regions of Fe stress) Moore et al., 2013) and hence the ability to retrieve such information globally at high temporal frequency using remote sensing observations of chlorophyll fluorescence is an exciting possibility (Behrenfeld et al., 2009). However, thus far uncertainty in phytoplankton NPQ behaviour has limited realisation of this potential. Here we have developed and applied a dynamic *SST*-based NPQ correction for ϕ_{sat} and suggest there is a strong likelihood that the resulting product may be indicative of relative Fe stress levels. However, whilst our field data do span several biogeochemical provinces, we advise caution when interpreting *SST*-NPQ corrected ϕ_{sat} beyond the sampled region. Two factors of particular concern are (i) the applicability of such an NPQ correction in other regions and seasons, and (ii) potential artefacts associated with satellite retrieved chlorophyll concentrations and fluorescence when chlorophyll is less than 0.1 mg m^{-3} (Huot et al., 2013).

Characterising NPQ behaviour throughout the world's oceans may ultimately allow less biased global maps of ϕ_{sat} to be attained. Although conducting sufficient numbers of dedicated experiments would be a significant task, as suggested above, fluorescence data routinely collected from ships underway flow through systems could allow broad characterisation of NPQ regimes. Establishment of robust relationships could subsequently facilitate less ambiguous attribution of variability in ϕ_{sat} to Fe stress across broad spatio-temporal scales.

6 Overall conclusions and future directions

6.1 Overall conclusions

AS set out in the introduction, the aim of this thesis has been to improve understanding of phytoplankton physiological status and nutrient limitation patterns in the South Atlantic and Southern Ocean. This has been achieved using field measurements and bioassay experiments on three research cruises in these regions and by developing a new method for evaluating the quantum yield of fluorescence in the hope that, with further work, regions of Fe-stressed phytoplankton communities can be mapped confidently at a high spatial and temporal resolution on a global scale.

In chapter two, sections of photophysiological parameters were presented for two crossings of the south subtropical convergence (SSTC) in the South Atlantic. As perhaps may have been predicted *a priori*, although certainly not with a high degree of confidence, marked differences were seen between the two systems throughout the surface mixed layer. Strongly depressed dark-acclimated F_v/F_m values were observed in ACC type waters that were shown not to be a result of photodamage or photoacclimation, and did not correlate with expected signatures of phytoplankton community structure. These low F_v/F_m values were shown to be a direct result of community level Fe stress, as evidenced by marked positive F_v/F_m responses over 24 hours to Fe addition relative to control bottles with no treatment. Conversely, high F_v/F_m values were found consistently throughout the water column in subtropical gyre type regimes that did not respond to Fe amendment. This was even the case in waters of the Agulhas Current where seawater dissolved Fe concentrations descended to values lower than that of many samples from

the sub-Antarctic sector. Phytoplankton in these waters were concluded to be living under steady state nitrate limitation, where nitrate concentrations were limiting the overall phytoplankton standing crop, yet the phytoplankton present were not being starved of the nutrient due to effective re-supply through rapid recycling. A significant finding therefore was that Fe limitation itself could not be predicted using seawater dissolved Fe concentrations alone. The Fe: nitrate ratio, or even nitrate concentrations themselves, were a much better predictor of identifying regions where Fe stress had developed, consistent with the idea that the supply ratios of these two nutrients effectively dictate nutrient limitation patterns on large spatial scales.

Chapter 3 presented photophysiological and ancillary data through a gradient in micronutrient availability from the North Scotia Ridge to the Drake Passage in the Southern Ocean. Three photophysiological regimes were delineated along this transect on the basis of trends in environmental parameters and night time values of F_v/F_m and σ_{PSII}. F_v/F_m values showed a clear reduction between the Scotia Ridge and the central Scotia Sea - Drake Passage, consistent with the expected reduction in micronutrient availability. On the other hand σ_{PSII} remained high until entering the Drake Passage, where depressed values were observed. This observation is inconsistent with previous field studies and was suggested to be a result of a micronutrient stress-induced disconnection between light harvesting antennae and RCII, brought about as a result of a low cellular requirement of photosynthate under low growth rates. For this study an attempt was made to use electron transport rate (ETR) light curve parameters to put these photophysiological signatures into perspective with regard to the effect on electron flow through RCII and therefore, indirectly, primary production.

Chapter 4 presented results from Fe and volcanic ash amendment experiments. These were conducted with the aim of determining the response of natural phytoplankton

communities in HNLC regions to ash supply. Somewhat unexpectedly, these experiments showed not only that ash supply could relieve phytoplankton Fe limitation as effectively as $FeCl_3$, but that in a number of cases phytoplankton responded to the supply of ash where there was no response at all to Fe amendment. Although a number of possible causes could be hypothesised, a process of elimination using ancillary data suggested that this was most likely a result of (co-)limitation by another trace-metal micronutrient, namely manganese (Mn). This hypothesis was particularly well supported by the dissolved concentrations of Mn that were amongst the lowest that have ever been measured in seawater. This would be an important finding, as currently phytoplankton growth in the Southern Ocean is widely assumed to be limited by the availability of Fe only (and seasonally, light). The results and interpretation of this study would suggest that Mn in addition to Fe would be necessary to stimulate phytoplankton growth in Drake Passage in austral summer time (and possibly other times of the year), and that volcanic eruptions could be an effective fertiliser for this system.

Chapter 5 presented non-photochemical quenching (NPQ) experiments throughout the cruise regions discussed in the first two chapters. The aim of these experiments were to assess for possible differences in NPQ responses of the various phytoplankton communities living under the variable environmental conditions encountered. Marked differences in phytoplankton NPQ behaviour were found, suggested to be driven by the variable mixing (and therefore light) environments the phytoplankton were growing under. The degree of NPQ measured showed large variability, empirically correlating well with sea surface temperatures that could therefore be used as a predictor for NPQ. Correcting sunlight induced chlorophyll fluorescence (SICF) retrieved by sensors on satellites is particularly important if this method is to be used to successfully exploit the unique fluorescence signatures of Fe-stressed phytoplankton to reveal regions of Fe-

limited phytoplankton growth. Correcting the fluorescence quantum yield for NPQ and comparing spatial patterns of resultant fields with areas experimentally-diagnosed as either Fe-stressed or Fe-replete, regions of high NPQ-corrected satellite fluorescence quantum yields were found to match up well with Fe-stressed regions. The findings presented in this chapter therefore suggested that this satellite derived parameter could be used successfully for this purpose, at least in the regions encountered and in the season field measurements were made.

6.2 Future directions

Whilst the work presented in Chapters 2-5 contributed significantly to diagnosing and understanding nutrient limitation patterns in the study regions encountered, many important questions remain to be answered. Some of these questions are considered below.

Physiologically, what causes low F_v/F_m or high chlorophyll normalised fluorescence in micronutrient-stressed phytoplankton? Laboratory studies are strongly suggesting the importance of 'energetically uncoupled' light harvesting complexes that appear to accumulate under Fe, oxidative, or salt stress (Behrenfeld and Milligan, 2013). If values of F_v/F_m do not reflect a quantum yield of photochemistry under these conditions, can they be used to estimate ETR or in turn carbon fixation? Work in this area focusing on phytoplankton species found in the open ocean (Macey et al., 2014), might reveal understanding that will necessitate re-interpretation of some published FRRf data.

Thus far, energetically uncoupled light harvesting complexes have been characterised using protein separation and Western Blot techniques (e.g., Schrader et al., 2011; Ryan-Keogh et al., 2011). An additional method of evaluating community level expression of energetically uncoupled complexes in the field could be to assess for characteristic

fluorescence lifetime signatures. The theory behind this approach is that energetically isolated light harvesting complexes are expected to show much shorter lived fluorescence lifetimes following illumination with a fully saturating blue light flash than a light harvesting complex coupled to a reaction centre. This expectation is a result of energy being supplied to a reaction centre through a connected light harvesting complex likely 'spilling over' into adjacent reaction centres, or being transferred backwards and forwards between a reaction centre and adjacent energy transfer pigments before fluorescing (Knox, 1975; Falkowski and Raven, 1997). Consequently this energy would, on average, take longer to emerge as fluorescence. Thus decay of fluorescence subsequent to a fully saturating light flash would take longer from cells with a higher fraction of energetically coupled reaction centres relative to uncoupled ones. Difficulties with pursuing this method might be that custom instrumentation would likely have to be built (i.e., a standard FRRf would not be able to perform these measurements), and furthermore the short fluorescence lifetimes of energetically isolated light harvesting complexes are predicted but have not yet been well characterised (e.g. Croce and van Amerongen, 2011).

An advantage of pursuing this line of research is that characterisation of the fluorescence behaviour of energetically coupled versus isolated light harvesting complexes could potentially be helpful in developing a mechanistic model of fluorescence quantum yield variability with irradiance. The simple model of NPQ presented in Chapter 5 performed well in its predictive capacity (i.e., predicting changes in fluorescence quantum yields with incident irradiance) and therefore correcting satellite retrieved fluorescence data, however the model delivers relatively limited physiological information (i.e., in terms of the relative roles of different components of NPQ). As noted in Chapter 5, the existing mechanistic model of Morrison (2003) was investigated as a means of fitting

fluorescence quantum yield versus irradiance data for the NPQ experiments conducted. Unfortunately, the fit quality of the model to the data was poor, possibly because the presence and quenching characteristics of a pool of energetically isolated pigment protein complexes are not accounted for in the model. Thus monitoring changes in fluorescence quenching with increasing irradiance, together with knowledge of the relative ratio of energetically coupled to isolated pigment protein complexes, could allow for an additional or modified term to be incorporated into existing models and thus potentially a better fit to the data in Fe-stressed waters.

Further work in this field could be particularly valuable because, as has been recently been proposed, the presence of energetically uncoupled pigment protein complexes in micronutrient-stressed regions may necessitate different treatment of these waters in primary production models that use satellite retrieved chlorophyll-a as a proxy for phytoplankton biomass (Behrenfeld et al., 2006; Schrader et al., 2011). New methodologies such as the approach described previously could potentially allow for effective characterisation of the relative abundance of energetically coupled versus isolated pigment protein complexes over large spatio-temporal scales. If the occurrence of energetically isolated pigment protein complexes turns out to be widespread across micronutrient-stressed regimes, the need for treating these regions separately in models of global primary production would be consistent with province-specific approaches for successful modelling of global primary production (Platt and Sathyendranath, 1988; Longhurst et al., 1995).

As a more general comment, the work synthesised by Cullen et al. (1992) concerning the influence of nutrient limitation on photosynthetic parameters (i.e., photosynthesis-irradiance curve parameters) remains to be clearly resolved for the most micronutrient limited natural systems in the world's oceans. For example no consistent trend in

chlorophyll-normalised light-saturated photosynthetic rates (P_{max}^{Chl}) or light limited slopes (α^{Chl}) between Fe-stressed and Fe-replete phytoplankton communities has been convincingly established. This is exemplified by the variable results of: Lindley and Barber, 1998; Maldonado et al., 1999, 2001; Gervais et al., 2002; Marchetti et al., 2006; Moore et al., 2007; and Hiscock et al., 2008.

For example, Hiscock et al. (2008) showed values of α^{Chl} to increase significantly in response to relief of Fe limitation in a mesoscale Southern Ocean Fe release experiment (with no significant change in P_{max}^{Chl}). This response to relief of Fe limitation thus appeared to be the physiological mechanism underlying the simultaneous increase in phytoplankton standing stocks observed. Increases in α^{Chl} were also observed in Fe-stressed waters of the Equatorial Pacific in response to a mesoscale Fe enrichment (Lindley and Barber, 1998). Conversely no response in α^{Chl} was observed by Gervais et al. (2002) in a separate mesoscale Fe release experiment in the Southern Ocean, nor Maldonado et al. (1999) or Moore et al. (2007) in bottle scale enrichment experiments in the North Pacific and Southern Ocean respectably.

This discrepancy could be important to resolve: if, as was suggested by Hiscock et al. (2008) and by the suite of rETR curves presented in Chapter 3, micronutrient stress is indeed a cause of depressed values of the light limited slope under Fe stress, this would considerably reduce primary production in these waters and mean that routinely used primary production algorithms (e.g., Behrenfeld and Falkowski, 1997) are incorrectly estimating production in these waters.

The variable results for these photosynthetic parameters are likely strongly influenced by severity of micronutrient stress (e.g., Cullen et al., 2002; Behrenfeld et al., 2004, 2013), influences of community structure (e.g., Bouman et al., 2005; Moore et al., 2007), and

photoacclimatory mechanisms (e.g., Cullen et al., 1992; Bouman et al., 2000, 2005; MacIntyre et al., 2002). Thus it is necessary to collect these ancillary data to aid with interpretation of photosynthesis-irradiance curve parameters under Fe-stressed and Fe-replete conditions. This would enable a more thorough appraisal of a question considered in Chapter 3: does micronutrient limitation ever influence the physiological performance of phytoplankton in the open ocean, or simply regulate the standing stock of phytoplankton present (Behrenfeld and Milligan, 2013; Cullen et al., 1992; Moore et al., 2008; Behrenfeld et al., 2004)? Again it is important to stress that changes in photosynthetic parameters with nutrient stress (e.g., Welschmeyer and Lorenzen, 1981; Cleveland and Perry, 1987; Cullen, 1990; Davey and Geider, 2001) would strongly influence models of primary production (e.g., Edwards et al., 2004; Hiscock et al., 2008; Behrenfeld and Falkowski, 1997) and more complex biogeochemical models (e.g., Vichi et al., 2013).

How reliably can night time F_v/F_m be used to diagnose a shift from proximal Fe to nitrate limitation or vice versa? For instance, would adding small quantities of nitrate to the Agulhas Current waters discussed in Chapter 2 have induced F_v/F_m reductions as has been reported in a laboratory study (Schrader et al., 2011)? Schrader et al. (2011) reported a Fe-nitrate colimited culture to have maximal F_v/F_m values. This was suggested to be a result of limited Fe availability restricting reaction centre synthesis and limited nitrate resources for constructing isolated light harvesting complexes. Addition of nitrate resulted in F_v/F_m reductions as the nutrient became available to synthesise energetically uncoupled light harvesting complexes. Whether this is observed in the field could be important to resolve: in areas where nitrate concentrations are low but measureable (and traditionally thought of as nitrate limited systems), for example in the Southern California Current (King and Barbeau, 2007; Hopkinson and Barbeau, 2008) or

the post-spring bloom high latitude North Atlantic (Ryan-Keogh et al., 2013), Fe stress could be important for regulating phytoplankton community structure and primary production (e.g., King and Barbeau, 2007; Hopkinson and Barbeau, 2008; Ryan-Keogh et al., 2013). Therefore the ability to use values of F_v/F_m, without resource intensive trace-metal-clean bioassay experiments to reliably diagnose Fe versus nitrate limitation and monitor future change in systems such as these would be valuable.

Are phytoplankton communities in Drake Passage limited by Mn? If so is this a proximal limitation or a colimitation alongside Fe? If this is a colimitation condition, what classification of colimitation does this represent (Arrigo, 2005; Saito et al., 2008), and therefore is the phytoplankton response to addition of both of these micronutrients additive or multiplicative (Boyd and Hutchins, 2012, after Folt et al., 1999)? For example, adding Fe appeared to result in no statistically significant phytoplankton response in a number of the experiments, yet it is possible that adding Mn on its own could result in no response either, or that adding Mn leads to some response yet adding both Fe and Mn together leads to an even larger response. Given the critical roles of these micronutrients in photosynthetic machinery, and their photochemical regulation in surface waters (Sunda and Huntsman, 1994; Barbeau et al., 2001; Tagliabue et al., 2009), the relevance of growth irradiance in the context of this colimitation would also be informative (e.g., Peers and Price, 2004; Sunda and Huntsman, 1997; Strzepek et al., 2012).

If Mn limitation is found to exist, an obvious question is: what is the spatial and depth resolved extent of this condition? For example it would be interesting to know if Mn concentrations are gradually depleted in open ocean regions throughout the growing season, such that onset on Mn limitation only occurs in late spring, or if they are simply dependant on episodic supply and vary in a fasion which is difficult to predict. Work

assessing the Fe:Mn ratio of various supply mechanisms and stoichiometric requirements of phytoplankton for these elements may help with predicting which micronutrient becomes depleted first. The comprehensive mapping exercise of seawater Mn concentrations in the Southern Ocean by Middag et al. (2011, 2012, and 2013) suggests that Mn concentrations can be low (~0.05 nM) over large spatial extents, even downstream of the Drake Passage – Scotia Ridge region. Furthermore, as Mn and Fe are likely to be often simultaneously drawn down to depleted levels, and that the solubility of Mn typically increases under elevated irradiance, does this induce diel patterns in the trace metal most limiting to to the extant phytoplankton community?

Convincing evidence of (co)limitation would likely stimulate significantly more research into the biogeochemical consequences of this finding. If future work reveals no evidence of (co)limitation by this micronutrient, the cause for phytoplankton responding to ash addition, but not $FeCl_3$, represents an uncertainty in current understanding of Southern Ocean biogeochemistry and thus remains important to address. Possible alternatives were outlined in Chapter 4, including the release kinetics of Fe from the ash relative to the $FeCl_3$ spike, and the possibility of ash releasing the more soluble (and thus more bioaccessible) Fe (II) compared with the Fe (III) present in the $FeCl_3$ spike. Testing each of these could be more complicated than a simple Mn addition. Two possible methods could be to: (i) add ligand bound (and thus more soluble) Fe as an artificial spike, which could address the issue of bioavailability of supplied Fe; or (ii) supply of small quantities of Fe over a period of time, possibly through the addition of a well characterised Fe containing soluble salt for which the Fe release kinetics may be more in line with that from the ash (e.g., Olgun et al., 2011).

What are the biogeochemical consequences of a volcanic eruption in an HNLC system? Preliminary work presented in Chapter 4 suggested the response will be strong,

but how long lived and exactly what parts of the marine biogeochemical system would be influenced remain to be investigated. Modelling could help with this, yet important parameters that would go into these are poorly constrained and could limit the usefulness of results obtained (e.g., Boyd and Mackie, 2008; see references listed in the section above). Even a large scale ash-release experiment (sensu Boyd et al., 2007), which whilst likely being highly informative, could be difficult to realise and would almost certainly still lead to further questions (Boyd et al., 2007). Perhaps the marine biogeochemistry community, like the volcanologists, atmospheric and climate scientists, should be ready to mount a field campaign capable of measuring a suite of informative parameters subsequent to natural ash fallout following any large volcanic eruptions in an HNLC region.

Predicting phytoplankton responses to ash supply will likely require a detailed evaluation of the ash being added to the system. For example ash particle size may exert a particularly important control on metal release, as for a given mass of ash addition metal release may be expected to be greater for ash samples with smaller grain sizes and thus larger surface area per bulk ash mass (assuming soluble salts on the ash surface scale positively with surface area). Performing additional leaching experiments would also likely yield valuable results. For example the results of the experiments presented in Chapter 4 indicated very high variability in Fe release between samples within a given ash type (around 100%), and it would be informative to track down the exact reason for this. Furthermore, obtaining more biogeochemically relevant values of metal release will require improvements in leaching methodologies currently employed. Carefully designed experiments detecting metal release from ash using conditions that best replicate, or ideally utilise, the natural ocean are needed if ash mass fluxes are to be used for projecting total metal (e.g., Fe) input to the surface ocean subsequent to an eruption and

thereby attempting to quantify primary production stimulated (c.f. Watson, 1997). For reasons outlined previously, such experiments should pay careful consideration to ash particle size, ash loading, and exposure time to best mimic natural ash depositions in the oceanic regime of interest (i.e. coastal versus open ocean waters).

How will the limitation patterns identified in this thesis be altered by projected global environmental changes? Carefully designed experiments examining phytoplankton response to combinations of the most critical environmental drivers will be a useful tool for an initial assessment of this (Boyd and Doney, 2002; Boyd et al., 2010; Boyd and Hutchins, 2012). For example, pronounced coincident environmental changes projected with global climate models (e.g., Sarmiento et al., 1998; Boyd and Doney, 2002) can be identified and natural phytoplankton communities can be exposed to these projected changes in controlled bottle experiments (Boyd et al., 2014). Observed responses of phytoplankton communities to such drivers may therefore give some level of appreciation of how phytoplankton may respond in the immediate term – for example, at least indicating to first order if there is an increase or decrease in phytoplankton biomass and/or a significant shift in community structure.

Of course, bottle scale experiments are only conducted for durations of several days or less - projected anthropogenically-induced changes are anticipated to occur over much longer (~1-100 year) timescales. Therefore, (i) any bottle scale experiments such as those described should be interpreted with this inherent limitation in mind; and (ii) methods of exploring potential longer term shifts in community structure and adaptation of phytoplankton to their growth environment should also be explored. For example, Lohbeck et al. (2012) monitored the response of the coccolithophore *Emiliania huxleyi* to a pH reduction over 500 generations in the laboratory and found that adaptation over this period significantly increased the ability of this species to function under less alkaline

conditions. Experiments such as these are rare - they inevitably take a long duration to conduct, are labour intensive, and have the inherent practical limitation of including only a single or a few drivers on monospecific cultures. An additional avenue of research being conducted that may yield insight into future phytoplankton responses is study of the geological record. The apparent response of phytoplankton in the geological record to well-constrained past environmental changes could enable more informed predictions regarding the longer term responses of phytoplankton to projected future change (e.g., Shen et al., 1987; Zachos et al., 2005; Sluijs et al., 2006). However, constraining environmental change in the geological past in sufficient detail, for example to include changes in nutrient supply patterns and stoichiometry's, is challenging (e.g., Barber et al., Falkowski, 1997; Doney et al., 2009). A multidisciplinary approach is warranted and is currently being pursued by the scientific community.

As recently reviewed by Moore et al. (2013), large gaps in our understanding even of modern day nutrient limitation patterns exist. As a well constrained baseline is necessary for successfully monitoring contemporary changes in marine ecosystems, it will be necessary to maintain research efforts focussed in this area. The international GEOTRACES programme (Henderson, et al., 2005) has already substantially improved knowledge of the ocean basin-scale distributions of micronutrients – recently made publically accessible through an intermediate data product (e.g., Morrison, 2014). In addition to this mapping exercise, the GEOTRACES programme has conducted dedicated process studies in an attempt to constrain mechanisms regulating dynamic micronutrient cycling in the surface ocean (Boyd et al.,2005; Strzepek et al., 2005). In addition to field-based programmes such as these, continued improvement of the performance, coverage, and understanding of remote sensing and autonomous instrument techniques will likely represent the best option for cost-effective quasi-synoptic

monitoring of current conditions and future change (Howe et al., 2010; Dickey et al., 2005).

References

Abbott, M. R. and Letelier, R.M. (1999), Algorithm theoretical basis document chlorophyll fluorescence, MODIS product number 20, NASA, http://modis.gsfc.nasa.gov/data/atbd/atbdmod22.pdf.

Achterberg, E. P., Moore, C. M., Henson, S. A., Steigenberger, S., Stohl, A., Eckhardt, S., et al. (2013), Natural iron fertilization by the Eyjafjallajokull volcanic eruption, *Geophys. Res. Lett., 40*, 921-926.

Allen, A. E., La Roche, J., Maheswari, U., Lommer, M., Schauer, N., Lopez, P. J., et al. (2008), Whole-cell response of the pennate diatom Phaeodactylum tricornutum to iron starvation, *Proc. Natl Acad. Sci. USA*, 105 (30), 10438-10443.

Aumont, O., Maier-Reimer, E., Blain, S., and Monfray, P. (2003), An ecosystem model of the global ocean including Fe, Si, P colimitations, *Global Biogeochemical Cy.*, 17, 1060.

Arrigo, K. R. (2005), Marine microorganisms and global nutrient cycles, *Nature*, 438 (7064), 122-122.

Ardelan, M. V., Holm-Hansen, O., Hewes, C. D., Reiss, C. S., Silva, N. S., Dulaiova, H., et al. (2010), Natural iron enrichment around the Antarctic Peninsula in the Southern Ocean, *Biogeosciences*, 7 (1), 11-25.

Arnon, D. I., Tsujimot H. Y., and McSwain, B. D. (1965), Photosynthetic phosphorylation and electron transport, *Nature*, 207 (5004), 1367.

Barbeau, K., Rue, E. L., Bruland, K. W., and Butler, A. (2001), Photochemical cycling of iron in the surface ocean mediated by microbial iron(III)-binding ligands, *Nature*, 413 (6854), 409-413.

Barber, R. T. (1992), Geologic and climatic time scales of nutrient variability, pp. 89–106 in Falkowski, P. G. and Woodhead, A. (eds.), *Primary productivity and biogeochemical cycles in the sea*, Plenum.

Barber, J. (2008), Photosynthetic generation of oxygen, *Philos. T. Roy. Soc. B.*, 363 (1504), 2665-2674.

Bay, R. C., Bramall, N., and Price, P. B. (2004), Bipolar correlation of volcanism with millennial climate change, *Proc. Natl Acad. Sci. USA*, *101*, 6341-6345.

Behrenfeld, M. J., Bale, A. J., Kolber, Z. S., Aiken, J., and Falkowski, P. G. (1996), Confirmation of iron limitation of phytoplankton photosynthesis in the equatorial Pacific Ocean, *Nature*, 383, 508-511.

Behrenfeld, M. J., and Falkowski, P. G. (1997), Photosynthetic rates derived from satellite-based chlorophyll concentration, *Limnol. Oceanogr.*, 42, 1-20.

Behrenfeld, M. J., Prasil, O., Kolber, Z. S., Babin, M., and Falkowski, P. G. (1998), Compensatory changes in Photosystem II electron turnover rates protect photosynthesis from photoinhibition. *Photosynth. Res.*, 58 (3), 259-268.

Behrenfeld, M. J., Prasil, O., Babin, M., and Bruyant, F. (2004), In search of a physiological basis for covariations in light-limited and light-saturated photosynthesis, *J. Phycol.*, *40*(1), 4-25.

Behrenfeld, M. J., Worthington, K., Sherrell, R. M., Chavez, F. P., Strutton, P., McPhaden, M., and Shea, D. M. (2006), Controls on tropical Pacific Ocean productivity revealed through nutrient stress diagnostics, *Nature*, 442, 1025-1028.

Behrenfeld, M. J., Halsey, K. H. and Milligan, A. J. (2008), Evolved physiological responses of phytoplankton to their integrated growth environment, *Philos. T. Roy. Soc. B.*, 363 (1504), 2687-2703.

Behrenfeld, M. J., Westberry, T. K., Boss, E. S., O'Malley, R. T., Siegel, D. A., Wiggert, J. D., et al. (2009), Satellite-detected fluorescence reveals global physiology of ocean phytoplankton, *Biogeosciences*, 6(5), 779-794.

Behrenfeld, M. J., and Milligan, A. J. (2013), Photophysiological expressions of iron stress in phytoplankton, *Ann. Rev. Mar. Sci.*, 5, 217-246.

Bertrand, E. M., Saito, M. A., Rose, J. M., Riesselman, C. R., Lohan, M. C., Noble, A. E., et al. (2007), Vitamin B-12 and iron colimitation of phytoplankton growth in the Ross Sea, *Limnol. Oceanogr.*, 52 (3), 1079-1093.

Bibby, T. S., Nield, J. and Barber, J. (2001), Iron deficiency induces the formation of an antenna ring around trimeric photosystem I in cyanobacteria, *Nature*, 412 (6848), 743-745.

Blain, S., Treguer, P., Belviso, S., Bucciarelli, E., Denis, M., Desabre, S., Fiala, M., Jezequel, V. M., Le Fevre, J., Mayzaud, P., Marty, J. C., and Razouls, S. (2001), A biogeochemical study of the island mass effect in the context of the iron hypothesis: Kerguelen Islands, Southern Ocean, *Deep-Sea Res. Pt. I*, 48, 163-187.

Blain, S., Sedwick, P. N., Griffiths, F. B., Queguiner, B., Bucciarelli, E., Fiala, M., Pondaven, P., and Treguer, P. (2002), Quantification of algal iron requirements in the Subantarctic Southern Ocean (Indian sector), *Deep-Sea Res. Pt. II*, 49, 3255-3273.

Blain, S., Queguiner, B., Armand, L., Belviso, S., Bombled, B., Bopp, L., Bowie, A., Brunet, C., Brussaard, C., Carlotti, F., et al. (2007), Effect of natural iron fertilization on carbon sequestration in the Southern Ocean, *Nature*, 446, 1070-1074.

Bouman, H. A., Platt, T., Kraay, G. W., Sathyendranath, S., and Irwin, B. D. (2000), Bio-optical properties of the subtropical North Atlantic. I. Vertical variability, *Mar. Ecol. Prog. Ser.*, 200, 3-18.

Bouman, H. A., Platt, T., Sathyendranath, S., Li, W. K., Stuart, V., Fuentes-Yaco, C., et al. (2003), Temperature as indicator of optical properties and community structure of marine phytoplankton: implications for remote sensing, *Mar. Ecol. Prog. Ser.*, 258, 19-30.

Bouman, H., Platt, T., Sathyendranath, S., and Stuart, V. (2005), Dependence of light-saturated photosynthesis on temperature and community structure, *Deep-Sea Res. Pt. I*, 52 (7), 1284-1299.

Bouman, H. A., Lepère, C., Scanlan, D. J., and Osvaldo, U. (2012), Phytoplankton community structure in a high-nutrient, low-chlorophyll region of the eastern Pacific Subantarctic region during winter-mixed and summer-stratified conditions, *Deep-Sea Res. Pt. I*, 69**,** 1–11.

Boyd, P. W., Watson, A. J., Law, C. S., Abraham, E. R., Trull, T., Murdoch, R., Bakker, D. C. E., Bowie, A. R., Buesseler, K. O., et al. (2000), A mesoscale phytoplankton bloom in the polar Southern Ocean stimulated by iron fertilization, *Nature*, 407, 695-702.

Boyd, P. W., and Abraham, E. R. (2001), Iron-mediated changes in phytoplankton photosynthetic competence during SOIREE, *Deep-Sea Res. Pt. II*, 48, 2529-2550.

Boyd, P. W. (2002), Environmental factors controlling phytoplankton processes in the Southern Ocean, *J. Phycol.*, 38 (5), 844-861.

Boyd, P. W. and Doney, S. C. (2002), Modelling regional responses by marine pelagic ecosystems to global climate change, *Geophys. Res. Lett.*, 29 (16).

Boyd, P. W., Law, C. S., Hutchins, D. A., Abraham, E. R., Croot, P. L., Ellwood, M. et al. (2005), FeCycle: Attempting an iron biogeochemical budget from a mesoscale SF6 tracer experiment in unperturbed low iron waters, *Global Biogeochem. Cy.*, 19(4), GB4S20.

Boyd, P. W., Jickells, T., Law, C. S., Blain, S., Boyle, E. A., Buesseler, K. O., et al. (2007), Mesoscale iron enrichment experiments 1993-2005: Synthesis and future directions, *Science*, *315*, 612-617.

Boyd, P. W. and Mackie, D. (2008), Comment on the Southern Ocean biological response to aeolian iron deposition, *Science*, 319 (5860).

Boyd, P. W. and Ellwood, M. J. (2010), The biogeochemical cycle of iron in the ocean, *Nat. Geosci.*, 3 (10), 675-682.

Boyd, P. W., Strzepek, R., Fu, F., and Hutchins, D. A. (2010), Environmental control of open-ocean phytoplankton groups: Now and in the future, *Limnol. Oceanogr.*, 55 (3), 1353-1376.

Boyd, P. W. and Hutchins, D. A. (2012), Understanding the responses of ocean biota to a complex matrix of cumulative anthropogenic change, *Mar. Ecol. Prog. Ser.*, 470, 125-135.

Boyd, P. W., Strzepek, R., Fu, F. X., and Hutchins, D. A. (2010), Environmental control of open-ocean phytoplankton groups: Now and in the future, *Limnol. Oceanogr.*, 55, 1353-1376.

Boyd, P. W., Arrigo, K. R., Strzepek, R., and Dijken, G. L. (2012), Mapping phytoplankton iron utilization: Insights into Southern Ocean supply mechanisms, *J. Geophys. Res.-Oceans*, 117.

Boyd, P. W., Doney, S. C., Glover, D., Lennartz, S. (2014) New approaches to designing complex environmental manipulations of marine phytoplankton. *AGU Ocean Sciences Hawaii 2014 conference abstract* (Abstract ID: 14570).

Boye, M., van den Berg, C. M., de Jong, J., Leach, H., Croot, P., and de Baar, H. J. (2001), Organic complexation of iron in the Southern Ocean, *Deep-Sea Res. Pt. I, 48*, 1477-1497.

Bricaud, A., A. Morel, M. Babin, K. Allali, and Claustre, H. (1998), Variations of light absorption by suspended particles with chlorophyll a concentration in oceanic (case 1) waters: Analysis and implications for bio-optical models, *J. Geophys. Res.-Oceans*, 103(C13), 31033-31044.

Broecker, W. S., and Peng, T. H., (1982), *Tracers in the Sea*, Lamont-Doherty Geological Observatory, Columbia University.

Browning, T. J., H. A. Bouman, C. M. Moore, C. Schlosser, G. A. Tarran, E. M.S Woodward, and Henderson, G. M. (2014), Nutrient regimes control phytoplankton ecophysiology in the South Atlantic, *Biogeosciences*, 11, 463-479.

Bruland, K. W., Donat, J. R. and Hutchins, D. A. (1991), Interactive influences of bioactive trace-metals on biological production in oceanic waters, *Limnol. Oceanogr., 36*, 1555-1577.

Bucciarelli, E., Blain, S., and Treguer, P. (2001), Iron and manganese in the wake of the Kerguelen Islands (Southern Ocean), *Mar. Chem.*, 73, 21-36.

Canfield, D. E. (1998), A new model for Proterozoic ocean chemistry, *Nature*, 396 (6710), 450-453.

Cassar, N., M. L. Bender, B. A. Barnett, S. Fan, W. J. Moxim, H. Levy, II, and Tilbrook B. (2007), The Southern Ocean biological response to Aeolian iron deposition, *Science*, 317(5841), 1067-1070.

Cather, S. M., Dunbar, N. W., McDowell, F. W., McIntosh, W. C. and Scholle, P. A. (2009), Climate forcing by iron fertilization from repeated ignimbrite eruptions: The icehouse-silicic large igneous province (SLIP) hypothesis, *Geosphere*, *5*, 315-324.

Censi, P., Randazzo, L. A., Zuddas, P., Saiano, F., Aricò, P., and Andò, S. (2010), Trace element behaviour in seawater during Etna's pyroclastic activity in 2001: Concurrent effects of nutrients and formation of alteration minerals, *J. Volcanol. Geoth. Res.*, 193 (1-2), 106-116.

Chekalyuk, A. M., and Hafez, M. A. (2008), Advanced laser fluorometry of natural aquatic environments, *Limnol. Oceanogr- Meth.*, 6, 591.

Ciotti, A. M., Lewis, M. R., and Cullen, J. J. (2002) Assessment of the relationships between dominant cell size in natural phytoplankton communities and the spectral shape of the absorption coefficient, *Limnol. Oceanogr.*, 47, 404-417.

Cleveland, J. S. and Perry, M. J. (1987), Quantum yield, relative specific absorption and fluorescence in nitrogen-limited chaetoceros-gracilis, *Mar. Biol.*, 94 (4), 489-497.

Cleveland, J. S., and Weidemann, A. D. (1993), Quantifying absorption by aquatic particles – a multiple-scattering correction for glass-fiber filters, *Limnol. Oceanogr.*, 38, 1321-1327.

Comiso, J. C., McClain, C. R., Sullivan, C. W., Ryan, J. P., and Leonard, C. L. (1993), Coastal zone color scanner pigment concentrations in the southern-ocean and relationships to geophysical surface-features, *J. Geophys. Res.-Oceans*, 98 (C2), 2419-2451.

Crawford, D. W., Lipsen, M. S., Purdie, D. A., Lohan, M. C., Statham, P. J., Whitney, F. A., et al. (2003), Influence of zinc and iron enrichments on phytoplankton growth in the northeastern subarctic Pacific, *Limnol. Oceanogr.*, 48 (4), 1583-1600.

Croce, R., and van Amerongen, H. (2011), Light-harvesting and structural organization of Photosystem II: from individual complexes to thylakoid membrane, *J. Photochem. Photobiol. B*, 104(1), 142-153.

Croot, P. L. and Laan, P. (2002), Continuous shipboard determination of Fe(II) in polar waters using flow injection analysis with chemiluminescence detection, *Anal. Chim. Acta*, *466*, 261-273.

Cullen, J. J. (1990), On models of growth and photosynthesis in phytoplankton, *Deep Sea Res.*, *37*(4), 667-683.

Cullen, J. J. (1991), Hypotheses to explain high-nutrient conditions in the open sea. *Limnol. Oceanogr.*, 36 (8), 1578-1599.

Cullen, J.J. (2009), Interactive comment on "Satellite-detected fluorescence reveals global physiology of ocean phytoplankton" by M. J. Behrenfeld et al., *Biogeosciences Discuss.*, 5, S2646-S2655.

Cullen, J.J. and Davis, R.F. (2003), The blank can make a big difference in oceanographic measurements, *Limnol. Oceanogr. Bulletin*, 12, 29-35.

Cullen, J. J. and Lewis, M. R. (1995), Biological processes and optical measurements near the sea surface: Some issues relevant to remote sensing, *J. Geophys. Res.-Oceans*, *100*(C7), 13255-13266.

Cullen, J. J., Yang, X., Macintyre, H. L. (1992), Nutrient limitation of marine photosynthesis, pp. 69–88 in Falkowski, P. G. and Woodhead, A. (eds.), *Primary productivity and biogeochemical cycles in the sea*, Plenum.

Cushing, D. H. (1989), A difference in structure between ecosystems in strongly stratified waters and in those that are only weakly stratified, *J. Plankton Res.*, 11, 1–13.

Dandonneau, Y., and Neveux, J. (1997), Diel variations of in vivo fluorescence in the eastern equatorial Pacific: an unvarying pattern, *Deep-Sea Res. Pt. II*, 44(9-10), 1869-1880.

Davey, M. and Geider, R. J. (2001), Impact of iron limitation on the photosynthetic apparatus of the diatom Chaetoceros muelleri (Bacillariophyceae), *J. Phycol.*, *37*(6), 987-1000.

Davey, M., Tarran, G. A., Mills, M. M., Ridame, C., Geider, R. J., and La Roche, J. (2008), Nutrient limitation of picophytoplankton photosynthesis and growth in the tropical North Atlantic, *Limnol. Oceanogr.*, 53, 1722-1733.

De Baar, H. J. W., J. T. M. De Jong, D. C. E. Bakker, B. M. Loscher, C. Veth, U. Bathmann, and Smetacek, V. (1995), Importance of iron for phytoplankton blooms and carbon-dioxide drawdown in the Southern-Ocean, *Nature*, 373(6513), 412-415.

De Baar, H. J., Boyd, P. W., Coale, K. H., Landry, M. R., Tsuda, A., Assmy, P., et al. (2005), Synthesis of iron fertilization experiments: From the iron age in the age of enlightenment, *J. Geophys. Res.-Oceans*, 110 (C9).

De Boyer Montégut, C., G. Madec, A. S. Fischer, A. Lazar, and Iudicone, D. (2004), Mixed layer depth over the global ocean: An examination of profile data and a profile-based climatology, *J. Geophys. Res.-Oceans*, 109, C12003.

Demmig-Adams, B., Adams, W. W., Heber, U., Neimanis, S., Winter, K., Krüger, A., et al. (1990), Inhibition of zeaxanthin formation and of rapid changes in radiationless

energy-dissipation by dithiothreitol in spinach leaves and chloroplasts, *Plant Physiol.*, 92(2), 293-301.

Desquilbet, T. E., Duval, J. C., Robert, B., Houmard, J., and Thomas, J. C. (2003), In the unicellular red alga Rhodella violacea iron deficiency induces an accumulation of uncoupled LHC, *Plant Cell Physiol.*, 44 (11), 1141-1151.

Detmer, A. E. and Bathmann, U. V. (1997), Distribution patterns of autotrophic pico- and nanoplankton and their relative contribution to algal biomass during spring in the Atlantic sector of the Southern Ocean, *Deep-Sea Res. Pt. II*, 44 (1-2), 299-320.

Dickey, T. D., and Bidigare, R. R. (2005), Interdisciplinary oceanographic observations: The wave of the future. *Scientia Marina*, 69(S1), 23-42.

Doney, S. C., Fabry, V. J., Feely, R. A., and Kleypas, J. A. (2009), Ocean acidification: the other CO2 problem, *Ann. Rev. Mar. Sci.*, 1, 169-192.

Duffy, J. E. and Stachowicz, J. J. (2006), Why biodiversity is important to oceanography: potential roles of genetic, species, and trophic diversity in pelagic ecosystem processes, *Mar. Ecol. Prog. Ser.* 311, 179-189.

Dugdale, R. C. and Goering, J. J.: Uptake of new and regenerated forms of nitrogen in primary productivity, *Limnol. Oceanogr.*, 12, 196-206, 1967.

Duggen, S., Croot, P., Schacht, U. and Hoffmann, L. (2007), Subduction zone volcanic ash can fertilize the surface ocean and stimulate phytoplankton growth: Evidence from biogeochemical experiments and satellite data. *Geophys. Res. Lett., 34*, L01612.

Duggen, S., Olgun, N., Croot, P., Hoffmann, L., Dietze, H., Delmelle, P., and Teschner, C. (2010), The role of airborne volcanic ash for the surface ocean biogeochemical iron-cycle: a review. *Biogeosciences, 7*, 827-844.

Duysens, L. M. N. and Sweers, H. E. (1963), Mechanisms of the two photochemical reactions in algae as studied by means of fluorescence, pp. 353-372 Japanese Society of Plant Physiologists (Ed.), *Studies on Microalgae and Photosynthetic Bacteria*, University of Tokyo Press, Tokyo.

Edwards, A. M., Platt, T. and Sathyendranath, S. (2004), The high-nutrient, low-chlorophyll regime of the ocean: limits on biomass and nitrate before and after iron enrichment, *Ecol. Model.*, 171 (1-2), 103-125.

Elrod, V. A., Berelson, W. M., Coale, K. H., and Johnson, K. S., (2004), The flux of iron from continental shelf sediments: A missing source for global budgets, *Geophys. Res. Lett.*, 31 (12).

Eppley, R. W. (1972), Temperature and phytoplankton growth in the sea, *Fish. Bull*, *70*(4), 1063-1085.

Eppley, R. W., and Peterson, B. J. (1979), Particulate organic-matter flux and planktonic new production in the deep ocean, *Nature*, 282, 677-680.

Falkowski, P. G. (1997), Evolution of the nitrogen cycle and its influence on the biological sequestration of CO2 in the ocean, *Nature*, 387 (6630), 272-275.

Falkowski, P. G., and D. A. Kiefer (1985), Chlorophyll-a fluorescence in phytoplankton – relationship to photosynthesis and biomass, *J. Plankton Res.*, 7(5), 715-731.

Falkowski, P., Scholes, R. J., Boyle, E. E. A., Canadell, J., Canfield, D., Elser, J., et al. (2000), The global carbon cycle: A test of our knowledge of earth as a system, *Science*, 290 (5490), 291-296.

Falkowski, P. G. (1994), the role of phytoplankton photosynthesis in global biogeochemical cycles, *Photosynth. Res.*, 39 (3), 235-258.

Falkowski, P. G., and Raven, J. A. (1997), *Aquatic photosynthesis*, Princeton University Press.

Falkowski, P. G., Barber, R. T. and Smetacek, V. (1998), Biogeochemical controls and feedbacks on ocean primary production, *Science*, 281 (5374), 200-206.

Falkowski, P. G. and Oliver, M. J. (2007), Mix and match: how climate selects phytoplankton. *Nat. Rev. Microbiol.*, 5 (10), 813-819.

Falkowski, P. G., Wyman, K., Ley, A. C., and Mauzerall, D. C. (1986), Relationship of steady-state photosynthesis to fluorescence in eukaryotic algae, *Biochim. Biophys. Acta*, 849 (2), 183-192.

Fan, S. M., Moxim, W. J. and Levy, H. (2006), Aeolian input of bioavailable iron to the ocean, *Geophys. Res. Lett.*, 33 (7).

Field, C. B., Behrenfeld, M. J., Randerson, J. T., and Falkowski, P. (1998), Primary production of the biosphere: Integrating terrestrial and oceanic components, *Science*, 281 (5374), 237-240.

Follows, M. J. and Dutkiewicz, S. (2011), Modeling Diverse Communities of Marine Microbes. *Ann. Rev. Mar. Sci., Vol 3* 3, 427-451.

Folt, C. L., Chen, C. Y., Moore, M. V., and Burnaford, J. (1999), Synergism and antagonism among multiple stressors, *Limnol. Oceanogr.*, 44 (3), 864-877.

Fontijn, K., Lachowycz, S.M., Rawson, H., Pyle, D.M., Mather, T.A., Naranjo, J.A., Moreno-Roa, H. (2014), Late Quaternary tephrostratigraphy of southern Chile and Argentina, *Quaternary Sci. Rev.*, 89, 70-84.

Fung, I. Y., Meyn, S. K., Tegen, I., Doney, S. C., John, J. G., and Bishop, J. K. (2000), Iron supply and demand in the upper ocean, *Global Biogeochem. Cy.*, *14*(1), 281-295.

Fraser, J. M., Tulk, S. E., Jeans, J. A., Campbell, D. A., Bibby, T. S., Cockshutt, A. M. (2013), Photophysiological and Photosynthetic Complex Changes during Iron Starvation in Synechocystis sp. PCC 6803 and Synechococcus elongatus PCC 7942, *PLoS ONE*, 8, e59861.

Geider, R. J., Greene, R. M., Kolber, Z., Macintyre, H. L., and Falkowski, P. G. (1993a), fluorescence assessment of the maximum quantum efficiency of photosynthesis in the Western North-Atlantic, *Deep-Sea Res. Pt. I*, 40, 1205-1224.

Geider, R. J., Laroche, J., Greene, R. M., and Olaizola, M. (1993b), Response of the photosynthetic apparatus of *Phaeodactylum-tricornutum* (Bacillariophyceae) to nitrate, phosphate, or iron starvation, *J. Phycol.*, 29, 755-766.

Gervais, F., Riebesell, U. and Gorbunov, M. Y. (2002), Changes in primary productivity and chlorophyll a in response to iron fertilization in the Southern Polar Frontal Zone, *Limnol. Oceanogr.*, 47 (5), 1324-1335.

Gibb, S. W., Barlow, R. G., Cummings, D. G., Rees, N. W., Trees, C. C., Holligan, P., and Suggett, D. (2000), Surface phytoplankton pigment distributions in the Atlantic Ocean: an assessment of basin scale variability between 50 degrees N and 50 degrees S, *Prog. Oceanogr.*, 45, 339-368.

Gibb, S. W., Cummings, D. G., Irigoien, X., Barlow, R. G., Fauzi, R., and Mantoura, C. (2001), Phytoplankton pigment chemotaxonomy of the northeastern Atlantic, *Deep-Sea Res. Pt. II*, 48, 795-823.

Gorbunov, M. Y., Kolber, Z. S., Lesser, M. P., and Falkowski, P. G. (2001), Photosynthesis and photoprotection in symbiotic corals, *Limnol. Oceanogr.*, 46, 75-85.

Greene, R. M., Geider, R. J., and Falkowski, P. G. (1991), Effect of iron limitation on photosynthesis in a marine diatom, *Limnol. Oceanogr.*, 36, 1772-1782.

Greene, R. M., Geider, R. J., Kolber, Z., and Falkowski, P. G. (1992), Iron-induced changes in light harvesting and photochemical energy-conversion processes in eukaryotic marine-algae, *Plant Physiol.*, 100, 565-575.

Greene, R. M., Kolber, Z. S., Swift, D. G., Tindale, N. W., and Falkowski, P. G. (1994), Physiological limitation of phytoplankton photosynthesis in the Eastern Equatorial Pacific determined from variability in the quantum yield of fluorescence, *Limnol. Oceanogr.*, 39, 1061-1074.

Hamme, R. C., Webley, P. W., Crawford, W. R., Whitney, F. A., DeGrandpre, M. D., Emerson, S. R., et al. (2010), Volcanic ash fuels anomalous plankton bloom in subarctic northeast Pacific, *Geophys. Res. Lett., 37*, L19604.

Hatta, M., Selph, K. E., Zhou, M., and Hiscock, W. T. (2012), Iron fluxes from the shelf regions near the South Shetland Islands in the Drake Passage during the austral-winter 2006, *Deep-Sea Res. Pt. II*, *90*, 89-101.

Anderson, R. F., Henderson, G. M., Adkins, J., Andersson, P., Eisenhauer, A., Frank, M., and Oschlies, A. (2007), GEOTRACES - An international study of the global marine biogeochemical cycles of trace elements and their isotopes, *Chemie Der Erde-Geochemistry* 67 (2), 85-131.

Hiscock, M. R., Lance, V. P., Apprill, A. M., Bidigare, R. R., Johnson, Z. I., Mitchell, B. G., et al. (2008), Photosynthetic maximum quantum yield increases are an essential component of the Southern Ocean phytoplankton response to iron, *Proc. Natl Acad. Sci. USA*, 105 (12), 4775-4780.

Hoffmann, L. J., Breitbarth, E., Ardelan, M. V., Duggen, S., Olgun, N., Hassellöv, M., and Wängberg, S. Å. (2012), Influence of trace metal release from volcanic ash on growth of *Thalassiosira pseudonana* and *Emiliania huxleyi*, *Mar. Chem.*, *132*, 28-33.

Holm-Hansen, O., Lorenzen, C. J., Holmes, R. W., and Strickland, J. D. H. (1965) Fluorometric determination of chlorophyll, *J. Cons. Perm. Int. Explor. Mer.*, 30:3-15.

Holm-Hansen, O., Naganobu, M., Kawaguchi, S., Kameda, T., Krasovski, I., Tchernyshkov, P., et al. (2004), Factors influencing the distribution, biomass, and productivity of phytoplankton in the Scotia Sea and adjoining waters, *Deep-Sea Res. Pt. II*, 51(12-13), 1333-1350.

Holeton, C. L., Nedelec, F., Sanders, R., Brown, L., Moore, C. M., Stevens, D. P., et al. (2005), Physiological state of phytoplankton communities in the Southwest Atlantic sector of the Southern Ocean, as measured by fast repetition rate fluorometry, *Polar Biol.*, 29 (1), 44-52.

Holligan, P. M., Charalampopoulou, A., and Hutson, R. (2010), Seasonal distributions of the coccolithophore *Emiliania huxleyi* and of particulate inorganic carbon in surface waters of the Scotia Sea, *J. Mar. Syst.*, *82*(4), 195-205.

Hopkinson, B. M., Mitchell, B., Reynolds, R. A., Wang, H., Selph, K. E., Measures, C. I., et al. (2007), Iron limitation across chlorophyll gradients in the southern Drake Passage: Phytoplankton responses to iron addition and photosynthetic indicators of iron stress, *Limnol. Oceanogr.*, *52*, 2540-2554.

Hopkinson, B. M. and Barbeau, K. A. (2008), Interactive influences of iron and light limitation on phytoplankton at subsurface chlorophyll maxima in the eastern North Pacific, *Limnol. Oceanogr.*, 53 (4), 1303-1318.

Howe, B. M., Chao, Y., Arabshahi, P., Roy, S., McGinnis, T., and Gray, A. (2010), A smart sensor web for ocean observation: fixed and mobile platforms, integrated

acoustics, satellites and predictive modelling, *IEEE J. Sel. Topics Appl. Earth Observ.*, 3(4), 507-521.

Horton, P., Ruban, A. V., and Walters, R. G. (1996), Regulation of light harvesting in green plants, *Ann. Rev. Plant Phys.*, 47, 655-684.

Hu, C., F. E. Muller-Karger, C. J. Taylor, K. L. Carder, C. Kelble, E. Johns, and C. A. Heil (2005), Red tide detection and tracing using MODIS fluorescence data: A regional example in SW Florida coastal waters, *Remote Sens. Environ.*, *97*(3), 311-321.

Huot, Y., C. A. Brown, and Cullen, J. J. (2005), New algorithms for MODIS sun-induced chlorophyll fluorescence and a comparison with present data products, *Limnol. Oceanogr-Meth.*, 3, 108-130.

Huot, Y., Franz, B. A., and Fradette, M. (2013), Estimating variability in the quantum yield of Sun-induced chlorophyll fluorescence: A global analysis of oceanic waters, *Remote Sens. Environ.*, 132, 238-253.

Hudson, R. J. M., and Morel, F. M. M., (1990), Iron transport in marine phytoplankton: Kinetics of cellular and medium coordination reactions, *Limnol. Oceanogr.*, 35, 1002-1020.

Huntsman, S. A. and Sunda, W. G. (1980), Role of trace metals in regulating phytoplankton growth with emphasis on Fe, Mn and Cu, in pp. 285-328 I. Moris (ed.), *Studies in Ecology, Physiological Ecology of Phytoplankton*, Blackwell Scientific, Oxford.

Hutchins, D. A., DiTullio, G. R., Zhang, Y., and Bruland, K. W. (1998), An iron limitation mosaic in the California upwelling regime, *Limnol. Oceanogr.*, 43, 1037-1054.

Hutchins, D. A., Hare, C. E., Weaver, R. S., Zhang, Y., Firme, G. F., DiTullio, G. R., et al. (2002), Phytoplankton iron limitation in the Humboldt Current and Peru Upwelling, *Limnol. Oceanogr.*, *47*(4), 997-1011.

Hydes, D. J., Aoyama M., Aminot A., Bakker K., Becker S., Coverly S., Daniel A., Dickson A. G., Grosso O., Kerouel R., Van Ooijen J., Sato K., Tanhua T., Woodward E. M. S., Zhang J. Z. (2010), Determination of dissolved nutrients (N,P,Si) in seawater with high precision and inter-comparability using gas-segmented continuous flow analysers, *The GO-SHIP Repeat Hyrography Manual: a collection of expert reports and guidelines*; IOCCP report No.14, ICPO publication series No. 134, version 1.

Ito, T., Parekh, P., Dutkiewicz, S., and Follows, M. J. (2005), The Antarctic Circumpolar Productivity Belt, *Geophys. Res. Lett.*, 32, L13604.

Johnson, K. S., Gordon, R. M., and Coale, K. H. (1997), What controls dissolved iron concentrations in the world ocean? *Mar. Chem.*, 57, 137-161.

Jones, M. T. and Gislason, S. R. (2008), Rapid releases of metal salts and nutrients following the deposition of volcanic ash into aqueous environments, *Geochim. Cosmochim. Acta* 72 (15), 3661-3680.

Karl, D. M. (2002), Nutrient dynamics in the deep blue sea, *Trends Microbiol.*, 10 (9), 410-418.

Katz, M. E., Finkel, Z. V., Grzebyk, D., Knoll, A. H., and Falkowski, P. G. (2004), Evolutionary trajectories and biogeochemical impacts of marine eukaryotic phytoplankton, *Annu. Rev. Ecol. Evol. S.*, 35, 523-556.

Kiefer, D. A., Chamberlin, W. S., and Booth, C. R. (1989), Natural fluorescence of chlorophyll-a – relationship to photosynthesis and chlorophyll concentration in the western South-Pacific gyre, *Limnol. Oceanogr.*, 34(5), 868-881.

Kiefer, D. A., and Reynolds, R. A. (1992), Advances in understanding phytoplankton fluorescence and photosynthesis, in *Primary Productivity and Biogeochemical Cycles in the Sea*, edited by P. G. Falkowski and A. D. Woodhead, pp. 155−174, Plenum, New York.

King, A. L. and Barbeau, K. (2007), Evidence for phytoplankton iron limitation in the southern California Current System, *Mar. Ecol. Prog. Ser.*, 342, 91-103.

Kirk, J. T. O. (1994), *Light and photosynthesis in aquatic ecosystems*, Cambridge University Press.

Kishino, M., Sugihara, S., and Okami, N. (1984), Influence of fluorescence of chlorophyll a on underwater upward irradiance spectrum, *La mer*, *22*, 224-232.

Kishino, M., Takahashi, M., Okami, N., and Ichimura, S. (1985), Estimation of the spectral absorption–coefficients of phytoplankton in the sea, *B. Mar. Sci.*, 37, 634-642.

Knox, R. S. (1975), *Excitation energy transfer and migration: Theoretical considerations*, Bioenergetics of photosynthesis, Academic Press, New York, 183-221.

Kolber, Z. S., Zehr, J., and Falkowski, P. (1988), Effects of growth irradiance and nitrogen limitation on photosynthetic energy conversion in photosystem-II, *Plant Physiol.*, 88, 923-929.

Kolber, Z. S., Wyman, K. D., and Falkowski, P. G. (1990), Natural variability in photosynthetic energy-conversion efficiency – a field-study in the Gulf of Maine, *Limnol. Oceanogr.*, 35, 72-79.

Kolber, Z. S., Barber, R. T., Coale, K. H., Fitzwater, S. E., Greene, R. M., Johnson, K. S., Lindley, S., and Falkowski, P. G. (1994), Iron limitation of phytoplankton photosynthesis in the Equatorial Pacific-Ocean, *Nature*, 371, 145-149.

Kolber, Z. S., Prasil, O., and Falkowski, P. G. (1998), Measurements of variable chlorophyll fluorescence using fast repetition rate techniques: defining methodology and experimental protocols, *BBA-Bioenergetics*, 1367, 88-106.

Korb, R. E. and Whitehouse, M. (2004), Contrasting primary production regimes around South Georgia, Southern Ocean: large blooms versus high nutrient, low chlorophyll waters, *Deep-Sea Res. Pt. I*, 51 (5).

Korb, R. E., Whitehouse, M. J., Atkinson, A., and Thorpe, S. E. (2008), Magnitude and maintenance of the phytoplankton bloom at South Georgia: a naturally iron-replete environment, *Mar. Ecol. Prog. Ser.*, 368, 75-91.

Kruskopf, M., and Flynn, K. J. (2006), Chlorophyll content and fluorescence responses cannot be used to gauge reliably phytoplankton biomass, nutrient status or growth rate, *New Phytol.*, 169, 525-536.

Krause, G. H. and Weis, E. (1991), Chlorophyll fluorescence and photosynthesis - the basics, *Ann. Rev. Plant Phys.*, 42, 313-349.

Laney, S. R. (2003), Assessing the error in photosynthetic properties determined by fast repetition rate fluorometry, *Limnol. Oceanogr.*, 48, 2234-2242.

Langmann, B., Zakšek, K., Hort, M., and Duggen, S. (2010), Volcanic ash as fertiliser for the surface ocean, *Atmos. Chem. Phys, 10*(8), 3891-3899.

Lavaud J., Strzepeck, R. F., and Kroth, P. G. (2007), Photoprotection capacity differs among diatoms: possible consequences on the spatial distribution of diatoms related to fluctuations in the underwater light climate, *Limnol. Oceanogr.*, 52, 1188-1194.

Lawrenz, E., Silsbe, G., Capuzzo, E., Ylöstalo, P., Forster, R. M., Simis, S. G., et al. (2013), Predicting the Electron Requirement for Carbon Fixation in Seas and Oceans, *PLoS ONE*, 8 (3).

Lee, Z. P., Carder, K. L., and Arnone, R. A. (2002), Deriving inherent optical properties from water color: a multiband quasi-analytical algorithm for optically deep waters, *Appl. Optics*, 41(27), 5755-5772.

Le Quéré, C. , Harrison, S. P., Prentice, I. C., Buitenhuis, E. T., Aumont, O., Bopp, L., et al., (2005), Ecosystem dynamics based on plankton functional types for global ocean biogeochemistry models, *Global Change Biol.*, *11*(11), 2016-2040.

Lefèvre, N., and Watson, A. J. (1999), Modeling the geochemical cycle of iron in the oceans and its impact on atmospheric CO2 concentrations, *Global Biogeochemical Cy.*, 13(3), 727-736.

Letelier, R. M., Abbott, M. R., and Karl, D. M. (1997), Chlorophyll natural fluorescence response to upwelling events in the Southern Ocean, *Geophys. Res. Lett.*, 24(4), 409-412.

Letelier, R. M., and Karl, D. M. (1989), Phycoerythrin-containing cyanobacteria in surface waters of the Drake Passage during February 1987, *Antarct. J. US*, *24*(5), 185-188.

Lindley, S. T. and Barber, R. T. (1998), Phytoplankton response to natural and experimental iron addition, *Deep-Sea Res. Pt. II*, 45 (6), 1135-1150.

Llido, J., Garcon, V., Lutjeharms, J. R. E., and Sudre, J. (2005), Event-scale blooms drive enhanced primary productivity at the Subtropical Convergence, *Geophys. Res. Lett.*, 32, L15611.

Longhurst, A.R. (1998), *Ecological Geography of the Sea*. Academic Press, San Diego.

Longhurst, A., Sathyendranath, S., Platt, T., and Caverhill, C. (1995), An estimate of global primary production in the ocean from satellite radiometer data, *J. Plankton Res.*, 17 (6), 1245-1271.

Lorenzen, C. J. (1966). A method for the continuous measurement of *in vivo* chlorophyll concentration, in *Deep Sea Research and Oceanographic Abstracts* (13, 2, pp. 223-227).

Lutjeharms, J. R. E. (1985), Location of frontal systems between Africa and Antarctica – some preliminary results, *Deep-Sea Res. Pt. a*, 32, 1499-1509.

MacIntyre, J. G., Cullen, J. J., and Cembella, A. D. (1997), Vertical migration, nutrition and toxicity in the dinoflagellate Alexandrium tamarense, *Mar. Ecol. Prog. Ser.*, 148, 201-216.

MacIntyre, H. L., Kana, T. M., Anning, T., and Geider, R. J. (2002), Photoacclimation of photosynthesis irradiance response curves and photosynthetic pigments in microalgae and cyanobacteria, *J. Phycol.*, 38 (1), 17-38.

Macey, A. I., Ryan-Keogh, T. J., Richier, S., Moore, C. M., and Bibby, T. S. (2014) Photosynthetic protein stoichiometry and photophysiological responses of phytoplankton communities to iron stress in the high latitude North Atlantic. *AGU Ocean Sciences Hawaii 2014 conference abstract* (Abstract ID: 15865).

Mackey, M. D., Mackey, D. J., Higgins, H. W., and Wright, S. W. (1996), CHEMTAX - A program for estimating class abundances from chemical markers: Application to HPLC measurements of phytoplankton, *Mar. Ecol. Prog. Ser.*, 144(1-3), 265-283.

Maldonado, M. T., Boyd, P. W., Harrison, P. J., and Price, N. M. (1999), Co-limitation of phytoplankton growth by light and Fe during winter in the NE subarctic Pacific Ocean, *Deep-Sea Res. Pt. II*, 46 (11-12), 2475-2485.

Maldonado, M. T., Boyd, P. W., Harrison, P. J., and Price, N. M. (2001), Iron uptake and physiological response of phytoplankton during a mesoscale Southern Ocean iron enrichment, *Limnol. Oceanogr.*, 46 (7), 1802-1808.

Malkin, S. and Kok, B. (1966), Fluorescence induction studies in isolated chloroplasts .i. Number of components involved in reaction and quantum yields, *Biochim. Biophys. Acta*, 126 (3), 413.

Marchetti, A., Sherry, N. D., Juneau, P., Strzepek, R. F., and Harrison, P. J. (2006), Phytoplankton processes during a mesoscale iron enrichment in the NE subarctic Pacific: Part III - Primary productivity, *Deep-Sea Res. Pt. II*, 53 (20-22), 2131-2151.

Margalef, R. (1978), Life-forms of phytoplankton as survival alternatives in an unstable environment, *Oceanol Acta* 1, 493–509.

Maritorena, S., A. Morel, and B. Gentili (2000), Determination of the fluorescence quantum yield by oceanic phytoplankton in their natural habitat, *Appl. Optics*, 39(36), 6725-6737.

Martin, J. H., Bruland, K. W., and Broenkow, W. W. (1976), Cadmium transport in the California Current, *Marine pollutant transfer*, 159-184.

Martin, J. H., and Knauer, G. A. (1973), The elemental composition of plankton, *Geochim. Cosmochim. Ac.*, *37*(7), 1639-1653.

Martin, J. H. and Fitzwater, S. E. (1988), Iron-deficiency limits phytoplankton growth in the northeast pacific subarctic, *Nature*, 331 (6154), 341-343.

Martin, J. H., Gordon, R. M. and Fitzwater, S. E. (1990), Iron in Antarctic waters, *Nature*, *345*, 156-158.

Matano, R. P. (1993), On the separation of the Brazil Current from the coast, *J. Phys. Oceanogr.*, 23, 79-90.

Mauzeral.D (1972), Light-induced fluorescence changes in chlorella, and primary photoreactions for production of oxygen, *Proc. Natl Acad. Sci. USA*, 69 (6), 1358.

Measures, C. I., Brown, M. T., Selph, K. E., Apprill, A., Zhou, M., Hatta, M., and Hiscock, W. T. (2012), The influence of shelf processes in delivering dissolved iron to the HNLC waters of the Drake Passage, Antarctica, *Deep-Sea Res. Pt. II*, *90*, 77-88.

Mélançon, J., Levasseur, M., Lizotte, M., Delmelle, P., Cullen, J., Hamme, R. C., et al. (2014), Early response of the northeast subarctic Pacific plankton assemblage to volcanic ash fertilization, *Limnol. Oceanogr*, *59*(1), 55-67.

Middag, R., De Baar, H. J. W., Laan, P., Cai, P. H., and Van Ooijen, J. C. (2011), Dissolved manganese in the Atlantic sector of the Southern Ocean, *Deep-Sea Res. Pt. II*, *58*(25), 2661-2677.

Middag, R., Baar, H. J. W., Laan, P., and Huhn, O. (2012), The effects of continental margins and water mass circulation on the distribution of dissolved aluminum and manganese in Drake Passage, *J. Geophys. Res.-Oceans (1978–2012)*, *117*(C1).

Middag, R., de Baar, H. J., Klunder, M. B., and Laan, P. (2013), Fluxes of dissolved aluminum and manganese to the Weddell Sea and indications for manganese co-limitation, *Limnol. Oceanogr., (58)1*, 287-300.

Milligan, A. J., Aparicio, U. A., and Behrenfeld, M. J. (2012), Fluorescence and nonphotochemical quenching responses to simulated vertical mixing in the marine diatom Thalassiosira weissflogii, *Mar. Ecol.-Prog. Ser.*, 448, 67-78.

Milne, A., Landing, W., Bizimis, M., and Morton, P. (2010), Determination of Mn, Fe, Co, Ni, Cu, Zn, Cd and Pb in seawater using high resolution magnetic sector inductively coupled mass spectrometry (HR-ICP-MS), *Analytica Chimica Acta*, 665, 200-207.

Mitchell, B. G., and Holm-Hansen, O. (1991), Bio-optical properties of Antarctic Peninsula waters - differentiation from temperate ocean models, *Deep-Sea Res. Pt. a*, 38(8-9), 1009-1028.

Mitchell, B. G., Brody, E. A., Holm-Hansen, O., McClain, C., and Bishop, J. (1991), Light limitation of phytoplankton biomass and macronutrient utilization in the southern-ocean, *Limnol. Oceanogr.*, 36 (8), 1662-1677.

Montegut, C. D., Madec, G., Fischer, A. S., Lazar, A., and Iudicone, D. (2004), Mixed layer depth over the global ocean: An examination of profile data and a profile-based climatology, *J. Geophys. Res.-Oceans*, 109, C102003.

Moore, C. M., Lucas, M. I., Sanders, R., and Davidson, R. (2005), Basin-scale variability of phytoplankton bio-optical characteristics in relation to bloom state and community structure in the Northeast Atlantic, *Deep-Sea Res. Pt. I*, 52, 401-419.

Moore, C. M., Mills, M. M., Milne, A., Langlois, R., Achterberg, E. P., Lochte, K., Geider, R. J., and La Roche, J. (2006a), Iron limits primary productivity during spring bloom development in the central North Atlantic, *Global Change Biol.*, 12, 626-634.

Moore, C. M., Suggett, D. J., Hickman, A. E., Kim, Y. N., Tweddle, J. F., Sharples, J., Geider, R. J., and Holligan, P. M. (2006b), Phytoplankton photoacclimation and photoadaptation in response to environmental gradients in a shelf sea, *Limnol. Oceanogr.*, 51, 936-949.

Moore, C. M., Seeyave, S., Hickman, A. E., Allen, J. T., Lucas, M. I., Planquette, H., Pollard, R. T., and Poulton, A. J. (2007), Iron-light interactions during the CROZet natural iron bloom and EXport experiment (CROZEX) I: Phytoplankton growth and photophysiology, *Deep-Sea Res. Pt. II*, 54, 2045-2065.

Moore, C. M., Mills, M. M., Langlois, R., Milne, A., Achterberg, E. P., La Roche, J., and Geider, R. J. (2008), Relative influence of nitrogen and phosphorus availability on phytoplankton physiology and productivity in the oligotrophic sub-tropical North Atlantic Ocean, *Limnol. Oceanogr.*, 53, 291-305.

Moore, C. M., Mills, M. M., Arrigo, K. R., Berman-Frank, I., Bopp, L., Boyd, P. W., Galbraith, E. D., Geider, R. J., et al. (2013), Processes and patterns of oceanic nutrient limitation, *Nat. Geosci.*, 6, 701-710.

Moore, J. K., and Abbott, M. R. (2002), Surface chlorophyll concentrations in relation to the Antarctic Polar Front: seasonal and spatial patterns from satellite observations, *J. Marine Syst.*, 37(1), 69-86.

Moore, J. K., Doney, S. C., and Lindsay, K. (2004), Upper ocean ecosystem dynamics and iron cycling in a global three-dimensional model, *Global Biogeochemical Cy.*, 18, GB4028.

Morales, F., Moise, N., Quílez, R., Abadía, A., Abadía, J., and Moya, I. (2001), Iron deficiency interrupts energy transfer from a disconnected part of the antenna to the rest of Photosystem II, *Photosynth. Res.*, 70 (2), 207-220.

Morel, A., and Bricaud, A. (1981), Theoretical results concerning light-absorption in a discrete medium, and application to specific absorption of phytoplankton, *Deep-Sea Res. Pt. a*, 28(11), 1375-1393.

Morel, F. M. M., & Reinfelder, R. (1994), Zinc and carbon co-limitation of marine-phytoplankton, *Nature*, 369 (6483), 740-742.

Morel, F. M. M., Milligan, A. J. and Saito, M. A. (2003), *Marine Bioinorganic Chemistry: The Role of Trace Metals in the Ocean Cycles of Major Nutrients*, Treatise on Geochemistry Vol. *6*, 113–143.

Morel, F. M. (2008), The co-evolution of phytoplankton and trace element cycles in the oceans, *Geobiology*, *6*(3), 318-324.

Morrison, J. R. (2003), In situ determination of the quantum yield of phytoplankton chlorophyll a fluorescence: A simple algorithm, observations, and a model, *Limnol. Oceanogr.*, 48(2), 618-631.

Morrison, J. R., and D. S. Goodwin (2010), Phytoplankton photocompensation from space-based fluorescence measurements, *Geophys. Res. Lett.*, 37, L06603.

Morrison, J. (2014), Digital atlas shows oceans' iron levels, *Nature News*, doi:10.1038/nature.2014.14774

Moseley, J. L., Allinger, T., Herzog, S., Hoerth, P., Wehinger, E., Merchant, S., and Hippler, M. (2002), Adaptation to Fe-deficiency requires remodeling of the photosynthetic apparatus, *Embo Journal* 21 (24), 6709-6720.

Müller, P., Li, X. P. and Niyogi, K. K. (2001), Non-photochemical quenching. A response to excess light energy, *Plant Physiol.*, 125(4), 1558-1566.

Nair, A., Sathyendranath, S., Platt, T., Morales, J., Stuart, V., Forget, M. H., et al. (2008), Remote sensing of phytoplankton functional types, *Remote Sens. Environ.*, *112*(8), 3366-3375.

Narcisi, B., Petit, J. R., Delmonte, B., Scarchilli, C., and Stenni, B. (2012), A 16,000-yr tephra framework for the Antarctic ice sheet: a contribution from the new Tabs Dome core, *Quaternary Sci. Rev.*, *49*, 52-63.

Naveira Garabato, A. C., Polzin, K. L., King, B. A., Heywood, K. J., and Visbeck, M. (2004), Widespread intense turbulent mixing in the Southern Ocean, *Science*, 303(5655), 210-213.

Nelson, D. M. and Smith, W. O. (1991), sverdrup revisited - critical depths, maximum chlorophyll levels, and the control of southern-ocean productivity by the irradiance-mixing regime, *Limnol. Oceanogr.*, 36 (8), 1650-1661.

Nielsdóttir, M. C., Bibby, T. S., Moore, C. M., Hinz, D. J., Sanders, R., Whitehouse, M., et al. (2012), Seasonal and spatial dynamics of iron availability in the Scotia Sea, *Mar. Chem.*, 130, 62-72.

Olgun, N., Duggen, S., Croot, P. L., Delmelle, P., Dietze, H., Schacht, U., et al. (2011), Surface ocean iron fertilization: The role of airborne volcanic ash from subduction zone and hot spot volcanoes and related iron fluxes into the Pacific Ocean, *Global Biogeochem. Cy.*, *25*, GB4001.

Olgun, N., Duggen, S., Andronico, D., Kutterolf, S., Croot, P. L., Giammanco, S., et al. (2013), Possible impacts of volcanic ash emissions of Mount Etna on the primary productivity in the oligotrophic Mediterranean Sea: Results from nutrient-release experiments in seawater, *Mar. Chem.*, *152*, 32-42.

Olson, R. J., Sosik, H. M., Chekalyuk, A. M., and Shalapyonok, A. (2000), Effects of iron enrichment on phytoplankton in the Southern Ocean during late summer: active fluorescence and flow cytometric analyses, *Deep-Sea Res. Pt. II*, 47, 3181-3200.

Orsi, A. H., Whitworth III, T., and Nowlin, Jr., W. D. (1995), On the meridional extent and fronts of the Antarctic Circumpolar Current, *Deep-Sea Res. I*, 42, 641-673.

O'Reilly, J. E., Maritorena, S., Siegel, D. A., O'Brien, M. C., Toole, D., Mitchell, B. G., et al., (2000), Ocean color chlorophyll a algorithms for SeaWiFS, OC2, and OC4: Version 4, *SeaWiFS post launch calibration and validation analyses, Part, 3*, 9-23.

Parekh, P., Follows, M. J., and Boyle, E. A. (2005), Decoupling of iron and phosphate in the global ocean, *Global Biogeochemical Cy.*, 19, GB2020.

Parkhill, J. P., Maillet, G., and Cullen, J. J. (2001), Fluorescence-based maximal quantum yield for PSII as a diagnostic of nutrient stress, *J. Phycol.*, 37, 517-529.

Peers, G., and Price, N. M. (2004), A role for manganese in superoxide dismutases and growth of iron-deficient diatoms, *Limnol. Oceanogr.*, 49, 74-83.

Price, N. M. and Morel, F. M. M. (1990), Cadmium and cobalt substitution for zinc in a marine diatom, *Nature*, 344 (6267), 658-660.

Planquette, H., Statham, P. J., Fones, G. R., Charette, M. A., Moore, C. M., Salter, I., Nedelec, F. H., Taylor, S. L., French, M., Baker, A. R., Mahowald, N., and Jickells, T. D. (2007), Dissolved iron in the vicinity of the Crozet Islands, Southern Ocean, *Deep-Sea Res. Pt. II*, 54, 1999-2019.

Platt, T., Gallegos, C. L., and Harrison, W. G. (1980), Photoinhibition of photosynthesis in natural assemblages of marine-phytoplankton, *J. Mar. Res.*, 38, 687-701.

Platt, T. and Sathyendranath, S. (1988), Oceanic primary production - estimation by remote-sensing at local and regional scales, *Science*, 241 (4873), 1613-1620.

Platt, T. and Sathyendranath, S. (2007), Modelling primary production (series).

Quigg, A., Irwin, A. J., and Finkel, Z. V. (2011), Evolutionary inheritance of elemental stoichiometry in phytoplankton, *P. Roy. Soc. B-Biol. Sci.*, 278, 526-534.

Raiswell, R., Benning, L. G., Tranter, M., and Tulaczyk, S. (2008), Bioavailable iron in the Southern Ocean: the significance of the iceberg conveyor belt, *Geochem. T.*, 9:7.

Raven, J. A. (2011), The cost of photoinhibition, *Physiol. Plantarum*, 142, 87-104.

Raven, J. A. and Geider, R. J. (1988), Temperature and algal growth, *New Phytologist*, 110 (4), 441-461.

Raven, J. A., Evans, M. C. W. and Korb, R. E. (1999), The role of trace metals in photosynthetic electron transport in O-2-evolving organisms, *Photosynth. Res.*, 60 (2-3).

Reay, D. S., Priddle, J., Nedwell, D. B., Whitehouse, M. J., Ellis-Evans, J. C., Deubert, C., and Connelly, D. P. (2001), Regulation by low temperature of phytoplankton growth and nutrient uptake in the Southern Ocean, *Mar. Ecol. Prog. Ser.*, 219, 51-64.

Reynolds, R. A., Stramski, D., and Mitchell, B. G. (2001), A chlorophyll-dependent semianalytical reflectance model derived from field measurements of absorption and backscattering coefficients within the Southern Ocean, *J. Geophys. Res.-Oceans*, 106(C4), 7125-7138.

Rose, J. M., Feng, Y., DiTullio, G. R., Dunbar, R. B., Hare, C. E., Lee, P. A., et al. (2009), Synergistic effects of iron and temperature on Antarctic phytoplankton and microzooplankton assemblages, *Biogeosciences*, 6 (12), 3131-3147.

Ryan-Keogh, T. J., Macey, A. I., Cockshutt, A. M., Moore, C. M., and Bibby, T. S. (2012), The cyanobacterial chlorophyll-binding protein IsiA acts to increase the in

vivo effective absorption cross-section of PSI under iron limitation, *J. Phycol.*, 48, 145-154.

Ryan-Keogh, T. J., Macey, A. I., Nielsdottir, M. C., Lucas, M. I., Steigenberger, S. S., Stinchcmbe, M. C., Achterberg, E. P., Bibby, T. S., and Moore, C. M. (2013), Spatial and temporal development of phytoplankton iron stress in relation to bloom dynamics in the high-latitude North Atlantic Ocean, *Limnol. Oceanogr.*, 58(2), 533-545.

Ryther, J. H., and Dunstan, W. M. (1971), Nitrogen, phosphorous and eutrophication in coastal marine environment, *Science*, 171, 1008-1013.

Saito, M. A., Goepfert, T. J. and Ritt, J. T. (2008), Some thoughts on the concept of colimitation: Three definitions and the importance of bioavailability, *Limnol. Oceanogr.*, 53 (1), 276-290.

Saito, M. A., Moppett, J. W., Chisholm, S. W., and Waterbury, J. B. (2002), Cobalt limitation and uptake in Prochlorococcus, *Limnol. Oceanogr.*, 47 (6), 1629-1636.

Sakshaug, E., and Holm-Hansen, O. (1977), Chemical composition of skeletonema-costatum (grev) cleve and pavlova (monochrysis) lutheri (droop) green as a function of nitrate-limited, phosphate-limited, and iron-limited growth, *J. Exp. Mar. Biol. Ecol.*, 29(1), 1-34.

Sarmiento, J. L., Hughes, T. M., Stouffer, R. J., & Manabe, S. (1998), Simulated response of the ocean carbon cycle to anthropogenic climate warming, *Nature*, 393(6682), 245-249.

Sathyendranath, S. and Platt, T. (1988), The spectral irradiance field at the surface and in the interior of the ocean - a model for applications in oceanography and remote-sensing, *J. Geophys. Res.-Oceans*, 93 (C8), 9270-9280.

Sathyendranath, S., Cota, G., Stuart, V., Maass, H., and Platt, T. (2001), Remote sensing of phytoplankton pigments: a comparison of empirical and theoretical approaches, *Int. J. Remote Sens.*, 22(2-3), 249-273.

Scasso, R. A., Corbella, H. and Tiberi, P. (1994), Sedimentological analysis of the tephra from the 12-15 August 1991 eruption of Hudson Volcano, *Bull. Volcanol.*, *56*, 121-132.

Schallenberg, C., Lewis, M. R., Kelley, D. E., and Cullen, J. J. (2008), Inferred influence of nutrient availability on the relationship between Sun-induced chlorophyll fluorescence and incident irradiance in the Bering Sea, *J. Geophys. Res.-Oceans*, 113, C07046.

Schlosser, C., De La Rocha, C. L. and Croot, P. L. (2011), Effects of iron surface adsorption and sample handling on iron solubility measurements, *Mar. Chem.*, *127*, 48-55.

Schrader, P. S., Milligan, A. J., and Behrenfeld, M. J. (2011), Surplus Photosynthetic Antennae Complexes Underlie Diagnostics of Iron Limitation in a Cyanobacterium, *PLoS ONE*, 6, e18753.

Scollo, S., Del Carlo, P. and Coltelli, M. (2007), Tephra fallout of 2001 Etna flank eruption: Analysis of the deposit and plume dispersion, *J. Volcanol. Geoth. Res.*, *160(1)*, 147-164.

Sedwick, P. N., DiTullio, G. R., Hutchins, D. A., Boyd, P. W., Griffiths, F. B., Crossley, A. C., et al. (1999), Limitation of algal growth by iron deficiency in the Australian Subantarctic region, *Geophys. Res. Lett.*, *26*(18), 2865-2868.

Shaked, Y., and Lis, H. (2012), Disassembling iron availability to phytoplankton, *Front. Microbiol.*, 3, 123.

Shaked, Y., Kustka, A.B., and Morel, F. M. M. (2005), A general kinetic model for iron acquisition by eukaryotic phytoplankton, *Limnol. Oceanogr.*, 50, 872-882.

Sheen, K. L., Brearley, J. A., Naveira Garabato, A. C., Smeed, D. A., Waterman, S., Ledwell, J. R.., et al. (2013), Rates and mechanisms of turbulent dissipation and mixing in the Southern Ocean: Results from the Diapycnal and Isopycnal Mixing Experiment in the Southern Ocean (DIMES), *J. Geophys. Res.-Oceans*, 118 (6), 2774-2792.

Shen, G. T., Boyle, E. A., Lea, D. W. (1987), Cadmium in corals as a tracer of historic upwelling and industrial fallout, *Nature*, 328, 794-796.

Sigman, D. M., Hain, M. P., and Haug, G. H. (2010), The polar ocean and glacial cycles in atmospheric CO2 concentration, *Nature*, *466* (7302), 47-55.

Silsbe, G. M., and Kromkamp, J. C. (2012), Modeling the irradiance dependency of the quantum efficiency of photosynthesis, *Limnol. Oceanogr.-Methods*, 10, 645-652.

Sluijs, A., Schouten, S., Pagani, M., Woltering, M., Brinkhuis, H., Damsté, J. S. S. et al. (2006), Subtropical Arctic Ocean temperatures during the Palaeocene/Eocene thermal maximum, *Nature*, 441(7093), 610-613.

Smetacek, V., Klaas, C., Strass, V. H., Assmy, P., Montresor, M., Cisewski, B., et al. (2012), Deep carbon export from a Southern Ocean iron-fertilized diatom bloom, *Nature*, *487*, 313-319.

Sokolov, S., and Rintoul, S. R. (2007), On the relationship between fronts of the Antarctic Circumpolar Current and surface chlorophyll concentrations in the Southern Ocean, *J. Geophys. Res.*, 112(C7), C07030.

Sosik, H. M., and Olson, R. J. (2002), Phytoplankton and iron limitation of photosynthetic efficiency in the Southern Ocean during late summer, *Deep-Sea Res. Pt. I*, 49, 1195-1216.

Steeman-Nielsen, E., (1952), The use of radioactive carbon (C^{14}) for measuring organic production in the sea, *J. Cons. Perm. Int. Explor. Mer.*, 18: I, 17- 140.

Stern, C. R. (2008), Holocene tephrochronology record of large explosive eruptions in the southernmost Patagonian Andes, *Bull. Volcanol.*, *70*, 435-454.

Sterner, R. W., and Elser, J. J. (2002), *Ecological stoichiometry: the biology of elements from molecules to the biosphere*, Princeton University Press.

Strzepek, R. F., and Harrison, P. J. (2004), Photosynthetic architecture differs in coastal and oceanic diatoms, *Nature*, 431(7009), 689-692.

Strzepek, R. F., Maldonado, M. T., Higgins, J. L., Hall, J., Safi, K., Wilhelm, S. W., and Boyd, P. W. (2005), Spinning the "Ferrous Wheel": The importance of the microbial community in an iron budget during the FeCycle experiment, *Global Biogeochem. Cy.*, 19(4), GB4S26.

Strzepek, R. F., Hunter, K. A., Frew, R. D., Harrison, P. J., and Boyd, P. W. (2012), Iron-light interactions differ in Southern Ocean phytoplankton, *Limnol. Oceanogr.*, 57 (4), 1182-1200.

Stuart, V., Sathyendranath, S., Head, E. J. H., Platt, T., Irwin, B., and Maass, H. (2000), Bio-optical characteristics of diatom and prymnesiophyte populations in the Labrador Sea, *Mar. Ecol.-Prog. Ser.*, 201, 91-106.

Suga, T., Motoki, K., Aoki, Y., and Macdonald, A. M. (2004), The North Pacific climatology of winter mixed layer and mode waters, *J. Phys. Oceanogr*., 34, 3-22.

Suggett, D. J., MacIntyre, H. L., and Geider, R. J. (2004), Evaluation of biophysical and optical determinations of light absorption by photosystem II in phytoplankton, *Limnol. Oceanogr.-Methods*, 2, 316-332.

Suggett, D. J., Moore, C. M., Marañón, E., Omachi, C., Varela, R. A., Aiken, J., and Holligan, P. M. (2006), Photosynthetic electron turnover in the tropical and subtropical Atlantic Ocean, *Deep-Sea Res. Pt. II*, 53 (14-16), 1573-1592.

Suggett, D. J., Moore, C. M., Hickman, A. E., and Geider, R. J. (2009), Interpretation of fast repetition rate (FRR) fluorescence: signatures of phytoplankton community structure versus physiological state, *Mar. Ecol.-Prog. Ser.*, 376, 1-19.

Suggett, D. J., Moore, C. M., and Geider, R. J. (2010), Estimating aquatic productivity from active fluorescence measurements, in *Chlorophyll a Fluorescence in Aquatic Sciences: Methods and Applications* (pp. 103-127), Springer Netherlands.

Sullivan, C. W., Arrigo, K. R., McClain, C. R., Comiso, J. C., and Firestone, J. (1993), Distributions of phytoplankton blooms in the southern-ocean, *Science*, 262 (5141), 1832-1837.

Sunda, W. G. (2012), Feedback Interactions between Trace Metal Nutrients and Phytoplankton in the Ocean, Front. Microbiol., 3, 204.

Sunda, W. G. and Huntsman, S. A. (1994), Photoreduction of manganese oxides in seawater, *Marine Chemistry*, 46 (1-2), 133-152.

Sunda, W. G. and Huntsman, S. A. (1997), Interrelated influence of iron, light and cell size on marine phytoplankton growth, *Nature*, 390 (6658), 389-392.

Tagliabue, A., Bopp, L., Aumont, O., and Arrigo, K. R., et al. (2009), Influence of light and temperature on the marine iron cycle: From theoretical to global modelling, *Global Biogeochem. Cy.*, 23.

Takahashi, T., Sutherland, S. C., Sweeney, C., Poisson, A., Metzl, N., Tilbrook, B. et al. (2002), Global sea-air CO2 flux based on climatological surface ocean pCO2 and seasonal biological and temperature effects, *Deep-Sea Res. Pt. II*, 49 (9-10), 1601-1622.

Tarran, G. A., Burkill, P. H., Edwards, E. S., and Woodward, E. M. S. (1999), Phytoplankton community structure in the Arabian Sea during and after the SW monsoon, 1994, *Deep-Sea Res. Pt. II*, *46*(3), 655-676.

Tarran, G. A., Zubkov, M. V., Sleigh, M. A., Burkill, P. H., and Yallop, M. (2001), Microbial community structure and standing stocks in the NE Atlantic in June and July of 1996, *Deep-Sea Res. Pt. II*, 48 (4-5), 963-985.

Thamatrakoln, K., Bailleul, B., Brown, C. M., Gorbunov, M. Y., Kustka, A. B., Frada, M., et al. (2013), Death-specific protein in a marine diatom regulates photosynthetic responses to iron and light availability, *Proc. Natl Acad. Sci. USA*, 110 (50), 20123-20128.

Thomson, R. E., and Fine, I. V. (2003), Estimating mixed layer depth from oceanic profile data, *J. Atmos. Ocean. Tech.*, 20, 319-329.

Topliss, B. J. (1985), Optical measurements in the Sargasso Sea - solar stimulated chlorophyll fluorescence, *Oceanologica Acta*, 8 (3), 263-270.

Topliss, B. J., and T. Platt (1986), Passive fluorescence and photosynthesis in the ocean - implications for remote-sensing, *Deep-Sea Res. Pt. a*, 33(7), 849-864.

Trees, C. C., Clark, D. K., Bidigare, R. R., Ondrusek, M. E., and Mueller, J. L. (2000), Accessory pigments versus chlorophyll a concentrations within the euphotic zone: A ubiquitous relationship, *Limnol. Oceanogr.*, 1130-1143.

Twining, B. S., and Baines, S. B. (2013). The trace metal composition of marine phytoplankton. *Ann. Rev. Mar. Sci.*, *5*, 191-215.

Vassiliev, I. R., Kolber, Z., Wyman, K. D., Mauzerall, D., Shukla, V. K., and Falkowski, P. G. (1995), Effects of iron limitation on photosystem-II composition and light utilization in *Dunaliella-tertiolecta*, *Plant Physiol.*, 109, 963-972.

Veldhuis, M. J. W., and Kraay, G. W. (2004), Phytoplankton in the subtropical Atlantic Ocean: towards a better assessment of biomass and composition, *Deep-Sea Res. Pt. I*, 51(4), 507-530.

Venables, H., and Moore, C. M. (2010), Phytoplankton and light limitation in the Southern Ocean: Learning from high-nutrient, high-chlorophyll areas, *J. Geophys. Res.-Oceans*, 115, C02015.

Vichi M., Cossarini G., Gutierrez Mlot E., Lazzari P., Lovato T., Mattia G., Masina S., McKiver W., Pinardi N., Solidoro C., Zavatarelli M. (2013), *The Biogeochemical Flux Model (BFM): Equation Description and User Manual*. BFM version 5 (BFM-V5). Release 1.0; BFM Report series N. 1. March 2013, Bologna, Italy, http://bfm-community.eu, pp. 87.

Volk, T., and Hoffert, M. I., in *The Carbon Cycle and Atmospheric CO_2: Natural Variations Archean to Present*, E. T. Sunquist and W. S. Broeker, Eds. (American Geophysical Union, Washington, DC, 1985), 32, pp. 99–110.

Walker, N. D. (1986), Satellite-observations of the Agulhas Current and episodic upwelling south of Africa, *Deep-Sea Res. Pt. a*, 33, 1083-1106.

Walker, G. P. L. (1981), Generation and dispersal of fine ash and dust by volcanic-eruptions, *J. of Volcanol. Geoth. Res.*, *11*, 81-92.

Watson, A. J. (1997), Volcanic iron, CO2, ocean productivity and climate, *Nature*, *385*, 587-588.

Watson, A. J., Ledwell, J. R., Messias, M. J., King, B. A., Mackay, N., Meredith, M. P., et al. (2013), Rapid cross-density ocean mixing at mid-depths in the Drake Passage measured by tracer release, *Nature*, 501 (7467), 408.

Watt, S. F. L., Pyle, D. M., Mather, T. A., Martin, R. S., and Matthews, N. E. (2009), Fallout and distribution of volcanic ash over Argentina following the May 2008 explosive eruption of Chaiten, Chile, *J. Geophys. Res.-Sol. Ea. 114*, B04207.

Welschmeyer, N. A. and Lorenzen, C. J. (1981), Chlorophyll-specific photosynthesis and quantum efficiency at sub-saturating light intensities, *J. Phycol.*, 17 (4), 283-293.

Westberry, T. K., Behrenfeld, M. J., Milligan, A. J., and Doney S. C. (2013), Retrospective satellite ocean color analysis of purposeful and natural ocean iron fertilization, *Deep-Sea Res. Pt. I*, 73, 1-16.

Williams, R.G. and Follows, M.J. (2011), *Ocean Dynamics and the Carbon Cycle*, Cambridge Univ. Press, Cambridge.

Williams, R. J. P., and Rickaby, R. (2012), *Evolution's Destiny: co-evolving chemistry of the environment and life*, Royal Society of Chemistry, Cambridge.

Woodward, E. M. S., Rees, A. P. (2001), Nutrient distributions in an anticyclonic eddy in the North East Atlantic Ocean, with reference to nanomolar ammonium concentrations, *Deep-Sea Res. Pt. II*, 48, 775–794.

Wright, S. W., Thomas, D. P., Marchant, H. J., Higgins, H. W., Mackey, M. D., and Mackey, D. J. (1996), Analysis of phytoplankton of the Australian sector of the Southern Ocean: Comparisons of microscopy and size frequency data with interpretations of pigment HPLC data using the 'CHEMTAX' matrix factorisation program, *Mar. Ecol.-Prog. Ser.*, 144(1-3), 285-298.

Yentsch, C. S., and Phinney, D. A. (1989), A bridge between ocean optics and marine ecology, *Limnol. Oceanogr.*, 34, 1694-1705.

Zachos, J. C., Röhl, U., Schellenberg, S. A., Sluijs, A., Hodell, D. A., Kelly, D. C. et al., (2005), Rapid acidification of the ocean during the Paleocene-Eocene thermal maximum, *Science*, 308(5728), 1611-1615.

Zubkov, M. V., Fuchs, B. M., Tarran, G. A., Burkill, P. H., and Amann, R. (2003), High rate of uptake of organic nitrogen compounds by Prochlorococcus cyanobacteria as a key to their dominance in oligotrophic oceanic waters, *Appl. Environ. Microb.*, 69, 1299-1304.

Appendicies

Appendix A1: Example Rapid Light Curves (RLCs)

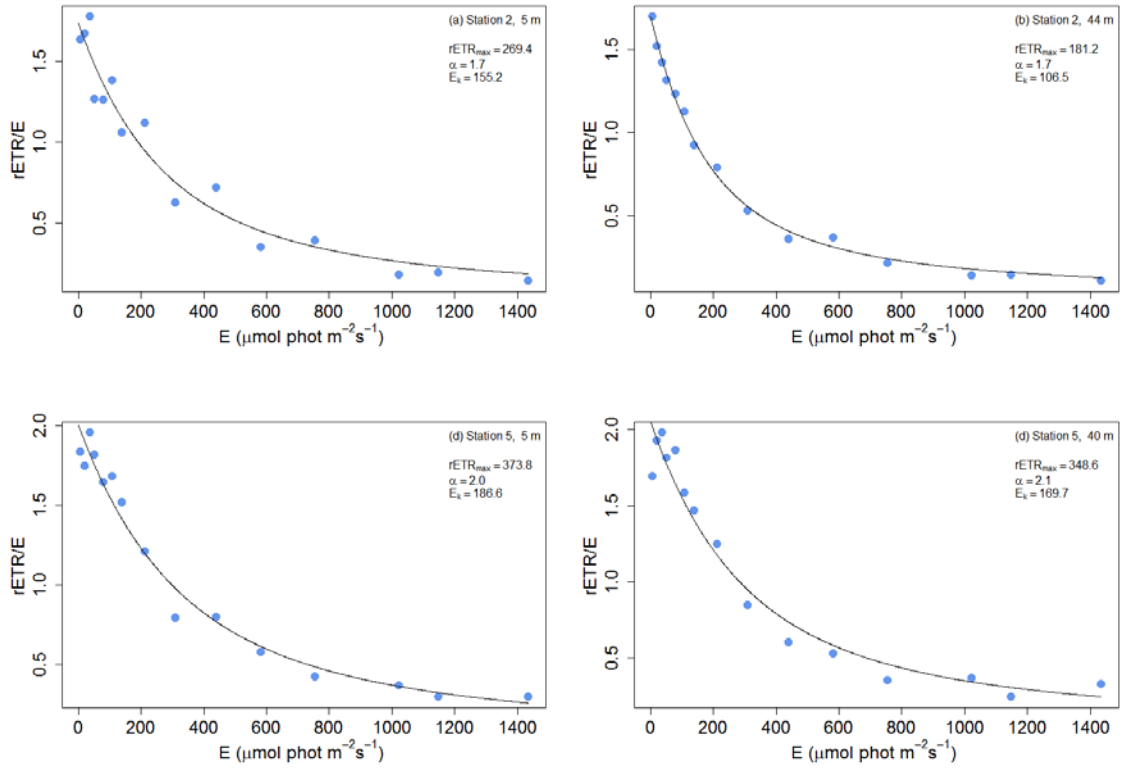

Figure A1.1: Example rETR/E versus E data and curve fits for the JC068 cruise. Blue dots are data points, the back line is the model fit to the data (see Equation 2.2). (a)-(b) are experiments conducted in subtropical gyre type waters (Station 2) north of the SSTC for near-surface and sub-chlorophyll maximum samples respectably; (c)-(d) are for experiments in the sub-Antarctic waters (Station 5) south of the SSTC. Units are as follows: rETR = electrons RCII^{-1} s^{-1}; α = electrons RCII^{-1} (µmol photons m^{-2})$^{-1}$; E_k = µmol photons m^{-2}s^{-1}; rETR/E = electrons RCII^{-1} (µmol photons m^{-2})$^{-1}$.

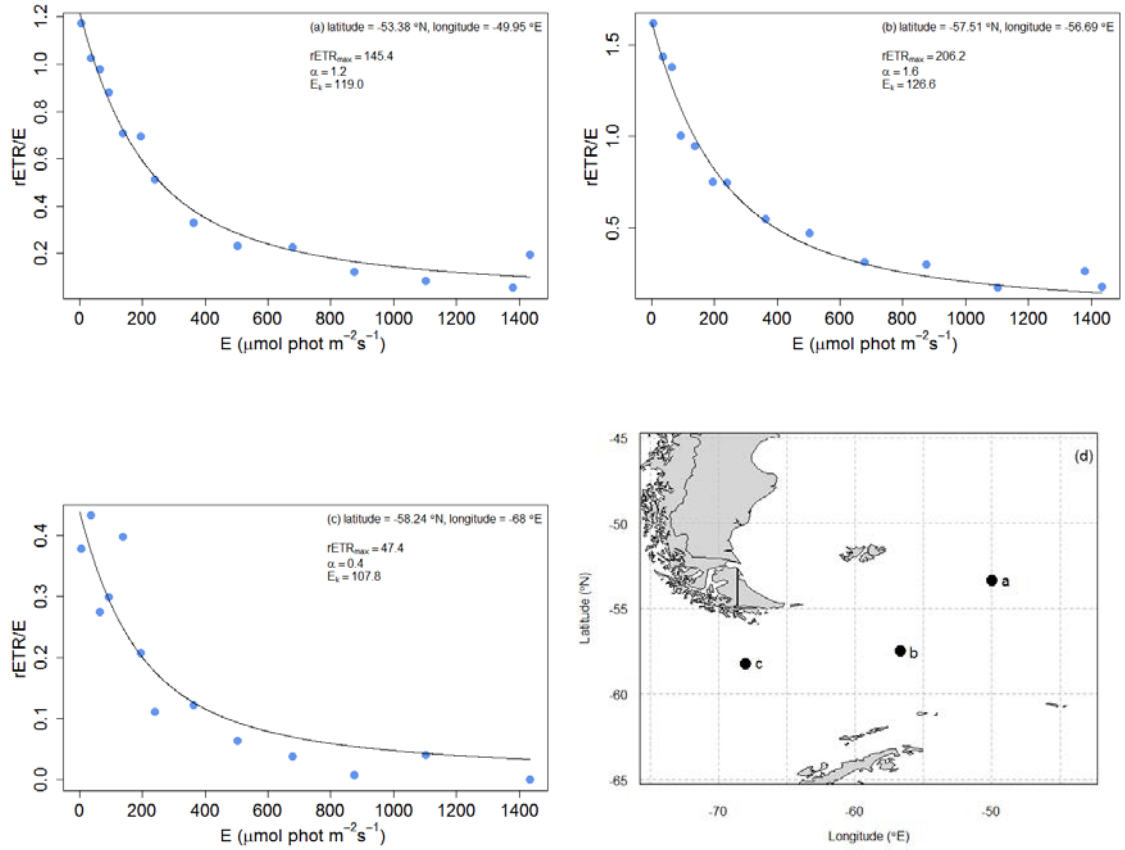

Figure A1.2: Example rETR/E versus E data and curve fits for the JC069 cruise. In (a)-(c) blue dots are data points, the back line is the model fit to the data (see Equation 3.3). Plots a-c show example experiments from the three ecophysiological regimes identified in Chapter 3. Exact locations of the 3 experiments are identified in (d). All 3 experiments were conducted on samples collected at night (i.e., fully dark acclimated). Units are as follows: rETR = electrons $RCII^{-1}$ s^{-1}; α = electrons $RCII^{-1}$ (µmol photons m^{-2})$^{-1}$; E_k = µmol photons $m^{-2}s^{-1}$; rETR/E = electrons $RCII^{-1}$ (µmol photons m^{-2})$^{-1}$.

Appendix A2: Incubation experiment results

Table A2.1: F_v/F_m values for incubation experiments conducted on JC068 and JC069.

IF1		I	C	Fe
	1	0.605	0.554	0.630
	2	0.547	0.643	0.581
	3	0.532	0.638	0.606
Average		0.561	0.612	0.606
SD		0.039	0.050	0.024

IF2		I	C	Fe
	1	0.520	0.648	0.527
	2	0.476	0.531	0.554
	3	0.503	0.632	0.554
Average		0.499	0.604	0.545
SD		0.022	0.063	0.015

IF3		I	C	Fe
	1	0.213	0.262	0.418
	2	0.214	0.238	0.395
	3	0.179	0.234	0.385
Average		0.202	0.244	0.399
SD		0.020	0.015	0.017

IF4		I	C	Fe
	1	0.171	0.211	0.317
	2	0.173	0.206	0.320
	3	0.160	0.204	0.322
Average		0.168	0.207	0.320
SD		0.007	0.004	0.002

IF5		I	C	Fe
	1	0.228	0.298	0.371
	2	0.223	0.281	0.381
	3	0.233	0.310	0.351
Average		0.228	0.296	0.368
SD		0.005	0.015	0.015

IF6		I	C	Fe
	1	0.227	0.237	0.350
	2	0.238	0.251	0.350
	3	0.252	0.302	0.353

Average	0.239	0.264	0.351
SD	0.012	0.034	0.002

IF7	I	C	Fe
1	0.268	0.292	0.360
2	0.267	0.259	0.376
3	0.260	0.308	0.355
Average	0.265	0.286	0.363
SD	0.004	0.025	0.011

IF8	I	C	Fe
1	0.252	0.295	0.375
2	0.237	0.295	0.353
3	0.250	0.320	0.371
Average	0.246	0.303	0.366
SD	0.008	0.014	0.012

IF9	I	C	Fe
1	0.333	0.375	0.347
2	0.328	0.341	0.362
3	0.317	0.375	0.371
Average	0.326	0.363	0.360
SD	0.008	0.020	0.012

IF10	I	C	Fe	Basalt
1	0.384	0.407	0.402	0.368
2	0.371	0.390	0.393	0.360
3	0.384	0.381	0.394	0.387
Average	0.380	0.393	0.396	0.372
SD	0.007	0.013	0.004	0.013

IF11	I	C	Fe
1	0.508		0.506
2	0.442	0.506	0.516
3	0.416	0.535	0.530
Average	0.456	0.520	0.518
SD	0.047	0.021	0.012

IF12	I	C	Fe	Rhyolite
1	0.450	0.412	0.426	0.406
2	0.473	0.425	0.422	0.403
3	0.463	0.447	0.375	0.457
Average	0.462	0.428	0.408	0.422
SD	0.012	0.018	0.028	0.030

IF13	I	C	Fe

1	0.461	0.435	0.443
2	0.467	0.414	0.474
3	0.439	0.441	0.445
Average	0.456	0.430	0.454
SD	0.015	0.014	0.018

IS1	I	C	Fe
1	0.465	0.617	0.501
2	0.449	0.494	0.598
3	0.476		0.551
Average	0.463	0.556	0.550
SD	0.014	0.088	0.048

IS8	I	C	Fe
1	0.350	0.376	0.452
2	0.394	0.435	0.468
3	0.389	0.446	0.411
Average	0.378	0.419	0.444
SD	0.024	0.038	0.030

IS18	I	C	Fe
1	0.424	0.433	0.413
2	0.409	0.409	0.427
3	0.421	0.406	0.421
Average	0.418	0.416	0.420
SD	0.008	0.015	0.007

IS22	I	C	Fe
1	0.346	0.383	0.365
2	0.446	0.419	0.406
3	0.436	0.380	0.339
Average	0.409	0.394	0.370
SD	0.055	0.022	0.034

IF14	I	C	Fe	Basalt	Rhyolite
1	0.378	0.366	0.381	0.370	0.368
2	0.370	0.375	0.374	0.364	0.372
3	0.344	0.357	0.362	0.364	0.374
Average	0.364	0.366	0.372	0.366	0.372
SD	0.018	0.009	0.010	0.004	0.003

IF15	I	C	Fe	Basalt	Rhyolite
1	0.375	0.400	0.452	0.449	0.467
2	0.384	0.393	0.471	0.472	0.481
3	0.384	0.376	0.456	0.480	0.481
Average	0.381	0.389	0.460	0.467	0.476

SD		0.005	0.012	0.010	0.016	0.008

IF16	I	C	Fe	Basalt	Rhyolite
	1	0.317	0.407	0.365	0.377	0.401
	2	0.299	0.409	0.356	0.408	0.423
	3	0.304	0.383	0.369	0.402	0.397
Average		0.307	0.400	0.363	0.395	0.407
SD		0.009	0.015	0.007	0.017	0.014

IF17	I	C	Fe	Basalt	Rhyolite
	1	0.382	0.412	0.426	0.450	0.433
	2	0.410	0.413	0.432	0.467	0.480
	3	0.414	0.416	0.441	0.477	0.467
Average		0.402	0.414	0.433	0.465	0.460
SD		0.018	0.002	0.008	0.014	0.024

IF18	I	C	Fe
	1	0.397	0.412	0.422
	2	0.423	0.410	0.420
	3	0.376	0.435	0.419
Average		0.398	0.419	0.420
SD		0.023	0.014	0.002

IF19	I	C	Fe
	1	0.394	0.380	0.410
	2	0.416	0.380	0.415
	3	0.403	0.379	0.409
Average		0.404	0.380	0.411
SD		0.011	0.000	0.003

IF20	I	C	Fe
	1	0.411	0.382	0.435
	2	0.404	0.376	0.444
	3	0.395	0.382	0.426
Average		0.403	0.380	0.435
SD		0.008	0.004	0.009

IF21	I	C	Fe
	1	0.336	0.356	0.331
	2	0.315	0.351	0.332
	3	0.320	0.355	0.339
Average		0.324	0.354	0.334
SD		0.011	0.003	0.005

IF22	I	C	Fe
	1	0.424	0.424	0.411

	2	0.426	0.426	0.387
	3	0.417	0.417	0.376
Average		0.422	0.422	0.391
SD		0.005	0.005	0.018

IF23	I	C	Fe
1	0.385	0.430	0.415
2	0.377	0.423	0.407
3	0.412	0.406	0.402
Average	0.392	0.420	0.408
SD	0.018	0.012	0.006

IF24	I	C	Fe
1	0.269	0.270	0.339
2	0.265	0.271	0.348
3	0.277	0.261	0.358
Average	0.270	0.267	0.349
SD	0.006	0.006	0.010

IF25	I	C	Fe
1	0.391	0.424	0.417
2	0.394	0.413	0.412
3	0.399	0.397	0.414
Average	0.394	0.411	0.414
SD	0.004	0.013	0.003

IF26	I	C	Fe	Basalt	Rhyolite
1	0.247	0.296	0.271	0.303	0.305
2	0.267	0.269	0.339	0.320	0.348
3	0.273	0.319	0.269	0.323	0.318
Average	0.263	0.295	0.293	0.315	0.324
SD	0.014	0.025	0.040	0.011	0.022

IF27	I	C	Fe
1	0.331	0.345	0.357
2	0.352	0.308	0.349
3	0.312	0.332	0.356
Average	0.332	0.329	0.354
SD	0.020	0.019	0.004

IF28	I	C	Fe
1	0.285	0.304	0.264
2	0.322	0.303	0.309
3	0.293	0.313	0.315
Average	0.300	0.307	0.296
SD	0.019	0.006	0.028

IF29	I	C	Fe	Basalt	Rhyolite
1	0.335	0.333	0.336	0.364	0.384
2	0.318	0.330	0.329	0.373	0.366
3	0.312	0.333	0.337	0.379	0.354
Average	0.322	0.332	0.334	0.372	0.368
SD	0.012	0.002	0.004	0.007	0.015

IF30	I	C	Fe	Basalt
1	0.300	0.298	0.301	0.330
2	0.258	0.279	0.297	0.327
3	0.288	0.300	0.300	0.317
Average	0.282	0.292	0.299	0.325
SD	0.022	0.012	0.002	0.007

IF31	I	C	Fe	Basalt	Rhyolite
1	0.236	0.278	0.313	0.342	0.354
2	0.266	0.286	0.312	0.338	0.360
3	0.269	0.284	0.294	0.366	0.328
Average	0.257	0.283	0.306	0.349	0.348
SD	0.018	0.004	0.011	0.015	0.018

IF32	I	C	Fe	Basalt	Rhyolite
1	0.239	0.365	0.329	0.495	0.347
2	0.267	0.336	0.436	0.388	0.496
3	0.264	0.289	0.456	0.395	0.407
Average	0.257	0.330	0.407	0.426	0.417
SD	0.016	0.038	0.068	0.060	0.075

IF33_24hr	I	C	Fe	Basalt	Rhyolite
1	0.257	0.295	0.319	0.363	0.365
2	0.230	0.299	0.355	0.425	0.373
3	0.258	0.275	0.292	0.336	
4				0.368	
Average	0.248	0.290	0.322	0.373	0.369
SD	0.016	0.013	0.032	0.037	0.006

IF33_48hr	I	C	Fe	Basalt	Rhyolite
1	0.257	0.261	0.356	0.420	0.434
2	0.230	0.284	0.297	0.466	0.410
3	0.258	0.316	0.314	0.416	
4				0.441	
Average	0.248	0.287	0.323	0.436	0.422
SD	0.016	0.028	0.030	0.023	0.017

IF and IS refer to ‘Incubation Fish’ (near-surface waters from the trace-metal-clean towed fish) and ‘Incubation Station’ (SCM waters sampled by the trace-metal-clean titanium frame CTD-rosette system) respectively. I = initial bottles, C = control bottles, Fe = iron amended bottles, Basalt and Rhyolite = bottles amended with the two respective ash types. Numbers 1-3 represent the bottle replicate number. ‘Average’ = mean; ‘SD’ = standard deviation. All experiments were conducted for 24 hours unless stated otherwise (i.e., Experiment IF33). Experiments IF1 to IS22 were conducted on JC068; experiments IF14 to IF33 were conducted on JC069. Experiments which included an ash amendment are referred to as experiments 1 to 12 in Chapter 4 (following the sequential order presented in the table above).